UNIVERSITA' DEGLI STUDI DI GENOVA

DOCTORATE SCHOOL IN SCIENCES AND TECHNOLOGIES OF CHEMISTRY AND MATERIALS

Curriculum in pharmaceutical, food and cosmetic sciences

XXX cycle

PhD Thesis

Design, synthesis and biological evaluation of pyrazolo-pyrimidines and related isosteres as inhibitors of protein kinases, potential antineoplastic agents

Monica Sanna

Advisor: Prof. Silvia Schenone

Defense date: 15th March 2018

TABLE OF CONTENTS

Table of contents

Table of contents

SUMMARY

The protein kinase enzyme family is one of the largest super-families of homologous proteins and are responsible for modifying an estimated one third of the human proteome. These enzymes catalyze the transfer of the terminal phosphate group of ATP to a hydroxyl group of serine, threonine or tyrosine present in a target protein. Depending on the substrate, protein kinases can be classified into serine-threonine kinases and tyrosine kinases.

According to their cellular location, both classes can be further divided into receptor kinases (located in the cell membrane) or cytoplasmic kinases (located within the cell).

Protein kinases are key regulators of cell functions. They direct the activity, localization and other functions of many proteins, and serve to orchestrate the activity of almost all cellular processes. It has also been firmly demonstrated that kinase activity alterations, leading to the disruption of cell signalling cascades, play important roles in many diseases, including cancer, inflammation, neurological disorders and diabetes. For all these reasons, kinases represent important targets for drug therapy. It is estimated that over 30% of the drug discovery efforts in pharmaceutical and biotech companies are directed towards finding and validating protein kinase inhibitors.

My PhD project was aimed at synthesizing inhibitors of the tyrosine kinases Src, Fyn and Hck and the serine-threonine kinase Sgk1.

Src family kinases are a group of highly homologous non-receptor tyrosine kinases that are involved in the regulation of several phases of cell life (e.g. growth, differentiation, apoptosis). The hyperactivation of c-Src, a member of this family of enzymes, has been proved to be closely connected with the development and progression of several tumor types. In this context, the research group where I worked has synthesized a large library of pyrazolo[3,4-*d*]pyrimidines; many of these molecules resulted to be nanomolar inhibitors of the cytoplasmic tyrosine kinase c-Src. This family of compounds also showed a good antiproliferative activity against several cancer cell lines: neuroblastoma, chronic myeloid leukaemia, rhabdomyosarcoma, osteosarcoma, prostate cancer, and mesothelioma. Important results have been obtained in several mouse models of cancer.

Recently, c-Src has been shown to be frequently hyperactivated or overexpressed also in glioblastoma, a brain tumour characterized by a high degree of proliferation, angiogenesis, necrosis, and invasiveness. Src inhibition reduced glioblastoma cell growth, viability and

migration both *in vitro* and in mouse models. In this context, I synthesized a library of pyrazolo[3,4-*d*]pyrimidines; some of these compounds demonstrated a good activity towards Src in enzymatic assays and on different glioblastoma cell lines.

At the same time, the pyrrolo[2,3-*d*]pyrimidine scaffold is also being extensively investigated and in the last few years, many of such compounds resulted active as kinase inhibitors. For this reason, I synthesized a family of pyrrolo[2,3-*d*]pyrimidines which have been tested on Src in enzymatic assays and as antiproliferative agents on a specific cancer cell line.

Fyn is another member of Src family kinases and it phosphorylates a variety of target proteins involved in different signalling pathways. To date, the implication of Fyn in solid and in hematologic malignancies has become more evident and its abnormal activity has been shown to be related to severe central nervous system pathologies such as Alzheimer's and Parkinson's disease.

The research group where I worked synthesized a library of pyrazolo[3,4-*d*]pyrimidines active as Fyn inhibitors endowed with K_i values in the nanomolar range. Some of these compounds inhibited the phosphorylation of the protein Tau in an Alzheimer's model cell line and showed antiproliferative activities against different cancer cell lines. On the basis of these interesting results, I decided to expand the structure-activity relationship (SAR) on this family of inhibitors and planned the synthesis of new compounds.

Hematopoietic cell kinase (Hck) is another member of Src family kinases and it is expressed in hematopoietic cells, particularly myelomonocytic cells and B-lymphocytes. High levels of Hck are involved in chronic myeloid leukemia and in other hematologic tumors, but its activity is also connected with viral infections, including HIV-1. In this context, our research group developed a docking study to identify new Hck inhibitors. We screened some molecules of our in house library of pyrazolo[3,4-*d*]pyrimidines and some commercial compounds, and we tested, in enzymatic and cellular assays, the most promising compounds which showed an activity towards Hck in the low micromolar range. On the basis of these results, I synthesized some new pyrazolo[3,4-*d*]pyrimidines, analogs of the most active inhibitors, and some derivatives of the commercial compound, which showed the best Hck inhibitory activity, in detail 5,6,7,8-tetrahydro[1]benzothieno[2,3-*d*]pyrimidine molecules. Enzymatic assays of these compounds are still in progress.

Sgk1 is a member of the serum- and glucocorticoid-regulated kinase family that is involved in antiapoptotic functions and in the regulation of cell survival, proliferation, and differentiation.

A pivotal role of Sgk1 in carcinogenesis and in resistance to anticancer therapy has been suggested. For all these reasons, we decided to develop an *in silico* screening in order to see if some our pyrazolo[3,4-*d*]pyrimidines, already active as Src and/or Abl inhibitors, were also active towards Sgk1. One of these compounds, showed a very interesting activity. On the basis of these interesting results, I synthesized a small library of pyrazolo[3,4-*d*]pyrimidines, analogue of the most active compounds, in order to develop a lead optimization study. Other synthesis and biological studies are in progress.

During the third year of my PhD, I also spent a research period at the School of Pharmacy of the University of Nottingham under the supervision of Prof. Cameron Alexander. In these months, I developed a new miniaturized screening process, based on an inkjet printing technologies, able to identify the best formulation to enhance the apparent water solubility of some pyrazolo[3,4-*d*]pyrimidine derivatives, using as little of the sample as possible. I chosen five compounds of our in-house library of pyrazolo[3,4-*d*]pyrimidines and I synthesized a new analogue. Then I combined these derivatives with seven different hydrophilic commercial available polymers that are able to inhibit crystallization and to create an amorphous solid dispersion. The applied amount of compounds used in the reported strategy ranged from 5 to 10 μg per formulation which were dispensed by an inkjet 2D printer directly into a 96-well plate. The selected polymer/drug formulations with high water solubility demonstrated improved cytotoxicity against a human lung adenocarcinoma cancer cell line (A549) compared to the free drugs. The enhanced efficacy was attribute to the improved apparent-solubility of the drug molecules achieved via this methodology. This novel miniaturized method showed promising results in terms of water solubility improvement of the highly hydrophobic pyrazolo[3,4-*d*]pyrimidine derivatives, requiring only a few micrograms of each drug per tested polymeric formulation. In addition, the reported experimental evidence may facilitate identification of suitable polymers for combination with drug, leading to investigations on biological properties or mechanisms of action in a single formulation.

CHAPTER 1. Introduction

1.1 The protein kinase enzyme family

Protein kinases are ATP-dependent phosphotransferases that deliver a single phosphoryl group from the γ-position of ATP to the hydroxyl groups of serine, threonine and tyrosine in protein substrates (**Fig. 1**). This phosphorylation process produces a signal transduction that implicates a biological response. Protein kinases can regulate a wide range of processes including cell growth, survival, division, differentiation, proliferation, apoptosis, angiogenesis and also carbohydrate and lipid metabolism, neurotransmitter biosynthesis, DNA transcription and replication, organelle trafficking and smooth muscle contraction.[1]

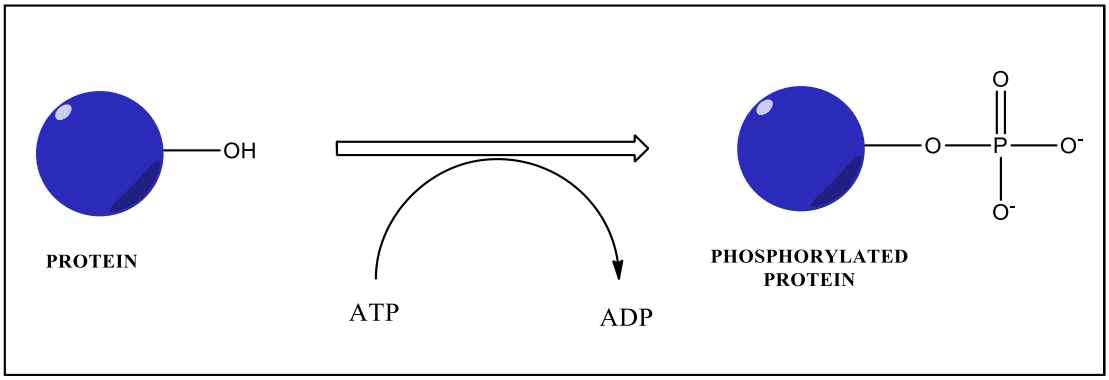

Fig. 1. Protein kinase phosphorylation mechanism.

Based on the nature of the phosphorylated OH group, these enzymes are classified as protein serine-threonine kinases and protein-tyrosine kinases.

Manning *et al*. identified 478 typical and 40 atypical human protein kinase genes (total 518) that correspond to nearly 2% of all human genes and are responsible for modifying an estimated one third of the human proteome (**Fig. 2**).[2] In the early 1990s, X-ray crystallography showed that the catalytic domains of serine/threonine and tyrosine kinases share a common architecture. Indeed, this is the key feature that distinguishes protein kinase family members from other proteins.

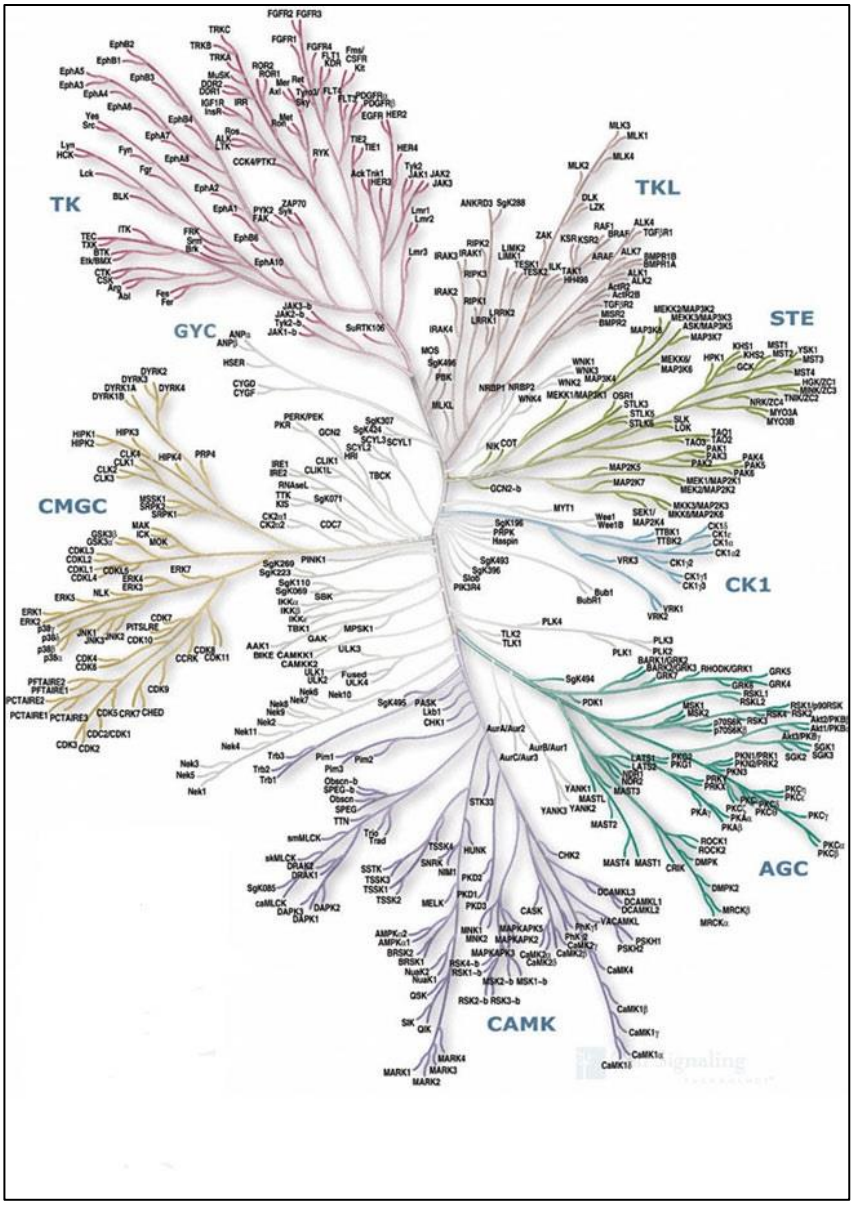

Fig. 2. Human protein kinases. (From Cell Signaling Technology®).

Protein phosphorylation was discovered as a regulatory mechanism by Krebs and Fischer (Nobel prize 1992) in the late 1950s through their studies of glycogen phosphorylase and their subsequent discovery of phosphorylase kinase.[3]

The mechanism requires an essential bivalent metal ion, usually Mg^{2+} (or Mn^{2+}) to facilitate the phosphoryl transfer reaction and assist in ATP-binding. Protein kinases operate on two substrates which are the protein and MgATP and produce the corresponding phosphoprotein and MgADP[4]. They possess extraordinary catalytic power, accelerating phosphorylation rates

by 9-11 orders of magnitude. This finding comes from the presumption that the alkoxide of serine or threonine or the phenolate of tyrosine, formed by the interaction with the Mg^{2+} ion, should be a better general nucleophile than the alcohol or phenol form and, thus, would enhance phosphoryl group donation.

It is known that protein kinases share a conserved region of approximately 200-250 amino acids that confers kinase activity and consists of two lobes, the N-terminal lobe (N-lobe) which contains five β strands and a universally conserved αC-helix, interacts with the ATP through the glycine-rich loop which coordinates the phosphate groups, and the C-terminal lobe, which contains mostly helices plus a β sheet and provides substrate-binding sites for ATP and peptides. The helical subdomain of the C lobe, which is extremely stable, forms the core of the kinase and the subdomain, comprising four β short strands, contains much of the catalytic machinery associated with the transfer of the phosphate from ATP to the protein substrate and is anchored through hydrophobic residues to the helical core. The C-terminal domain includes the activation loop (A-loop), a segment typically containing tyrosine, serine or threonine residues that can be phosphorylated. In its non-phosphorylated state, the A-loop tends to hinder substrate binding. Phosphorylation of these residues increases kinase activity. Among the amino acids of the conserved region, there are key residues extremely important for the interaction with ATP. Asp-184, a strictly conserved residue, interacts with the essential Mg^{2+}, which chelates the β and γ phosphates of ATP. The chelation of this ion may position the terminal phosphate for direct transfer to the hydroxyl acceptor.

Another key residue is Lys-72, which interacts with α and β phosphates of ATP, giving additional stabilization and facilitating the phosphoryl group transfer without influencing ATP-binding (**Fig. 3**).

In addition to the catalytic domain, the structure of protein kinases includes other well characterized domains (e.g. SH3 and SH2 in cytoplasmic tyrosine kinases). Typically, these domains mediate inter- and intramolecular interactions of protein kinases, thus playing an important role in their functional regulation.[1]

It has been demonstrated that kinase activity alterations (especially hyperactivation, hyperproduction or mutations), leading to the disruption of cell signalling cascades, play important roles in several diseases, including cancer, inflammation, neurological disorders and diabetes, making kinases attractive targets for several therapies.[5]

Thus, kinases are the focus of intense basic and drug discovery research, and the US Food and

Drug Administration (FDA) and the European Medical Agency (EMA) have so far approved more than 30 small-molecule kinase inhibitors.[6,7]

The kinase inhibitors market is expected to see a staggering growth, with the current market valued at USD 15 billion in 2012, and anticipated to reach USD 36 billion in 2018. This exponential growth is predicted due to a rise in the incidence of various cancers, a rise in aging population and, consequently, increased focus of pharmaceutical companies on R&D to come up with potential medicines for the treatments of cancers.

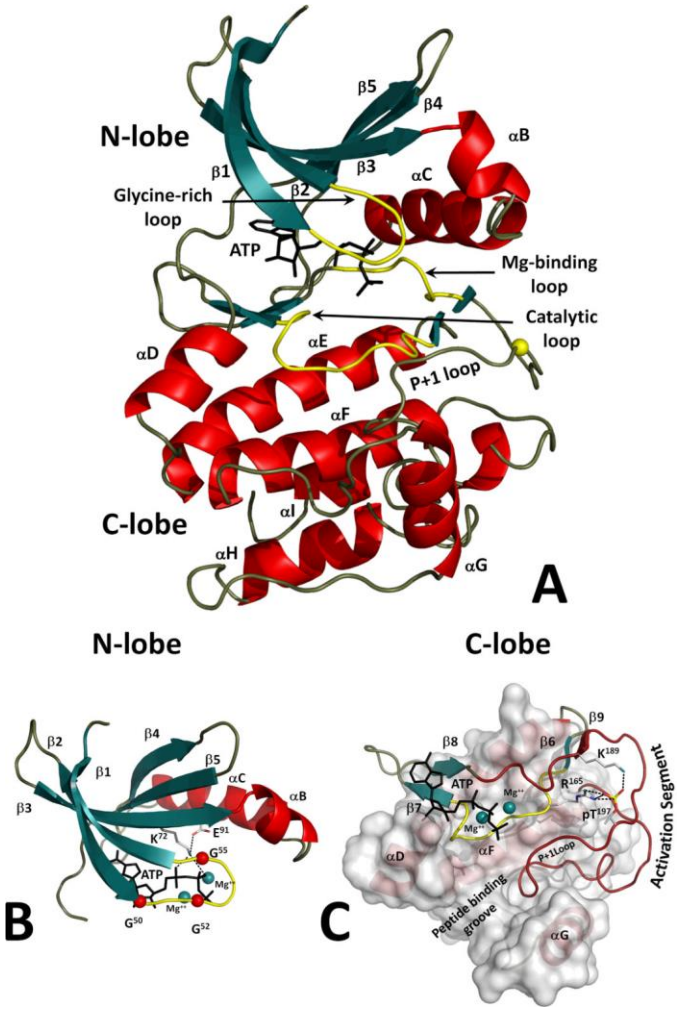

Fig. 3. A. Structure of the conserved protein kinase core. An ATP molecule is bound to a deep cleft between the lobes. Major catalytically important loops are colored yellow. **B**. N-lobe structure. Three conserved glycines are shown as red spheres. **C**. C-lobe structure. Catalytic and regulatory machinery is bound to the rigid helical core.

1.1.1 Tyrosine kinases

Tyrosine kinases (TKs) are a subclass of protein kinases that catalyze phosphorylation of selected tyrosine residues in target proteins, using ATP.

TKs are conserved throughout eukaryotes and regulate processes in both unicellular and multicellular organisms. They contain highly conserved catalytic domains similar to those of serine/threonine kinases, but with unique subdomain motifs typical of TKs.[8] The reaction catalyzed by tyrosine kinases involves the transfer of the γ-phosphate of ATP to the hydroxyl of the substrate tyrosine and requires the presence of a divalent metal ion. In detail, the substrate binds to a platform on the TK C-terminal lobe, with the hydroxyl group of the tyrosine to be phosphorylated pointing toward the γ-phosphate of ATP. This platform is partially formed by residues from the activation loop (A-loop), the conformation of which is stabilized by the phosphorylation of one or more tyrosine residues in most tyrosine kinases. Residues important for catalysis or for the correct architecture of the catalytic site come from different parts of the structure, such as the P-loop (glycine-rich or nucleotide-binding loop), β strand 3 and αC-helix, all within the N-terminal lobe and the catalytic loop (β strands 6 and 7) and the A-loop (about 20 residues located between strand 8 and αC-helix). Many of these structural elements correspond to regions with highly conserved sequences.

The structures of TKs in the active state are all very similar, despite the fact that they have different substrate specificities and different mechanisms of control. This similarity results from the constraints on the spatial arrangement of residues important for catalysis. In this way, the structural elements on which these amino acids reside tend to have the same relative orientation. In cells under resting conditions, most TKs are held in an inactive state, which usually involves a conformation that disrupts the active arrangement of the catalytic residues or blocks the protein from binding cofactors or substrates. Unlike active kinases where the structures are very similar, inactive kinases have structurally diverse conformations. Structural biology has revealed several different mechanisms of self-regulation. In most cases, the position of C-helix and/or the A-loop is involved, and very often regions outside the kinase domain fold back to block the binding sites or cause conformational changes that render the kinase inactive. Many of these mechanisms are shared by kinases from distinct tyrosine kinase subgroups and also with non-tyrosine kinases.[9]

TK activation regulates many key processes in cell growth, survival, organ morphogenesis, neovascularization, and tissue repair and regeneration.[10] In normal cells, TK activity is strictly

regulated, while deregulation or constitutive activation of TKs has been found in a wide range of disease and, in particular, in cancer. The deregulated activation occurs by gain-of-function mutations, gene rearrangement, gene amplification, overexpression or abnormal autocrine, endocrine or paracrine stimulation of both enzyme and ligand, and, in some cases, it has been shown to correlate with the development and progression of numerous human cancers. Since TKs have been implicated in many aspects of the malignant phenotype, they emerged as promising therapeutic targets. Cancer therapy targeting TKs may be successful only if the targeted TK is a major regulator of cancer cell survival, but cancer cells usually contain multiple genetic and epigenetic abnormalities. Despite this complexity, cancer cell survival and/or proliferation can often be impaired by the inactivation of a single oncogene. This phenomenon, called "oncogene addiction", provides a rationale for molecular targeted therapies. A convincing evidence for the concept of oncogene addiction comes from the increasing number of examples of the therapeutic efficacy of antibodies or small molecules that target a specific oncogene. Evidence is provided by the therapeutic efficacy of drugs that target various oncogenic protein kinases; examples include imatinib, which targets the Bcr-abl oncogene in chronic myeloid leukemia and also targets the c-kit oncogene in gastrointestinal stromal tumors, and gefitinib and erlotinib, which target the epidermal growth factor receptor in non-small cell lung cancer, pancreatic cancer, and glioblastoma.[11]

Two classes of TKs are present in human cells, the transmembrane receptor TKs, and the cytoplasmic or non-receptor TKs.

1.1.1.1 Receptor tyrosine kinases

The family of receptor tyrosine kinases (RTKs) includes 20 subclasses (ALK, AXL, DDR, EGFR, EPH, FGFR, INSR, MET, MUSK, PDGFR, PTK7, RET, ROS, ROR, RYK, TIE, TRK, VEGFR, AATYK and the uncharacterized DKFZp761P1010). All these enzymes are transmembrane glycoproteins formed by an extracellular part, which works as a receptor, and an intracellular portion endowed with the kinase catalytic activity. The RTKs are activated by the binding of their cognate ligands and transduce the extracellular signal to the cytoplasm by phosphorylating tyrosine residues on the receptors themselves (autophosphorylation) and on downstream signalling proteins.

RTKs activate numerous signalling pathways within cells, leading to cell proliferation, differentiation, migration or metabolic changes.[12]

Activation of RTKs typically stimulates two processes: the enhancement of intrinsic catalytic activity and creation of binding sites to recruit downstream signalling proteins. For the majority of RTKs, both of these processes are accomplished by autophosphorylation on tyrosine residues, a consequence of ligand-mediated oligomerization. Therefore, the inactive state of RTKs is monomeric or oligomeric. The activation of the receptor requires the binding of its ligand to stabilize specific relationships between individual receptor molecules. Ligand binding to the extracellular portion of RTKs mediates the noncovalent oligomerization of monomeric receptors or induces a structural rearrangement in heterotetrameric receptors (e.g. the insulin receptor), facilitating tyrosine autophosphorylation in the cytoplasmic domains. All members of RTKs family consist of a single transmembrane domain that separates the intracellular tyrosine kinase region from the extracellular portion. The latter exhibit a variety of elements including immunoglobulin (Ig)-like or epidermal growth factor (EGF)-like domains, fibronectin type III repeats or cysteine-rich regions that are characteristic for each subfamily of RTKs. The catalytic domain is located in the intracellular portion, and displays the highest level of conservation, includes the ATP-binding site that catalyses receptor autophosphorylation and tyrosine phosphorylation of RTK substrates (**Fig. 4**). [13]

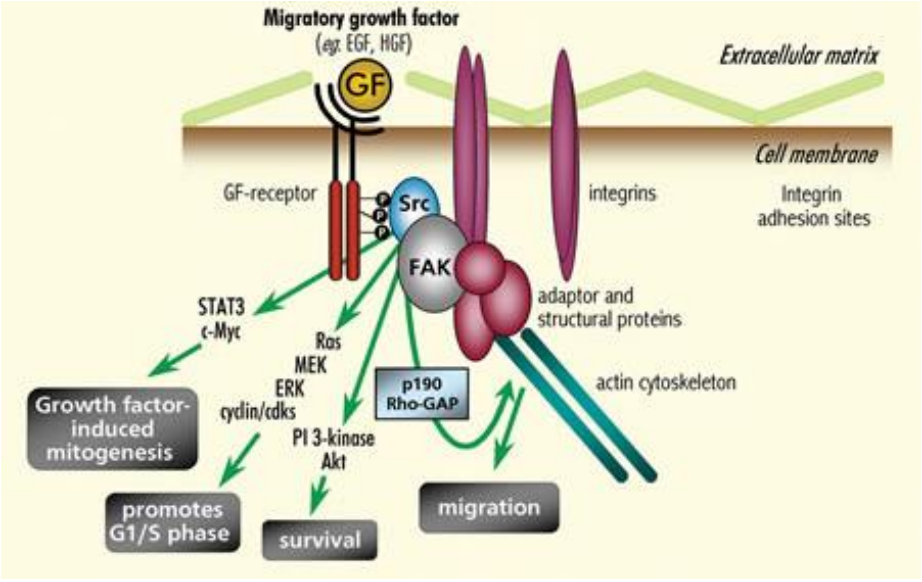

Fig. 4. A receptor tyrosine kinase and intracellular pathways activated by it.

1.1.1.2 Non-receptor tyrosine kinases

The family of non-receptor tyrosine kinases (NRTKs) includes 10 subfamilies (Abl, Ack, Csk, Fak, Fes, Frk, Jak, Src, Tec, Syn), indirectly regulated by extra-cellular signals **(Fig. 5)**.

Some NRTKs are anchored to the cell membrane through amino-terminal modifications, such as myristoylation or palmitoylation. The catalytic domain is located between the N-lobe and the C-lobe, as reported for other protein kinases, and shares a common structure. In addition, NRTKs possess domains that mediate protein-protein, protein-lipid, and protein-DNA interactions. The most commonly found protein-protein interaction domains in NRTKs are the Src homology 2 (SH2) and 3 (SH3) domains. The SH2 domain is a compact domain of ~100 residues that binds phosphotyrosine residues in a sequence-specific manner. The smaller SH3 domain (~60 residues) binds proline-containing sequences capable of forming a polyproline type II helix. Some NRTKs lack SH2 and SH3 domains but possess subfamily-specific domains used for protein-protein interactions. The most common theme in NRTK regulation is tyrosine phosphorylation. With few exceptions, phosphorylation of tyrosines in the activation loop of NRTKs leads to an increase in enzymatic activity. Activation loop phosphorylation occurs via *trans*-autophosphorylation or phosphorylation by a different NRTK. On the other hand, phosphorylation of tyrosines outside of the activation loop can negatively regulate kinase activity.[10] A description of all cytoplasmic TKs has been reviewed by Tsygankov.[14]

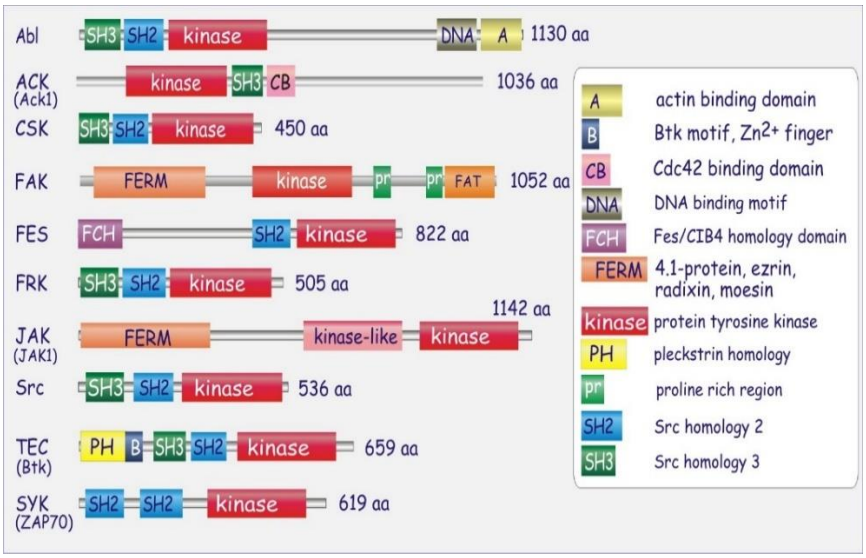

Fig. 5. Examples of non-receptor tyrosine kinases.

1.1.2 Serine-threonine kinases

The serine-threonine kinases (STKs) are a subfamily of protein kinases which catalyze the phosphorylation of serine or threonine residues in their substrates, they have important functions in normal and pathological cellular processes, as they regulate cell survival, metabolism, motility, growth, division, and differentiation.[15]

STKs have been implicated in human cancer as well. Moreover, many high-throughput strategies have been exploited to implicate STKs in the initiation and progression of cancer either by searching for activating mutations or by identifying misregulated expression in gene profiling experiments.[16] Similarly to TKs, STKs can be divided in two classes: receptor STKs and cytoplasmic STKs.

1.1.2.1 Receptor serine-threonine kinases

In contrast to the large number of receptor tyrosine kinases, there are only 12 receptor serine/ threonine kinases.[2] They are all members of a single extended family that binds ligands in the TGFβ family of cytokines and transduces signals that promote growth arrest and differentiation. Signalling by this type of receptor kinase is accomplished through the binding of a TGFβ family member, which induces the formation of a heterodimer containing a type I TGFβ receptor and a type II TGFβ receptor. Within this dimer, the constitutively active type II receptor phosphorylates the inactive type I receptor in the complex, and thereby activates it to phosphorylate downstream cytoplasmic target proteins.[17,18]

1.1.2.2 Non-receptor serine-threonine kinases

Non-receptor serine/threonine kinases are the largest group of eukaryotic protein kinases comprising 376 out of the total of 518 protein kinases in humans.[2] Examples are protein kinase C (PKC), the mitogen activated protein kinases (MAPK), Akt (or protein kinase B, PKB) and Sgk (Serum- and glucocorticoid-regulated kinase). Cytoplasmic serine threonine kinases (like Raf, Akt, Tpl-2 and Sgk1) are also mutated or activated in several types of human malignancies.[16]

CHAPTER 2. Src family kinases

The Src family of protein tyrosine kinases (SFKs) counts nine members: Src, Fyn, Yes, Blk, Yrk, Fgr, Hck, Lck, and Lyn. They play key roles in regulating signal transduction from a diverse set of cell surface receptors in the context of a variety of cellular environments. SFKs are involved in the regulation of fundamental cellular processes, including cell growth, differentiation, migration and survival, cell shape and specialized cell signals.[19] Moreover, many members of this family have been identified as cellular oncogenes. The pleiotropic functions of Src family members underscore the importance of these kinases in physiologic and pathologic conditions.[20]

2.1 c-Src structure and activation

Human c-Src is a protein of 536 amino acids and has a structure that shares common features with the other SFK members. From the N- to C-terminus, Src presents a conserved domain organization which includes a N-terminal Src homology domain (SH4), an unique domain, a SH3 domain, a SH2 domain, a poly-proline type II (PPII) domain, a catalytic domain (SH1) and finally a short C-terminal regulatory segment (**Fig. 6**).[21]

The SH4 domain, whose N-terminal is always myristoylated and sometimes palmitoylated,[22] is the membrane-targeting region that allows the association between the protein and the inner surface of the cell membrane. The unique domain is a sequence of 50-70 residues and it is different among SFK members. It is probably involved in protein-protein interactions. SH2 and SH3 are two domains highly conserved in SFKs and play a critical role in regulating Src activity. SH2 (~100 amino acid residues) presents a central three-stranded β-sheet with a single helix packed against each side; this structure leads to the formation of two recognition pockets. SH3 domain (~60 amino acid residues) is a β-barrel consisting of five antiparallel β-strands and two loops (RT and n-Src loops) that bind the poly-proline type II domain (PPII), a linker segment located between the SH2 and the kinase domains. The PPII domain is characterized by proline-rich sequences that adopt a helical conformation in complex with the SH3 domain, binding with aromatic amino acid side chains on the SH3 surface. The catalytic domain SH1, responsible for the TK activity, presents a bilobal structure, similarly to the majority of kinases, with a small N-terminal lobe and a large C-terminal lobe, that form the ATP and substrate

binding site at the interlobe cleft.

The N-terminal lobe is composed of five β-strands and a single α-helix (C-helix), with a glycine-rich G-loop (or P-loop, because of the phosphate binding site) that binds and locates ATP appropriately for γ-phosphate transfer to the substrate. The C-terminal lobe is mainly formed of α-helix. The positive regulatory activation loop (A-loop) is located in it, and contains the key residue Tyr419 (in human Src). The flexible chain that connects N- and C-lobes is called the "hinge region".[21]

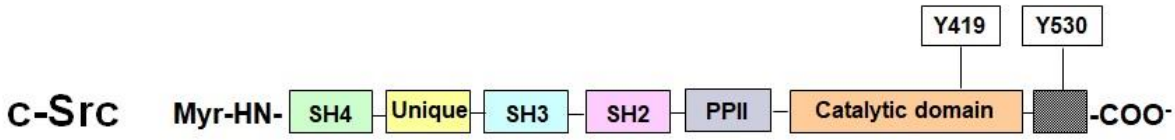

Fig. 6. Human c-Src structure.

Src exists in two forms: a closed, inactive conformation and an open and active one. There are two key elements that regulate Src conformation: the amino acids Tyr419 and Tyr530. When Tyr419 is phosphorylated and Tyr530 dephosphorylated, Src is in the active state, while, when Tyr 419 is dephosphorylated and Tyr530 phosphorylated, the kinase is in the inactive state.

The inactive enzyme is forced in a closed conformation by intramolecular contacts among the SH2 and SH3 domains and the catalytic site. In detail, SH3 and SH2 pack against the N-lobe and the C-lobe, respectively, on the opposite site of the catalytic cleft. Furthermore, this closed conformation is stabilized by intramolecular interactions of SH3 with the PPII domain and of SH2 with the phosphorylated C-terminal tail.

Although the position of the SH2 and SH3 domains does not sterically occlude the catalytic cleft, this conformation causes the inactivation of the enzyme, mainly for three reasons:

- A catalytically important residue is removed from the active site as a consequence of the C-helix displacement.
- In this conformation, the A-loop does not allow the phosphorylation of the positive regulatory Tyr419 or the protein binding.
- The relative orientation of N- and C-lobes is not convenient for the kinase activity.[20]

The dephosphorylation of Tyr530 and the autophosphorylation of Tyr419 lead to the active and open conformation: the molecular associations between SH2 and SH3 are disrupted, different interactions are formed, and the phosphorylation of Tyr419 in the A-loop causes conformational

changes that allow the access of substrates to the catalytic site. Under basal condition in vivo, 90-95% of Src is present in the inactive form (pTyr530). C-terminal Src kinase (Csk) and Csk homologous kinase (Chk) are the two kinases known up today to specifically phosphorylate Src on Tyr530 causing its inactivation (Fig. 7).

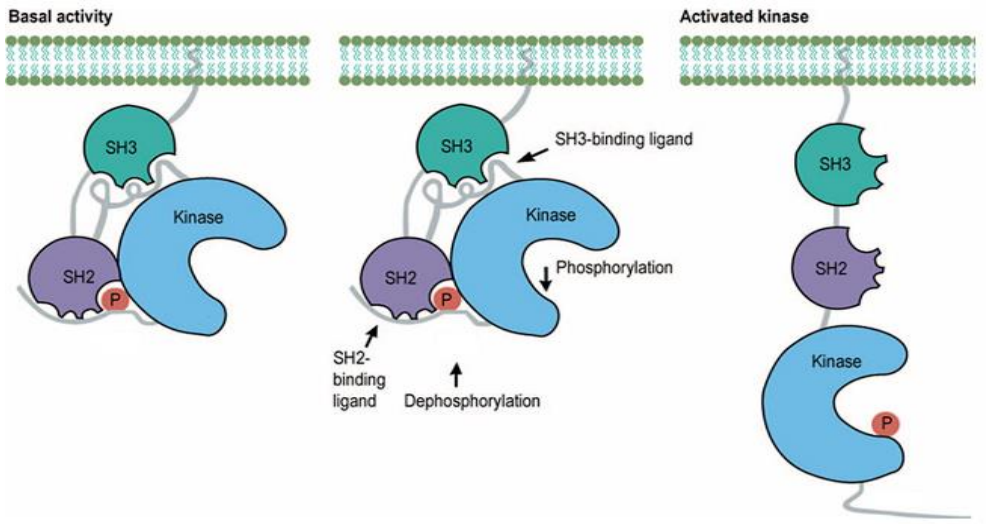

Fig. 7. Src activation/inactivation.

On the other hand, several phosphatases can dephosphorylate Tyr530, leading to enzyme activation. Some transmembrane tyrosine phosphatases[23] and the cytosolic proteins PTP1B (protein tyrosine phosphatase 1B), Shp1 and Shp2 are the enzymes involved in this reaction. Ligand-bound cell-surface receptors and cytoplasmatic proteins can activate Src, by binding the SH3 and SH2 domains and displacing such regulatory subunits from the kinase domain. This permits Tyr419 autophosphorylation.

In particular, several extracellular molecules can activate Src binding receptors, such as growth factor receptors, integrins and other adhesion receptors, guanosine phosphate binding-coupled receptors (GPCRs), cytokine receptors and ion channels. Src, in response to these extracellular signals, becomes activated and phosphorylates various downstream targets, regulating multiple signal transduction pathways, including Ras/Raf, RhoGAP, PI3K/Akt pathways and many others (**Fig. 8**).

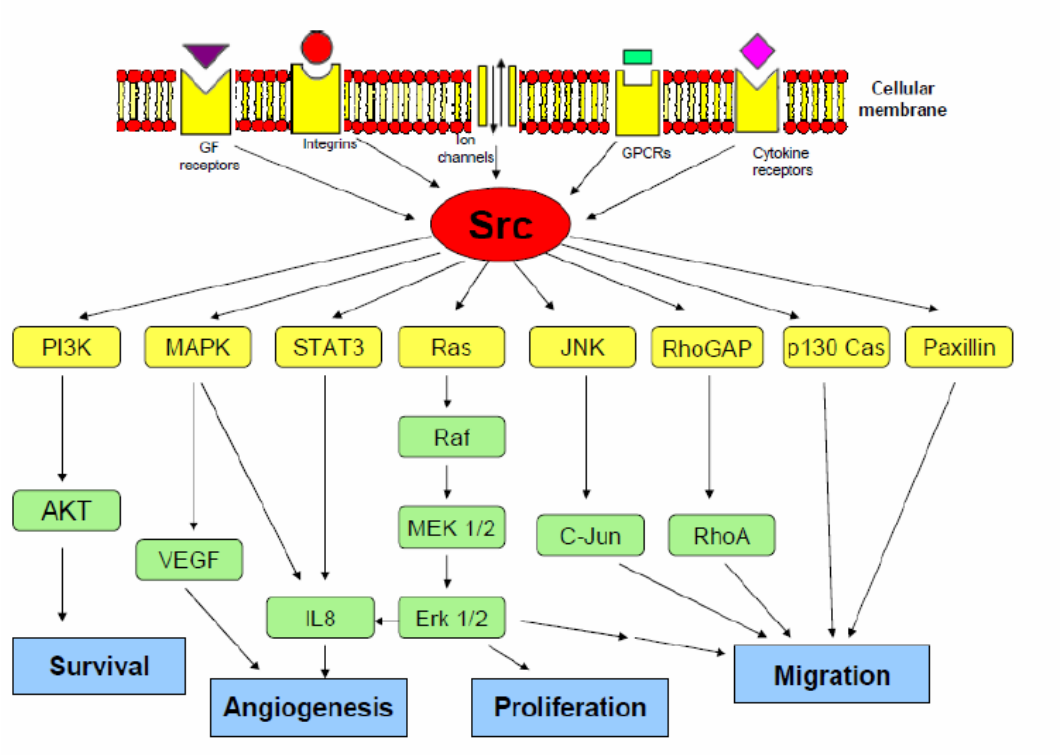

Fig. 8. Schematic representation of Src signalling pathway.

2.2 Src and cancer

SFKs have a key role in cell signalling and are involved in the development of numerous diseases, first of all cancer (**Fig. 9**).[24,25] Src is the first kinase, among SFKs, which has been reported as implicated in cancer biology, in particular in cancer progression. An increased Src activity is found transiently in almost every aspect of a normal cell life in response to different physiological conditions, including mitogenesis, proliferation, survival, adhesion and motility, all of them deregulated during cancer progression.[26] Malignant activation of Src is concomitant with a cell's inability to downregulate such activity. Four of the six "hallmarks of the transformed state" (in detail, self-sufficiency in growth signals, evasion of apoptosis, sustained angiogenesis and tissue invasion and metastasis) are heavily dependent on tyrosine kinase (including Src) signalling.[27]

Many studies have been performed on the oncogenic behaviour of mutated Src in the etiology of human cancer, starting from the discovery that v-Src, the viral homologous of c-Src, characterized by the lack of the C-terminal negative regulation site, causes sarcoma in chickens and in other animal species.[28] A deregulated SFKs activity probably mainly depends on

overexpression or hyperactivation of the enzyme, even if the presence of mutations in advanced human colon cancer has been also described.[29] The point mutation introduces a stop codon corresponding to the amino acid 531, and this truncated form, termed Src-531, shows enhanced activity.

Changes in the levels of Src and/or in its kinase activity appear to be correlated with the grade of malignance of tumors. Malignant activation of SFKs, characterized by constitutively high enzymatic levels, is present in many human cancers: breast, gastric, colon, pancreatic, ovarian, prostate, head, neck, lung, bladder cancer, neuronal tumors, and leukemias, lymphomas and myelomas.[30]

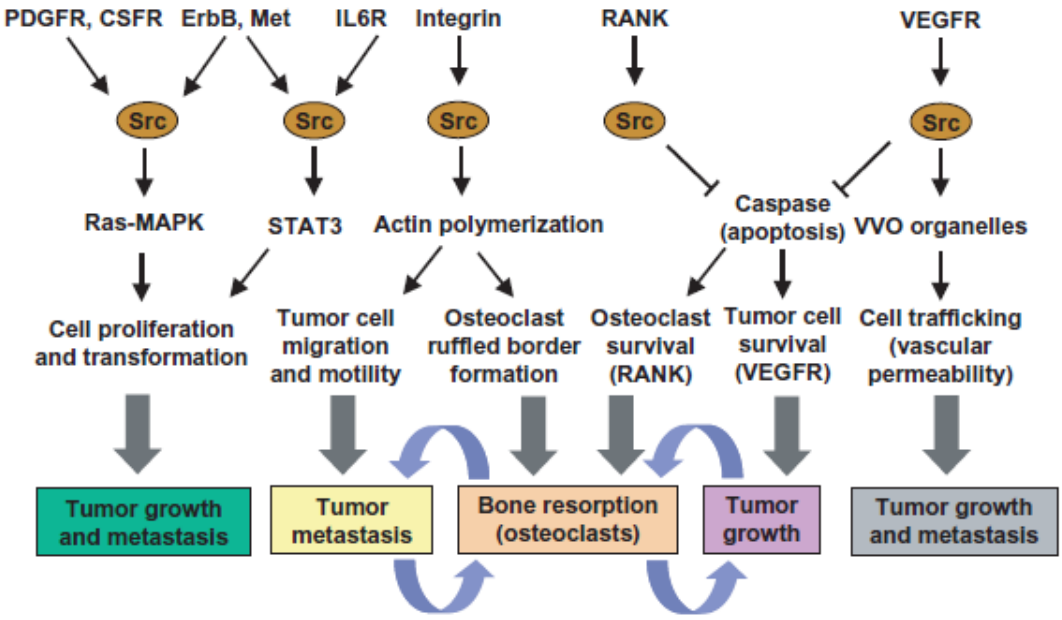

Fig. 9. Involvement of Src in the onset and progression of tumors. Ann Oncol 2008[24]

2.2.1 Src and glioblastoma

Glioblastoma (GB) is the most common and aggressive primary tumor of the central nervous system (CNS). According to the World Health Organization classification, GB is a grade IV astrocytoma[31] and can develop either *de novo* or through the malignant progression of lower-grade astrocytomas. About 50% of the people diagnosed with GB die within one year, while 90% within three years.[32] GB is characterized by increased proliferation and demand of nutrient and oxygen, as revealed by frequent evidence of microvascularity and necrosis.[33]

The current standard of care for GB consists of surgical resection, followed by radiotherapy combined with chemotherapy and, then, by an adjuvant course of chemotherapy. However, despite this intensive therapy, the prognosis remains extremely poor. Indeed, following the first-line treatment, nearly all the patients with GB experience recurrence and the available salvage therapies have not been proven to improve survival.

New therapeutic targets for GB, including receptors for growth factors and other tyrosine kinases involved in intracellular signal transduction processes, are actively studied.[34,35]

Among these, SFK members have been proposed as key kinases able to drive GB carcinogenesis and progression.[36] Initial studies have found elevated Src activity in GB compared with normal brain samples, and have revealed its oncogenic properties for brain tumors.[37] Src is a key downstream intermediate of growth factor receptors frequently overexpressed in brain tumors, including epidermal growth factor receptor (EGFR) and platelet-derived growth factor receptor (PDGFR), involved, in association with focal adhesion kinase (Fak), in cytoskeletal-linked cell survival and migration.[38,39] In preclinical models of GB, genetic and pharmacologic blockade of Src resulted effective in inhibiting cell proliferation and invasion.[40–42]

2.2.2 Src and neuroblastoma

Neuroblastoma (NB) is a rare cancer of the sympathetic nervous system. It is the most common extracranial solid tumor in childhood and the most frequently diagnosed neoplasm during infancy.[43] The prognosis of NB patients over 1 year of age tends to be poor, whereas that of patients under 1 year of age is usually more favourable, with tumors having a potential to differentiate or to regress spontaneously.[44] The disease is characterized by a broad spectrum of clinical behaviour. Although during the past few decades a substantial improvement in the treatment of certain, well-defined, subsets of patients has been observed, the outcome of the disease for children with a high-risk clinical phenotype has improved modestly, with a long-term survival less than 40%. The therapeutic options for the clinical managing of NB consist of a multimodality approach, which includes surgery, chemotherapy, radiotherapy, differentiation therapy, immunotherapy and in selected cases "careful observation only".[45] The current chemotherapeutic treatment for high-risk neuroblastoma uses dose-intensive cycles of cisplatin and etoposide, alternating with vincristine, doxorubicin, and cyclophosphamide.[43] Furthermore, isotretinoin is used during the first remission. Despite the intensive multimodal

therapy, the outcome of patients with advanced stage NB remains poor, and development of a novel therapeutic approach is warranted for these patients.

It has been reported that c-Src also plays a key role in the differentiation, adhesion, and survival of NB cells, due to its hyperactivation rather than overexpression.[46] c-Src was also hypothesized to have an oncogenic role in the progression of aggressive NB forms.[47] Addressing this kinase with small molecule inhibitors and thereby inhibiting its catalytic activity has recently been reported as a potential approach to the treatment of NB.[48,49]

2.2.3 Src and medulloblastoma

Medulloblastoma (MB) is the most common malignant brain tumor in children and accounts for 15-20% of pediatric brain tumors with an overall cure rate that ranges from 40% to 90% depending on the molecular subtype.[50] The current treatment for MB consists of surgery followed by craniospinal irradiation and chemotherapy. Because irradiating the CNS can be damaging to the developing brain, radiation therapy is usually avoided in children under the age of three, but this can compromise disease control and survival.[51] The combination of radiotherapy and chemotherapeutic agents, including ifosfamide, cisplatin, and etoposide, improved the survival rate and also reduced the risk of radiotherapy-related cognitive and endocrine effects.[52,53]

Despite the improvements in the overall survival rate following the multimodality treatment, a small but significant number of patients has a recurrent or progressive disease. Several attempts to further reduce the morbidity and mortality associated with medulloblastoma have been limited by the toxicity of conventional treatments and the low permeability of the blood-brain barrier (BBB), which hinders the entry of hydrophilic or large lipophilic compounds into the brain.[50,54] Therefore, it is important to develop innovative therapeutic agents that could cross the BBB more easily, in order to achieve a higher control of the disease and less neurocognitive toxic effects. Over the past decade, several discoveries have increased our understanding of medulloblastoma formation, identifying a crucial role for different proteins, including various RTKs and telomerase. Sikkema *et al*.[55] identified a panel of tyrosine kinase associated with pediatric brain tumors such as medulloblastoma, astrocytoma, and ependymoma. In particular, the researchers showed high Src family kinase activity in these tumors, as established by high levels of phosphorylation, in comparison with normal tissues. This observation suggests that Src could have a key role in the development of medulloblastoma. It has been reported that

some pyrazolo[3,4-*d*]pyrimidines reduced the growth rate of medulloblastoma cells by inhibiting Src in a mouse model.[56]

2.2.4 Src and colon cancer

Colon cancer is one of the leading tumours in the world with lung, prostate and breast cancer.[57] Early stages of colon cancer are amenable to surgery. However, at diagnosis, colon cancer has often metastasized and requires chemotherapy. Chemotherapy is not very effective in these cases, with survival rates < 10% in the presence of metastasis. Therefore, very important advances have occurred in the field of treatments of this common disease: adjuvant chemotherapy was demonstrated to be effective, chiefly in stage III patients, and surgery was optimized in order to achieve the best results with a low morbidity.[58]

An increased Src activity is related to colon cancer in 80% of patients, which indicates its importance in the disease.[59,60] Gradual increases in Src activity have been observed during premalignant ulcerative colitis, polyps formation, invasive tumors and in metastatic lesions.[61] An activating mutation of *Src* gene is found in 12% of patients. This mutation accounts for only a small proportion of Src activation in colon cancer.[30] Furthermore, several other studies have not detected a Src mutation in colon cancer.[62] Analysis of different aspects of Src regulation have been performed, such as the contribution of Csk and Chk, the two negative regulators of the C-terminal portion of Src. Sirvent *et al*. reported that SFK-driven colon cancer cell invasion is induced by the delocalization of Csk in the membrane, defining a novel mechanism for SFK oncogenic activation in human colorectal cancer cells.[63] The overexpression of Src in colon cancer cells increases cell adhesion, invasion, and migration but not cell proliferation, which indicates the role of Src in the progression of colon cancer.[64] Therefore, the inhibition of Src may facilitate the treatment of colon cancer to increase the survival rate.[65]

2.2.5 Src and breast cancer

Breast cancer is the most frequently diagnosed life-threatening cancer in women and the leading cause of cancer death among women. Although several Src family members have been reported to be expressed in either breast cancer cells or tissues, Src has been the most widely studied enzyme to date, and considerable data support its role in the progression of this disease.[66,67] Src plays a critical role in several key pathways that overall contribute to the growth of breast cancer. For example, through association with receptor tyrosine kinases, particularly those of

the EGFR family, Src acts in the regulation of cellular proliferation. Different members of the EGFR receptor family are overexpressed in as many as 60% of breast cancers,[68] often with concomitant Src overexpression.[69,70] Indeed, Src and EGFR have been shown to synergise, enhancing the neoplastic growth of mammary epithelial cells.[71]

Consequently, inhibition of Src activity can prevent EGFR mediated proliferation.[72,73] Src is also involved in heregulin-mediated growth and survival of breast cancer cells through Her2-dependent and independent mechanisms.[74] In addition, some reports have demonstrated a role for Src in mediating Her2–Her3 heterodimerisation, followed by an increase of their signalling capacity and biological function.[75] Moreover, Src may be indirectly involved in the stimulation of c-Met receptor signalling in breast cancer through the inappropriate activation of transcription of its ligand, the hepatocyte growth factor (HGF).[76] These data provide further evidence of a role for Src as a contributor to the development of a severe breast cancer phenotype through modulation of the activity of receptors associated with a poor prognosis.[77,78] Moreover, breast cancer cell lines expressing higher levels of Her1 and Src have also higher levels of phosphorylated Shc, increased activation of MAPK, and increased tumorigenicity compared with those that do not show overexpression of EGFR and Src.[79]

Breast tumors with elevated Src activity frequently express the progesterone receptor, indicating the possibility that SFKs may contribute to hormone dependent cell growth signalling.[80] Furthermore, some studies have demonstrated that Src could be activated in this type of cancer by a tyrosine phosphatase-dependent dephosphorylation of the regulatory tyrosine, involving the PTP1B.[81] Recently, a clinical study has been developed to investigate the effect of dasatinib (a Src inhibitor) with the anti-Her2 antibody trastuzumab and paclitaxel as first line therapy for patients with Her2-overexpressing advanced breast cancer.[82]

2.2.6 Src and pancreatic cancer

Pancreatic cancer is one of the deadliest of all of the solid malignancies. An overexpression and hyperactivation of Src are present in pancreatic carcinoma cell lines compared to normal pancreatic cells.[83] Several preclinical data showed that inhibition of Src should be a potentially effective therapeutic target in metastatic pancreatic cancer.[84,85] Moreover, it has been demonstrated that c-Src is subjected to tyrosine nitration in pancreatic carcinoma cells, indicating that this nitration may contribute to c-Src activation.[86]

It may be more therapeutically effective and scientifically rational to consider Src inhibition in

combination with cytotoxic therapies, based on the following caveats. First of all, constitutively active Src is associated with increased chemoresistance in pancreatic cancer cells;[87,88,89] secondly, inhibition of Src reduces tumor expression of thymidylate synthase, the target enzyme of 5-fluorouracil; thus, lowering thymidylate synthase levels is associated with subsequent 5-fluorouracil chemoresistance reversal, resulting in substantially decreased *in vivo* tumor growth and inhibition of progressive distant metastases.[90] Finally, Dasatinib (a Src inhibitor) can inhibit oxaliplatin-induced Src activation, and, consequently, Src inhibition can also increase oxaliplatin activity both *in vitro* and *in vivo*.[91]

Therefore, all these studies demonstrate that Src inhibition represents a potentially good strategy for the treatment of pancreatic cancer.[92]

2.2.7 Src and angiogenesis

Angiogenesis is the growth of blood vessels from the existing vasculature, is regulated by both activator and inhibitor molecules. Different studies have demonstrated the implication and the importance of Src in angiogenesis.[93] v-Src, the viral form of Src, induces vascular endothelial growth factor (VEGF) expression. VEGF is a signal protein produced by cells that stimulates vasculogenesis and angiogenesis, and it is part of the system that restores the oxygen supply to tissues when blood circulation is inadequate.[94]

The induction of VEGF occurs through activation of STAT374 and c-Src is required for hypoxia-induced VEGF production in a number of cell types.[95] Actually, SFKs are activated in response to stimulation by different growth factors such as VEGF and FGF, which are angiogenic molecules. It was also demonstrated that tumor necrosis factor (TNF)-related activation-induced cytokine (TRANCE), an angiogenic stimulating molecule, acts through activation of Src and of phospholipase C in human endothelial cells, confirming the importance of Src in angiogenesis.[96]

CHAPTER 3. Fyn kinase

Fyn is another non-receptor or cytoplasmatic TK belonging to the SFKs. It has been identified and characterized by Kipta *et al*. in 1988 both in normal and polyoma virus transformed cells.[97] It is primarily localized to the cytoplasmatic side of the plasma membrane, where it phosphorylates tyrosine residues of enzymes involved in different signalling pathways and works downstream of several cell-surface receptors. A number of biological functions in which Fyn activity is involved have been reported and includes regulation of cell growth and survival, cell adhesion, integrin-mediated signalling, cytoskeletal remodeling, cell motility, immune response and axon guidance.[98] Active Fyn plays different roles in growth factor and cytokine receptor signalling, ion channel functions, platelet activation, T-cell and B-cell receptor signalling, axon guidance, fertilization, entry into mitosis, differentiation of natural killer cells, oligodendrocytes and keratinocytes.[99] Fyn is primarily involved in several transduction pathways in the CNS where it is involved in myelination and morphological differentiation associated with the formation of neurite in oligodendrocytes, oligodendrocyte differentiation, synapse formation and regulation.[100]

Recent evidences suggest that Fyn hyperactivation/deregulation might contribute to Alzheimer's disease (AD)[101] and other tauopathies pathogenesis.[102] It is also involved in the peripheral immune system, playing in this latter important roles in regulation and functions of T-cell development and activation.[103]

Fyn is also known to mediate integrin adhesion and cell-cell interactions. For all these reasons, it is also involved in the onset of cancer.[104,105]

3.1 Fyn structure and regulation

Fyn is a 59-kDa protein comprising 537 amino acids, encoded by the *Fyn* gene that is located on chromosome 6q21. There are three isoforms of Fyn: isoform 1, or FynB, which is mainly expressed in the brain, isoform 2 or FynT, first identified, which tends to be expressed in T-cells and differs from isoform 1 in the linker region between the SH2 and the SH1 domain,[106] and finally, isoform 3, also called FynDelta7, which has been found in peripheral blood mononuclear cells and differs from isoform type 1 as it misses the sequence 233-287.[107] Even if most tissues express a mixture of the first two isoforms, FynB is highly expressed in the brain

and FynT is highly expressed in T-cell. Fyn, similarly to the other SFK members, is composed of several functional parts connected together in a single protein chain. These functional portions include the unique domain, the SH3 and the SH2 domains, and the SH1 (or catalytic) domain (**Fig. 10**).[108]

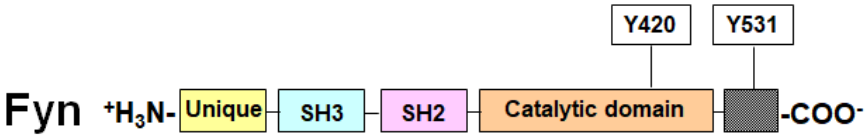

Fig. 10. Schematic representation of Fyn structure.

Fyn is characterized by a common regulatory mechanism with the other SFKs. Indeed, the activation or inhibition of kinase activity depends on intramolecular interactions between SH2 and SH3 with the kinase domain and on phosphorylation/dephosphorylation of two critical tyrosine residues. The first tyrosine is situated in the A-loop (Tyr420) and the second (Tyr531) in the C-terminal region. Fyn is able to interact with almost 300 different proteins and, through these interactions, participates in many cellular pathways, both in physiological and pathological situations.[109–111]

3.2 Fyn functions in CNS

Fyn is deeply implicated both in brain development and in adult brain physiology. Biological functions of Fyn in the brain have been extensively investigated using transgenic animal models.[112,113] These studies indicated that Fyn is a key element required for the development and functions of CNS (**Fig. 11**).[104] Fyn is involved in many processes critical for the development of the brain; it regulates neuronal migration during corticogenesis, oligodendrocyte maturation, myelin production, long-term potentiation, and excitatory and inhibitory neuronal receptors.[114] Indeed, its activity in the brain is highest during the myelination.[105] Sperber *et al*. demonstrated a severe myelin deficit in forebrain at all ages (from 14 days to 1 year) in Fyn (-/-) null mutant mice, which do not express Fyn. This study, based on the count of oligodendrocytes and of myelinated fibres and on the use of an inactivated form of Fyn (bearing a single amino acid substitution), showed that Fyn plays a unique role in

myelination.[115]

Recently, Miyamoto *et al*. demonstrated the relation between myelination and protein markers and myelin ultrastructure utilizing transgenic mice, which express active Fyn under the control of a glial fibrillary acidic protein promoter. This promoter induces protein expression in the initiation stage of myelination in the peripheral nervous system (PNS).[105]

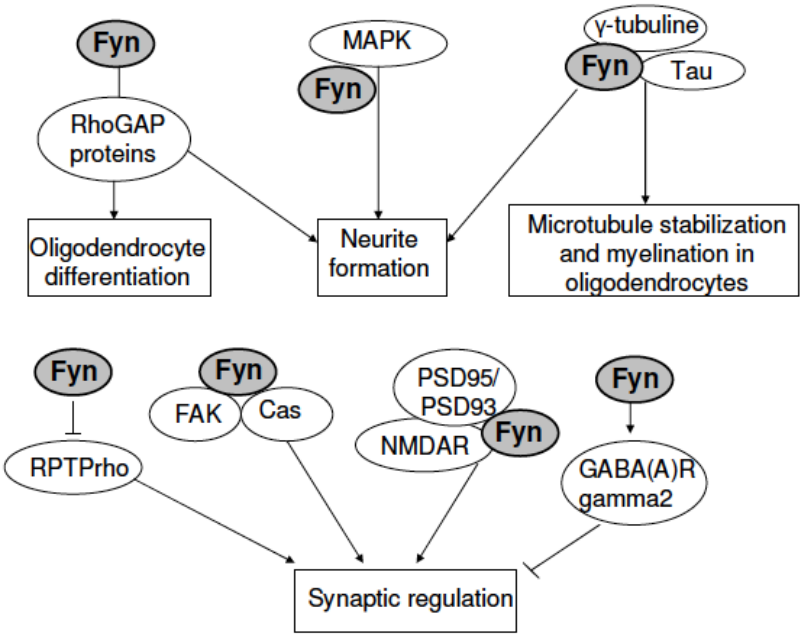

Fig. 11. Fyn functions in CNS.[104]

Moreover, Fyn is involved in the morphological differentiation that leads to neurite formation in oligodendrocytes. Indeed, Fyn interacts with γ-tubulin, a member of the tubulin family, which plays a central role in neurite construction. In more detail, membrane associated γ-tubulin forms complex with Fyn, participating in the signalling cascade that leads to membrane-associated microtubule nucleation. This has been demonstrated by the fact that pretreatment of P19 embryonal carcinoma cells with SFK inhibitors blocked the nucleation activity of the γ-tubulin complexes.[116]

This process is promoted by Fyn interaction with the cytoskeletal proteins Tau that, binding with tubulin, stabilizes the microtubules in the brain. Other evidences demonstrated that Tau-Fyn interactions could play a pathogenic role in some human CNS neurodegenerative diseases where axonal degeneration is the key factor in clinical decline.[117,118]

Fyn and other SFK members play important roles in synaptic transmission and plasticity at excitatory synapses; indeed, these enzymes are localized to the postsynaptic density (PSD), the primary cytoskeleton specialization at neuronal excitatory synapses, constituted by many proteins, including PSD95 (postsynaptic density protein 95), NMDAR (N-methyl-D-aspartate receptor) and AMPAR (α-amino-3-hydroxy-5-methyl-4-isoxazolepropionic acid receptor).[119] Particularly, NMDAR forms a multiprotein complex in which PSD95 plays a critical role, directly binding to the NMDA Receptor 2 (NR2) subunit of NMDAR. PSD95 also interacts with the SH2 domain of Fyn and has been proposed to promote Fyn-mediated tyrosine phosphorylation of NMDAR subunit NR2A.[120,121] In this way, Fyn (and also Src) regulates the NMDAR complex phosphorylation and upregulates NMDAR functions, leading to the production of NMDAR-dependent synaptic potentiation.[122] Phosphorylation by Fyn of the NMDAR subunit NR2A and Fyn involvement in the interactions between NR2A and PSD95 have been observed after brain ischemia/reperfusion; moreover, increased tyrosine phosphorylation of NR2A and increased interaction involving NR2A, PSD95, Src and Fyn have been detected in ischemic episodes.[123] Fyn phosphorylates also PSD93, another protein tightly associated to the NMDAR complex. In more details, PSD93 serves as a membrane-anchored substrate of Fyn and plays a role in the regulation of Fyn mediated modification of NMDAR functions. This connection could explain the involvement of Fyn in brain diseases.[124]

Jurd *et al*. demonstrated that Fyn phosphorylates the GABA(A)R (gamma aminobutyric acid A receptor) gamma2 subunit on Tyr365/7. This phosphorylation is an important mechanism for modulating inhibitory synaptic function in the mammalian brain. Tyrosine phosphorylation of the gamma2 subunit is significantly reduced in the hippocampus of Fyn knockout mice, suggesting that Fyn substantially contributes to the phosphorylation of this subunit *in vivo*; however Tyr367 phosphorylation is not completely abolished in these mice, suggesting that other SFKs, such as Src, also contribute to maintaining and regulating the endogenous phosphorylation level.[125]

Fyn is also involved in the modulation of other CNS signalling proteins: it collaborates with Cellular apoptosis susceptibility (Cas) and with other kinases of the Fak family in regulating the morphology of dendritic spines, the specialized microscopic protrusion on dendrites that are the primary sites, where the postsynaptic components of excitatory synapses are located in the mammalian CNS.[126]

Fyn plays also a role in the signalling pathway starting from reelin, a large glycoprotein

involved in cortical formation and in postnatal brain functions, such as dendrite development. Isosaka *et al*. demonstrated that the levels of several phosphoproteins, and in particular NR2A and NR2B subunits of NMDAR, are regulated by reelin level in a Fyn-dependent manner in the mouse brain.[127]

Fyn activation is required for a signalling cascade which involves MAPK and lipid rafts, starting from the transmembrane form of the extracellular matrix heparin sulphate proteoglycan agrin (TM-agrin) that is primarily expressed in the CNS on axons and dendrites during the phase of active neurite extension.[128]

Yuasa *et al*. demonstrated that Fyn plays an important role in memory formation in contextual fear conditioning.[129] Accordingly, the same authors, using the SFK inhibitor PP2 showed that downregulation of hippocampal Fyn activity facilitates the extinction of contextual fear memory. Probably Fyn inhibition causes a downregulation of CDK5 (activated by Fyn-phosphorylation on Tyr15) that facilitates extinction of contextual fear. Both Fyn and CDK5 in hippocampus are probably involved in fear extinction by crosstalk for synaptic remodelling through cytoskeletal rearrangement.[130]

It has been reported that recombinant Fyn directly binds to metabotropic Glutamate Receptor 1a (mGluR1a) at a consensus binding motif located in the intracellular C-terminus of mGluR1a *in vitro*. Similarly, endogenous Fyn interacts with mGluR1a in adult rat cerebellar neurons *in vivo*. Active Fyn phosphorylates mGluR1a at a conserved tyrosine residue in the C.terminus region. In cerebellar neurons and transfected HEK293T cells, the Fyn-mediated tyrosine phosphorylation of mGluR1a is constitutively active and acts to facilitate the surface expression of mGluR1a and to potentiate the mGluR1a postreceptor signalling. These results support mGluR1a to be a novel substrate of Fyn.[131]

3.3 Fyn and Alzheimer's disease

AD is the most common causes of dementia and one of the great health-care challenges of the 21st century.[132] It is characterized by a gradual loss of neurons, particularly in the cortex and hippocampus and, as a consequence, by progressive impairments of memory, judgment, decision making, orientation to physical surroundings, and language. Pathologically, AD is characterized by the presence of extracellular neuritic plaques containing the β-amyloid peptide (Aβ) and neurofibrillary tangles (NFTs) composed of hyperphosphorylated Tau protein in the brain.[133] In 1906, Alois Alzheimer reported the case of a woman who presented a "peculiar"

dementia at the age of 51 years. Alzheimer correlated the woman's cognitive and behavioral features with histopathological findings of extracellular "miliary foci" (senile plaques) and fibrils inside the neurons (neurofibrillary tangles) in her cerebral cortex.[134]

AD is classified into two subtypes according to the age of onset. About 1-5% of AD cases present an early-onset (before the age of 65, typically in the late 40s or early 50s) and are classified as having early-onset Alzheimer disease (EOAD), whereas more than 95% of patients develop the disease after the age of 65 years and are classified as having late-onset Alzheimer disease (LOAD).[135]

In 1984, Glenner first proposed that cerebral Aβ drives all the subsequent pathologies, and this central thesis was later reinterpreted and reported as the amyloid cascade hypothesis of AD, which affirms that the accumulation of Aβ is the primary driver of AD-related pathogenesis, including neurofibrillary tangle formation, synapse loss, and neuronal cell death.[136–138] Although the amyloid cascade is only one possible mechanism proposed, the pathophysiology of AD is attributed to a number of factors such as the cholinergic dysfunction,[139] amyloid/tau toxicity[140] and oxidative stress/mitochondrial dysfunction.[141]

As previously reported, Fyn hyperactivation/deregulation is involved in different tauopathies, characterized by alteration of the Tau protein, abnormally phosphorylated on serine and threonine residues.[142] Subsequent studies indicated that Tau is phosphorylated also on tyrosine. Lee *et al*. demonstrated that Fyn phosphorylates Tau at its amino terminus on Tyr18 and that tyrosine phosphorylated Tau is present in the neurofibrillary tangles in AD brain, giving further insights in the involvement of Fyn in tauopathies.[143] Recently, Lau *et al*. demonstrated that Fyn also co-localises with Tau in a proportion of neurons containing Tau tangles in AD. Hence, Tau-Fyn interactions could play a pathogenic role in AD. They report the identification of critical proline residues, Pro213, Pro216, and Pro219, located within the fifth and sixth Pro-X-X-Pro motifs in the proline-rich region of Tau, that are important for its binding to Fyn. These residues in Tau are flanked by numerous phosphorylation sites. In this study, the identification of the binding site between tau and Fyn may facilitate the development of compounds that can inhibit tau-fyn interactions, as a potential alternative therapeutic strategy for AD.[118]

Moreover, using transgenic mice expressing both human AAP (amyloid precursor protein) and Fyn, it has been demonstrated that Fyn induces synaptic and cognitive impairments in a transgenic mouse model of AD. Indeed, increased Fyn expression is sufficient to trigger prominent neuronal deficits in the context of even relatively moderate Aβ levels, and for this

reason inhibition of Fyn activity may help to counteract Aβ-induced impairments. These and other data support that Fyn takes part in the synaptotoxicity and neurotoxicity mediated by Aβ.[112]

Ho *et al*. demonstrated that Fyn levels were decreased in the synapses and increased in the neuronal cell bodies where localized together with neurofibrillary tangles from autopsy cases, suggesting that alterations in Fyn localization might be associated with neurofibrillary pathology and synapse loss in AD.[144]

Williamson *et al*. examined the response of primary human and rat brain cortical cultures to Aβ administration and they found a marked increase in the tyrosine phosphorylation content of several neuronal proteins, including Tau and Fak; furthermore, immunoprecipitation of Fyn from Aβ-treated neurons showed an increased association of Fyn with Fak. The increased tyrosine phosphorylation was blocked by addition of the SFK inhibitor PP2. The rapid changes in Fak/Fyn and Tau tyrosine phosphorylation may be critical in the early pathogenic events initiated by Aβ. Early cognitive deficit characteristic of early AD seems to be produced by a soluble form of Aβ, Aβ25-35, produced in AD patients by enzymatic cleavage of Aβ1-40.[145]

Hence, Peña *et al*. demonstrated the involvement of Fyn in the Aβ25-35-induced disruption of hippocampal network activity *in vitro*. Interestingly, they found that such phenomenon is not observed in slices obtained from Fyn-knockout mice, suggesting that Aβ25-35 affects hippocampal function through a Fyn-dependent mechanism.[146]

Further connections among Fyn-Tau-Aβ, called the toxic triad, have been proposed by Haass *et al*. Briefly, the toxicity of the triad is at least in part due to Tau and Fyn localization in the different compartments of the neuron (soma, axon, dendrites). Indeed, in normal conditions Tau protein is primarily located in neuron axons, but also interacts with Fyn targeting it into neuron dendrites. As reported before, Fyn phosphorylates NMDAR, resulting in the stabilization of this receptor's interaction with PSD95. This stabilization, in turn, strengthens signalling by the excitotoxic neurotransmitter glutamate, which enhances Aβ toxicity. During AD pathogenesis enhanced redistribution of abnormally hyperphosphorylated Tau from axon to the soma and to the dendrites may increase Tau-dependent sorting of Fyn to the dendrites, leading to abnormal NMDA signalling and increasing the toxic effects of Aβ on neurons.[147] This hypothesis takes shape from the work of Ittner *et al*., which suggested how Tau may mediate Aβ toxicity. Indeed, they first generated transgenic mice that overexpressed a variant of Tau (Δtau) lacking the C-terminus and thus binding to Fyn but not to microtubules. This Tau modification caused

sequestration of Fyn in the soma.

Similarly, loss of Tau also prevented postsynaptic targeting of Fyn. The reduced Fyn localization to dendrites decreases NMDAR signalling and consequently Aβ toxicity. The study also suggests that the targeting of Fyn to dendrites depends on normal Tau, even if all the factors involved in this Tau function are not yet completely identified. Very interestingly, this Fyn-Tau connection in dendritic spines could be exploited to develop new therapeutic strategies for treating AD. Indeed, when phosphorylation of NMDAR by Fyn is blocked by a synthetic peptide previously constructed, neurons are protected from excitotoxic damage.

Consistently, when Ittner *et al*. treated their transgenic AD mice with this peptide,[148] memory deficits were ameliorated and there was improved survival, similar to that observed when Fyn was sequestered by Δtau. Probably also other agents that inhibit Fyn activity could be offer a therapeutic opportunity to treat AD.[148]

Recent evidence indicates that Tau phosphorylation at specific residues, and not only its presence or absence, can modulate the interaction among Fyn, PSD95, Tau and the NMDAR. Phosphorylation at T205 on Tau through activation of the p38 MAPK prevents the association of the Fyn-PSD95-Tau-NMDAR complex, and ameliorates Aβ toxicity both in cellular and mouse models of AD. The presumed effect of T205 phosphorylation is the functional inhibition of Fyn-mediated signalling critical to Aβ toxicity *in vitro* and *in vivo*.[149]

Cellular Prion Protein (PrPC) is one of the highest affinity Aβ receptors identified, with an estimated K_d of 0.4 nM, exclusively engaging oligomeric Aβ.[150] PrPC-interacting Aβ emerges at the time of cognitive impairment in several AD mouse lines, supporting a role for this specific Aβ assembly in the pathophysiology of AD in preclinical models.[151] Critically, PrPC interacting Aβ has been consistently found in human AD brain homogenates, strongly suggesting that the signalling cascade characterized in preclinical models of AD may also be present in human disease.[152–154]

3.4 Fyn and Parkinson's disease

Parkinson's disease (PD) is another complex neurological disorder. It is the second most common age-related neurodegenerative disease with movement disorders and is clinically characterized by parkinsonism and widespread Lewy body pathology in CNS, PNS, and autonomic nervous system (ANS). PD affects about 1% of people over 65 years and approximately 4% of the population aged over 80. Almost 6 million people worldwide are

suffering from PD, with millions of cases in the United States alone suffering from PD.[155] The first detailed description of PD was made almost two centuries ago, but the knowledge of the disease continues to evolve.

The crucial pathological feature of PD is the loss of dopaminergic neurons within the Substantia Nigra pars compacta (SNpc). Results of clinical-pathological correlation studies showed that moderate to severe dopaminergic neuronal loss within this area is probably the cause of motor features, bradykinesia and rigidity, in advanced PD. Findings from pathology confirm that moderate loss of nigral neurons is also present in early stages of the disease but also provide evidence for a population of potentially salvageable dopaminergic neurons.[156]

Another hallmark of PD is Lewy pathology. Aggregation of abnormally folded proteins has emerged as a common theme in neurodegenerative diseases, including PD. Each neurodegenerative disease is categorised according to the protein that is most abundant in the associated protein inclusions. In PD, this protein was identified as α-synuclein, following the discovery that mutations in its gene, SNCA, cause a monogenic form of the disease. In a misfolded state, α-synuclein becomes insoluble and aggregates to form intracellular inclusions within the cell body (Lewy bodies) and processes (Lewy neurites) of neurons.[157]

Two different research groups simultaneously reported that Fyn phosphorylates α-synuclein, a presynaptic protein of unknown function that has been implicated in the pathogenesis of several neurodegenerative diseases, including PD. Consistently, phosphorylation by Fyn on α-synuclein Tyr125 was inhibited by the SFK inhibitor PP2.[158,159]

Using Fyn knockout mice, it has been demonstrated that the dopamine dependent trafficking of striatal NMDAR requires Fyn and consequently strategies that prevent NMDAR redistribution through inhibition of Fyn could offer a new strategy in the treatment of PD.[160,104]

Panicker *et al* examined the role of Fyn in microglial activation and neuroinflammatory mechanisms in cell culture and animal models of PD. On the basis of experimental evidence from cell culture, primary culture, and *in vivo* models using both Fyn and PKC knock-out mice they demonstrate that Fyn activation plays an upstream regulatory role in eliciting proinflammatory signalling following both acute and chronic states of microglia stimulation. Their mechanistic studies revealed that Fyn serves as a major upstream regulator of proinflammatory signalling involving PKC, MAPK, and the Nuclear factor κB (NFκB, a transcription factor that plays an important role in carcinogenesis as well as in the regulation of inflammatory response NFκB pathways). Thus, Fyn could be exploited as a potential signalling

node in the development of novel antineuroinflammatory drug candidates for treating PD and other related neurodegenerative diseases with associated microglia-mediated proinflammatory processes.[161]

Dopamine replacement therapy with levodopa (L-DOPA) is the treatment of choice for PD; however, its long-term use is frequently associated with L-DOPA-induced dyskinesia (LID).

Recently, Sanz-Blasco *et al*. found that mice lacking Fyn displayed reduced LID, ΔFosB accumulation and NR2B phosphorylation compared to wild-type (wt) control mice. Pre-administration of saracatinib, an inhibitor of Fyn activity, also significantly reduced LID in dyskinetic wt mice. These results support that Fyn has a critical role in the molecular pathways affected during the development of LID and identify Fyn as a novel potential therapeutic target for the management of dyskinesia in PD.[162]

3.5 Fyn and cancer

Fyn is implicated (as other SFK members) in several physiological processes, including not only cellular growth and proliferation, but also morphogenesis and cellular motility, whose aberration may cause cancer development. Its role as a potential oncogene has been investigated since 1988, when Kawakami *et al*. demonstrated that Fyn overexpression induces morphologic transformation and anchorage-independent growth in NIH 3T3 cells. In addition, even if a relatively low frequency, Fyn acquired properties of a dominant-acting oncogene capable of inducing the fully tumorigenic phenotype.[163]

Fyn is involved in several signalling pathways hyperactivated in cancer **(Fig. 12)**. Together with other SFK members it is a mediator of growth-factor induced antiapoptotic activity of Akt/PKB (protein kinase B); indeed its overexpression results in promotion of antiapoptotic activity of Akt and in the regulation of Rac and Rho GTPases and of ERKs (extracellular signal–regulated kinases)/MAPKs, that are enzymatic pathways hyperactivated in cancer, as deeply reported by Posadas *et al*.[99]

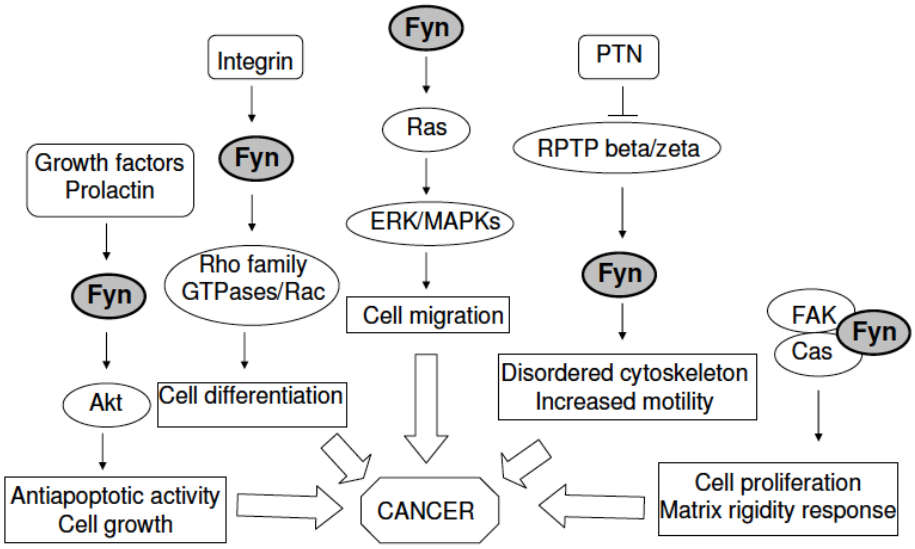

Fig. 12. Fyn involvement in cancer.[104]

Fyn is also involved in proliferation processes of different cell lines: as an example expression of inactive Fyn inhibited the PDGF-induced fibroblast proliferation.[164] Moreover, lymphocytes from Fyn-deficient mice were blocked in cytokinesis, the process in which the cytoplasm of a single eukaryotic cell is divided to form two daughter cells.[165] Fyn is involved in matrix rigidity, which is important in cell motility and spreading, matrix remodelling and anchorage independency. All these processes, if altered, can lead to cancer development and metastasis formation. Indeed, an increased matrix rigidity (the cell behaviour in response to the mechanical properties of the environment) leads to tissue disorganization and malignant transformation.[166] Cas proteins form complexes with SFKs, including Fyn, that are implicated in the regulation of cytoskeleton organization and cell proliferation. In pathological conditions, Cas complexes deregulation has been supposed to play a role in oncogenic transformation and perhaps metastasis formation.[167][168] In more details, soon after cell attachment, Fak is activated and binds directly to Cas. Fak then phosphorylates Cas, creating a high affinity site for binding by the SH2 domain of SFKs (including Src, Lyn, Fyn).

Kostic *et al*. demonstrated that the matrix rigidity response through increased spreading and growth correlates with the recruitment of Fyn, but not of c-Src. Moreover, the authors confirmed that Cas, downstream substrate of Fyn, is also required for a rigidity response and is phosphorylated in a Fyn-dependent process. Furthermore, increased Cas phosphorylation by Fyn well correlates with anchorage independency of NB-39-nu neuroblastoma cell lines.

Consistently, treatment of NB-39-nu cells with PP2 suppresses Cas phosphorylation, suggesting that the anchorage-independent process is associated with the activity of SFKs, in particular of Fyn.[169]

3.5.1 Fyn and breast cancer

Breast cancer cell lines (MDA-MB-231, T47D and SK-Br3) express elevated levels of different oncogenes, including Fyn, which may promote metastasis formation through the facilitation of epithelial to mesenchymal transition (EMT), a cell transformation program characterized by loss of cell adhesion, repression of E-cadherin expression, and increased cell mobility. A study reported that 48% of breast tumor specimens analyzed contained elevated expression/activity of SFKs, including Fyn and Yes, relative to normal tissue. Moreover, Fyn expression in breast cancer cells from patients is associated with poor survival and neoangiogenesis, correlated with c-Met and Fak kinases upregulation.[170]

Elias *et al*. demonstrated that Fyn is upregulated in tamoxifen-resistant breast cancer cell lines and plays a key role in the resistance mechanism. Further, the cellular localization of Fyn within cancer cells of primary ER+ breast tumor tissue may serve as a prognostic marker.[171]

Very recently it has been shown that the inhibition of protein phosphatase N23 promotes breast cancer development via activation of Fyn.[172]

3.5.2 Fyn and ovarian cancer

Lysophosphatidic acid (LPA), known as the "ovarian cancer activating factor" is present at high concentrations in the plasma and ascites of ovarian cancer patients; it causes junction dispersal in ovarian cancer SKOV3 cells by inducing morphological changes, including membrane ruffling, lamellipodia formation, cell-cell dissociation and single cell migration, events that could lead to the first steps of metastasis formation.

Huang *et al*. demonstrated that LPA acts by activating Fyn (but not c-Src) and increasing its association with p120-catenin at the cell-cell junctions.[173]

Yang *et al*., very recently, documented that the activation of Fyn can cause dissociation of cell-cell junctions and adhesion, resulting in paracellular hypermeability. They detected high expression levels of Fyn in vessel endothelial cells, and suggested a possible mechanism (involving Fyn activity) by which the ovarian tumor cells cross the endothelial barrier and transform to an invasive phenotype.[174]

3.5.3 Fyn and prostate cancer

Posadas *et al*. demonstrated that Fyn is upregulated in prostate cancer and is functionally distinct from other SFKs, since it interacts with Fak and paxillin (PXN) that are regulators of cell morphology and motility. Data showed a greater Fyn expression in prostate cancer than in normal tissue, specific for Fyn and not present for other SFKs. Expression of Fyn in prostate cancer cell lines (LNCaP, 22Rv1, PC3, DuPro) was detected using quantitative real-time PCR (qRT-PCR) and immunoblotting. Comparing normal with cancer samples, it has been detected a 2.1-fold increase of Fyn level, a 1.7-fold increase in Fak and a doubling in PXN. These studies support the hypothesis that Fyn and its related signalling partners are upregulated in prostate cancer, and warrant further investigation into the role of Fyn as a therapeutic target.[175] In 2015, the same research group demonstrated that Fyn is strongly up-regulated in human neuroendocrine prostate cancer (NEPC) tissues and xenografts, as well as cells derived from a NEPC transgenic mouse model. These data indicated that the neuroendocrine differentiation that occurs in prostate cancer cells is, at least in part, regulated by Fyn. The understanding of the role of Fyn in the regulation of neuroendocrine markers should provide further support for ongoing clinical trials of SFK and MET inhibitors in castration-resistant PCa patients.[176] Based on the hypothesis that the treatment with the Fyn inhibitor saracatinib would increase the time required to develop new metastatic lesions, the same group performed a clinical study on a number of prostate cancer patients. Unfortunately, this study was unable to determine if saracatinib had potential as metastasis inhibitor.[177]

3.5.4 Fyn and melanoma

Huang *et al*. reported that Fyn is selectively activated among SFKs in the K-1735 murine melanoma cell line with high metastatic potential, where significant tyrosine phosphorylation of cortactin (a cytoplasmatic protein promoting polymerization and rearrangement of the actin cytoskeleton and involved in cell migration), stable complex formation between activated Fyn and cortactin, and co-localization of cortactin with Fyn at cell membranes have been observed. The authors showed that cortactin is a specific substrate and a cooperative effector of Fyn in integrin-mediated signalling processes regulating metastatic potential.[178]

More recently, Fyn has been also identified as a melanoma biomarker which contributes to the tumor development.[179]

3.5.5 Fyn and squamous cell carcinoma

Integrin beta6 is expressed in invasive oral squamous cell carcinoma (SCC) and is correlated with oral tumor progression. Li *et al*. investigated to determine whether integrin beta6 signalling activates Fyn and thus promotes SCC progression and demonstrated that upon ligation of the integrin beta6 with fibronectin, beta6 forms a complex with Fyn and activates it. Fyn activation recruits and activates Fak to this complex that in turn stimulates the Raf-ERK/MAPK pathway. This pathway transcriptionally activates the matrix metalloproteinase-3 gene and promotes oral SCC cell proliferation and experimental metastasis *in vivo*. These findings indicate that integrin beta6 signalling activates Fyn and thus promotes oral cancer progression.[180] Successively the same group also demonstrated that the activation of Fyn, as well as local growth factor concentration, modulates EMT in oral SCC, rendering the tumor more aggressive.[181]

Recently, Lee *et al*. determined that SCC growth in 3-dimensional multicellular spheroid (MCS) approximates epithelial to mesenchymal transition. Organization of an MCS requires the full-length β6 integrin subunit and its maintenance requires MAPK. Limiting Fyn activation results in the down-regulation of E-cadherin, β-catenin and an increase in expression of N-cadherin and SNAIL. These results indicate that the microenvironment and growth patterns in an MCS are complex and require MAPK and Fyn.[182]

3.5.6 Fyn and brain tumors

Regarding brain tumors, it has been reported that *Fyn* gene, together with other genes involved in brain development and neural differentiation, was strongly enriched in astrocytoma, a common and lethal human malignancy. Moreover, Fyn and c-Src are effectors of oncogenic EGFR signalling in GB patients and enhance invasion and tumor cell survival *in vivo*. Consistently, the pan-SFK inhibitor dasatinib inhibited invasion, promoted tumor regression, and induced apoptosis *in vivo*, significantly prolonging mice survival in an orthotopic GB model. This study demonstrated a mechanism linking EGFR signalling with Fyn and Src activation to promote tumor progression and invasion and provided the rationale for combined anti-EGFR and anti-SFK targeted therapies.[183]

Very recently, Comba *et al*. confirmed that Fyn expression correlates positively with GB cell aggressiveness. The histopathological evaluation of gliomas indicates that loss of Fyn reduced malignant features such as pseudopalisades, necrosis, and hypervascularization. This study indicates an important role for Fyn in modulating many glioma cellular processes and its

relevance as a novel regulator of GB behaviour and therapy response.[184]

3.5.7 Fyn and pancreatic cancer

Chen *et al*. demonstrated that upregulation of Fyn expression is correlated with human pancreatic cancer metastasis. Indeed, the inhibition of Fyn activation by kinase-dead Fyn transfection decreased liver metastasis of PC3 pancreatic cancer cells in nude mice. Further analyses showed that Fyn activity modulated pancreatic cell metastasis through the regulation of proliferation and apoptosis.[185]

In 2014, it has been demonstrated that the suppression of the messenger RNA expressions of Yes1, Lyn, Fyn, Frk, and Src by specific small interfering RNA transfection caused the suppression of cell proliferation by 16.7% to 47.3% in PANC-1 cells. Knockdown of any of these five SFKs suppressed proliferation in other pancreatic cancer cell lines by 3.0% to 40.5%. The knockdowns significantly reduced pancreatic cancer cell migration by 24.9% to 66.7% and completely inhibited invasion. These results suggest that the knockdown of Yes1, Lyn, Fyn, Frk, or Src reduce human pancreatic cancer cell proliferation, migration, and invasion.[186]

Recently, Jiang *et al*. reported that the suppression of Fyn activity and/or overexpression of heterogeneous nuclear ribonucleoprotein E1 (hnRNP E1) decreased the metastasis of pancreatic cancer cells. The study demonstrated a novel mechanism by which Fyn/hnRNP E1 signalling regulates pancreatic cancer metastasis by affecting the alternative splicing of integrin β1.[187]

3.5.8 Fyn and mesothelioma

Menges *et al*., applying a phosphotyrosine proteomic screen, identified novel signalling molecules, including Janus kinase 1 (Jak1), STAT1, cortactin, FER, p130Cas, c-Src and Fyn, as tyrosine phosphorylated and activated in human malignant mesothelioma. They also confirmed that known signal transduction pathways previously implicated in mesothelioma, such as EGFR and Met, are co-activated in the majority of human mesothelioma specimens and tested cell lines. Since all these enzymes seem to be hyperactivated in malignant mesothelioma cell lines, dual or multitargeted inhibition of some of these kinases is likely to be more efficacious than inhibition of a single tyrosine kinase for a potential antiproliferative activity.[188]

Further studies showed that double RNA interference knockdown of Fyn and Lyn induced apoptosis accompanied by caspase-8 activation in mesothelioma cell line.[189]

3.5.9 Fyn and leukemia

Fyn involvement has also been shown in haematological malignancies, including chronic myeloid leukemia (CML), some types of acute leukemias and multiple myeloma. It has been reported that Hck, Lyn and Fyn strongly phosphorylate the SH3-SH2 region of Bcr-Abl, the constitutively active cytoplasmatic tyrosine kinase that is the etiologic agent of CML. Seven phosphorylation sites were identified, namely Tyr89 and Tyr134 in the Abl SH3 domain, Tyr147 in the SH3-SH2 connector and Tyr158, Tyr191, Tyr204 and Tyr234 in the SH2 domain. Tyr89 in the SH3 domain, the most prominent phosphorylation site *in vitro*, is strongly phosphorylated in CML cells in a SFK-dependent manner. The positions of these tyrosine residues in the crystal structure of c-Abl (the normal protein form present in healthy cells) together with the transformation defect of the corresponding Bcr-Abl mutants suggest that phosphorylation of the SH3-SH2 region by Src family kinases impacts Bcr-Abl protein conformation and signalling.[190] Small interfering RNA experiments and pharmacologic approaches identified Fyn as a candidate for resistance to imatinib, the first line drug for CML. This study provides a comprehensive picture of the transcriptional events associated with imatinib and identify Fyn as a new potential target for therapeutic intervention in CML.[191]

Using a tissue microarray, Chandra *et al*. demonstrated that Fyn expression is significantly increased in CML blast crisis (the terminal phase of the disease) compared with the chronic phase. Cells overexpressing Bcr-Abl *in vitro* and *in vivo* display an upregulation of Fyn protein and its mRNA. Moreover, knockdown of Fyn with short hairpin RNA (shRNA) slows leukemia cell growth, inhibits clonogenicity and leads to increased sensitivity to imatinib, indicating that Fyn mediates CML cell proliferation.[192] The authors also proposed a mechanism explaining the heightened levels of Fyn in CML cells: Bcr-Abl is one of the several oncoproteins that raise ROS (reactive oxygen species) concentration; ROS is in turn responsible for the upregulation of Fyn mRNA and protein levels.

The identification of these novel downstream signals is particularly important in the effort to overcome the unresolved problem of treatment of blast crisis CML and management of kinase inhibitor resistance.[193] Fyn has been proposed as a putative target for treating Bcr-Abl expressing acute lymphoblastic leukemias; in fact together *IL-15*, *Fyn* gene has hub-like properties, potentially showing the highest biologic importance among other factors involved in the proliferation of malignant leukemic blasts.[194]

Singh *et al*. discovered a role of Fyn in promoting Bcr-Abl1 mediated cell growth and sensitivity to imatinib. They demonstrate that Fyn contributes to Bcr-Abl1 induced genomic instability, a feature of blast crisis CML. Bone marrow cells and mouse embryonic fibroblasts derived from Fyn knockout mice transduced with Bcr-Abl1 display slowed growth and clonogenic potential as compared to Fyn wt Bcr-Abl1 expressing counterparts.[195]

Recently, Chougule *et al*. studied the role of Fyn in Fms-like tyrosine kinase 3 (FLT3) (a RTK) signalling in respect to acute myeloid leukemia (AML) and they reported that Fyn cooperates with the oncogenic variant FLT3-ITD (internal tandem duplication) in cellular transformation by selective activation of the STAT5 pathway. Therefore, Fyn inhibition, in combination with FLT3 inhibition, could be beneficial for AML patients.[196]

CHAPTER 4. Hck kinase

The hematopoietic cell kinase (Hck) is another non-receptor or cytoplasmic TK belonging to the SFKs.[2] Hck, together with Lyn and Fgr, is predominantly expressed in myeloid cells and represents the prevalent SFK member involved in inflammation.[197,198] It induces production of multiple cytokines and chemokines such as TNF-α, interleukin-1 (IL-1), and interleukin-6 (IL-6) in macrophages upon activation by lipopolysaccharide (LPS).[199] Hck, toghether with Fgr, is also involved in integrin-mediated cell signalling to promote macrophage migration and attachment to the sites of inflammation.[200] Since it has a role in the inflammatory response, Hck is involved in inflammatory diseases, but it also demonstrated to possess a role in other diseases, including several types of leukemia and in human immunodeficiency virus-1 (HIV-1) infection, which are caused by alterations of immune system cells. Thus Hck has been identified as a potential target for the treatment of CML[201] and HIV-1 infection.[198,202]

4.1 Hck structure and functions

Human Hck, independently discovered in 1987 by two groups, shares the same overall structure architecture of the other SFKs and includes five distinct regions: a unique N-terminal region, with sequences for lipid attachment, the regulatory SH3 and SH2 domains, a catalytic domain SH1, followed by a negative regulatory C-terminal tail.[203]

Alvarado *et al*. determined the crystal structure of a truncated Hck protein constituted by the SH2 and SH3 domains plus the linker between the SH3 and the SH2 domains. Despite the absence of the kinase domain, the structures and relative orientations of the SH2 and SH3 domains in this shorter protein are very similar to those observed in the full-length Hck. However, the SH2 kinase linker adopts a modified topology and fails to engage the SH3 domain. This structure suggests that the non-catalytic regions work together as a "conformational switch" that modulates kinase activity in a manner unique to the SH3 domain (**Fig. 13**).[204]

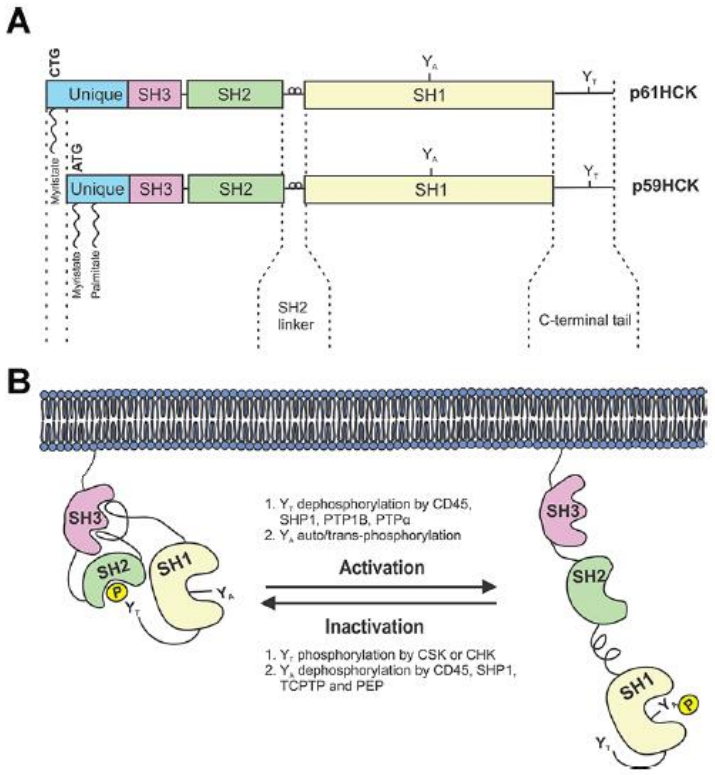

Fig. 13. Schematic representation of Hck structure and regulation[197]

In humans, Hck is expressed as two isoforms, p59Hck and p61Hck, generated simultaneously and in equal amounts by alternative translation of a single mRNA.[197] Compared to p59Hck, p61Hck presents an additional 21 amino acid peptide at the N-terminal end which is myristoylated, while the N-terminal domain of p59Hck is myristoylated or palmitoylated.[205] Thus, the two Hck isoforms only differ in a portion of their N-terminal domains, and are 100% identical in their other sequences, but they show different subcellular localizations and lead to distinct phenotypes when ectopically expressed in fibroblasts.[206] In more detail, p59Hck is mainly associated to the plasma membrane and p61Hck to the lysosome membrane.[207]

The expression of a constitutively activated variant of p61Hck induces the de novo formation of podosome rosettes, which are structures involved in cell adhesion and extracellular matrix degradation, whereas p59Hck triggers the formation of plasma membrane protrusions.[208]

Hck is especially expressed in myeloid cells and is primarily involved in inflammatory signalling.[209] Thus, Hck levels are relatively low in immature monocytes and granulocytes, but rise much folds as these cells differentiate. An increase in Hck expression occurs when mature

macrophages are treated with LPS, which induces transcription of genes encoding for proinflammatory regulators of the immune response.[210] The protein levels also rise after cell exposure to interferon gamma and macrophage colony-stimulating factor (M-CSF), which activate Hck among other signalling molecules.[211] Hck expression is particularly high in fully differentiated phagocytes (i.e. neutrophils, monocytes, macrophages, dendritic cells and mast cells) which are specialized cells of the immune system and are able to detect the chemotactic factors released by the infected tissue and/or microorganisms. In these cells, Hck plays important roles in phagocytosis, adhesion and migration, and regulates the formation of membrane protrusions, lysosome exocytosis, podosome formation, and actin polymerization.[212] T-lymphocyte adhesion plays a critical role in both inflammatory and autoimmune responses. It has been demonstrated that Hck facilitates the phosphorylation of C3G, a Rap1 guanine nucleotide exchange factor involved in the regulation of T-cell adhesion. These findings indicate that both C3G and Hck are promising potential therapeutic targets for the treatment of T cell-dependent autoimmune disorders.[213] Asai *et al*. demonstrated that Hck, together with other factors, is involved in the regulation of antigen transcytosis across the epithelial barrier, a process critical in mucosal immunity.[214]

Other studies evidenced new target proteins for Hck. For example, it has been reported that Hck plays an important role in Toll like receptor (TLR)-mediated proinflammatory cytokine production, and hence in the control of inflammation. TLRs are a family of transmembrane noncatalytic proteins, which provide specific recognition of a range of bacterial, viral, fungal and endogenous ligands, and are able to initiate a response against a wide range of physical and environmental insults.[215] Increasing evidence suggests that TLRs are involved in pathologies such as autoimmune diseases, atherosclerosis and cancer. Using primary human macrophages in combination with adenoviral overexpression and small interfering RNA knockdown studies, Smolinska *et al*. showed that Hck has an important role in LPS/TLR4-induced TNF and IL-6 production. In fact, Hck mediates TLR4-induced transcription of both TNF and IL-6. These data suggest the possibility of targeting this kinase for the alleviation of inflammation.[216]

Several studies indicated Hck involvement not only in inflammatory pathways, but also in cancer development. The expression of a constitutively active form of p56Hck (a murine form of Hck) in HeLa cells (derived from cervical cancer) leads to membrane protrusion and F-actin redistribution. In addition, both p56Hck and its constitutive active form enhance cell motility and invasion.[217]

In 2015, Awad *et al*. demonstrated a specific interaction between the SH3 domain of Hck and the polyproline motif of Eukaryotic EnguLfment and cell Motility 1 (ELMO1), that is a protein involved in cell migration and actin remodeling.[218]

4.2 Hck and Leukemias

4.2.1 Hck and CML

Several studies report the involvement of Hck in the Bcr-Abl driven transformation that typically occurs in CML cells. It was first observed that the hematopoietic transformation of IL-3-dependent myeloid cell line 32D by transfection with Bcr-Abl induces the activation of at least two SFK members, p53/56Lyn and p59Hck.[219] It was successively demonstrated that Hck phosphorylates Bcr-Abl on Tyr177 within the Bcr region, providing a docking site for the Growth factor receptor-bound protein 2 (Grb2) SH2 domain and thus a possible link to the Ras pathway, whose hyperactivation is involved in many malignancies.[220] Further studies indicated that Hck binds Bcr-Abl in at least four independent regions, one in Bcr, one in the region comprising the SH3 and SH2 domain of Abl, one in the SH1 domain of Abl, and one in the C-terminal domain of Abl. In Hck, deletion of the SH2 and/or the SH3 region abolishes the binding to Bcr-Abl, while deletion of the Hck SH1 domain enhances the binding of Hck to Abl and Bcr-Abl.[221] Using matrix-assisted laser desorption ionization time-of-flight mass spectrometry, Chen *et al*. observed that seven tyrosine residues in the Bcr-Abl SH3-SH2 regions are phosphorylated by the SFK members Hck, Lyn and Fyn, which in this way modulate Bcr-Abl transforming activity. In particular, Tyr89 localizes to a binding surface of the SH3 domain that engages the SH2-kinase linker in the crystal structure of the c-Abl core. Phosphorylation of this tyrosine residue by Hck disrupts negative regulatory interactions and leads to enhanced Abl kinase activity and cellular signalling.[222] Using a kinase-defective mutant of Hck, it has been demonstrated that Hck participates with Bcr-Abl in cell modification to cytokine independence, suggesting that SFK activation may be necessary for Bcr-Abl transformation signalling. STAT5 is constitutively activated by Bcr-Abl. Klejman *et al*. got further insights in this activation pathway and demonstrated that the Bcr-Abl SH3 and SH2 domains interact with Hck, leading to the stimulation of Hck catalytic activity. Active Hck in turn phosphorylates STAT5B on Tyr699, which is an essential step in STAT5B activation. A kinase-dead Hck mutant and the Hck inhibitor PP2 abrogate Bcr-Abl-dependent activation of STAT5. This study indicated that Bcr-Abl-Hck-STAT5 signalling pathway plays an important role in Bcr-Abl-

mediated transformation of myeloid cells.[223] Interestingly, Hck and Src prevent nuclear localization of STAT5 in the presence of Bcr-Abl. Consistently, in CML cells STAT5 is unexpectedly present at podosome-like structures in the cytoplasm, while in normal macrophages it is not at podosomes but in the nucleus. Phosphorylated-STAT5 associates to podosomes in a process dependent on constitutive activation of Hck. This observation indicates that STAT5, previously classified as a transcription factor, could play another role outside the nucleus, elicited by the Bcr-Abl/Hck transforming pathway. The cytoplasmic retention of activated STAT5, mediated by Src and Hck in Bcr-Abl positive cells, has been confirmed.[224] STAT5 tyrosine phosphorylation can occur in response to genotoxic activation of Bcr-Abl, Hck, and Jak2, a non-receptor TK implicated in signalling by members of the type II cytokine receptor. Apparently, STAT5 phosphorylation occurs in a complex constituted by Bcr-Abl, Hck, and Jak2. Moreover, Hck together with STAT5B regulates Insulin-like Growth Factor 1 (IGF-1) expression, which is increased in CML blast crisis, the last and fatal stage of the diseases.[225] SFKs, in particular Hck and Fgr, interact with c-Abl in the regulation of myeloid cell migration. Indeed, c-Abl associates to integrin-bound Hck and Fgr and its phosphorylation is regulated by these SFKs. Additionally, inhibition of c-Abl activity results in a marked reduction of mouse macrophage and human neutrophil migration and polarization.[226] A study performed by using a chemical-genetic approach demonstrated that Hck has a non-redundant function as a key downstream signalling partner for Bcr-Abl and may represent a potential drug target in CML (**Fig. 14A**).[227] It has been successively confirmed that Hck mediates imatinib-resistance in CML patients, who do not harbour Bcr-Abl mutations, and that an elevated Hck and Lyn kinase activity is sufficient to induce imatinib-resistance through a mechanism that may involve phosphorylation.[228]

4.2.2 Hck and other haematological malignancies

A study performed on B-lymphoid leukemia cells expressing Bcr-Abl indicates that the SFK members Hck, Lyn and Fgr are implicated in Ph(+) acute B lymphoblastic leukemia (B-ALL) and suggests that simultaneous inhibition of SFKs and Bcr-Abl may benefit patients with Ph(+)ALL.[229] Hck also takes part in the development of human AML, interfering with the activation of FLT3. As briefly reported in the previous chapter, this kinase is overexpressed and hyperactivated by activating mutations, i.e. internal tandem duplications (ITD) in the juxtamembrane region in about 30% of AML patients. The mechanism of association between

Hck and FLT3 has been analyzed and it was demonstrated that Hck phosphorylates tyrosine residues 589 and 591 in the juxtamembrane region of wt FLT3 and ITD FLT3 via its SH2 domain, and interferes with FLT3 maturation in a kinase-dependent manner.[230] Saito *et al*., using immunofluorescence labelling, evaluated the expression of nine different proteins in leukemia stem cells (LSCs), which are cell cycle-quiescent and chemotherapy-resistant in human AML. The authors found that the genes encoding Hck and the transcription factor Will Tumor 1 (WT1) are overrepresented in the greatest proportions of LSC samples, analyzed in situ in the bone marrow endosteal region. This finding confirms that Hck is a promising target for the treatment of chemotherapy-resistant LSCs.[231]

Lopez *et al*. reported that AML cells carrying FLT3-ITD mutations are dependent on CDK6 for cell proliferation while CDK4 is not essential. They showed that FLT3-ITD signalling is responsible for CDK6 overexpression, through a pathway involving Hck. Accordingly, FLT3-ITD failed to transform primary hematopoietic progenitor cells from Cdk6-/- mice. Their results demonstrate that CDK6 is the primary target of CDK4/CDK6 inhibitors in FLT3-ITD positive AML. Furthermore, they delineate an essential protein kinase pathway (FLT3/HCK/CDK6) in the context of AML with FLT3-ITD mutations.[232]

Diffuse large B-cell lymphoma (DLBCL) is the most common lymphoid malignancy. It accounts for approximately 30% of non-Hodgkin lymphomas and over 80% of aggressive lymphomas. Hck is overexpressed at the mRNA level in DLBCL cells. Moreover, phosphorylation of Src, Lyn and Hck is much higher in DLBCL cells than in resting B cells. This suggested a role of SFKs, including Hck, in this disease.[233] Clinical data, transgenic mouse models and signalling studies support the role of IL-6 as the major growth factor for multiple myeloma (MM) cells. Hck becomes activated by IL-6 and associates with gp130, and in this way, it is involved in IL-6 signal transduction pathway in MM. Moreover, the expression of a kinase inactive Hck mutant (K269R) in 7TD1 cells (whose growth is IL-6 dependent) causes a dominant negative effect on cell number increase, thus providing further evidence that SFKs, particularly Hck, are required for gp130 signalling in MM (**Fig. 14B**).[234,198]

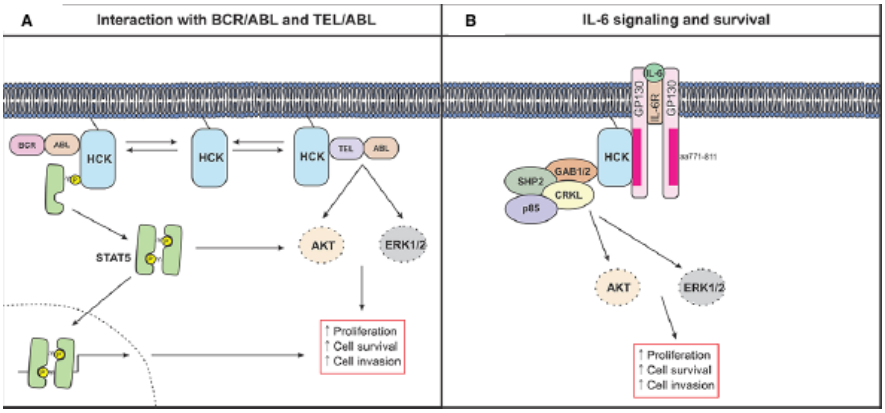

Fig. 14. Schematic Hck signaling pathway in cancer cells. **A.** Interaction with Bcr-Abl. **B.** Interaction with IL-6.

4.3 Hck and HIV

The HIV infection, that is the cause of Acquired Immune Deficiency Syndrome (AIDS) was first identified in early 1980's.[235,236] The most common mode of transmission of HIV-1 is through sexual contact, while the second one is via blood and blood products. The third most common mode is maternal-fetal transmission. HIV transmission is not known to occur via casual, non-sexual contact or via insect vectors such as flies and mosquitoes.[237] The early-stage of HIV is characterized by different symptoms (fever, muscle ache, enlarged glands, weakness and weight loss); in many cases, after this period, the initial symptoms disappear for several years. During this time, the virus carries on developing and damaging the immune system; if left untreated, HIV infection causes reduction in the numbers of CD4-bearing helper T cells weakening the ability to fight infections and the person becomes vulnerable to serious illnesses. This stage of infection is known as AIDS.[238]

4.3.1 HIV-1 infection

The HIV is grouped to the genus Lentivirus within the family of Retroviridae, subfamily Orthoretrovirinae. Retroviruses are small envelope viruses that contain a diploid, single-stranded RNA genome. The virus particle is formed by an inner core that contains the viral nucleic acids, as well as enzymes required for early replication events. This inner core is surrounded by capsid proteins. The capsid itself is surrounded by a lipid membrane. A virus matrix protein is inserted into the inner surface of the membrane. The envelope glycoprotein, an integral membrane protein, protrudes through the membrane and forms the outer surface of

the virus particle.[239]

Infection begins when a virus particle or a cell-producing virus encounters a cell with a high-affinity receptor for the virus. A specific high-affinity binding reaction occurs between the virus surface envelope glycoprotein and the CD4 molecule. CD4 is a surface glycoprotein found on a variety of cells of hematopoietic origin. The CD4 protein is present in low concentration on monocytes, macrophages, and antigen presenting dendritic cells. Entry occurs by fusion of virus and cell membranes. The envelope proteins gp120 and gp41 bind to CD4+ cell receptors and coreceptors on the outside of CD4+ cells and macrophages. The C-C chemokine receptors type 5 (CCR5) and C-X-C chemokine receptor type 4 (CXCR4) facilitate viral entry. T-cell tropic viruses require CXCR4 to bind, and macrotropic strains of the virus require CCR5. The joining of the proteins and the receptors and coreceptors fuses the HIV membrane with the CD4+ cell membrane, and the virus enters the CD4+ cell and macrophage. The HIV membrane and the envelope proteins remain outside of the CD4+ cell, whereas the core of the virus enters the CD4+ cell. CD4+ cell enzymes interact with the viral core and stimulate the release of viral RNA and the viral enzymes reverse transcriptase, integrase, and protease. The HIV RNA must be converted to DNA before it can be incorporated into the DNA of the CD4+ cell. This incorporation must occur for the virus to multiply. The conversion of HIV RNA to DNA is known as reverse transcription and is mediated by the HIV enzyme reverse transcriptase. The result is the production of a single strand of DNA from the viral RNA. The single strand of this new DNA then undergoes replication into double-stranded HIV DNA. Once reverse transcription has occurred, the viral DNA can enter the nucleus of the CD4+ cell. The viral enzyme integrase then inserts the viral DNA into the CD4+ cell's DNA. This process is known as integration. The CD4+ cell has now been changed into a factory used to produce more HIV. The new DNA, which has been formed by the integration of the viral DNA into the CD4+ cell, causes the production of messenger RNA that initiates the synthesis of HIV proteins. The HIV proteins and viral RNA, all the components needed to make a new virus, gather at the CD4+ cell membrane to form new viruses. These new viruses push through the different parts of the cell wall by budding. They leave the CD4+ cell and contain all the components necessary to infect other CD4+ cells. The new virus has all the components necessary to infect other CD4+ cells, after a process of maturation. During this process, the HIV protease enzyme cuts the long HIV proteins of the virus into smaller functional units that then reassemble to form a mature virus (**Fig. 15**).[240]

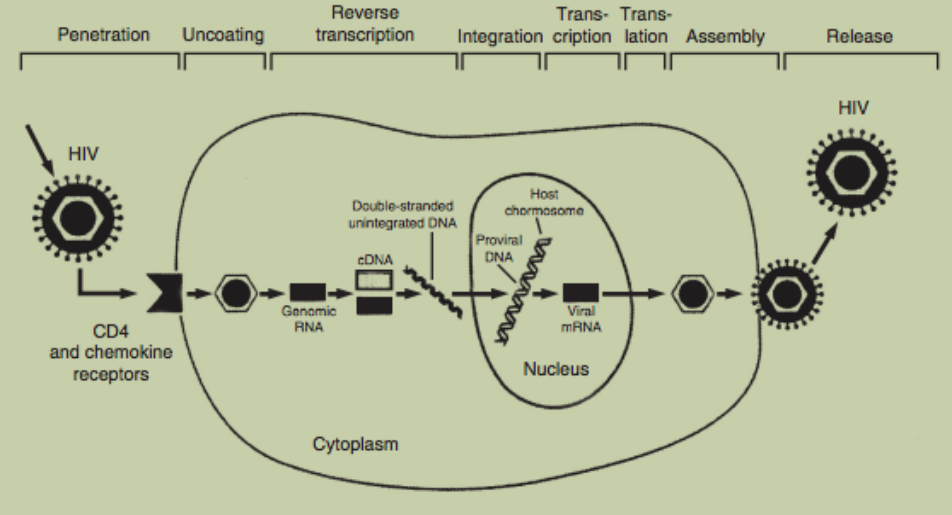

Fig. 15. Schematic diagram of the HIV life cycle.

4.3.2 Role of Hck in HIV infection and AIDS

There are some viral accessory proteins that act late in the virus life cycle with different functions, such as assisting virus maturation, releasing and increasing the virus particle infectivity and viability. These proteins are Nef (Negative regulatory factor), Vif (Virus infectivity factor), Vpu (Viral protein U) and Vpr (Viral protein R).[198,241] Nef, the most important regarding the link with Hck, has no known catalytic function and is believed to promote viral pathogenicity by altering signalling pathways in infected cells through its interactions with surface receptors and cellular proteins.[242] Initially, it was thought that Nef was an inhibitor of viral pathogenesis, since it was shown to decrease viral transcription and replication in culture and was thus named “negative factor”. Successively, much evidence has demonstrated the strongly positive effect of Nef on HIV pathogenesis, including enhancing infected cell survival and optimized host environment for viral replication and infectivity. Even if more recent advances in the field reported that Nef effects range from inhibition to activation on T-cell antigen receptor (TCR) signalling cascade, it has been generally demonstrated that Nef is essential for AIDS pathogenesis.[243]

When hematopoietic differentiated cells derived from mesenchymal stem cells become permissive to HIV infection, an increased Hck expression has been observed.[244]

Nef has been shown to interact with the Hck SH3 domain and stimulate its tyrosine kinase activity *in vivo*. Myristoylation of Nef does not affect SH3 domain binding. The crystal structure of Nef in complex with the Hck SH3-SH2 domains has been determined with a resolution of

1.86 Å (PDB code: 4U5W).[245] **Fig. 16** shows the structure of the Nef-Hck SH3-SH2 complex.

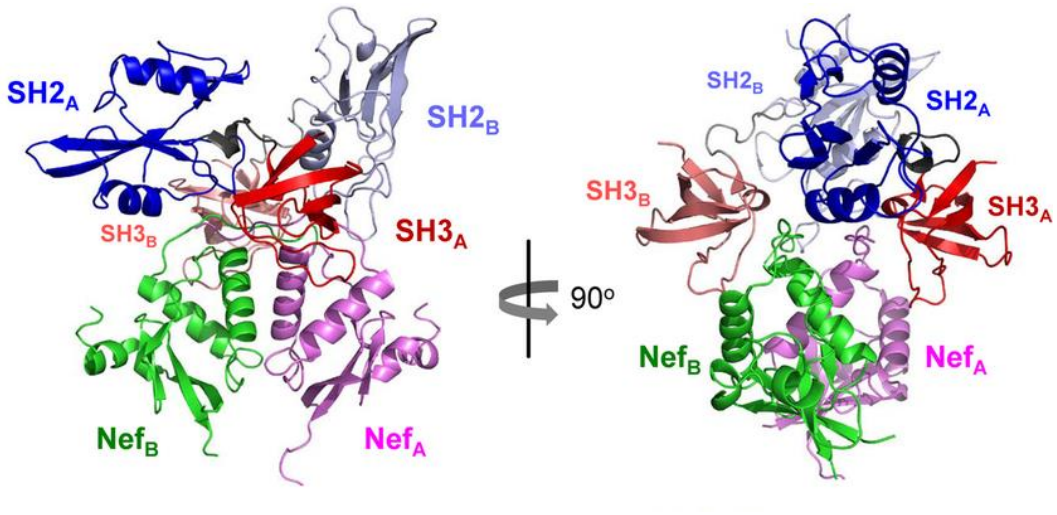

Fig. 16. Crystal structure of Nef in complex with SH3-SH2 domains of Hck.[245]

There are two Nef-Hck SH3-SH2 domain complexes in the unit of the crystal. The SH3 domain of Hck binds to the PxxP (polyproline motif) loop of Nef by means of its RT-loop (region ranging from residue 86 to 101). In detail, hydrophobic contacts were detected between the PxxPxR motif and residues Tyr90, Tyr92, Trp118, Pro133 and Tyr136 of Hck. Hydrogen bonds involve SH3 residues Tyr136 and Trp118 with Pro72 and Val74, respectively, of Nef. Moreover, a salt-bridge between the conserved arginine in the Nef PxxPxR motif (Arg77) and the SH3 Asp99 was found. An intermolecular-intercomplex interaction was observed in the Nef-Hck dimeric structure involving a salt bridge between Nef Arg105 from one complex and the SH3 Glu93 of the opposite complex. Furthermore, each SH2 domain establishes van der Waals interactions with both Nef molecules of the complex and in particular with Nef residues Phe68, Pro69, Leu76 and Tyr115. These contacts between Nef and SH2 Hck could guide the proper placement of the PxxPxR motif for its interaction with the SH3 domain.[245] It was successively confirmed that Nef specifically binds to the SH3 domain of Hck *in vitro* with high affinity.[198] Furthermore, the Hck-Nef binding is blocked by proline-to-alanine mutations.[246] Lee *et al*. showed that Ile96, which is in a Hck loop positioned close to conserved SH3 residues implicated in the binding of proline-rich motifs, forms hydrophobic interactions with a hydrophobic pocket within the Nef core, and the mutation of Ile96 abrogates Nef binding to Hck.[247]

Other residues within the Nef hydrophobic pocket, such as Tyr120, have also been found to be

critical for Nef-mediated binding and activation of Hck. Nef interactions both with Hck SH3 domain and with Hck Ile96 are necessary, but not independently sufficient, for high affinity binding of Nef to the Hck SH3 domain.[212]

Hck activation by Nef has been revealed also in other cell-based assays. Briggs *et al*. demonstrated that Hck SH3 engagement by Nef is sufficient to activate this kinase in rat fibroblasts.[248] Amino acid sequence alignment with active Nef proteins revealed differences in regions not previously implicated in Hck activation, including a large internal flexible loop absent from available Nef structures. Substitution of these residues in active Nef compromises Hck activation without affecting SH3 domain binding. These findings show that residues at a distance from the SH3 domain binding site can allosterically influence Nef interactions.[249]

A study by Kim *et al*. indicated that Hck is also implicated in CNS HIV infections, that cause HIV-associated neurocognitive disorders (HAND), also reported as AIDS dementia. Macrophages and microglia are infected by HIV-1 and play a pivotal role in the pathogenesis of AIDS dementia. They express CD45, which are a family of transmembrane protein tyrosine phosphatases. In particular, microglia expresses the two subtypes CD45RB and CD45RO. The authors treated the microglia with a CD45 agonist antibody (alphaCD45RO) and observed that it inhibits HIV-1 replication. They also demonstrated that this antibody prevents HIV-1 Nef-induced autophosphorylation of Hck. This study showed that in myeloid lineage cells, Nef interacts with the Hck SH3 domain, and this activity results in autophosphorylation of Hck and in increased HIV-1 transcription. Thus, in microglia Hck is phosphorylated following HIV-1 infection in a Nef-dependent manner.[250]

Recently, Shinya *et al*. demonstrated the involvement of the association of Nef with Hck and p21-activated kinase 2 (PAK2), and that Hck, which is expressed strongly in dendritic cells, augmented this mutual interaction. Hck might be another therapeutic target to preserve the function of HIV-1 infected dendritic cells, which are potential reservoirs of HIV-1 even after antiretroviral therapy.[251]

Hck is also involved in the interaction with another HIV-1 protein, Vif, which is critically required for the infection of host cells. Vif plays a key role in replication and transmission of the virus in non-permissive cells, such as primary T cells and macrophages.[252] Vif interacts with a variety of host proteins, including Hck, and is able to cause kinase activation. In fact, using a yeast growth suppression assay, it has been shown that purified Vif is a potent activator of Hck *in vitro* and *in vivo*.[253]

CHAPTER 5. Sgk1 kinase

The Sgk family consists of three members, Sgk1, Sgk2 and Sgk3, all displaying serine/threonine kinase activity. They are products of three distinct genes localized on different chromosomes.[254]

5.1 Sgk1 structure and functions

Sgks are members of the AGC (protein A, G, C) kinase group and share structural and functional similarities with Akt, PKC and S6K1–3 (Ribosomal S6 Kinase).[255, 256] They present a conserved structure with an N-terminal variable domain, a catalytic domain and a hydrophobic C-terminal domain (**Fig. 17**).[257]

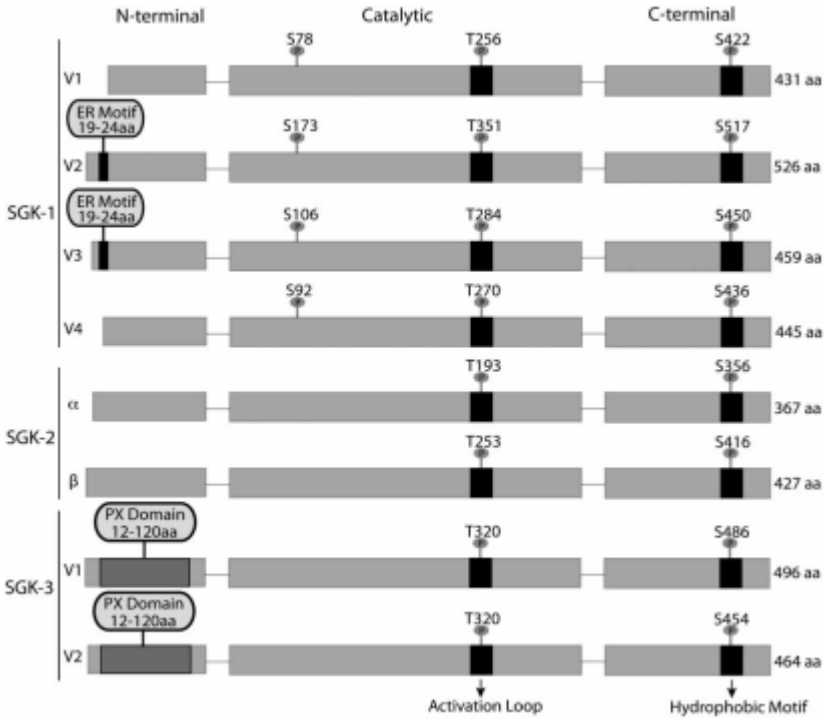

Fig. 17. Sgk isoforms and variants.[257]

For each Sgk isoform, several variants have been identified. Sgk1 has four variants that differ in the amino-terminus which impacts on both substrate specificity and turnover of the protein. Sgk2 has two variants named alpha and beta, which differ in the amino-terminus, while Sgk3 exists in two forms, with variant 2 lacking an alternate in-frame exon, compared to variant 1,

resulting in a shorter protein. The functional consequence of the differing variants of Sgk2 and Sgk3 is as yet unknown. Sgk isoforms have been implicated in the regulation of a great diversity of cellular factors including ion channels, membrane transporters, cellular enzymes and transcription factors. This diversity is reflected in Sgks involvement in a wide variety of cellular processes including hair growth, locomotive behaviour, cell stress, survival, proliferation and transport of ions, nutrients and amino acids (**Fig. 18**).[258]

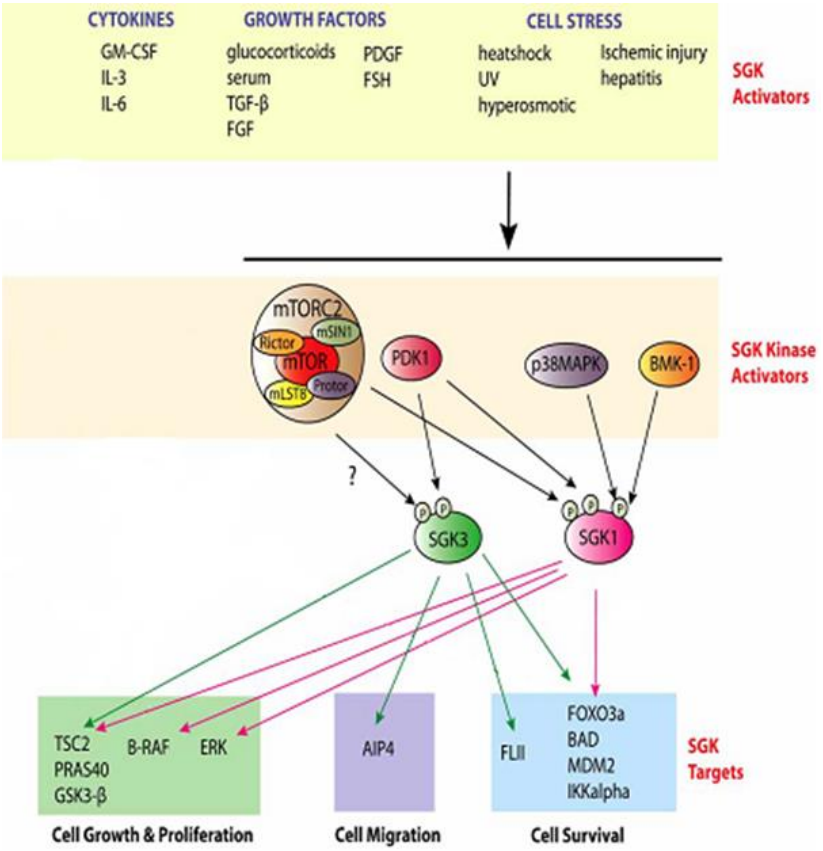

Fig. 18. Activators of Sgk1 and Sgk3 and substrates involved in cell proliferation, migration and survival.[257]

5.2 Regulation and activation of Sgk

Similarly to the Akt isoforms, Sgk activity is regulated by post-translational modification, most frequently by phosphorylation and dephosphorylation mediated via the PI3K pathway and protein phosphatase 2A, respectively.[259] Sgk1 was originally described as a key enzyme in the hormonal regulation of sodium absorption by the amiloride sensitive sodium channel (ENaC).[260] The activity of ENaC, through Sgk1, is regulated by cAMP,[261] insulin,[261,262]

glucocorticoids,[263] IL-2[264] and IGF-1[265] and other survival signal proteins in normal and cancer cells. Subsequently, *Sgk1* gene transcription has been shown to be upregulated by a multitude of different stimuli, including growth factors,[266,267] the p53 tumour suppressor protein[268] and various cellular stressors including ischaemic injury, heat shock and ultraviolet stress.[269–272] It has been proposed that Sgk1 degradation may be mediated by the E3 ubiquitin-protein ligase Nedd4-2. Sgk1 phosphorylation of Nedd4-2 increases Sgk1 degradation, thus, through a feedback inhibition mechanism, Sgk1 is likely to induce its own degradation.[273]

Sgk1 activity is strictly correlated with its post-translational modifications. It becomes a substrate of mTOR (mammalian target of rapamycin) kinase that phosphorylates Sgk1 hydrophobic motif (H-motif) on Ser422. Then, 3-phosphoinositide-dependent kinase-1 (Pdk1) binds to the H-motif of Sgk1, at the level of phospho-Ser422, and further phosphorylates the protein at Thr256.[274] Given the substantial homology in the hydrophobic motif between the Sgk isoforms, it is likely that the kinase responsible for phosphorylation of Sgk1 will also be responsible for Sgk2 and Sgk3 phosphorylation. In addition to the PI3K activation of Sgk1, big mitogen-activated protein kinase-1 (BMK-1) in response to EGF stimulation[275] and p38 MAPK in response to interleukin IL-6 stimulation[276] can activate Sgk1 through a Pdk1-independent phosphorylation of serine-78.[257]

5.3 Sgk1 and cancer

Sgk1 is a kinase that has recently gained the attention in the field of molecular oncology, its antiapoptotic function suggests a possible involvement in human carcinogenesis.[277] Ectopic expression of wt Sgk1 is able to revert apoptosis mediated by growth factor withdrawal.[278] Moreover, Sgk1 mediates glucocorticoid dependent antiapoptotic signals in mammary epithelial and breast cancer cells[279] and IL-2 dependent antiapoptotic signals in kidney cancer cells.[264] Interestingly, active Sgk1 regulates cell survival, proliferation, and differentiation through Murine Double Minute 2 (MDM2), that directs p53 to ubiquitylation and proteosomal degradation,[280] and, through RAN-binding protein 1 (RANBP1), affects mitotic stability and taxol sensitivity of RKO colon carcinoma cells in culture.[281] Sgk1 activates N-Myc down-regulated gene 1 (NDRG1), by catalysing its phosphorylation on Thr346. The NDRG1 factor is considered to be a specific Sgk1 substrate.[282] NDRG1 has an important role in cell proliferation and differentiation[283] and a debated role in oncogenesis.

Indeed, it mainly behaves like an oncosuppressor in several tumor models,[284,285] but it appears to be a key determinant of resistance towards alkylating chemotherapy in malignant gliomas.[286] Moreover, it is associated with aggressive tumor behaviour in hepatocellular carcinoma (HCC), where NDRG1 suppression induces apoptosis.[287] Taken together, these observations suggest an important role of Sgk1 in carcinogenesis and in resistance to hormonal therapy and chemotherapy.[288]

An increased Sgk1 expression has been found in several human tumors, including prostate,[289] colon,[290] endometrial,[291] and breast cancer,[292] non-small cell lung cancer (NSCLC),[293] HCC,[294,295] GB.[296,297]

Recently, Dattilo *et al*. reported that Sgk1 controls cell transformation and tumor progression. In detail, Sgk1 affects mitotic stability by regulating the expression of RANBP1/RAN; the authors demonstrated that Sgk1 fluctuations indirectly modify the maturation of precursor micro RNAs (pre-miRNAs) by modulating the equilibrium of the RAN/RANBP1/RANGAP1 axis, the main regulator of nucleo-cytoplasmic transport. The levels of pre-miRNAs and mature miRNAs were assessed by qRT-PCR, in total extracts and after differential nuclear/cytoplasmic extraction. The RANBP1 expression is the limiting step in the regulation of Sgk1-SP1 dependent nuclear export. These results were validated in tumor models and primary human fibroblasts and corroborated in tumor-engrafted nude mice. Experiments using RANGTP conformational antibodies confirmed that Sgk1, through RANBP1, decreases the level of the GTP-bound state of RAN. This novel mechanism may play a role in the epigenomic regulation of cell physiology and fate.[298]

5.3.1 Sgk1 and prostate cancer

Androgens, through their actions on the androgen receptor (AR), are required for the development of the prostate and contribute to the pathological growth dysregulation observed in prostate cancers. Consequently, androgen ablation has become an essential component of the pharmacotherapy of prostate cancer. Sherk *et al*. explored the utility of targeting processes downstream of AR as an alternate approach for therapy. Specifically, they demonstrate that the *sgk1* gene is an androgen-regulated target gene in cellular models of prostate cancer. Furthermore, functional Sgk1 protein, as determined by the phosphorylation of its target Nedd4-2 was also increased with androgen treatment. Importantly, the authors determined that RNAi mediated knockdown of Sgk1 expression attenuates androgen-mediated growth of the

prostate cancer cell line, LNCaP. Data suggested that the androgen ablation and the inhibition of pathways downstream of AR are likely to have therapeutic utility in prostate cancer.[299]

Szmulewitz *et al*. have studied the role of Sgk1 and glucocorticoid receptor (GR) in prostate cancer. They reported that Sgk1 expression was strong in 79% of untreated cancers versus 44% in androgen-deprived cancers. Conversely, GR expression was present in a higher proportion of androgen-deprived versus untreated cancers (78% vs. 38%). High-grade cancers were nearly twice as likely to have relatively low Sgk1 staining compared to low-grade cancers (13.8% vs. 26.5%). Low Sgk1 expression in untreated tumors was associated with increased risk of cancer recurrence, 5-year progression-free survival 47.8% versus 72.6%. The Sgk1 expression is high in most untreated prostate cancers and declines with androgen deprivation. However, these data suggest that relatively low expression of Sgk1 is associated with higher tumor grade and increased cancer recurrence, and is a potential indicator of aberrant AR signalling in these tumors. GR expression increased with androgen deprivation, potentially providing a mechanism for the maintenance of androgen pathway signalling in these tumors.[300]

Despite new treatments for castrate-resistant prostate cancer (CRPC), the prognosis of patients with CRPC remains bleak due to acquired resistance to AR-directed therapy. The GR and AR share several transcriptional targets, including the anti-apoptotic genes *Sgk1* and *MKP1* dual specificity phosphatase 1 (*DUSP1*). Because GR expression increases in a subset of primary PCa following androgen deprivation therapy, Isikbay *et al*. sought to determine whether GR activation can contribute to resistance to AR-directed therapy. They studied several PCa models before and following treatment with androgen blockade and found that increased GR expression and activity contributed to tumor-promoting PCa cell viability. Increased GR-regulated Sgk1 expression appears, at least in part, to mediate enhanced PCa cell survival. Therefore, GR and/or Sgk1 inhibition may be useful adjuncts to AR blockade for treating CRPC.[289]

Recently, Liu *et al*. investigated the cellular responses to GSK650394 (a competitive Sgk inhibitor) treatment and Skg1 silencing (or overexpression) in PCa cell lines and PC3 xenografts using flow cytometry, western blotting, immunofluorescence, transmission electron microscopy and immunohistochemistry. The authors demonstrated that Sgk1 inhibition exhibits significant antitumour effects against PCa *in vitro* and *in vivo*.[301]

5.3.2 Sgk1 and colon cancer

Studies on Sgk1 knockout murine models and Sgk1-specific RNA silencing in the RKO human colon carcinoma cell line point to this kinase as a central player in colon carcinogenesis and in resistance to taxanes. In this regards, Amato *et al*. investigated the mechanisms through which Sgk1 regulates cell proliferation. They adopted a proteomic approach to identify up- or downregulated proteins after Sgk1-specific RNA silencing. The authors reported that Sgk1-dependent regulation of RANBP1 has functional consequences on both mitotic microtubule activity and taxol sensitivity of cancer cells.[281] In 2015 the same group described the biologic effects of a recently identified kinase inhibitor, SI113, characterized by a substituted pyrazolo[3,4-*d*]pyrimidine scaffold, that shows specificity for Sgk1.[290] The compound possesses antiproliferative activity on colon cancer cells and potentiate cell sensitivity to paclitaxel.

Recently, Liang *et al*. developed a novel analog of GSK650394, and evaluated its effects on colorectal cancer cells (CRC) and tumor growth both *in vitro* and *in vivo*. They found that new developed GSK650394 analog QGY-5-114-A has lower IC_{50} value, and treatment with QGY-5-114-A significantly inhibited CRC cell proliferation and migration *in vitro*. Besides that, QGY-5-114-A is also active *in vivo*.[302]

5.3.3 Sgk1 in endometrial problems and cancer

Sgk1 seems to be involved in unjustified infertility. Indeed, its overexpression in endometrial surface epithelium leads to infertility in animal models. On the other hand, during pregnancy, endometrial Sgk1 activity shows some protective effects. So further insights in the role of Sgk1 in infertility and pregnancy are needed.[303]

Endometrial cancer is often characterized by PI3K/Akt pathway deregulation. However, the role of Sgk1 in endometrial cancer has been poorly investigated. Recently, Conza *et al*. demonstrated that Sgk1 expression is increased in tissue specimens from neoplastic endometrium. The Sgk1 inhibitor SI113, previously cited in the context of colon cancer,[290] induced a significant reduction of endometrial cancer cells viability, measured by the (3-(4,5-dimethylthiazol-2-yl)-2,5-diphenyl tetrazolium bromide assay. This effect was associated to the increase of autophagy, as revealed by the increase of the markers LC3B-II and beclin I, detected by both immunofluorescence and western blot analysis. SI113 treatment caused also apoptosis of endometrial cancer cells, evidenced by the cleavage of the apoptotic markers Poli ADP-

Ribose Polymerase (PARP) and Caspase-9. Increased expression of Sgk1 in endometrial cancer tissues suggests a role for Sgk1 in this type of cancer, as reported for other malignancies.[291]

5.3.4 Sgk1 and breast cancer

Some breast cancer cell lines are resistant to Akt inhibitors. It has been reported that increased SGK1 expression represents one mechanism predicting Akt inhibitor resistance. For this reason, it would be very interesting to explore the therapeutic utility of SGK1 inhibitors or dual Akt/SGK1 inhibitors in treating Akt-resistant cancer cells possessing elevated SGK1.[292]

Salis *et al.* investigated the cytotoxic effect of fluvastatin on MCF-7 breast cancer cells and define the transcriptional regulation of specific genes during the occurrence of this cytotoxic effect. Their data suggested that the antiproliferative effects of Fluvastatin may be related to the decreased expression levels of Sgk1 and caveolin-1 (CAV1).[304]

Recently, Castel *et al*. demonstrated that in breast cancer cells resistant to PI3Kα inhibitors, targeting Sgk1 restores the antitumoral effects of PI3Ka inhibition.[305]

5.3.5 Sgk1 and non-small cell lung cancer

Lung cancer represents one of the most frequent cause of death for cancer. In NSCLC, which accounts for the vast majority of this disease, only early detection and treatment, when possible, may significantly affect patient's prognosis. An important role in NSCLC malignancy is attributed to the signal transduction pathways involving PI3K, with consequent activation of the Akt family factors and of Sgk1. Abbruzzese *et al*. used qRT-PCR and immunohistochemistry (IHC) to determine respectively mRNA and protein expression of Sgk1 (total and phosphorylated/activated) in archival NSCLC samples from patients with a well-documented clinical history. The data confirm the oncogenic role of Sgk1, since higher mRNA expression appears to be present in patients with worse prognostic indicators. Moreover, the significantly higher Sgk1 expression in the squamous cell subtype of NSCLC could indicate this factor as central in establishing prognostic/predictive parameters. For this reason, Sgk1 might be employed in the management of patients with squamous cell lung cancer.[293]

Recently, Shi *et al*., revealed that different dosing strategies of wogonin (5,7-dihydroxy-8-methoxyflavanon, an *O*-methylated flavone from *Scutellaria baicalensis*) can induce different outcomes of NSCLC A549 cells, including cell cycle arrest, senescence, and apoptosis. In these cells, there are significant differences in Sgk1 oscillation frequency, amplitude, and cycle

during different cell responses. Data suggest that the timing and end point of different cell responses are associated with the dynamics of Sgk1. Sgk1 protein dynamics may be an important part of cellular signalling that directly influences cellular response decisions.[306]

5.3.6 Sgk1 and hepatocellular carcinoma

Analysis of gene expression in human HCC cells demonstrates that Sgk1 and Akt1 are equally overexpressed when compared with normal human hepatocytes, suggesting that both kinases might have roles in hepatocellular dysregulation.[294,307]

Talarico *et al.* demonstrated that SI113, which was previously cited for its activity to induce cell death in colon carcinoma and in endometrial cancer cells,[290,291] also inhibits tumour growth in hepatocarcinoma models *in vitro* and *in vivo*. Data show that direct Sgk1 inhibition can be effective in hepatic cancer models, either alone or in combination with radiotherapy.[295]

Recently, Salis *et al.* correlated the activity of fluvastatin in reducing human hepatocellular carcinoma (Hep3B) cell migration with the expression of some genes, including *Sgk1*.[308]

5.3.7 Sgk1 and glioblastoma

Talarico *et al*. found that Sgk1 expression is correlated with high-grade glial tumors in a cohort of n a cohort of GB patients. Thus, they expanded the analysis of SI113 efficacy in GB cellular models and demonstrated that SI113 produces a dramatic decrease in cell viability by inducing apoptosis in GB cell lines only, sparing normal mice fibroblasts. They demonstrated that this Sgk1 inhibitor enhances the effects of ionizing radiations in the induction of cell death and distortion of cell cycle progression. Indeed, SI113 synergizes with oxidative stress, the primary mechanism of the radio-dependent tumor killing, and modulates the autophagic response and the reticulum stress. Taken together, these data demonstrate the importance of Sgk1 as molecular target in cancer therapy and the effectiveness of the SI113-dependent Sgk1 inhibition also in GB treatment, where this compound appears effective as a single agent and also in combination with radiotherapy.[296]

The importance of copper in the metabolism of cancer cells has been widely studied in the last years and a clear-cut association between copper levels and cancer deregulation has been established. Recently, the same authors studied the combined effects of $^{64}CuCl_2$ and SI113 on human GB cell lines with variable p53 expression. They demonstrate that $^{64}CuCl_2$ is able to induce a time and dose dependent modulation of cell viability in highly malignant gliomas and

that the co-treatment with SI113 leads to additive/synergistic effects in terms of cell death. Evidence reported in this study underlines the therapeutic potential of the combined treatment with SI113 and $^{64}CuCl_2$ in GB cells.[297]

A subpopulation of cells known as GB stem-like cells (GB-SCs) has the capacity to initiate and sustain tumor growth and possess molecular characteristics similar to the parental tumor. GB-SCs are known to be enriched in hypoxic niches and may contribute to therapeutic resistance. Kulkarni *et al*. identified the genes required for the growth and survival of GB stem cells under both normoxic and hypoxic conditions and confirmed Sgk1 as a novel potential drug target for GB.[309]

5.4 Sgk1 and metabolic syndrome

Hypertension, obesity and susceptibility to develop type II diabetes are hallmarks of metabolic syndrome, a condition associated with enhanced morbidity and mortality from cardiovascular diseases and very common in developed countries. Sgk1 plays a critical role in the hypertensive effects of glucocorticoids.[310] In humans a certain variant of the *Sgk1* gene is associated with moderately enhanced blood pressure and with insulin-sensitivity of blood pressure increase.[311] The same *Sgk1* gene variant is associated with an increased body mass index. Accordingly, the *Sgk1* gene variant is more prevalent in patients with type II diabetes than in individuals without family history of diabetes.[312] Sgk1 presumably participates in the pathophysiology of the metabolic syndrome (**Fig. 19**).

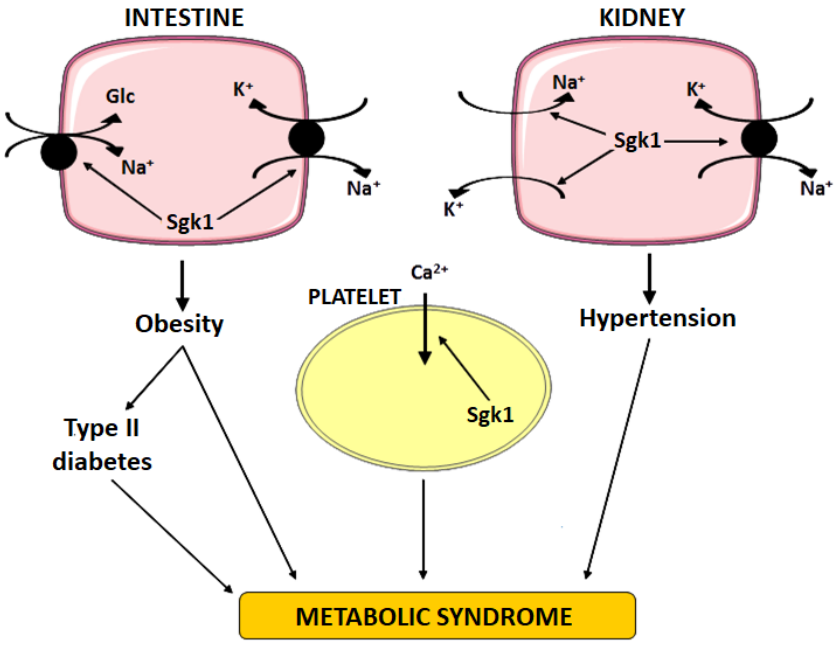

Fig. 19. Sgk1 in metabolic syndrome.

5.4.1 Sgk1 and blood pressure

Owing to its influence on renal salt excretion and salt intake, Sgk1 is expected to participate in blood pressure control.[313] Notably, induction of hyperinsulinemia in mice by pretreatment with a high-fructose diet sensitizes arterial blood pressure to high-salt intake in wt but not Sgk1-deficient animals. Thus Sgk1 mediates the salt-sensitizing effect of hyperinsulinism on blood pressure.[258]

5.4.2 Sgk1 in obesity and diabetes

Sgk1 participates in the development of obesity,[258,314] which is well known to cause insulin resistance and ultimately impair insulin release leading to type II diabetes. The mechanisms involved in the development of insulin resistance in obese individuals include intracellular lipid-induced inhibition of insulin-stimulated insulin-receptor substrate (IRS)-1 tyrosine phosphorylation, resulting in reduced IRS-1-associated PI3K activity and subsequent decrease of insulin-stimulated GLUT4 (glucose transporter type 4) activity.[315]

Sgk1 fosters the development of obesity at least partially by stimulation of the Na^+ coupled glucose transporter SGLT1, which accelerates the intestinal uptake of glucose. The rapid intestinal glucose absorption leads to excessive insulin release and fat deposition, with

subsequent decrease of plasma glucose concentration, which triggers repeated glucose uptake and thus obesity. Conversely, obesity could be counteracted by inhibitors of SGLT1. In diabetes mellitus, the excessive plasma glucose concentrations could, at least in part, upregulate intestinal Sgk1 expression and the enhanced Sgk1-dependent stimulation of SGLT1 could contribute to the maintenance of obesity.[316]

CHAPTER 6. SFKs and Sgk inhibitors

It has been estimated that a large part of the current research and development budget of the pharmaceutical industry is spent on kinases, and particularly on their inhibitors. In fact, in the last years, a large number of small molecule inhibitors of different kinases have received FDA and EMA approval and are entered into clinical therapy for the treatment of solid and haematological malignancies, and many other compounds are being tested both in preclinical and clinical trials. All these inhibitors contain at least one nitrogen heterocycle, but belong to very different chemical families. Some of these molecules are very promising as drug candidates, in particular towards mutated kinases resistant to the first generation inhibitors.

6.1 Classification of TK inhibitors

The structure of the enzyme-bound inhibitors complex is used for the classification of TK inhibitors, which can be divided, on the basis of the protein region they interact with in:

- kinase domain inhibitors. This group includes the majority of inhibitors and, in turn, is constituted by two subtypes of inhibitors (types I and II). Type I and II inhibitors target the conserved catalytic cleft and are ATP-competitive. Type I inhibitors target the ATP-binding site in the active open conformation (DFG-in). These compounds typically mimic the interactions of the adenine moiety of ATP, forming from 1 to 3 hydrogen bonds with the hinge region of the kinase. Structural studies allowed to divide the region occupied by these inhibitors into subregions: the hydrophobic regions I and II, the adenine region, the ribose region and the phosphate-binding region (**Fig. 20**).[317] Structural studies have also revealed that the presence of the deep hydrophobic region I plays important roles in the potency and selectivity of small-molecule inhibitors. The size and shape of this pocket vary considerably among kinases and depend on the activation state of the enzyme.[20] Type II inhibitors target the ATP-binding site of the enzyme in the inactive closed conformation (DFG-out) and also occupy the adjacent hydrophobic pocket I (sometimes defined as allosteric pocket) that is only accessible when the kinase is in an inactivated configuration;[317]
- allosteric inhibitors, defined as type III and type IV, have been reported for different kinases. They bind or the allosteric pocket near the catalytic site (type III) or a different allosteric pocket (type IV) far from the catalytic site. They act by inducing

conformational changes to modulate enzymatic activity. This type of inhibitors could be useful to overcome clinically acquired resistance mutations to the first generation of ATP-competitive kinase inhibitors;[318]

- covalent inhibitors, defined as type V, bind the catalytic site forming covalent linkages.

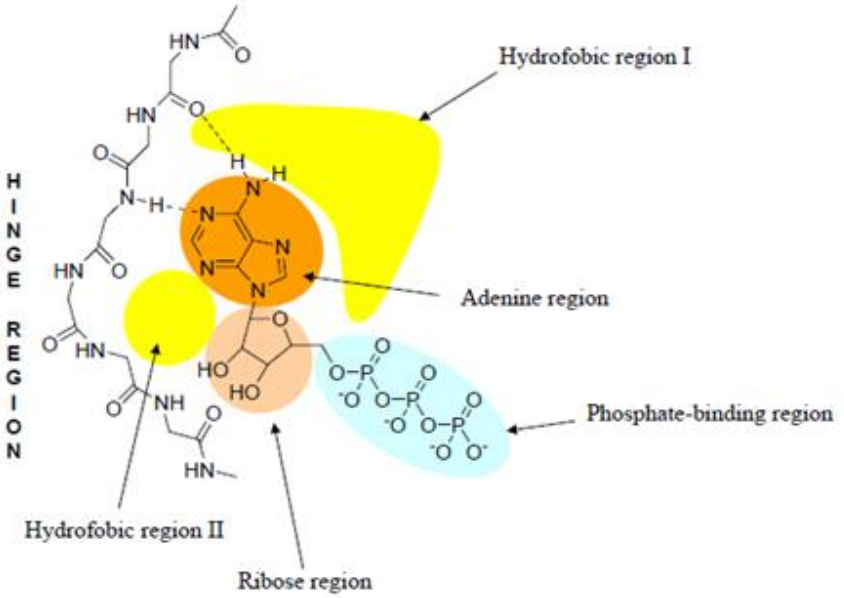

Fig. 20. Schematic representation of subregions in the ATP-binding site.

6.2 Src inhibitors

6.2.1 PH006

PH006 **1** is an ATP-competitive Src inhibitor, which selectively inhibits c-Src with an IC_{50} of 0.38 μM among a panel of 14 TKs. PH006 potently reduces c-Src phosphorylation and c-Src-dependent signal transduction, resulting in inhibition of cell proliferation, migration, and invasion in human breast cancer MDA-MB-231 cells and in animal models.[319]

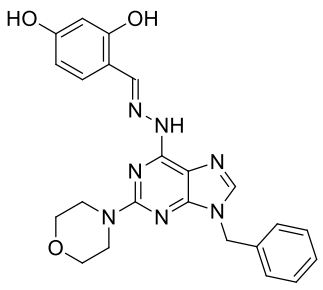

1 PH006

6.2.2 Purine derivatives

Huang *et al*. reported some purine derivatives, with potent and selective inhibitory activity against c-Src. These inhibitors were discovered by adopting a strategy that integrated focused combinatorial library design, virtual screening, chemical synthesis, and bioassays. Thirty-two compounds were synthesized and showed inhibitory activity against c-Src with IC_{50} values ranging from 3.14 to 0.02 μM. Among these, compound **2** was identified as the most potent and selective agent (IC_{50} of 20 nM).

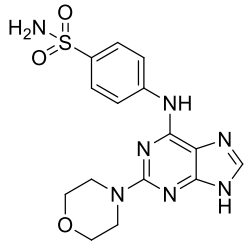

2

It is 100-fold and 300-fold less potent against Kit and c-Abl, respectively and possesses weak inhibitory effect on many other kinases, with IC_{50} values of above 10 μM.[320]

6.2.3 KX2-391

KX2-391 (or KX-01, **3**), synthesized by Kinex Pharmaceuticals is one of the few examples of type III inhibitors. It is a highly selective non-ATP Src inhibitor with an IC_{50} value of 20 nM.[321] KX2-391 inhibits Src catalyzed trans-phosphorylation of Fak, Shc, PXN as well as Src kinase autophosphorylation, while it does not have any effect on PDGFR, EGFR, Jak1, Jak2 and Lck. It is also found to be an inhibitor of tubulin polymerization through binding to the unique conformation on heterodimeric tubulin. In cellular assays, KX2-391 shows growth inhibition in NIH3T3/c-Src527F and SYF/c-Src527F cells.[321,322] KX2-391 is efficient against a variety of solid tumors and many leukaemia types. It inhibits primary tumor growth and suppresses metastasis and is currently being tested in 9 clinical trials for different tumors. (https://clinicaltrials.gov/ct2/results?cond=&term=KX2-391&cntry1=&state1=&recrs=).[323]

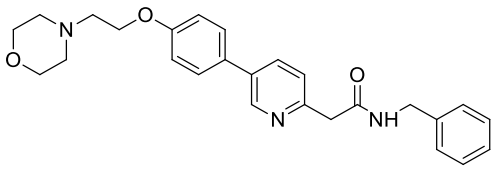

3 KX2-391

6.2.4 WH-4-124-2

Moroco *et al*. discovered a new c-Src inhibitor using a screening on a kinase-biased library with the aim of finding selective inhibitors of the Src/Fak complex versus c-Src alone. This approach led to the identification an aminopyrimidinyl carbamate compound, WH-4-124-2 **4**, with nanomolar activity for c-Src. Molecular docking studies indicate that WH-4-124-2 may preferentially inhibit the DFG-out conformation of the kinase active site.[324]

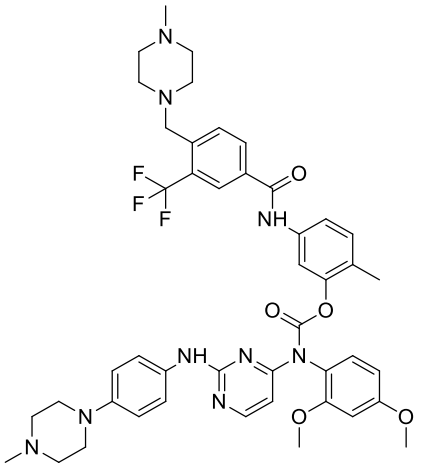

4

6.2.5 Bisubstrate inhibitors

Bisubstrate or bivalent inhibitor are molecules, which interact both with the ATP and protein substrate-binding sites. This kind of inhibition represent a promising strategy for the identification of kinase inhibitors with increased potency and selectivity. However, in the literature there are few examples where the potency and selectivity advantages are fully realized.[325–328]

In this context, Brandvold *et al*. have developed a modular approach to bisubstrate inhibition of TKs. Their strategy utilizes a promiscuous ATP-competitive inhibitor that is then linked to a peptide derived from known substrates for the target kinase. They applied our methodology to c-Src and identified a highly selective bisubstrate inhibitor for this target, compound **5**, which showed a K_d value of 0.28 nM. In addition, they developed a novel screening methodology to identify non-ATP-competitive inhibitors of c-Src and they discovered one of the most potent non-ATP-competitive inhibitor reported to date, compound **6**.[329]

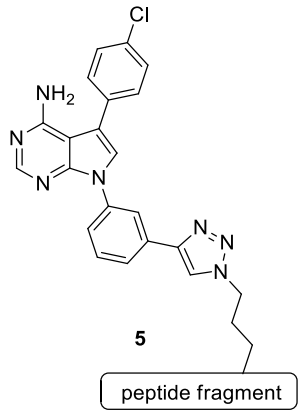

5

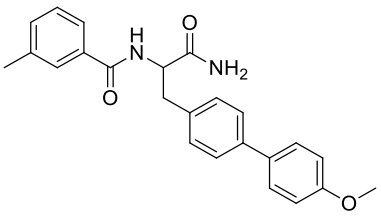

6

6.3 Dual Src/Abl inhibitors

Because of the high structural homology between Src and Abl (another cytoplasmic TK), several compounds originally synthesized as Src inhibitors have also been shown to be potent Abl inhibitors, useful in overcoming the onset of some types of resistance to drugs that only target Bcr-Abl. The excellent clinical results and the observation that dual or multi-targeted inhibitors might be better than selective inhibitors encouraged the development of such compounds. Indeed, even if a selective inhibitor reduces the risk of undesired effects, multi-targeted compounds, usually inhibiting different cell pathways or compensatory mechanisms, could be more effective than selective inhibitors, especially in tumors, where different mechanisms and pathways are generally involved. Several clinical trials on dual Src/Abl inhibitors are ongoing or just terminated, while others are recruiting patients both with hematological and solid tumors. Some dual Src/Abl inhibitors reported below have been approved for the treatment of CML. Notwithstanding the promise shown by these inhibitors, it is not clear whether dual Src/Abl inhibitors will provide a viable strategy for the treatment of

solid tumors. Indeed, some clinical trials have been disappointing and the future of clinical applications is uncertain.[330]

6.3.1 PP1 and PP2

The pyrazolo[3,4-*d*]pyrimidines PP1 **7** and PP2 **8**, by Pfizer, are the first dual inhibitors reported in literature,[331] and showed IC_{50} values of ~1 μM and 0.5 μM, respectively, for Src and of 0.3 μM and 0.5 μM, respectively, for Abl. They have been discovered during a program to find specific inhibitors for SFK members; only later, the activity towards Abl was found out, opening a new field of research.[332] These compounds remain the references for the synthesis of new molecules targeting SFKs, even if they have not been developed as therapeutic agents. On the other hand, their activities are still investigated as demonstrated by several published articles. For example, Kong *et al*. showed that PP2 efficiently reduced cervical cancer cell proliferation, inhibiting both Src and EGFR activity, two factors involved with different roles in this type of tumor.[333] It has recently discovered PP1 and PP2 involvement in adipogenesis.[334]

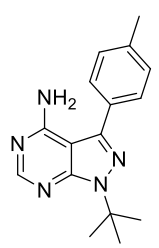

7 PP1

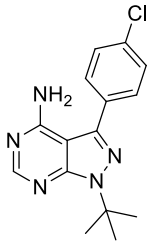

8 PP2

6.3.2 Dasatinib

Dasatinib, (BMS-354825, Sprycel™, **9**), the thiazole-carboxamide derivative synthesized by Bristol-Myers Squibb, is the most important dual Src/Abl inhibitor reported to date, being the first one used for CML therapy, also useful to overcome several imatinib-resistances, with the notable exception of the T315I mutation. Dasatinib is a type I inhibitor and shows IC_{50} values of 0.5 and 1 nM for Src and Abl, respectively.[335] Nevertheless, the molecule is not selective for these two TKs, inhibiting other TKs, including Kit, PDGFR, EPHA, and the Tec kinase Btk.

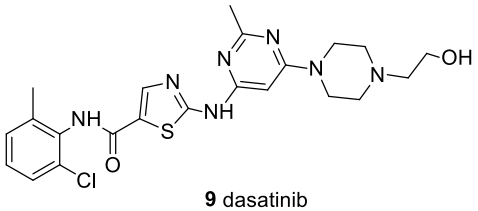

9 dasatinib

The importance of the dual Src/Abl inhibition in CML progenitor cells has been investigated and confirmed: dasatinib inhibits both Bcr-Abl-dependent and-independent Src activity (in contrast to imatinib that inhibited only Bcr-Abl-dependent Src activity), blocking downstream signalling pathways in CML progenitor cells: it suppresses CML colony-forming cells and long-term culture-initiating cells; nevertheless, it has been pointed out that dasatinib does not induce a strong proapoptotic response.[336] This very interesting profile of activity, supported by a number of preclinical and clinical studies, culminated in 2006 with the approval of dasatinib by FDA and successively by EMA for the treatment of CML patients with resistance or intolerance to prior therapy, including imatinib mesylate, and more recently as first line CML therapy. Then, a large number of publications and clinical trials have been reported, investigating the use of dasatinib in both hematologic and solid cancers and confirming the high expectations for this compound.

Lilly *et al*. showed that dasatinib also induced rapid hematologic and cytogenetic responses in adult patients with Philadelphia chromosome positive acute lymphoblastic leukemia (Ph^+ ALL) with resistance or intolerance to imatinib. Several studies investigated the application of dasatinib for the treatment of solid tumors and leukemia in children. A pediatric phase I trial was performed to evaluate the side effects and the best dose of dasatinib in treating young patients with recurrent or refractory solid tumors or Ph+ ALL or CML that did not respond to imatinib mesylate.

Aplenc *et al*. concluded that disposition and tolerability of dasatinib were similar to those observed in adult patients (NCT00316953).[337]

6.3.3 Bosutinib and derivatives

Bosutinib **10** (SKI-606), a 7-alkoxy-3-quinolinecarbonitrile derivative, is an orally potent Src and Abl inhibitor reported by Boschelli *et al*. in Wyeth Pharmaceuticals.[338] Bosutinib acts with an ATP-competitive mechanism, docking inside the active sites of both c-Src and Abl (type I

inhibitor). In detail the analysis of bosutinib docked into the active site of c-Src, showed the formation of three hydrogen bonds:

- between the backbone NH of Met341 and N1 of quinoline;
- between the side chain hydroxyl group of Thr338 and the nitrogen atom of the CN group;
- between the quinoline C2 and the carbonyl oxygen of Glu339.

The anilino group is positioned in the kinase-specific pocket, while the 4-methylpiperazine is oriented towards the solvent region (near the ribose pocket). Computational studies demonstrated that the orientation and hydrogen bonding interaction of bosutinib are similar in both Src and Abl kinases.[339]

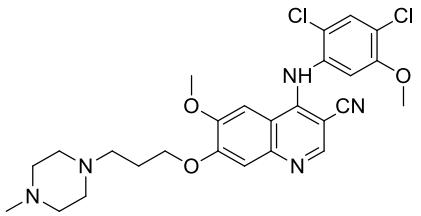

10 bosutinib

Bosutinib showed an IC_{50} of 1.2 nM in an enzymatic assay and an IC_{50} of 100 nM on Src cell proliferation.[338] SKI-606 was found to be also an Abl kinase inhibitor with an IC_{50} of 1 nM in an Abl enzymatic assay. Moreover, this compound inhibits the growth of three Brc-Abl positive leukemia cell lines (K562, KU812 and MEG-01) with IC_{50} values of 20, 5, 20 nM, respectively. Once-daily oral administration of SKI-606 at 100 mg/kg for 5 days caused complete regression of large K562 xenografts in nude mice.[340] Furthermore, bosutinib significantly decreased the proliferation of imatinib-resistant human cell lines, but it showed to be inactive on the T315I mutation.[341]

The clinical efficacy of bosutinib in CML has been supported by several clinical trials and finally, the compound has been approved by FDA and EMA for the treatment of CML patients resistant to prior therapies.

Bosutinib is also investigated for its application in solid tumors, such as breast, prostatic, pancreatic, lung and cervical cancers. Phase I data showed that bosutinib is generally well tolerated with predominantly gastrointestinal adverse effects (NCT00195260).[341]

Recently, Tesar *el al*. conducted a phase II study to evaluate the efficacy and safety of bosutinib in patients with autosomal dominant polycystic kidney disease (ADPKD) which is related to

hyperactivation of Src. They demonstrated that bosutinib is able to reduce kidney growth in patients with ADPKD showing a good toxicity profile (NCT01233869).[342]

6.3.4 Saracatinib

The anilino-quinazoline saracatinib **11**, (AZD0530) is a potent, high selective, dual Src/Abl inhibitor (type I) by AstraZeneca, active in the low nanomolar range against both the enzymes, inhibiting Src and Abl with an IC_{50} of 2.7 and 30 nM, respectively.[343]

Hennequin *et al*. reported the crystal structure of AZD0530 complexed with c-Src in the inactivated form: the quinazoline ring is located in the adenine region, the tetrahydropyran ring fits tightly in the ribose pocket and the chlorobenzodioxole moiety is buried in the hydrophobic pocket I. The authors pointed out that interactions with the protein are predominantly hydrophobic and are formed with the G-loop in the N-terminal domain (Leu273, Gly274) and with Leu393 and Ser345 in the C-terminal domain.

Saracatinib is orally available, displaying excellent pharmacokinetic parameters in animals, with good aqueous solubility and moderate binding to plasma proteins. It inhibits tumor growth in a c-Src-transfected 3T3-fibroblast xenograft model *in vivo* and led to a significant increase in animal survival in an orthotopic model of human pancreatic cancer.[344]

It has been reported that AZD0530 specifically inhibits the growth of CML and Ph^+ ALL cell lines, but not the Ph- ALL; probably the antiproliferative effect of saracatinib results from the inhibition of both Src and Bcr-Abl kinases, with consequent downregulation of survival signalling pathways (STAT5, Erk, PI3K/Akt) in Ph+ cells, resistant or sensitive to imatinib. Moreover, AZD0530 inhibits the growth of imatinib-resistant Ba/F3 cells, expressing the mutations Y253F and E255K. However, AstraZeneca researchers reported that AZD0530 activity on Abl is not currently considered sufficient to provide a strong rationale for its clinical development in Bcr-Abl-driven leukemias.

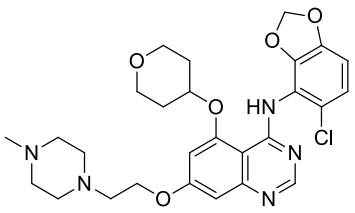

11 saracatinib

The compound inhibited tumor growth in different xenografts models.

Obtained data suggest that the compound may provide clinical benefit by preventing or delaying tumor progression through inhibition of tumor cell migration and invasion, rather than by reduction of primary tumor growth.[343]

AZD0530 inhibits Src activity in different breast cancer cell lines and interestingly suppresses the motile and invasive nature of endocrine-resistant breast cancer cells. Moreover, treatment of these cells with AZD0530 in combination with tamoxifen results in a reduction of Src and Fak activity together with a complete abrogation of their invasive behaviour *in vitro*.[345]

It has been reported that the combination of saracatinib and the ER (Estrogen Receptor) blocking fulvestrant, led to arrest of the ER-positive breast cancer cell cycle via p27, an enzyme that inhibits cyclin-dependent kinases. This combination slowed xenograft tumor growth *in vivo* more than either of the drugs alone. In contrast, saracatinib monotherapy rapidly gave rise to drug resistance, supporting further clinical investigation of this combination for women with ER-positive breast cancer.[346]

Saracatinib is also active in prostate cancer, it inhibited Src activation in a rapid and dose dependent manner in cells and reduced orthotopic DU145 xenograft growth by 45% in mice.[347]

Saracatinib is currently being tested in 33 clinical trials, mainly as anticancer agent, used alone or in combination with other drugs.

https://clinicaltrials.gov/ct2/results?cond=&term=saracatinib&cntry1=&state1=&recrs=

6.3.5 Purine derivatives

ARIAD Pharmaceutical researchers reported AP23464 **12** as a dual Src/Abl, ATP-competitive inhibitor, potently active on wt Bcr-Abl and on a panel of Bcr-Abl mutants (except T315I) with subnanomolar IC_{50} values.[348] In further optimization, they focused on inhibitors bearing an N-9 trans double bond and constructed a library of compounds bearing different C2 groups and aromatic/heteroaromatic moieties as double bond substituents, obtaining new cyclic and acyclic derivatives, which inhibited both Src and Abl at low nanomolar concentrations.

A very interesting derivative of this series is AP24283 **13**, C2 unsubstituted, bearing a dimethylphosphinoxide substituted aniline in C6 and a vinyl-linked methylindazole group in N9; **13** potently inhibits Src and Abl (IC_{50} values < 0.46 nM) and also the proliferation of cell lines driven by Bcr-Abl (K562 and wt Ba/F3) with at least 10-fold greater potency than imatinib. Interestingly, despite early concerns about the potential metabolic instability of the

vinyl linkage, the compound possessed good pharmacokinetic properties. In fact, the N-linked double bond was not rapidly metabolized. The compound is not orally bioavailable, presumably due to the rapid bioconjugation of the indazole NH. From a structural point of view, its most important feature is the trans vinyl linkage at N9 on the purine core, which projects hydrophobic substituents into the selectivity pocket behind the ATP site. Moreover, docking studies demonstrated that the vinyl-linked 4-substituted indazole preserves the intricate series of H-bonds observed in the crystal structure of compound **12**, previously reported by the authors. These purines bind to the DFG-in conformation of Src and Abl in a manner similar to dasatinib. Subsequently, with the aim to obtain purine derivatives targeting the DFG-out conformations of Src and Abl, the authors inserted privileged DFG-out targeting structural fragments, i.e. diarylamide groups in N9, as suggested by docking studies and by the analysis of previously reported crystal structures. The new DFG-out targeted dual Src/Abl inhibitors bear substituents only at the 6 and 9 positions of the purine scaffold as opposed to the 2,6,9-trisubstitution present in some of the DFG-in binder purines previously reported by the same company.

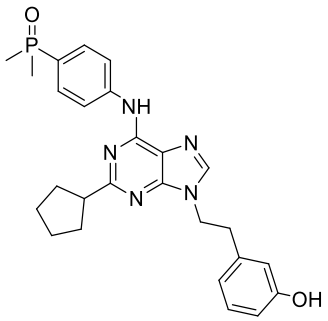

12 AP23464

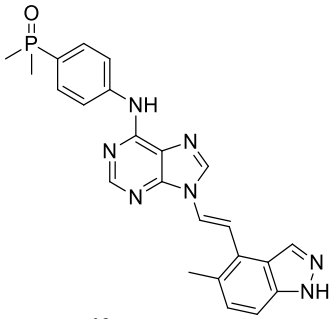

13 AP24283

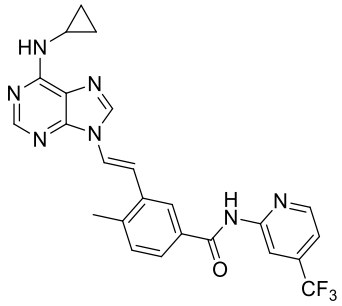

14 AP24226

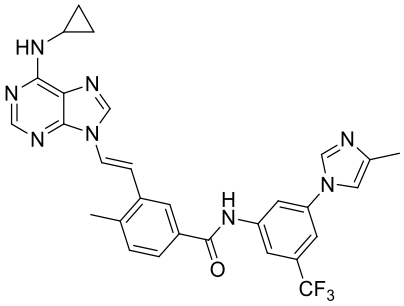

15 AP24163

In particular, compound AP24226 **14**, bearing a 4-methyl-N-[4-(trifluoromethyl)pyridine-2-yl]benzamide on the double bond, a C6 cyclopropylamino group instead of the

anilinophenylphosphine substituent (present in previously reported compounds) and C2 unsubstituted, proved to be the most interesting of the series, inhibiting Src and Abl with IC_{50} of 7 and 20 nM, respectively, in enzymatic assays and blocking K562 cell proliferation with potency in the low nanomolar range. Once-daily oral administration of AP24226 at a dose of 10 mg/kg significantly prolonged the survival of mice injected intravenously with wt Bcr-Abl expressing Ba/F3 cells. The compound also elicited dose-dependent tumor shrinkage with complete tumor regression in mice bearing subcutaneous xenografts of Src Y527F expressing NIH 3T3 cells. It inhibited both Src and Abl (with IC_{50} values of 7.6 and 25 nM respectively) and showed antiproliferative activity against a broad panel of Ba/F3 cells expressing clinically relevant Bcr-Abl mutants, included the T315I mutation, for which it showed an IC_{50} of 420 nM. Another interesting compound is AP24163 **15**. In enzymatic assays, it showed an IC_{50} value of 478 nM on T315I Abl. It is important to point out that the compound is the first DFG-out inhibitor that shows activity, even not high, on the mutant T315I, both in cellular and enzymatic assays and that it is active also on Src, differently from the majority of the DFG-out binders. Importantly it does not inhibit untransformed Ba/F3 cells up to a concentration of 5 μM.

The authors performed further studies to explain the biological behaviour of AP24163. In more detail they reported the crystal structures of Abl in complex with their inhibitors (both type I and type II) and demonstrated that, at least in part, AP24163 activity on Abl T315I can be attributed to the incorporation of a less sterically demanding vinyl linkage proximal to the increased bulk due to the presence of isoleucine as gatekeeper residue.

Moreover, a privileged DFG-out binding element (i.e. the N9 diarylamide substituent) is necessary to obtain activity on Abl T315I.[349]

6.3.6 Ponatinib

Ponatinib, AP24534, **16** is an imidazo[1,2-*b*]pyridazine synthesized by Ariad Pharmaceuticals Inc. researchers as a dual Src/Bcr-Abl kinase inhibitor that potently inhibits Src (IC_{50} = 4 nM) and Bcr-Abl in the low nanomolar range; in particular, it blocks native Abl (IC_{50} = 0.37 nM), Abl T315I (IC_{50} = 2.0 nM) and other clinically important Abl kinase domain mutants (IC_{50} = 0.30-0.44 nM).[350,351]

It has been approved by FDA for the treatment of resistant or imatinib-intolerant CML and Ph+ ALL patients, especially those harbouring the T315I mutation. It was soon temporarily suspended because of the increasing numbers of vascular occlusive events observed in

ponatinib-treated patients. On January 2014, the drug was re-authorized by FDA after a revised indication statement and a boxed warming, with alerts to the risk associated with its use.[352]

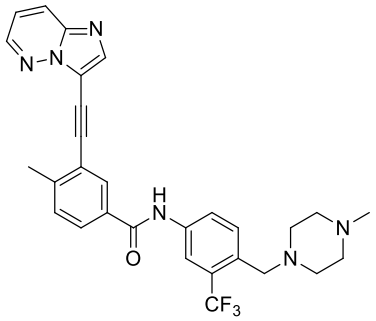

16 Ponatinib

Ponatinib activity is probably due to the inflexible acetylene linkage, a very unusual feature; the C-C≡C-C structural motif should be chemically and pharmacologically more stable than the corresponding N-C≡C-C moiety, present in other derivatives reported by the authors.

Ponatinib binds Abl and Src in the DFG-out mode; specifically, the imidazo[1,2-*b*]pyridazine core occupies the adenine pocket of the enzyme, the methylphenyl group fits to the hydrophobic pocket behind the gatekeeper residue and the trifluoromethylphenyl substituent binds tightly to the pocket induced by the DFG-out conformation of the protein.[330]

The rigid ethynyl linkage reduces steric repulsions with the bulk of the isoleucine side chain of the T315I mutant and is involved in favorable van der Waals interactions with Ile315.

The piperazine tail confers excellent cellular potency and improved aqueous solubility with reduced plasma protein binding, leading to good pharmacokinetic properties following oral dosing in rats and mice. Daily oral administration of the compound significantly prolonged survival of mice injected intravenously with Bcr-Abl T315I-expressing Ba/F3 cells.[330]

Ponatinib is a very promising drug for patients with CML and Ph^+ ALL who failed with imatinib, dasatinib and nilotinib therapy. This activity may be attributed to its ability to inhibit the T315I gatekeeper mutation and also to the fact that it targets a high number of kinases.[350]

6.3.7 HG7-85-01

During an iterative synthesis process followed by cellular assays, Weisberg *et al*. identified HG-7-85-01 **17** as a multitargeted inhibitor acting also on Abl and Src. In particular, HG-7-85-01 has been designed as a hybrid between the type I inhibitor dasatinib and the type II inhibitor

nilotinib; in fact it presents the aminothiazole hinge-interacting motif of dasatinib connected with the N-[3(trifluoromethyl)-phenyl]benzamide substructure of nilotinib, responsible for inducing the DFG-out flip, that is characteristic of type II kinase inhibitors. In a high-throughput screening on a panel of 353 human kinases (KINOMEscan), HG- 7-85-01 inhibited several kinases, including wt Bcr-Abl, T315I Bcr-Abl, Src, c-Kit and PDGFR in the low nanomolar range (1-10 nM). HG-7-85-01 potently and selectively inhibited the proliferation of 32D and Ba/F3 cells expressing wt Bcr-Abl and Bcr-Abl T315I and of two CML cell lines (K562 and KU812F), with IC_{50} values in the low micromolar range (IC_{50} = 0.06-0.14 μM). It also inhibited the proliferation of Ba/F3 cells transformed with human c-Src (IC_{50} = 190 nM). It has been shown that the inhibition of proliferation is mediated by selective inhibition of kinase activity, induction of apoptosis, and inhibition of cell-cycle progression. Very interestingly, an *in vivo* study demonstrated that combined treatment with nilotinib and HG-7-85-01 in mice harboring Bcr-Abl-positive leukemia led to a greater suppression of leukemic cell growth in mice than either drug alone. Crystallographic studies revealed that HG-7-85-01 binds to Src in the DFG-out inactive conformation forming the following hydrogen bonds:

- between the cyclopropyl amide NH and the backbone carbonyl of Met341;
- between the thiazole N and backbone NH of Tyr340 in the hinge region;
- between the benzamide carbonyl and the backbone NH of Asp404 of the DFG-motif;
- between the benzamide NH and side-chain carboxylate of Glu310 from the αC-helix;
- among the distal piperazine nitrogen (presumably protonated) and the backbone carbonyls of Val383 and His384.

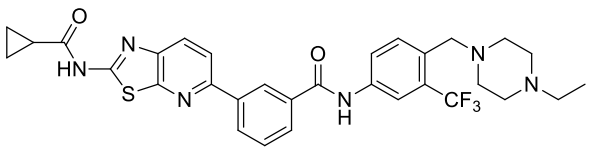

17

The most notable difference between the binding mode of HG-7-85-01 to Src compared with the binding mode of other inhibitors is the lack of a hydrogen bond between HG-7-85-01 and the side-chain hydroxyl of the gatekeeper residue Thr338. This loss is probably compensated by the formation of the extra hydrogen bond to the backbone of Met341 in the hinge region of the kinase. The authors point out that this type II ATP-competitive inhibitor showed the ability

to accommodate either a gatekeeper threonine, or a larger hydrophobic amino acid (such as isoleucine, methionine, or phenylalanine) without becoming a promiscuous kinase inhibitor. In fact, despite this tolerance at the gatekeeper position, HG-7-85-01 is a considerably more selective inhibitor than dasatinib.[353]

6.4 Fyn inhibitors

As previously reported above, Fyn overexpression or hyperactivation is involved both in brain pathologies and in tumors; for these reasons, the search for Fyn inhibitors represents an expanding field of study. Selective agents could result useful for their potential clinical implications and, in addiction, could be essential for elucidating the biological roles of the targeted enzyme. Unfortunately, because of the strict similarity of SFK members in their catalytic domains, at the moment no selective Fyn inhibitor has been reported. Indeed, all the published inhibitors also act on other members of SFKs, or in some cases also on other TKs. The design and the synthesis of inhibitors are frequently based on the study of the structure of the target enzyme. Regarding Fyn, only one three-dimensional structure of the kinase domain (2DQ7) is present in the Protein Data Bank (PDB); this structure reports the Fyn kinase domain bound with the "pan-kinase" inhibitor staurosporine **18** (**Fig. 21**), but unfortunately shows low resolution (2.8 Å).[354] In this structure the staurosporine molecule binds to the large groove between the N- and C-lobes by means of three hydrogen bonds and some hydrophobic interactions. The NH and keto oxygen of lactam ring of the inhibitor make a pair of hydrogen bonds with the backbone carbonyl oxygen of Glu343 and the backbone NH of Met345, respectively, defined as the hinge region, involved in the ATP-adenine ring binding. Their numbers in the crystal structure deposited in the PDB become respectively Glu83 and Met85. A third hydrogen bond occurs in the ribose binding pocket of Fyn. The methylamino nitrogen of the staurosporine glycosidic ring forms a hydrogen bond with Ala394 (Ala134 in the 2DQ7).[104]

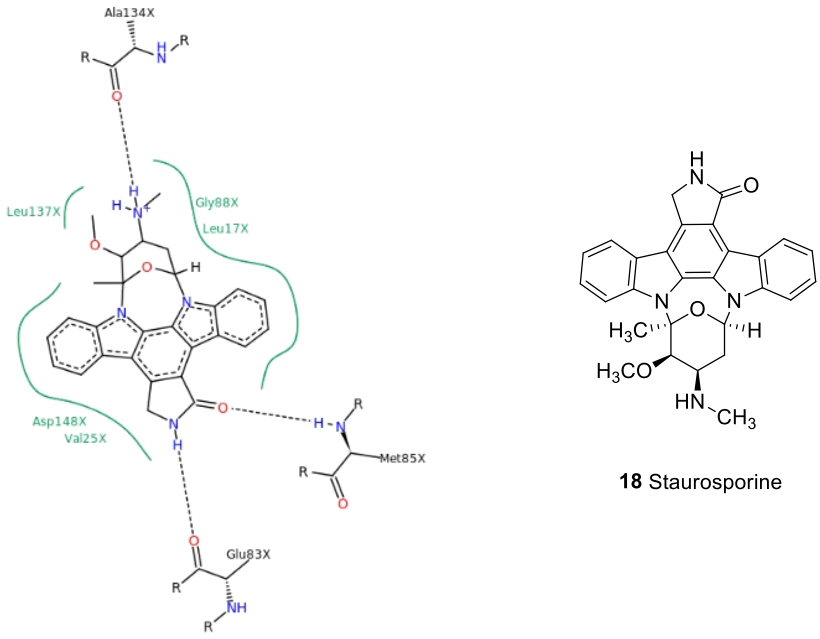

Fig. 21. Schematic representation of the interaction Fyn-staurosporine (2DQ7).

6.4.1 Pyrazolo[3,4-*d*]pyrimidines

The pyrazolo[3,4-*d*]pyrimidines PP1 (**7**) and PP2 (**8**) were previously discussed in "dual Src and Abl inhibitors" section. However, they represent the first nanomolar inhibitors of Fyn (IC_{50} = 4-6 nM) and they have become lead compounds for the development of new promising molecules. In fact, even if the poor biopharmaceutical property of PP1 and its analogs appeared to limit their potential use as drugs, their discovery represented a significant advance in the use of TK inhibitors in the study of different cell functions.

6.4.2 Purines

Derivative **19**, AP23464 is a purine compound developed by Ariad, which targets c-Src with picomolar affinity (450 pM). The compound showed also notable activity against Abl, Fyn, Yes, Lck, Lyn, EGFR, FGFR, PDGFR, C-Kit, b-Raf, all kinases characterized by a small gatekeeper residue.[355,317]

Another 2,6,9-trisubstituted purine, **20** again from Ariad, is a good Src inhibitor, even if it is less active than AP23464. The compound is however very interesting because incorporates in position 6 a bone-targeting anilino biphosphonate group that confers good affinity to hydroxyapatite, used by the authors to evaluate the affinity of the compound to the bone tissue.

It showed an IC_{50} value of 41 nM for Src and similar value for Fyn, with good selectivity over a panel of several kinases.[356]

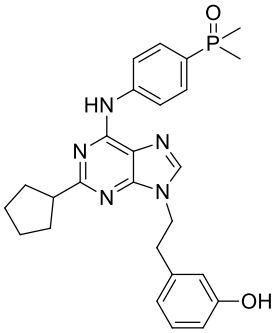

19 AP23464

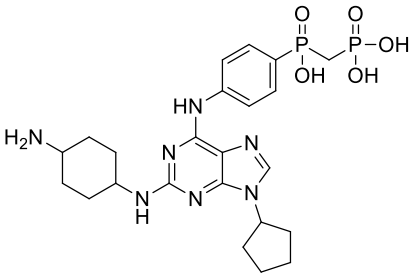

20

6.4.3 Other pyrimidines and fused-pyrimidines

Saracatinib (**11**), cited above, is active on the different members of this TK family in the low nanomolar range. Particularly, it inhibits Fyn with an IC_{50} value of 10 nM in enzymatic assay and it was studied in clinical trials for the treatment of AD.[357,358]

Quinazoline derivatives have been also reported in the patent literature. For example, Janssen Pharmaceutica patented a series of such derivatives as antitumor agents, acting as SFK inhibitors. Compound **21** inhibits Fyn with an IC_{50} value of 6.69 nM.[359]

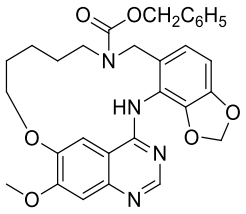

21

Moy *et al*. synthesized a type II inhibitor **22**, which exhibits nanomolar inhibitory activity against multiple kinases. The compound bears a pyrazolo[1,5-*a*]pyrimidine core linked to a tetramethylpiperidine-1-oxyl radical that, possessing a very slow electronic relaxation time and prolonged radical stability, is able to be used in the NMR spectroscopy of the complex with the enzyme. This derivative is particularly active on VEGFR2 (IC_{50} = 3.3 nM), Abl (IC_{50} = 5 nM)

and on SFKs, including Fyn (5 nM). Since the compound is very active and endowed with paramagnetic properties, it could represent a useful tool in a screen for non-ATP site binders.[360]

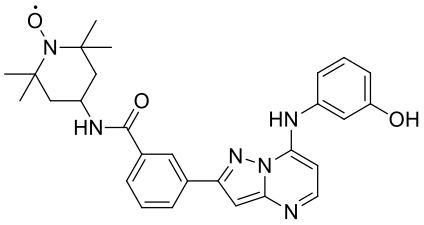

22

In a wide study, Bamborough *et al*. at GlaxoSmithKline tested more than 500 compounds against a panel of over 200 protein kinases chosen to represent kinase inhibitor space. Significant results include the identification of hits against new kinases and the expansion of the inhibition profiles of several literature compounds. A detailed analysis of the data through the use of affinity fingerprints gave interesting indications for biological target selection, the choice of tool compounds for target validation, lead discovery and optimization. These results show how broad cross-profiling can provide important insights to assist kinase drug discovery. Regarding Fyn inhibitors, they found that the bis-anilinopyrimidine **23** potently inhibits also Fyn with an IC_{50} value of 0.4 nM.[361]

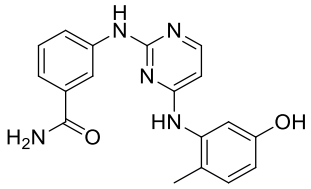

23

Amgen researchers synthesized a series of aminopyrimidine amides as potent, selective inhibitors of the lymphocyte specific kinase Lck. The compounds are active not only in Lck (IC_{50} in the subnanomolar range), but inhibit also other SFK members including c-Src and Fyn. The most interesting compound is **24** that possessed IC_{50} values of 3 nM against c-Src and Fyn and 0.6 nM against Lck.[362]

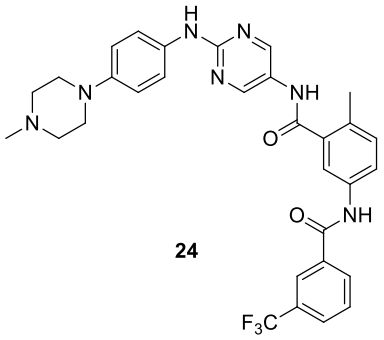

24

6.4.4 Quinolines and analogous derivatives

Using a high-throughput yeast-based assay, Wyeth Pharmaceuticals researchers identified a family of 4-anilinoquinoline-3-carbonitriles as interesting SFK inhibitors. Compounds **25**[363] and **26**[364] showed IC_{50} of 1.5 and 2.9 μM, respectively, in assays measuring Fyn-dependent cell proliferation on rat fibroblasts transfected with activated Fyn.

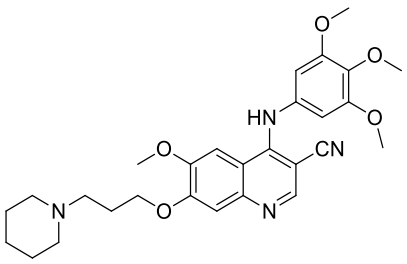

25

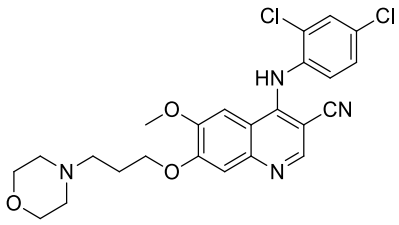

26

Subsequent SAR studies led to the optimization of the substitution of the anilino moiety and to the introduction at C7 of a 3-(4-methylpiperazin-1-yl)propoxy group, providing the most interesting compound of this chemical class, **10**, bosutinib, previously reported as dual Src/Abl inhibitor. Regarding Fyn, the compound has an IC_{50} value of 410 nM for the inhibition of Fyn dependent cell proliferation, with a selectivity for Src over Fyn of only about 4 fold in cell based assay.[338]

4-Anilino-7,8-dialkoxybenzo[*g*]quinoline-3-cabonitriles derived from structural modifications of 4-anilinoquinoline-3-carbonitriles, such as bosutinib, are subnanomolar and selective SFK inhibitors. One of the most active compounds, **27**, in cell based assays showed an IC_{50} value of 37 nM for Src-transformed fibroblasts and of 140 and 420 nM for Lyn- and Fyn-transformed fibroblasts, respectively, indicating some activity also on Fyn.[365]

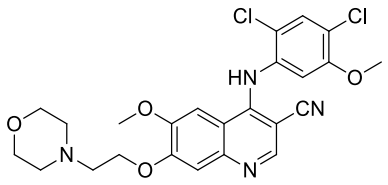

27

6.4.5 Thieno[2,3-*b*]pyridine carbonitriles

Wyeth researchers also synthesized a series of 2-alkenyl thieno[2,3-*b*]pyridine carbonitriles, bearing a thieno-pyridine core isoster to the quinolinic one of bosutinib, as potent inhibitors of protein kinase C theta (PKCθ), a serine/threonine kinase espressed in lymphocytes and mast cells and involved in the inflammatory response. In the screening to assess compounds selectivity, they found that the most active derivatives also inhibited SFKs. Interestingly, compound **28** possessed an IC_{50} value of 25 nM for Fyn and comparable inhibition also versus Hck and Lck, while the IC_{50} value for c-Src was significantly higher (330 nM).[366]

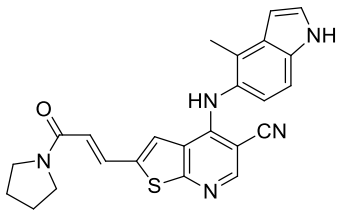

28

6.4.6 Thiazole-carboxamides

Dasatinib **9**, as reported above, demonstrated to be active towards Abl and many SFKs.

Li *et al*. performed an enzymatic and phosphoproteomic characterization of dasatinib action in NSCLC and identified nearly 40 different kinase targets of dasatinib. These include SFK members (Lyn, Src, Fyn, Lck and Yes), other non-receptor tyrosine kinases (Frk, Brk and Ack) and receptor tyrosine kinases (EPH, DDR1 and EGFR).

Using drug-resistant gatekeeper mutants, they showed that particularly Src and Fyn, as well as EGFR, are relevant targets for dasatinib action, getting further insight both in dasatinib action and in Fyn involvement in this particular malignancy.[367,104] Other thiazole derivatives, in particular a series of 2-amino-5-carboxamido-derivatives structurally similar to dasatinib previously reported by Bristol-Myers Squibb researchers as Lck inhibitors, are also active on

Fyn and on Src: compound **29** showed IC_{50} values of 35, 71 and 10 nM for Lck, Fyn and Src, respectively.[368] A family of compounds structurally related to dasatinib, bearing 2-aminoheteroaryl groups has been reported by the same authors as potent and orally active SFK inhibitors. Among these, compound **30** resulted one of the most interesting derivatives, possessing IC_{50} values of 1-2 nM for all SFKs, including Fyn, and excellent selectivity against receptor TK and serine/threonine kinases.[369]

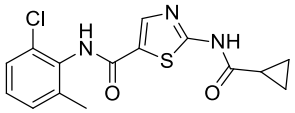

29

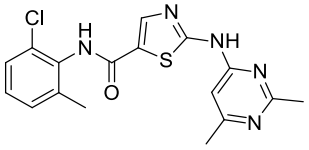

30

6.4.7 Different heterocyclic compounds

Indolinone derivatives represent an important family of TK inhibitors. Particularly **31**, SU6656, synthesized by Sugen, exhibits selectivity for Src and other members of SFK, including Fyn, with IC_{50} values of 280, 170, 20, 130 nM versus Src, Fyn, Yes and Lyn, respectively.[370]

Other tetrahydroindole-based indolin-2-ones, reported by the same company, bearing an amidic substituent in C3 of the tetrahydroindole moiety, showed to be potent SFK inhibitors.

Regarding Fyn inhibition, the most active compound is **32** that possessed an IC_{50} value of 50 nM on Fyn and similar data also on the other SFK members with moderate/good selectivity versus VEGFR2 and FGFR1.[371] Klic-Kurt *et al*. have synthesized a series of oxindole derivatives active as Fyn, Lyn e Hck inhibitors. Three of these compounds showed a selective activity toward Fyn. Docking study was developed to evaluate the receptor-binding properties of **33**, the most active compound, and it has been demonstrated that this molecule inhibits Fyn with an ATP-competitive mechanism.[372]

Bristol-Myers Squibb researchers synthesized a series of imidazo[1,5-*a*]pyrido[3,2-*e*]pyrazines as Lck inhibitors. The compounds were active on all SFK members, being **34**, BMS-279700 the most interesting derivative with IC_{50} values of 4, 4, 5, 0.5 nM versus Lck, Src, Fyn and Lyn, respectively.[373] A series of (6,7-dimethoxy-2,4-dihydroindeno[1,2-*c*]pyrazol-3-yl)phenylamines has been synthesized as inhibitors of PDGFR. One of the most active compounds, **35** showed some activity also on SFKs, with an IC_{50} value of 0.378 μM on Fyn.[374,104]

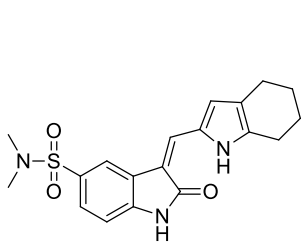

31 SU6656

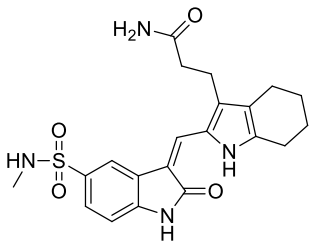

32

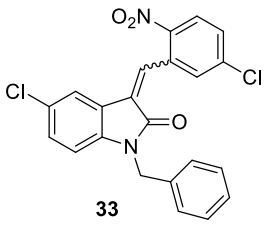

33

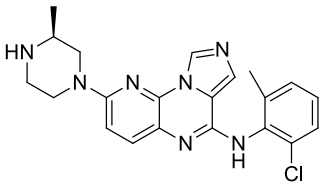

34 BMS-279700

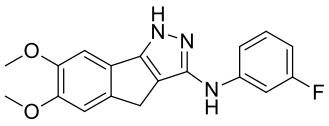

35

Rottapharm Biothec has patented a series of heterocycles active as Fyn inhibitors. In particular, the authors reported that these compounds should be potential drugs for Fyn-mediated diseases. Two of these molecules, **36** and **37** showed an inhibitory activity against Fyn with IC_{50} values of 9 nM and 4 nM, respectively.[375]

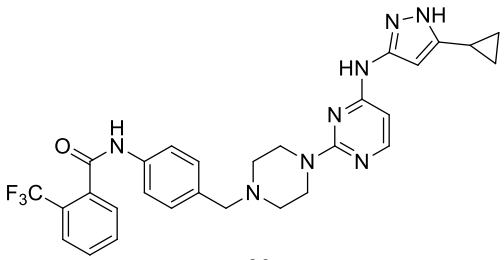

36

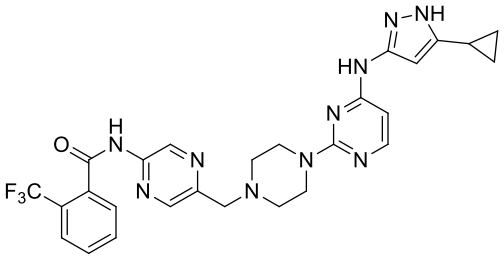

37

6.4.8 Phenolic compounds

Caffeic acid (3,4-dihydroxycinnamic acid) **38** is present in many foods, including coffee. Different studies suggested that caffeic acid exerts anticarcinogenic effects, but little is known about the underlying molecular mechanisms and specific target proteins. Kang *et al*. found that caffeic acid suppressed UVB-induced skin carcinogenesis by directly inhibiting Fyn kinase and downstream MAPKs. They also demonstrated that caffeic acid directly binds with Fyn in a non-ATP-competitive manner.[376,104]

Rosmarinic acid **39**, the ester of caffeic acid with 3,4-dihydroxyphenyl lactic acid, is a natural polyphenol antioxidant carboxylic acid found in many Lamiaceae herbs, including Salvia officinalis and Rosmarinus officinalis; it is responsible for antiinfective, antiinflammatory and antioxidative effects of these plants. It has been reported that the compound showed protective effects against Aβ-induced neurotoxicity in PC12 cells and reduced impairment of memory induced by Aβ in a mouse model. It also displayed anti-amyloidogenic effects for Alzheimer's Aβ fibrils *in vitro*. Moreover, rosmarinic acid induced apoptosis in Jurkat and peripheral T-cells.[104] Jelić *et al*., using immunochemical and in silico methods, discovered that rosmarinic acid is a Fyn inhibitor. In the homology model of Fyn prepared by the authors two possible binding modes of rosmarinic acid were evaluated, i.e. near to or in the ATP-binding site of Fyn kinase domain. Indeed, from docking experiments it resulted that rosmarinic acid could bind Fyn in the ATP-binding site or in the opposite site from the ATP-binding site. This "binding site 2" is in the kinase domain but oriented toward the linker which connects SH2 and the kinase domain. Enzyme kinetic experiments revealed that Fyn is inhibited in a linear-mixed non-competitive mechanism of inhibition by rosmarinic acid, indicating that rosmarinic acid binds to the "binding site 2" of Fyn. Inhibition value of Fyn by rosmarinic acid was also reported: the compound possessed an IC_{50} value of 1.3 μM, tested by ELISA method.[377]

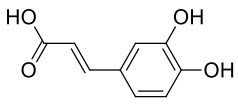

38 caffeic acid

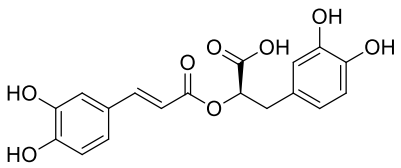

39 rosmarinic acid

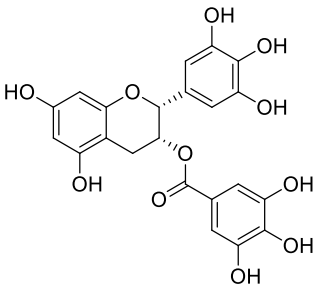

40 (-)-epigallocatechin gallate

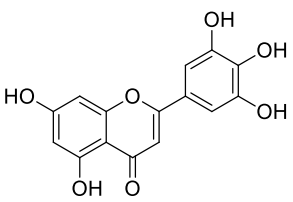

41 myricetin

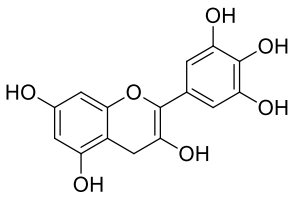

42 delphinidin

Also a number of flavonoids possessed inhibitory activity on Fyn. Dong *et al*. found that (-)-epigallocatechin gallate **40** (the ester of epigallocatechin and gallic acid), a flavonoid present in green tea and possessing cancer preventive action, inhibited EGF-induced Fyn kinase activity and phosphorylation. Very interestingly, it binds to the Fyn-SH2 domain (but not to the SH3 domain) with a K_d value of 0.367 μM in epidermal mouse skin cells (JB6 C141 cells) and inhibits cell transformation promoted by EGFR.[378]

Myricetin **41** is a naturally occurring flavonol, present in several foods, including red wine. Jung *et al*. reported that the compound inhibits the formation of non-melanoma skin cancer (related to chronic exposure to UVB radiation) in the SKH-1 hairless mouse model. Interestingly they demonstrated that myricetin activity is due to Fyn inhibition with subsequent attenuation of UVB-induced phosphorylation of MAPKs. Myricetin exerted similar inhibitory effects to that of PP2. Mouse skin tumorigenesis data clearly showed that pretreatment with myricetin significantly suppressed UVB-induced skin tumor incidence in a dose-dependent manner. Docking data suggest that myricetin is docked to the ATP-binding site of Fyn and behaves as an ATP-competitive inhibitor. Therapeutic inhibition of Fyn by myricetin might provide clinical benefits in skin cancer treatment.[379] Delphinidin **42**, a major anthocyanidin present in red wine and berries, inhibits TNF-alpha induced COX-2 expression by directly inhibiting Fyn kinase activity, consequently suppressing the activation of MAPK and PI3K pathways. The compound inhibits Fyn kinase activity and directly binds with Fyn in a non ATP-competitive manner. This effect suggests that delphinidin could contribute to the chemopreventive potential of red wine and berries.[380,104]

6.4.9 Prenylated polyphenol inhibitors

Prenylated natural compounds have demonstrated different biological effects and several studies were developed to evaluate the antioxidant and cytoprotective activity of prenylated polyphenol. *In vitro* studies and cell-based assays showed that kazinol E (**43**) is able to inhibit the Fyn phosphorylation with a similar effect to SU6656 (**31**). Treatment with **43** also inhibits the oxidative stress which is facilitated by Fyn phosphorylation.[381]

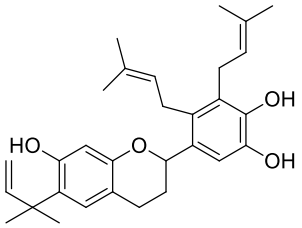

43 kazinol E

6.4.10 Cycloalkane-fused derivatives

Koo *et al*. have studied the possibility of cycloalkane-fused dithiolethiones (CDTs), or other congeners, to increase antioxidant capacity in association with Fyn inhibition.

It has been observed that oxidative injury caused by arachidonic acid and iron promoted the phosphorylation and the activation of Fyn which was decreased by SNU1A (**44**) treatment.

Also SU6656 (**31**), a Fyn inhibitor, shows a similar effect to SNU1A. These results demonstrated that the reduction of Fyn activity protects the mitochondria from oxidative injury.[382]

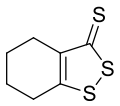

44 SNU1A

6.5 Hck inhibitors

6.5.1 Pyrazolo[3,4-*d*]pyrimidines

One of the first TK inhibitors reported to be also active on Hck is PP1 **7**, discussed above, which shows an IC_{50} value of 20 nM for this enzyme.[198] Sicheri *et al*., which determined the crystal structure of the autoinhibited form of Hck in complex with PP1, demonstrated that PP1 occupies the adenine binding pocket where establishes hydrogen bonds with Thr338, Glu339, Met341 and Lys295. In detail, the amino group of PP1 is hydrogen bonded to the hydroxyl group of Thr338 as well as to the backbone carbonyl of Glu339. The nitrogen at position 5 accepts a hydrogen bond from the NH backbone of Met341 and the nitrogen at position 2 interacts with Lys295 by a water molecule (W1). In addition to polar interactions, the inhibitor makes hydrophobic contacts with Ala293, Leu273 and Val281 in the N lobe as well as with Met341 and Leu393 in the C lobe. Residues 409-423 form a well-packed hydrophobic pocket, which

accommodates the methyl-phenyl group of PP1 and two well-ordered water molecules (W2 and W3). Also PP2, **8** that is closely related to PP1, potently inhibits SFKs, with an IC_{50} value of 5 nM for Hck, with a similar binding mode.[331]

A very active derivative, A-770041 **45**, shows IC_{50} values of 0.147, 1.22 and 1.18 μM on Lck, Hck and Lyn, respectively, while it is less active on the other SFK members (9.05 μM for Src and 44.1 μM for Fyn) and almost inactive on different TKs.

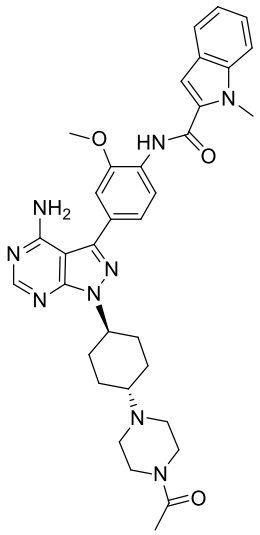

45 A-770041

Maly *et al.* described a new crosslinking strategy that enables rapid and quantitative profiling of protein kinase active sites in cell lysates and cells.[383] The authors applied this methodology to the SFK members Src and Hck and identified a series of conformation-specific, ATP-competitive inhibitors that have a distinct preference for the autoinhibited forms of the kinases, modulating binding interactions of the regulatory domains SH2 and SH3 of Src and Hck. Even though kinase phosphotransfer activity is essential for a huge number of cellular processes, new evidence suggests that kinases also have a number of important non-catalytic functions, such as protein scaffolding complex formation, allosteric regulation of other enzymes and modulation of protein-protein and protein-DNA interactions.[384] First, the authors prepared a cell-permeable, ATP-competitive photoprobe **69** that covalently modifies the ATP-binding sites of protein kinases if exposed to UV light. The probe is formed by three parts:

- a potent ATP-competitive inhibitor (dasatinib);
- a photoreactive benzophenone crosslinker;

- a hexylchloride tag that selectively labels the active site of the self-labelling protein called HaloTag.

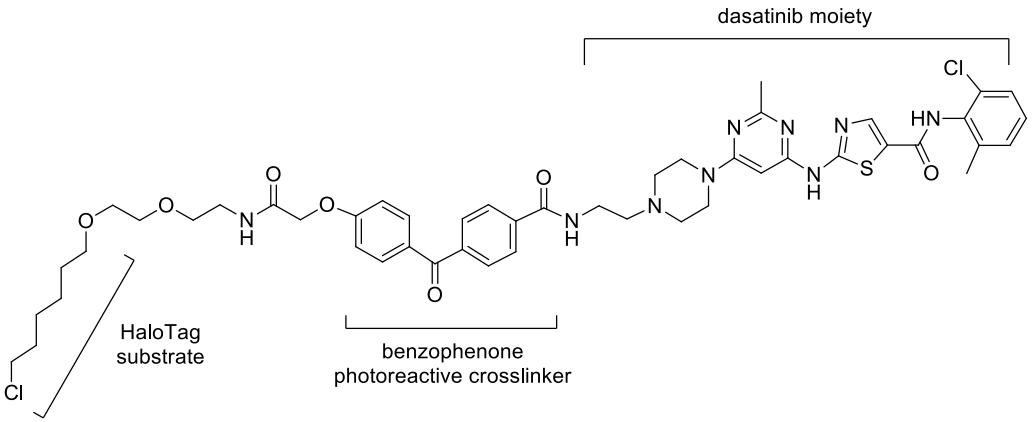

46

The probe was linked both to activated Src and Hck, and to autoinhibited forms of these kinases (i.e. Hck SH3eng and Hck SH2eng, which are inhibited forms of Hck). Then, a number of ATP-competitive SFK inhibitors were used in photocrosslinking competition assays with **46** and the purified SFK constructs. The IC_{50} values obtained in this test demonstrated that several inhibitors, including the pyrazolo[3,4-*d*]pyrimidines **47**, **48** and **49** are more effective competitors of the autoinhibited Hck constructs (Hck SH3eng and Hck SH2eng) than of activated Hck. These data have direct implications for the pharmacological inhibition of multidomain protein kinases, including SFKs. These inhibitors, which stabilize an inactive ATP-binding site conformation and promote the intramolecular recruitment of regulatory interactions, could prevent several kinase activation signals, providing important insights into the regulation of SFKs.[383]

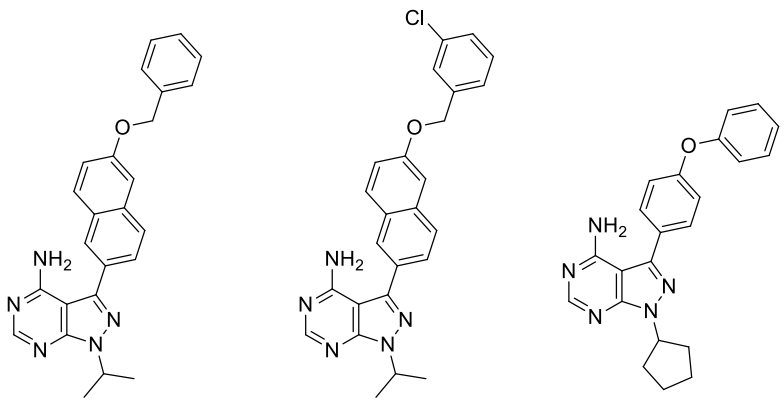

47 **48** **49**

Saito *et al.* performed a combination of a high-throughput enzyme inhibition assay, in silico screening and X-ray crystallography with the aim of identifying small molecule Hck inhibitors.[385] As a result, the pyrrolopyrimidine derivative **50**, RK-20449, was identified by screening about 48,000 commercially available small molecules. The compound showed an IC_{50} value of 0.43 nM on Hck in enzymatic assays. The crystal structure of Hck in complex with RK-20449 confirms that the compound binds the ATP-binding pocket with the same orientation of PP1. The phenoxy moiety established more hydrophobic contacts than the p–methyl group of PP1 within the hydrophobic pocket formed by Met314, Val323, Leu325, Ile336, Ala403, Phe405 and Leu407. In addition to the interactions with the hinge region and the hydrophobic pocket, the methyl-piperazine group of the ligand interacts with Asp368. These additional contacts are probably responsible for the higher potency of RK-20449 as compared to PP1 in the Hck inhibition.[385]

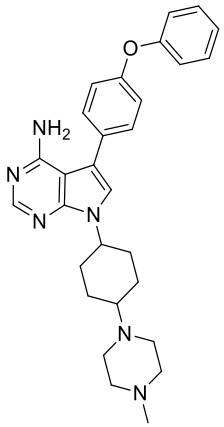

50 RK-20449, A-419259

Later, another crystal structure of RK-20449 and Hck, similar to Saito's one, was reported by Parker *et al*.[386]

Compound **50** had been already reported by Calderwood *et al*. with the name of A-419259 as a potent SFK inhibitor, with IC_{50} values in the low nanomolar range.[387] The same authors investigated the contribution of Hck to Bcr-Abl signalling. For this purpose, they developed an A-419259-resistant mutant of Hck by replacing the gatekeeper residue (Thr338) in the inhibitor binding site with a bulkier methionine residue (Hck-T338M). This mutation avoids the inhibitor from binding to the modified enzyme. Indeed, the T338M mutation induces dramatic resistance

to A-419259, increasing the IC_{50} value by almost 30-fold from 11.26 nM for wt Hck to 315.6 nM for the T338M mutant. Expression of Hck-T338M in K562 CML and Bcr-Abl-transformed TF-1 myeloid cells blocks the apoptotic and antiproliferative effects of A-419259. These effects correlate with persistence of Hck-T338M kinase activity in the presence of the compound. In contrast, control cells expressing equivalent levels of wt Hck retain sensitivity to the inhibitor. In this study, by pairing an inhibitor-resistant SFK mutant with a broad-spectrum SFK inhibitor, it was established new pharmacological evidence for Hck in Bcr-Abl survival signalling.[198]

Tintori *et al*., with the aim of identifying novel Hck inhibitors, applied a structure-based virtual screening protocol, which led to the selection of candidates to be tested in a cell-free assay. First, an in-house library of pyrazolo[3,4-*d*]pyrimidine derivatives, which were previously shown to be dual Abl and c-Src inhibitors,[388,389] was analyzed by docking studies within the ATP-binding site of Hck to select the best candidates. Next, the same computational protocol was applied to screen a database of commercially available compounds. Some compounds were found active against Hck, with the best ones showing inhibitory activity towards isolated Hck in the sub-micromolar range. Interestingly, the three identified hit compounds **51** (an in house compounds), **52** and **53** were predicted to be able to perfectly fill the enlarged hydrophobic cavity, which characterizes the inactive conformation of Hck. Furthermore, selected compounds showed an interesting antiproliferative activity profile against the human leukemia cell line KU-812, and were found to block HIV-1 replication at sub-toxic concentrations.[390]

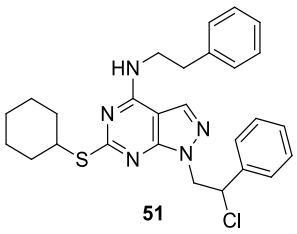

51

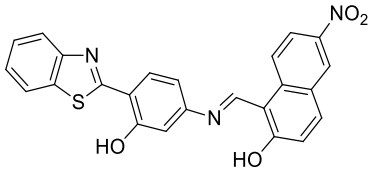

52

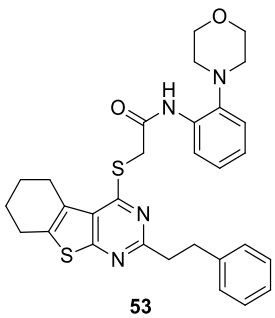

53

6.5.2 Type II inhibitors and photoaffinity probes

Some compounds designed by Maly *et al*., based on the central chemical scaffold of imatinib, demonstrated a good activity even towards Hck. The most active one is DSA7, **54**, which shows an enzymatic inhibitory activity with an IC_{50} value of 2.2 nM.[391]

Continuing their studies on kinases, the authors also prepared active site-directed probes for profiling kinases in cells. In detail, aside from compound **54**, they identified a number of ligands, including **55**, which specifically bind kinases in the DFG-out conformation. These inhibitors, commonly named type II inhibitors, contain moieties that make contacts similar to those of the adenine ring of ATP and hydrophobic substituents that occupy the pocket created by the movement of the Phe side chain in the DFG-motif [392]. Then, the authors designed and synthesized the photoaffinity probes **56** and **57** derived from **54** and **55**, respectively. Each probe contains three components:

- a high affinity ligand that selectively recognizes the active sites of protein kinases;
- a reactive group that is able to covalently modify probe-bound kinases;
- a photocrosslinking group that allows visualization and/or purification.

In the probes, **56** and **57** the 3-trifluoromethylphenyl groups of the precursors were replaced with 3-trifluoromethylphenyl diazirine moieties, and the para-substituents of the anilino group of these inhibitors were functionalized with alkyne tags. The compounds and the probes were tested on a panel of kinases, including Hck, on which they showed IC_{50} values in the low nanomolar range.[198]

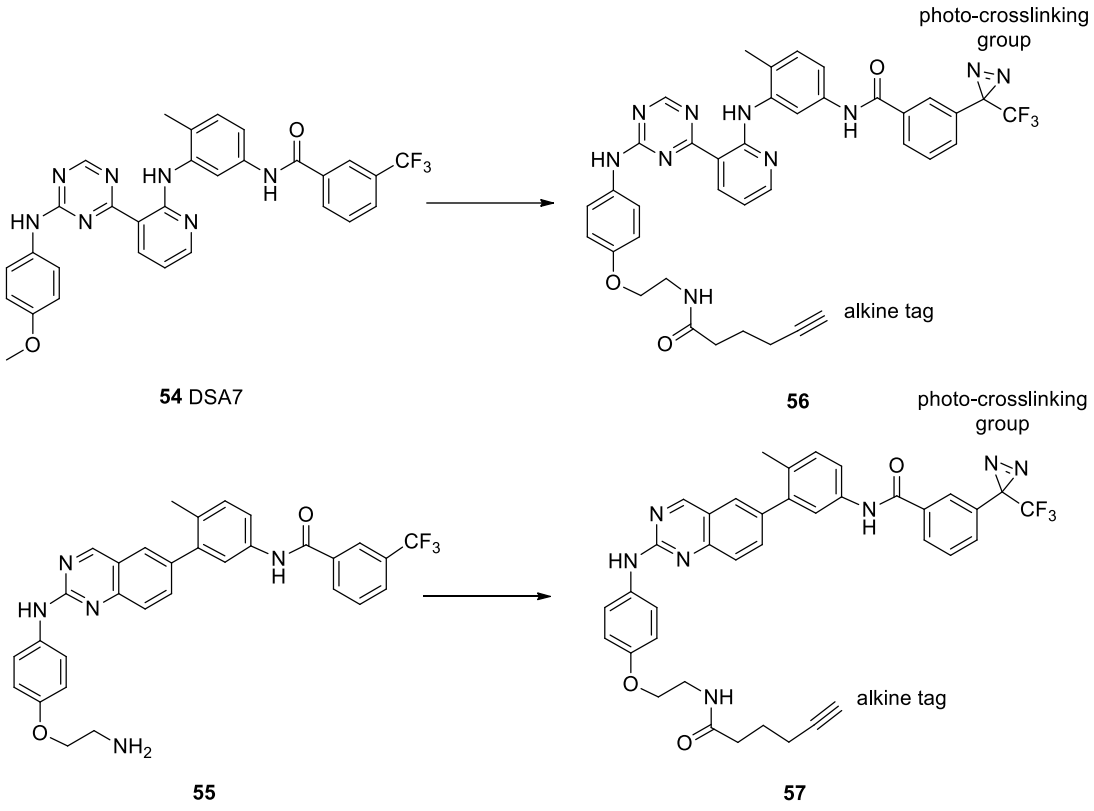

6.5.3 Compounds inhibiting the Hck-Nef binding

Because of its role in HIV-1 replication, Nef is an attractive target for drug discovery. Some derivatives have been reported to inhibit the binding Hck-Nef. Even if some of these compounds do not inhibit the catalytic activity of Hck, their actions are connected to the inhibition of Hck functions. In this regard, Smithgall *et al*. identified compounds that inhibit Nef-mediated Hck activity and also block Nef-dependent HIV-1 replication *in vitro*. The inhibitors have been discovered by a HTS (high-throughput screening) that couples Nef to the activation of Hck. Using this screen, the 4-amino substituted diphenylfuropyrimidine **58** was identified as a strong inhibitor of Nef-dependent Hck activation. This compound also exhibits remarkable antiretroviral effects, blocking Nef-dependent HIV replication in cell culture.

Moreover, structurally related analogs, including **59** and **60**, showed similar Nef-dependent antiviral activity, allowing to identify the diphenylfuropyrimidine substructure as a new scaffold for antiretroviral drug development. These ligands show a remarkable difference in both potency and efficacy for Nef-activated Hck versus Hck alone. For example, compound **60** shows an IC_{50} value > 30 μM when tested versus Hck alone and of 2.0 μM when tested on Hck

in the presence of Nef. This may be because Nef influences the conformation of the ATP-binding site of Hck and facilitate compound binding.[393]

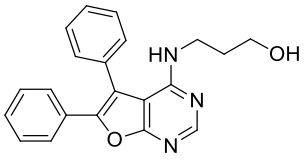

58 DFP-4AP

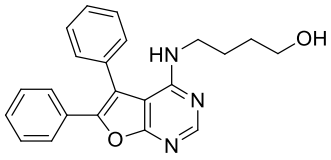

59 DFP-4AB

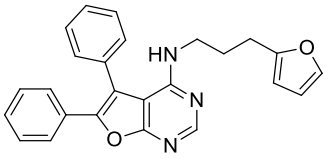

60 DFP-4APF

This study further demonstrated that coupling non-catalytic HIV accessory factors with host cell target proteins addressable by HTS may open new avenues for the discovery of anti-HIV agents. The same authors applied this HTS method on a larger and more diverse chemical library of about 220,000 compounds. Using this approach, they identified the phenylpyrazolo derivative **61**, which blocks Nef-dependent Hck activity in the low micromolar range and is also active on several Nef variants. The compound exhibits remarkable selectivity for Hck inhibition in the presence of Nef. Indeed, it blocks the kinase activity of the Nef-Hck complex *in vitro* with an IC_{50} value of 2.8 μM, whereas its activity against Hck alone is > 20 mM. The authors determined that the compound directly interacts with Nef, and prevents its dimerization, a property implicated in many Nef functions.[198]

Compound **62** is a small molecule that was previously shown to block several proline-rich motif-SH3 domain binding. Hassan *et al*. demonstrated that **62** is a non-kinase inhibitor that effectively inhibits Nef-Hck binding and blocks Nef-induced skewed Golgi localization of an active form of Hck (Hck-P2A), but shows no inhibition on Hck-P2A kinase activity.[394] Suzu *et al*. performed further studies on compound **62**, confirming that it competes for Nef binding with Hck and could be useful as anti-HIV agent, since it reduces Nef-mediated viral infectivity enhancement. In detail, this compound inhibits Hck SH3-Nef binding, and the inhibition is more evident when Nef was pre-incubated with **62** before its incubation with Hck, indicating that both Hck SH3 and **62** directly bind to Nef and that their binding sites overlap. The authors underlined that it remains to establish how **62** reduces Nef mediated infectivity enhancement. Since both **62** and the Hck SH3 domain bind directly to overlapping domains of Nef and reduce viral infectivity, the authors speculated that the inhibitory effects are due to the inhibition of the interaction of Nef with host proteins.[395]

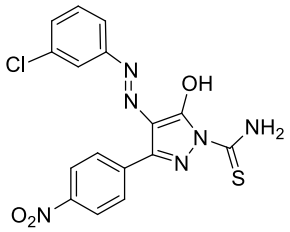

61

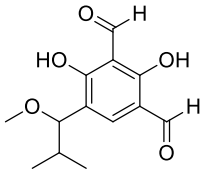

62

6.5.4 Other compounds

The anilino-quinazoline saracatinib **11** (reported above), potent and highly selective dual Src/Abl inhibitor previously discussed, demonstrated to reduce Hck phosphorylation in BV173 CML cells, at a dose of 0.5 μM.[396]

The ATP-based SFK inhibitor **63**, AP23846 inhibits Hck with an IC_{50} value of 0.3 nM, with a good selectivity profile when tested on a panel of different kinases.

Bristol-Myers Squibb synthesized differently substituted 5-carboxamidothiazoles as SFK inhibitors, also active on Hck. One of the first members of this family is derivative **64**, which was shown to be a potent SFK inhibitor, with a good activity towards Hck (IC_{50} = 310 nM). Successively, the same researchers reported another family of thiazole-5-carboxamides, bearing 2-aminoheteroaryl substituents, as potent and orally active Lck inhibitors. Actually, the most active compound, **65**, inhibits all the SFK members, including Hck, with similar potency (IC_{50} values in the range 1-2 nM).[369]

The benzimidazolo-pyrimidine **66**, PG-1009247, which was developed as a Lck inhibitor by Sabat *et al*., showed IC_{50} values of 46 nM towards Hck, together with a good inhibition of IL-2 production and good aqueous solubility.[198,397]

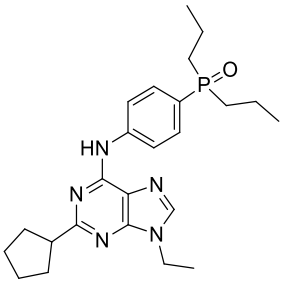

63 AP23846

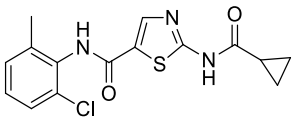

64

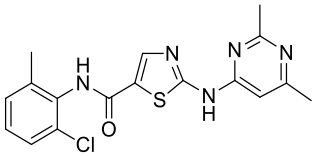

65

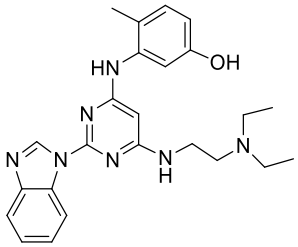

66 PG-1009247

Narita *et al.* patented a compound, **67**, for the treatment of AML, this molecule resulted a Hck inhibitor and stopped the leukemic cells proliferation.[398]

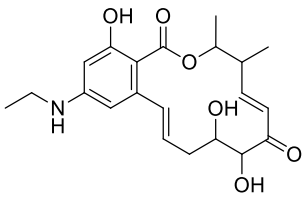

67

Bakuchiol **68** is a meroterpene present in the medicinal plant Psoralea corylifolia, which has been traditionally used in China, India, Japan and Korea for the treatment of different upsets. It has been recently reported that bakuchiol is able to inhibit EGF in neoplastic cells. Moreover, **68** reduces the motility of these cells and inhibits anchorage-independent growth of A431 human epithelial carcinoma cells. Hck, Blk and p38MAPK have been identified as targets of this compound.[399]

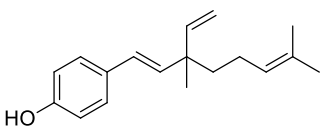

68

6.6 Sgk1 inhibitors

Different studies have shown that some "selective" inhibitors are actually active on many kinases, e.g. indolinone derivative SU6656 **31**, cited above as SFKs inhibitor, has been demonstrated to be also an inhibitor of other kinases, including STKs. Compounds CGP57380 **69**, D4476 **70** and SP600125 **71** are inhibitors of several kinases, including Sgk1 (IC_{50} in the micromolar range), unfortunately with low specificity.[400]

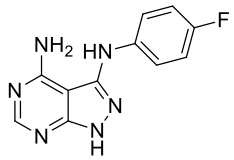

69 CGP57380

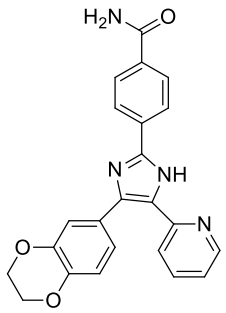

70 D4476

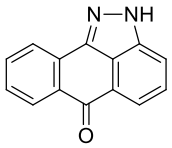

71 SP600125

GlaxoSmithKline has discovered some selective inhibitors of Sgk1, e.g. the pyrrol-pyridine GSK650394 **72** which has been the first Sgk1 inhibitor, reported in literature by Sherk *et al*.[299]

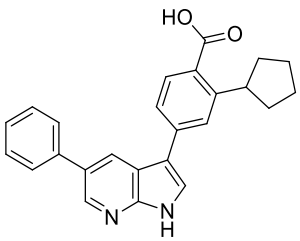

72 GSK650394

Initially, it has been observed that **72** was able to stop cell growth in different prostate cancer cell lines. More recently **72** has demonstrated, in *in vivo* assays, to have a synergic effect with cisplatin in the treatment of head and neck tumors.[401] However, toxicity data have not been clearly reported in literature. GSK650394 is equally active on Sgk1 and Sgk2, moreover, is 30 times more selective for Sgk1 than IGF1R, ROCK (Rho-associated protein kinase), Jak1, Jak3, Akt-1, Akt-2, Akt-3, DYRK1A (dual-specificity tyrosine phosphorylation-regulated kinase)

and Pdk1, and is 10 times more selective for Sgk1 versus Aurora kinases and JNK (c-Jun N-terminal kinase).[299,402]

EMD638683 **73**, a benzoylbenzohydrazinic compound, originally described as Sgk1 inhibitor for the metabolic syndrome therapy, has been later tested in an experimental model of colon cancer. The molecule shows proapoptotic activity and is able to decrease the number of colonic tumors following chemical carcinogenesis in Sgk1 knockout mice.[403]

The specificity of EMD638683, at 1 µM concentration, has been tested on an extended group of kinases. Data showed that EMD638683 have an inhibitory effect also on PKA (cAMP-dependent protein kinase), MSK1 (mitogen- and stress-activated protein kinase-1), PRK2 (protein kinase C-related kinase 2), Sgk2 and Sgk3. *In vivo* tests demonstrated that EMD638683 inhibits Sgk1 with an IC_{50} value of 3 µM.[404]

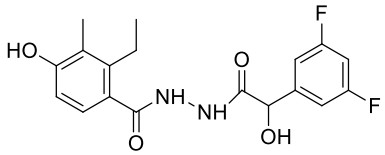

73 EMD638683

Sanofi has patented several sulphonamide derivatives of pyrazolo-pyrazines, which showed an inhibitory activity of Sgk1. These compounds should be suitable for the treatment of diseases involving Sgk1 alteration activity. In particular, compound **74** has shown an IC_{50} value of 1 nM in enzymatic assays on Sgk1.[405]

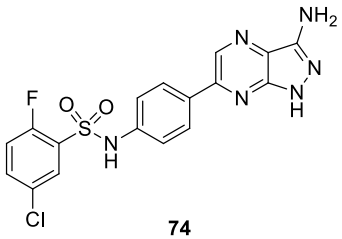

74

CHAPTER 7. Discussion. Synthesis of pyrazolo[3,4-*d*]pyrimidines and pyrrolo[2,3-*d*]pyrimidines as Src inhibitors active towards glioblastoma models

7.1 Synthesis of pyrazolo[3,4-*d*]pyrimidines

7.1.1 Background

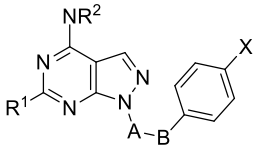

75

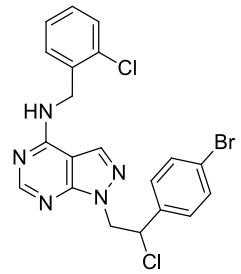

76 SI221

A-B = $-CH_2CH_2-$, -CH=CH-, $-CH_2CH(CH_3)-$, $-CH_2CH(Cl)-$, $-CH_2CH(OH)-$
R^1 = H, S-alkyl, amino groups
NR^2 = alyphatic and aromatic amino groups
X = H, F, Cl, Br

My research group synthesized a library of 4-amino substituted pyrazolo[3,4-*d*]pyrimidines bearing in N1 an alkylphenyl chain, **75**, which resulted active as ATP-competitive Src and Abl inhibitors, with IC_{50} values in the nanomolar range in enzymatic assays and a potent antiproliferative and proapoptotic activity toward different cancer cell lines.[389,406] Different studies demonstrated that Src is overexpressed also in GB,[36,407] which led to the decision to evaluate if some member of the in house pyrazolo[3,4-*d*]pyrimidines were active on this aggressive brain tumor. In particular, compound SI221, **76**, (K_i = 0.62 μM on Src) was able to reduce significantly cell viability and migration in GB cell lines without affecting non-tumor cells.[408] In detail, the antiproliferative activity of SI221 was evaluated in four GB cell lines (U-373MG, U-87MG, T98G, PRT-HU2) and in non-cancer cells (primary human skin fibroblasts) by MTS assay; the compound significantly reduced cell viability in all the GB cell lines (IC_{50} values of 17.9, 14.9, 12.5 and 14.3 μM, respectively) and didn't show toxic effect on normal fibroblasts.

Since SI221 was nearly ineffective on fibroblasts, the IC_{50} value for these non-tumor cells was not determinable at the range of concentrations used. The antiproliferative efficacy of SI221 was also compared with that of the well-known SFK inhibitor PP2 (**8**). Data showed that PP2

was nearly ineffective on U-373MG, U-87MG, and RT-HU2 cell lines, at the concentrations used, and had an efficacy lower than SI221 on T98G (**Fig. 22**). The analysis of SI221 ability to exert a long-term inhibition of GB cell growth, assessed by clonogenic assay, showed that SI221 treatment dramatically inhibited colony formation in all the GB cell lines.

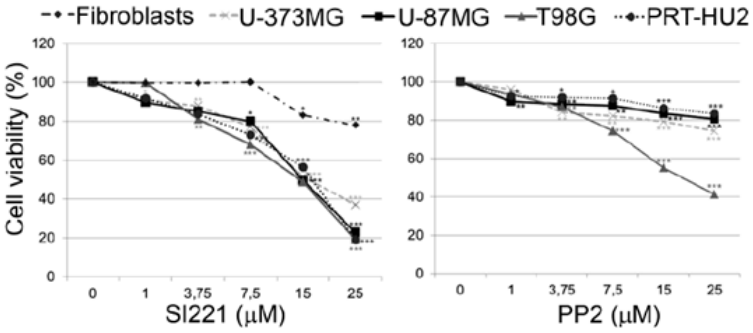

Fig. 22. Cell viability analysis by MTS assay in primary human skin fibroblasts, U-373MG, U-87MG, T98G, and PRT-HU2 cell lines 72 h after treatment with either SI221 or PP2 at the indicated concentrations.

7.1.1.1 ADME properties

SI221 was previously subjected to *in vitro* pharmacokinetic assays in order to preliminarily estimate its ADME properties[388] and later, another study was conducted in order to predict SI221 ability to passively cross the BBB. The parallel artificial membrane permeability (PAMPA)-BBB assay showed that SI221 had a good capability to cross the BBB, with an extremely low percentage of membrane retention. SI211 showed high SI221 metabolic stability. Two main metabolites of the compound have been identified using human liver microsomes (HLM) and LC-UV-MS. One is derived from an oxidative dechlorination reaction and the other one from an N-dealkylation reaction. However, the two metabolites were present in low percentages.[388]

7.1.2 Project

Despite its remarkable activities, this compound suffers from a low water solubility, which precludes oral administration. Accordingly, a series of more soluble pyrazolo[3,4-*d*]pyrimidine derivatives has been rationally designed and synthesized by my research group, through the introduction of polar groups in the solvent-exposed C6 position. This study led to the identification of the C4-anilino derivative **77**, which showed a beneficial profile in terms of both biological activity and ADME properties, being characterized by a high metabolic stability

(95%), good water solubility (1.7 μg/mL), an efficient membrane permeability (10 x 10^{-6} cm/s), and a potent inhibitory activity against isolated c-Src (K_i= 0.21 μM).

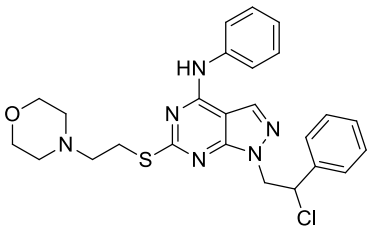

77

The X-ray crystal structure of c-Src in complex with compound **77** was obtained in good resolution (PDB code: 4O2P) (**Fig. 23**).

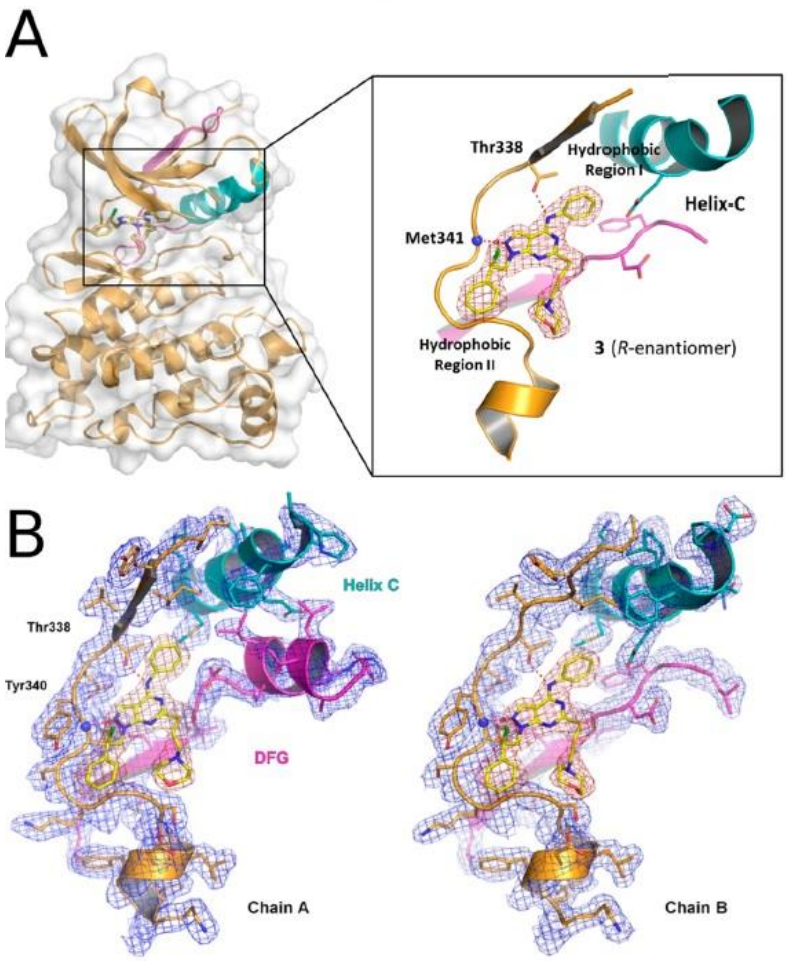

Fig. 23. A. Inhibitor **77** in complex with wild-type c-Src. **B.** Experimental electron density of chain A and B in complex with **77.**

The solved structure confirmed the binding mode previously predicted by us for C6-substituted derivatives within the ATP-binding site of c-Src. Starting from this crystal structure, a computationally driven hit-to-lead optimization primarily guided by results of free energy perturbations was successfully conducted, leading to the identification of novel derivatives with improved potencies against c-Src.[48] On the basis of these interesting results we decided to expand the library of pyrazolo[3,4-*d*]pyrimidines synthesizing compounds **78a-g** and to test the new molecules on GB cell lines. These compounds bear a 2-chloro-2-phenylethyl or 2-phenylethyl chain in N1, an anilino or benzylamino substituent in C4 and a thioethylmorpholino chain in C6. We decided also to expand the synthesis of this class of derivatives and synthesize compounds **79** bearing a [2-(4-methylpiperazin-1-yl)ethyl)]thio chain in C6, in order to improve the solubility of these molecules, following the suggestion of molecular modeling studies.

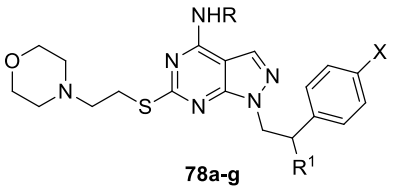

78a-g

a: R = C_6H_5, R^1 = H, X = H
b: R = C_6H_4-*m*F, R^1 = H, X = H
c: R = C_6H_4-*m*Br, R^1 = H, X = H
d: R = C_6H_4-*m*Cl, R^1 = H, X = F
e: R = C_6H_4-*m*Br, R^1 = Cl, X = H
f: R = $CH_2C_6H_4$-*o*F, R^1 = Cl, X = H
g: R = $CH_2C_6H_4$-*o*Cl, R^1 = Cl, X = H

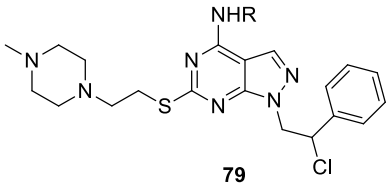

79

NHR = anilines or benzylamines

7.1.2.1 Chemistry

Compounds **78a-g** were synthesized by reacting the opportune (2-phenylethyl)hydrazine **80a,c**[409,410] with ethyl(ethoxymethylene)cyanoacetate in anhydrous toluene at 80 °C for 8 h, affording the ethyl 5-amino-1*H*-pyrazole-4-carboxylates **81a-c**. These intermediates were treated with benzoyl isothiocyanate in anhydrous tetrahydrofuran (THF) at reflux for 18 h to give compounds **82a-c**. These latter were cyclized to pyrazolo[3,4-*d*]pyrimidinones **83a-c** by treatment with 2 N NaOH at 100 °C for 10 min, followed by acidification with acetic acid. Alkylation with 4-(2-chloroethyl)morpholine at position C6 in the presence of NaOH in anhydrous dimethylformamide (DMF) and absolute EtOH at reflux for 6 h gave compounds **84a-c**. These intermediates were treated with the Vilsmeier complex ($POCl_3$/DMF, 1:1) in

$CHCl_3$ at reflux for 8 h to obtain the halogenated compounds **85a-c**. Finally, the reaction of **85a-c** with amines or anilines in opportune conditions gave the desired compounds **78a-g** (**Scheme 1**).

Scheme 1. Preparation of derivatives **78a-g.**

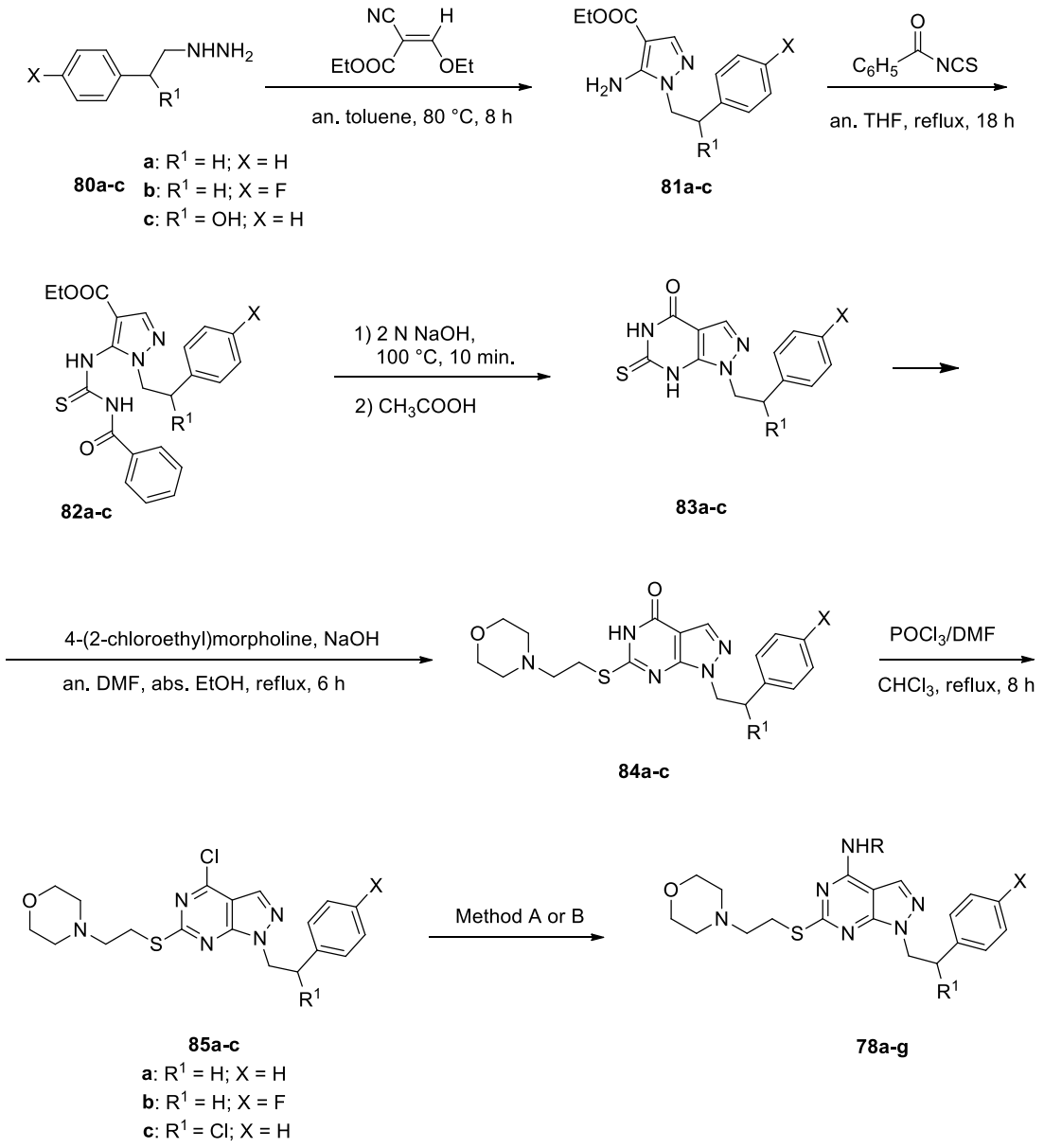

Method A: appropriate aniline, abs. EtOH, reflux, 3-5 h (to obtain compounds **78a-e**);
Method B: appropriate amine, an. toluene, r.t., 48 h (to obtain compounds **78f,g**).

Compound **86** was synthesized by alkylation at position C6 of intermediate **83c**, using 1-(2-chloroethyl)-4-methylpiperazine, KOH and KI in absolute EtOH at 80 °C for 12 h. The synthesis of the halogenated derivative **87** gave several problems and various attempts have been performed:compound **86** was treated with the Vilsmeier complex ($POCl_3$/DMF, 1:1) in $CHCl_3$ at reflux for 6-12 h, but the reaction formed a mixture of decomposition products;

- another reaction was performed with $POCl_3$ at 100 °C for 3 h but it didn't work;
- an attempt to directly obtain compounds **79** was made by reacting compound **86** with PCl_3 and the opportune aniline or amine in acetonitrile (ACN) at 80 °C for 5 h, but also this attempt failed (**Scheme 2**).

Scheme 2. Attempts to obtain compounds **79.**

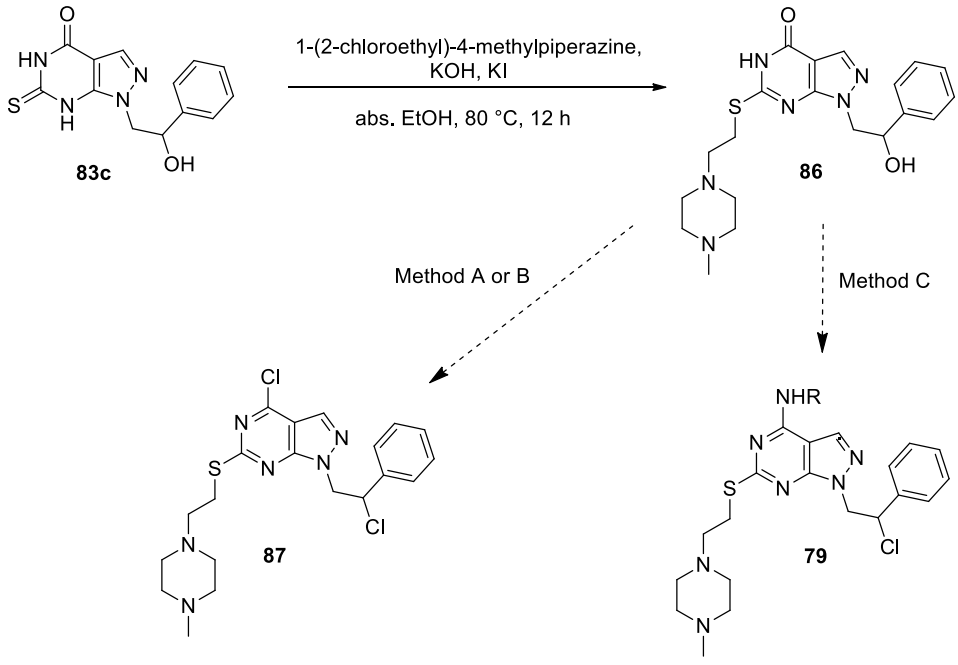

Method A: $POCl_3$/DMF, $CHCl_3$, reflux, 6-12 h.
Method B: $POCl_3$, 100 °C, 3 h.
Method C: PCl_3, opportune aniline or amine, ACN, 80 °C, 5 h.

Up to date, compounds **79** have not been obtained but other attempts will be made, using other chlorinating agents, in order to synthesize these molecules, since modeling studies show that compounds **79** may be good Src inhibitors endowed with better ADME properties (in particular solubility), than compounds **78**.

7.1.2.2 In vitro studies

The enzymatic assays were performed by the group of Dr. Maga of CNR of Pavia. The cellular assays were carried out by the group of Prof. Giordano of Sbarro Institute for Cancer Research and Molecular Medicine of Philadelphia.

Enzymatic Assay on Isolated Src: The kinase inhibition mechanism was studied in a cell free assay using recombinant human Src. To evaluate the affinity toward isolated c-Src the study was performed in a binding assay in the presence of [γ^{-32P}]ATP and a peptide substrate. Each experiment was done in triplicate, and mean values were used for the interpolation. Curve fitting was performed with the program GraphPad Prism. K_i values are reported in **Table I**; compound **77** was used as a reference.[408]

Cell Proliferation/Vitality Assay: up to date, this test was performed only on compound **78e**. U87-MG cells were treated at concentrations of **78e** ranging from 1 to 25 μM. Cell viability was evaluated 72 h after treatment by MTS assay to evaluate the IC_{50} values.

7.1.2.3 ADME studies

It is well-known that many kinase inhibitors, included our pyrazolo[3,4-*d*]pyrimidines, are generally affected by solubility issues because of their lipophilic nature. Therefore, the early evaluation of ADME properties in this field represents a key step to guide the drug candidate selection. Accordingly, *in vitro* ADME studies were conducted on the most potent c-Src inhibitor, **78e**, in order to early assess its absorption/stability. In particular, aqueous solubility, PAMPA, and human liver microsomes (HLM) stability were evaluated (**Table I**). Overall, optimal ADME properties were measured for **78e**. Indeed, the metabolic stability was found to be higher than 90%. Moreover, the membrane permeability value was of 5.27 x 10^{-6} cm/s, highlighting a sufficient ability to cross the cell membranes. Furthermore, water solubility is higher to that of reference **77**, with a value of 3.7 μg/mL.

Table I. Enzymatic activities, cellular activities and ADME properties of compounds **77** and **78a-g**.

	Biological Data		*In vitro* ADME		
Cpd	**c-Src K_i (μM)**	**U87-MG IC_{50} (μM)**	**Solubility (μg/mL)**	**PAMPA *Papp* 10^{-6} cm/s**	**Met. Stab. Human (%)**
77	0.24	ND	1.7	10.0	95
78a	NA	ND	ND	ND	ND
78b	NA	ND	ND	ND	ND
78c	NA	ND	ND	ND	ND
78d	NA	ND	ND	ND	ND
78e	0.13	5	3.7	5.27	96
78f	0.17	ND	ND	ND	ND
78g	0.29	ND	ND	ND	ND

NA = Not Active; ND = Not Determined

7.1.2.4 In vitro biological activity of compound 78e

Compound **78e**, which showed an IC_{50} value of 5 μM on U87-MG cells and good ADME properties, was tested in further *in vitro* assays.

Cellular assays

U87-MG cell lines were treated with compound **78e** and dasatinib to evaluate their apoptotic and antiproliferative effects (**Fig. 24, 25**). At 5 μM concentration **78e** induces apoptosis in 32% of cells and causes a 48% reduction of cell proliferation, showing a slightly higher effect than dasatinib (24% and 42%, respectively).

Compound **78e** was also tested on U87-TxR GB cells that express the gene of multi-drug resistance. Interestingly, the compound showed an IC_{50} value of 3.6 μM (**Fig. 26**).

Furthermore, the activity of **78e** in comparison to radiotherapy (RT) has been evaluated: **78e** alone is more effective than RT, and the association with RT determines a 73% reduction on the number of colonies (**78e** 1 μM) and an 88% reduction (**78e** 10 μM) (**Fig. 27**).

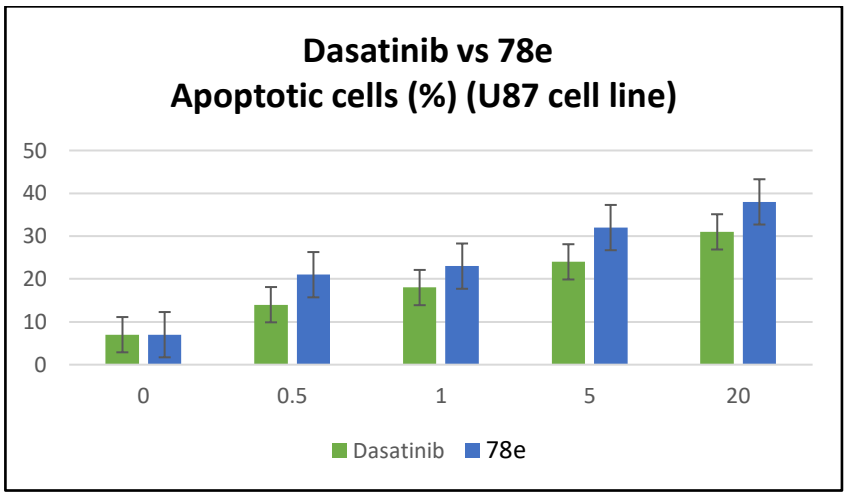

Fig. 24. Apoptotic effects of compound **78e** and dasatinib in U87-MG cell line.

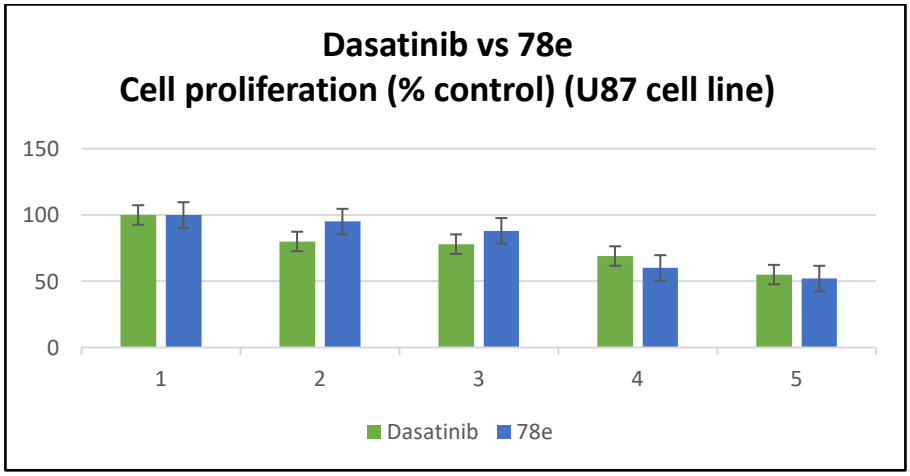

Fig. 25. Antiproliferative effects of compound **78e** and dasatinib in U87-MG cell line.

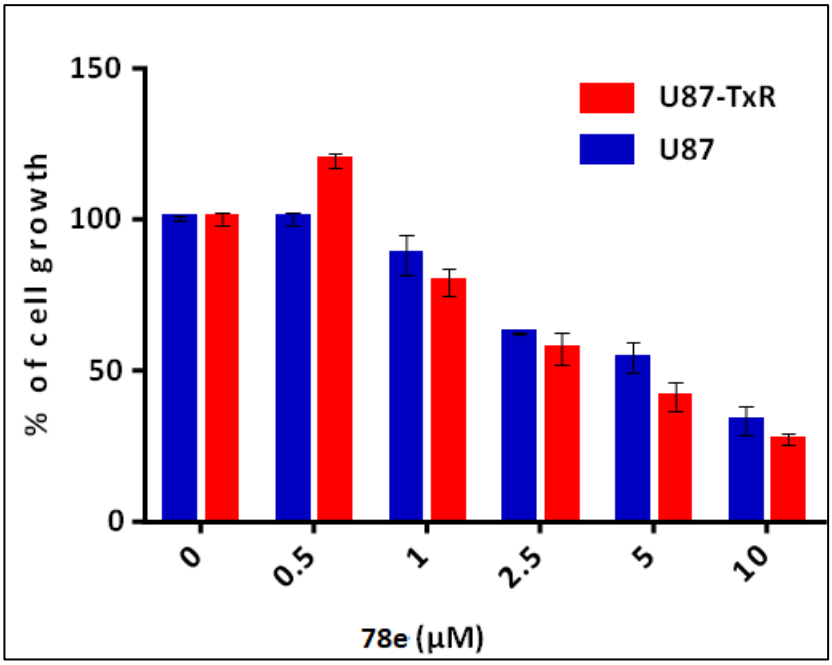

Fig. 26. Effects of compound **78e** on U87-TxR glioblastoma cells that express the gene of multi-drug resistance.

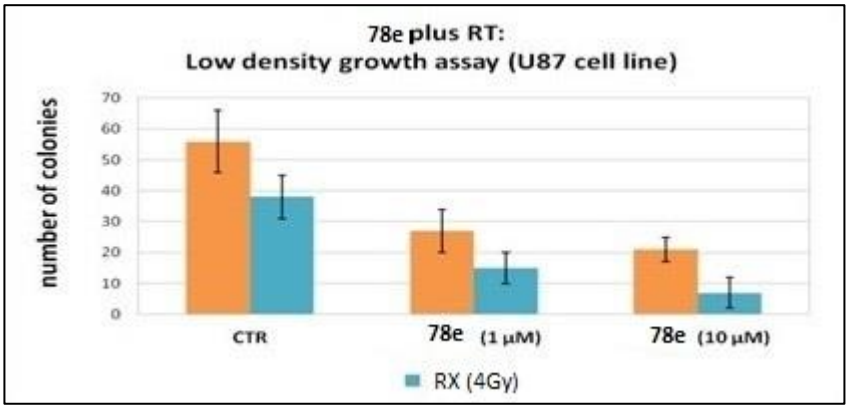

Fig. 27. Activity of **78e** in comparison to radiotherapy (RT).

7.1.2.5 In vivo assays

Xenograft mouse models, inoculated subcutaneously with U87 cells, were treated with **78e** at 50 mg/kg daily for 60 days. 50% tumor reduction (**78e** alone) and 80% tumor reduction (**78e** combined with RT) were observed. Moreover, mice did not show any sign of distress or weight loss (**Fig. 28**).

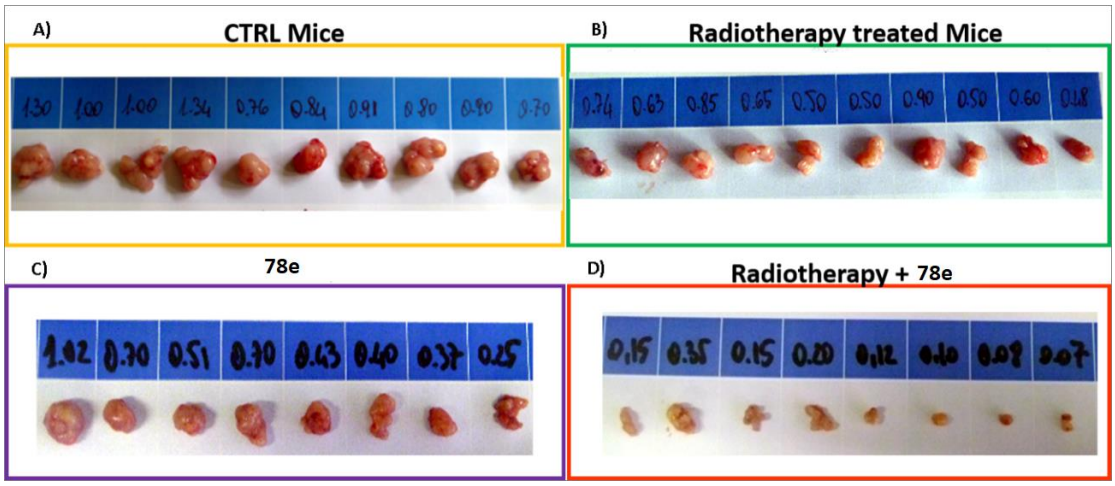

Fig. 28. *In vivo* effects on xenograft mouse models, inoculated with U87 cells. **A.** Control. **B.** Mice treated with RT. **C.** Mice treated with **78e** alone. **D**. Mice treated with **78e** in association with RT.

7.1.2.6 Conclusions

In summary, for the first time an X-ray crystal structure of c-Src in complex with one of our patented pyrazolo[3,4-*d*]pyrimidines, compound **77**, was obtained in good resolution. The solved structure confirmed the binding mode previously predicted by us for C6-substituted derivatives within the ATP-binding site of c-Src.

Starting from the promising results obtained with compound **77** and other analogs active as Src inhibitors, and on the basis of the knowledge that c-Src is overexpressed or hyperactivated in GB, we synthesized and tested compounds **78a-g** for their inhibitory activity on c-Src. Data showed that compounds **78a-d** bearing a 2-phenylethyl chain are not active, while compounds **78e-g** bearing a 2-chloro-2-phenylethyl chain in N1 display activity towards Src with K_i values in the nanomolar or submicromolar range. Among these, compound **78e**, bearing a 3-bromoaniline substituent in C4, is the most active of the series. Given these interesting results, **78e** has been selected to further *in vitro* and *in vivo* assays, in which it shows antiproliferative activity on GB cell lines and a 50% tumor reduction in U87 cell xenograft mouse model.

In conclusion, this study led to the identification of a compound with a good activity *in vivo*, which will be subjected to other studies. Furthermore, we think to design and synthesize other **78e** analogs to expand SAR evaluations.

7.2 Synthesis of pyrrolo[2,3-*d*]pyrimidines

7.2.1 Background

In the last few years, several pyrrolo-pyrimidine derivatives have been either approved by the US FDA and in other countries for the treatment of different diseases or are currently in phase I/II clinical trials.

The pyrrolo[2,3-*d*]pyrimidine scaffold is being extensively investigated and in the last few years many of such compounds resulted active as kinase inhibitors. To get further insight in this family of compounds, during my PhD course, I wrote two review articles on this topic.[411,412]

The Jak kinase inhibitors tofacitinib **88**,[413] ruxolitinib **89**[414] and oclacitinib **90**[415] are approved by the US FDA and in other countries for the treatment of rheumatoid arthritis, myelofibrosis and canine allergic dermatitis, respectively. AEE788, **91** is a dual EGFR/VEGFR inhibitor[416,417] which was evaluated in phase I/II clinical trials for its activity in patients with recurrent or relapsed GB. CCT128930, **92**[418] and AZD5363, **93**[419] inhibit Akt, a STK often deregulated in tumors, such as GB, breast and gastric cancer. Interestingly, some pyrrolo[2,3-*d*]pyrimidines are also active on Src.[420–422]

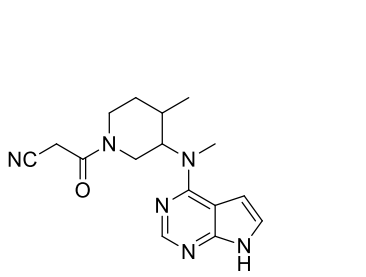

88 tofacitinib

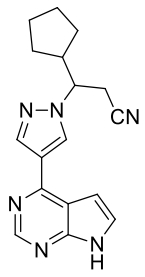

89 ruxolitinib

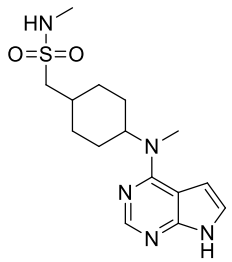

90 oclacitinib

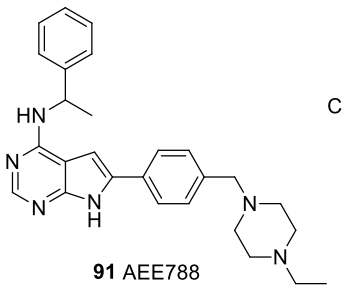

91 AEE788

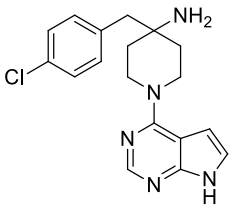

92 CCT128930

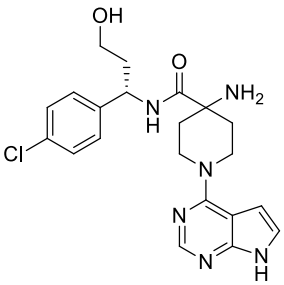

93 AZD5363

7.2.2 Project

Recently, different libraries of pyrazolo[3,4-*d*]pyrimidines active as SFK and/or Abl inhibitors have been synthesized.[389,406] In particular, our in house compounds **94** showed K_i values in the nanomolar range both in enzymatic and cell assays and possessed *in vivo* antitumor activity on xenograft models derived from different cell lines.[48,102,388]

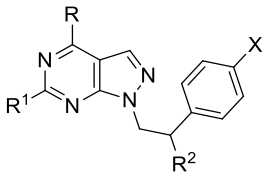

94

R = alyphatic or aromatic amino groups
R^1 = H, CH_3, Cl
R^2 = H, alkyl, thioalkyl and aminoalkyl groups
X = H, Cl, F, Br

With the aim of investigating if the deaza-isosteres of in house inhibitors **94** maintain the activity on Src both in enzymatic and in cell assays, we decided to synthesize a family of pyrrolo[2,3-*d*]pyrimidines **95a-j**, and to test them on Src in enzymatic assays and as antiproliferative agents on a specific cancer cell line. Some of compounds **95a-j** are strictly correlated with their pyrazolo[3,4-*d*]pyrimidine analogs **94** bearing a C2 thiomethyl group, a C4 amino group, and an N7 2-chloro-2-phenylethyl chain, whereas other derivatives are substituted in N7 with a benzylic chain, more easily accessible from a synthetic point of view.

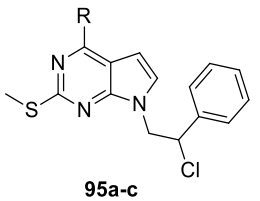

95a-c

a R = NHC_6H_5
b R = NHC_6H_4*m*-Cl
c R = $NHCH_2C_6H_5$

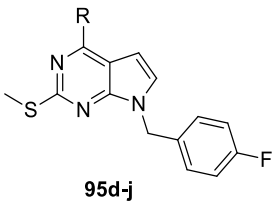

95d-j

d R = nC_4H_9
e R = 1-pyrrolidino
f R = 1-piperidino
g R = 4-morpholino
h R = $NHCH_2C_6H_5$
i R = $NHCH_2CH_2C_6H_5$
j R = $NHCH_2CH_2C_6H_4$-*p*Cl

7.2.2.1 Chemistry

The synthesis of compounds **95a-c** was performed starting from 6-amino-2-(methylthio)pyrimidin-4(3*H*)-one **96**, prepared following the procedure reported by Baker and coll.[423] Compound **96** was cyclized using an aqueous solution of chloroacetaldehyde in a

microwave open vessel apparatus to obtain 2-(methylthio)-7*H*-pyrrolo[2,3-*d*]pyrimidin-4-ol **97** in a higher yield compared to the literature method.[424] Then compound **97** was chlorinated in C4 to give 4-chloro-2-(methylthio)-7*H*-pyrrolo[2,3-*d*]pyrimidine **98** following a literature method.[424] Intermediate **98** was alkylated in N7 using 2-bromo-1-phenylethanone at room temperature in the presence of sodium hydride to obtain compound **99**. The latter was reduced to **100** with sodium borohydride in a mixture of THF and water. Intermediate **100** was in turn treated with the Vilsmeier complex ($POCl_3$/DMF, 1:1) in CH_2Cl_2 at reflux for 8 h to obtain compound **101**, bearing a 2-chloro-2-phenyethyl chain in N7. Finally, the reaction of **101** with the suitable anilines in absolute EtOH at reflux for 5 h gave the desired compounds **95a,b** in good yields, while compound **95c** was obtained by treating **101** with an excess of benzylamine in anhydrous toluene at room temperature for 24 h (**Scheme 3**).

Scheme 3. Preparation of derivatives **95a-c.**

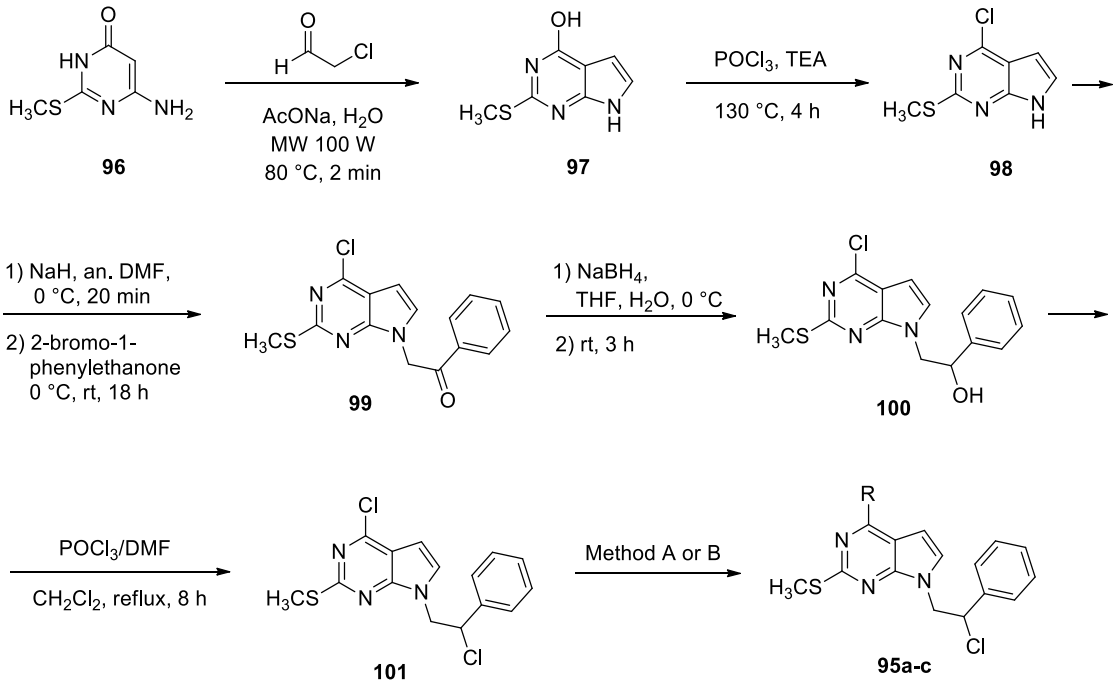

Method A: anilines, abs. EtOH, reflux, 5 h (to obtain compounds **95a,b**);
Method B: benzylamine, an. toluene, rt, 24 h (to obtain compound **95c**).

The synthesis of compounds **95d-j** was performed starting from 4-chloro-2-(methylthio)-7*H*-pyrrolo[2,3-*d*]pyrimidine **98** which was alkylated in N7 with sodium hydride and 4-

fluorobenzyl chloride in anhydrous ACN at 50 °C for 2 h to give 4-chloro-7-(4-fluorobenzyl)-2-(methylthio)-7*H*-pyrrolo[2,3-*d*]pyrimidine **102**. The compound was treated with the suitable amine in dimethylsulfoxide (DMSO) at 90-130 °C to obtain the desired compounds **95d-j** (**Scheme 4**).

Scheme 4. Preparation of derivatives **95d-j.**

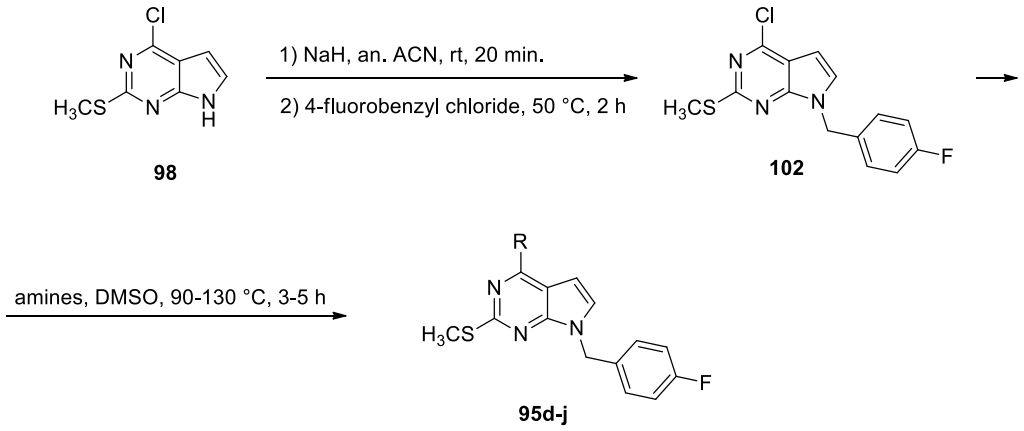

7.2.2.2 Molecular modeling studies

A molecular docking protocol has been employed in order to evaluate the ability of the new synthesized compounds **95a-j** to interact with the ATP-binding site of c-Src kinase. For this purpose, the X-ray crystal structure of Src in a complex with a pyrazolo[3,4-*d*]pyrimidine derivative, **77**,[48] previously cited, was used for computational studies. Compound **95b** has been scored as the best compound of the series thanks to the presence of the chlorine atom in the meta position on the C4 anilino substituent which interacts with Asp404 and Phe405 belonging to the DFG-motif.

Despite the binding poses of compounds **95a-j** present common features with those of the ligand **77**, pyrrolo-pyrimidines lack the nitrogen atom which usually interacts with the backbone of Met341 in the pyrazolo[3,4-*d*]pyrimidine analogs. The absence of this important point of contact with the hinge region makes our pyrrolo[2,3-*d*]pyrimidines less active than their pyrazolo counterpart, but they open the way to the study of a new promising scaffold which could be further optimized (**Fig. 29**).

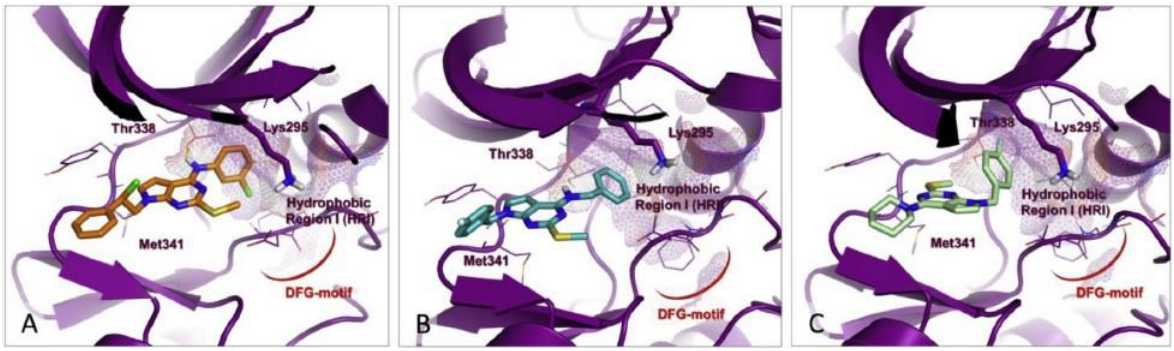

Fig. 29. Best predicted docking poses within the ATP-binding site of 4O2P crystal structure chain B of **A.** compound **95b** (orange); **B.** compound **95h** (deep teal); **C.** compound **95e** (pale green).

7.2.2.3 Enzymatic assays

All synthesized compounds were initially tested in a cell free assay to evaluate their affinity toward isolated c-Src (**Table II**). In agreement with our computational studies, **95b** resulted one of the best compounds of our small library of pyrrolo[2,3-*d*]pyrimidines, showing a good inhibitory effect of the enzymatic activity with a K_i value of 0.7 mM. As expected, **95c**, which has a longer side chain as R substituent, or **95a**, which lacks the mCl substituent, reduced the activity of the enzyme in a less efficient way than **95b**. In the series **95d-j** the substitution of the 2-chloro-2-phenylethyl side chain in R1 with a shorter 4-fluoro-benzyl group, which lacks the bulky Cl atom, gives the possibility to the compounds with a longer R substituent to better accommodate into the ATP-binding cleft and go deeply into the HR1. This is confirmed by the fact that **95h** also showed a good inhibitory activity against c-Src (0.5 mM), despite the presence of a long benzyl group as R substituent. In general, for all two series, it was observed that increasing the length of the linker at C4 position caused a high reduction of the inhibitory power against c-Src (compare **95c** with **95b** and **95j** with **95h**). On the other hand, compound **95d**, bearing a nC_4H_9 substituent in C4 and a 4-fluoro-benzyl chain in N7, showed to be too small for effectively bind the ATP cleft of Src (K_i = 3 µM). The compounds have been also tested on Fyn, another member of SFKs, and showed a certain degree of activity, probably due to the similarity among the members of this family of kinases. The most active compound is **95i**, which possesses a Ki value of 2 µM on this enzyme. On the other hand, the compounds resulted inactive when tested on a small panel of kinases, including c-Kit, Abl, AblT315I, FLT3 and EGFR, demonstrating a degree of selectivity toward c-Src.

Table II. Enzymatic and cellular activities of compounds **95a-j**.

Cpd	c-Src K_i (μM)	U87-MG IC_{50} (μM)
95a	1.5 ± 0.10	27.4 ± 0.16
95b	0.7 ± 0.20	143.1 ± 0.20
95c	6.0 ± 0.08	50.7 ± 0.18
95d	3.0 ± 0.10	20.7 ± 0.38
95e	2.0 ± 0.30	51.8 ± 0.21
95f	2.5 ± 0.30	50.7 ± 0.42
95g	4.7 ± 0.20	20.3 ± 0.15
95h	0.8 ± 0.06	7.1 ± 0.16
95i	0.5 ± 0.04	13.3 ± 0.16
95j	5.0 ± 0.10	46.1 ± 0.08

7.2.2.4 Cytotoxicity assays on U87 GB cell line

The compounds have been successively tested on U87 GB cell line, that has been chosen because of Src involvement in this aggressive tumor.[408] The most active compound was **95h**, with an IC_{50} value of 7.1 μM after 72h, while the other derivatives resulted less active with IC_{50} values higher than 10 μM (**Fig. 30**).

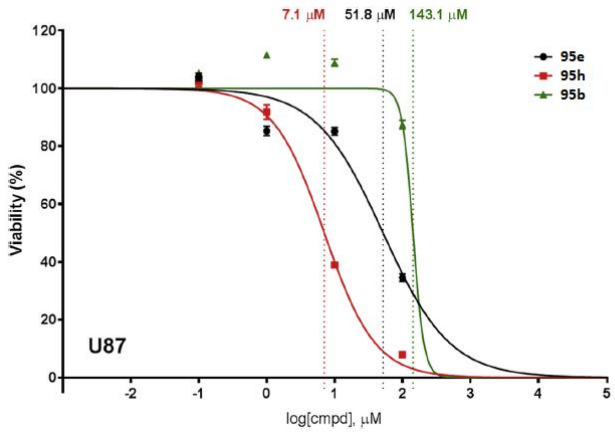

Fig. 30. Viability of U87 cell line evaluated at 72h is reported for the most active compound **95h** and for **95b** and **95e** as examples of less active compounds of each series.

7.2.2.5 Conclusions

A series of pyrrolo[2,3-*d*]pyrimidines has been synthesized and tested for their activity against c-Src. Molecular docking revealed our compounds possess profitable features for the binding to the catalytic site of c-Src, being able to act as ATP-competitive inhibitors of the enzyme. Compounds **95a-j** have been tested on a small panel of kinases. As a result, our pyrrolo[2,3-*d*]pyrimidines demonstrated a certain selectivity for c-Src, since they did not show any activity against other tyrosine kinases, with the only exception of **95i** which turned out moderately active against Fyn. The compounds have been finally tested *in vitro* for their cytotoxicity on U87 GB cell line and **95h** demonstrated to be active with an IC_{50} value of 7.1 μM. The inadequacy of the current therapies against GB raises the need of new drugs able to inhibit the growth of this aggressive tumor. In this contest, our pyrrolo[2,3-*d*]pyrimidine derivatives stand as a new promising scaffold with a good potency against GB and therefore worthy of further investigation.

CHAPTER 8. Discussion. Synthesis of pyrazolo[3,4-*d*]pyrimidines as Fyn inhibitors potentially active towards tauopathies and tumors

8.1 Background

Because of the involvement of Fyn in different tauopathies and tumors, the design and synthesis of Fyn inhibitors represent an expanding field of study.

Molecular modeling studies, performed in collaboration with the University of Siena, were combined with organic synthesis with the aim of developing novel Fyn kinase inhibitors. A docking study was employed with the purpose of identifying novel ATP-competitive Fyn kinase inhibitors. An in house library of pyrazolo[3,4-*d*]pyrimidines (consisting of about 300 structurally characterized compounds with > 98% purity) was chosen for this purpose, using the experimental pose of the known active ligands PP1 (**7**) and PP2 (**8**), selected as reference compounds.

Pyrazolo[3,4-*d*]pyrimidines were virtually screened against the active site of Fyn and then tested in an enzymatic assay towards this kinase. Derivative **103a** emerged as the most active compound. On the basis of this finding, a hit to lead optimization process was then initiated and new analogs of **103a**, among which **103b-e**, were synthesized.

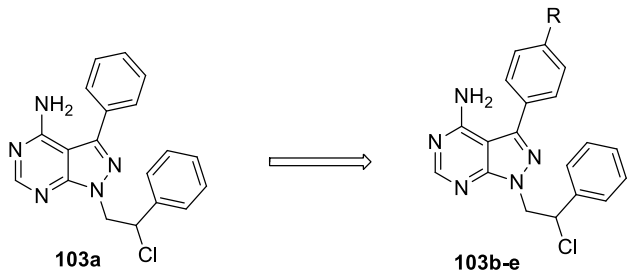

103a **103b-e**

b: R = F
c: R = Cl
d: R = CH_3
e: R = OCH3

8.1.1 Enzymatic assays

Compounds **103b-e** resulted potent *in vitro* inhibitors of Fyn, with K_i values in the nanomolar range (**Table III**). These activities were most likely due to the contribution of a substituent in the para position of the C3 phenyl ring.

Furthermore, to assess its specificity against Fyn, the most active compound, **103c**, was tested

against a panel of kinases including other SFK members (Hck, Blk, Fgr, Fyn, Src, Lck, Lyn, and Yes), TKs (Abl, EGFR, IGF1R, Jak2, PDGFR, KDR), as well as some STKs. **103c** proved to be more efficient against SFK members than towards the other investigated kinases, confirming such a compound as a useful probe to study SFK function. Furthermore, a high activity against Abl was also detected as expected for the high structural similarity between Abl and SFKs. Notably, **103c** was not able to significantly inhibit any of the STKs tested (Pim-1, mTOR, JNK, CDK5, Chl1). Moreover, the compound did not inhibit the STKs DYRK1a and GSK3-β that are implicated in AD.[425]

Table III. Enzymatic and cellular activities of compounds **103a-e,** toward isolated Fyn. kinase.

Cpd	Fyn K_i (μM)	IC_{50} ± SD (μM) (K562 cells)
103a	0.90	ND
103b	0.36	12.63±14.80
103c	0.07	0.56±0.01
103d	0.095	0.30±0.06
103e	1.485	ND

ND = not determined

8.1.2 Docking studies

To rationalize such biological data, docking studies were carried out and the resulting binding modes were compared with that previously identified for the hit **103a**. All studied compounds adopted a pose in line with that of **103a.**

8.1.3 Cellular assays

In AD, Fyn mediates the phosphorylation of Tau protein on the Tyr18 residue, an early and crucial step in the disease progression.[426] For this reason, the most interesting compounds identified during *in vitro* inhibition assays, **103c** and **103d**, were also evaluated for their ability to inhibit the Fyn mediated phosphorylation of residue Tyr18 of Tau in a cellular model of AD. Both compounds significantly affected amyloid beta 1-42 (Aβ_{42}**)** induced Tyr18-Tau phosphorylation with a similar degree and in a dose-dependent manner. Moreover, the inhibitory activity of **103c** and **103d** resulted constant over time, being effective up to 6 h after compound administration.

The three most active compounds in terms of enzymatic activities, **103b**, **103c**, and **103d**, were then evaluated for their antiproliferative activity on the human CML cell line K562 (**Table III**). The tested compounds showed an effective antiproliferative activity that well correlates with the K_i values determined by in vitro inhibition assays. The most active compounds, **103c** and **103d**, inhibited cell viability with IC_{50} values in the submicromolar range (**Table III**). Moreover, the antiproliferative effect of **103c** and **103d** was evaluated through cell cycle analysis (**Fig. 31**).

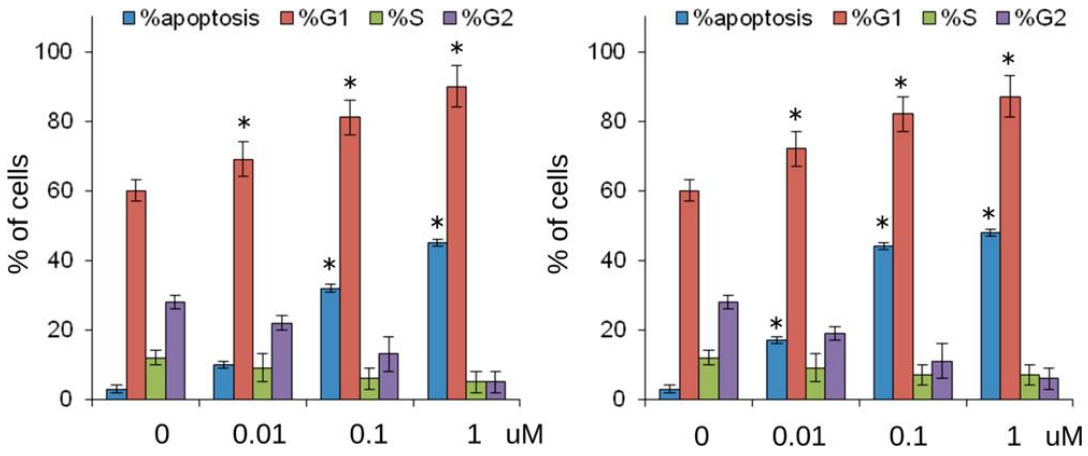

Fig. 31. Analysis of the cell cycle distribution of K562 cells after treatment with increasing concentrations of **103c** and **103d**.

Notably, the treatment with 0.1 μM **103d** induced apoptosis in about 50% of treated K562 cells. Compounds **103c** and **103d** were also tested on early hematopoietic progenitor cells (CD34+) from Ph+ CML patients who developed resistance to both imatinib mesylate and dasatinib. The percentage of apoptotic CD34+ after imatinib treatment was found equal to control, confirming drug resistance. By contrast, **103c** and **103d** increase apoptotic levels to 35% and 30%, respectively. It is important to note that these compounds, when tested in human normal fibroblasts, did not show any sign of cell toxicity.

Furthermore, compounds **103b-e**, were also evaluated on two solid human tumor cell lines, MDA-MD-231 (human breast cancer cell line) and U87 (human glioblastoma multiforme cell line). These cell lines, treated with **103c** and **103d**, showed similar response profiles, with a significant difference in cell growth starting from 20 h after treatment with respect to control cells, and a more evident inhibition of cell viability from 70 h after treatment. U87 cells resulted particularly responsive to SFKs inhibitors, indeed **103c** and **103d** showed IC_{50} values of 0.074 and 0.78 μM, respectively. Compounds **103c** and **103d** also showed an effective

antiproliferative activity on the MDA-MD-231 cell line, with IC_{50}s in the low micromolar range (3.7 and 8.3 μM for compounds **103c** and **103d**, respectively).

8.1.4 *In vitro* ADME studies

Compounds **103a-e** were profiled in vitro for aqueous solubility, liver microsomal stability, and membrane permeability (**Table IV**).

Table IV. In vitro ADME profile of compounds **103a-e**

Cpd	PAMPA P_{app} X 10^{-6} (cm/s)	PAMPA-BBB P_{app} X 10^{-6} (cm/s)	Water solubility (log S)	Metabolic stability (%)	Major metabolites (%)
103a	12.8	9.5	-7.26	78.9	M1=M-36 + 16 (18.0) M2=M-35 + 17 (3.0)
103b	16.5	12.9	-7.75	95.7	M1=M-36 + 16 (2.8) M2=M-35 + 17 (1.4)
103c	9.9	8.4	-7.60	85.2	M1=M-36 + 16 (14.7) M2=M-35 + 17 (<0.10)
103d	10.9	11.5	-7.30	90.0	M1=M-36 + 16 (2.4) M2=M-35 + 17 (5.0) M3=M + 16 (2.6)
103e	17.5	14.5	-8.25	95.6	M1=M-36 + 16 (2.5) M2=M-35 + 17 (0.9) M4= -14 (0.8)
caffeine		1.12			

Caffeine used as reference compound.

The aqueous solubility of these derivatives (-log S ranging from 7.26 to 8.25) was very low and constituted a deleterious parameter in terms of a suitable PK profile. However, passive membrane permeability in PAMPA assay indicated a good cell permeability for compounds **103a-e** (ranging from 9.9 to 17.5 X 10^{-6} cm/s). Similarly, all these compounds were found to cross the BBB in a specific PAMPA-BBB assay, with good permeability values (ranging from 8.4 to 14.5 X 10^{-6} cm/s). Moreover, stability tests disclosed that the compounds showed good (from 78.9 to 95.6%) metabolic stability in liver microsomes. Metabolite identification by LC-

MS analysis after incubation in human microsomes indicated the primary metabolites were actually the products of an oxidative dehalogenation at the chlorine atom on the N1 side chain, as previously reported by us for similar compounds.[427]

8.2 Project

On the basis of these interesting results, we decided to extend this family of compounds **103a-e**, resulted the most active in the previous studies, and, during my PhD course, I planned the synthesis of compounds **104a-j** bearing different aromatic groups in C3.

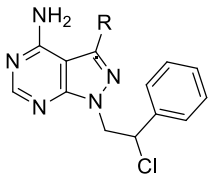

104a-j

a: R = C_6H_4-*p*CH_2OH
b: R = C_6H_4-*p*OH
c: R = C_6H_4-*p*NO_2
d: R = 5-indolyl
e: R = C_6H_4-*o*Cl
f: R = C_6H_4-*m*Cl
g: R = C_6H_4-*p*Br
h: R = C_6H_4-*p*I
i: R = C_6H_4-*p*C_2H_5
j: R = C_6H_4-*p*C_3H_7

8.2.1 Chemistry

The synthesis of compounds **104a,b** started with the reaction between 5-amino-1*H*-pyrazolo-4-carbonitrile **106,**[428] **(**obtained by reaction of (ethoxymethylene)-malononitrile **105** with hydrazine monohydrate) and formamide at 200 °C for 1 h, affording 1*H*-pyrazolo[3,4-*d*]pyrimidin-4-amine **107**.[428] Reaction of **107** with N-iodosuccinimide (NIS) in dry DMF at 80 °C for 14 h under nitrogen atmosphere gave 3-iodo-1*H*-pyrazolo[3,4-*d*]pyrimidin-4-amine **108**.[429] This last was in turn treated with a solution 1 M of tetrabutylammonium fluoride hydrate (TBAF) in anhydrous toluene at 70 °C for 1 h. Then 2-bromoacetophenone was added and the reaction was stirred at 70 °C for 2 h to afford 2-(4-ammino-3-iodo-1*H*-pyrazolo[3,4-*d*]pyrimidin-1-yl)-1-phenylethanone **109**. This last was reduced with $NaBH_4$ in MeOH at 0 °C for 3 h to obtain 2-(4-ammino-3-iodo-1*H*-pyrazolo[3,4-*d*]pyrimidin-1-yl)-1-phenylethanol **110.** This intermediate was treated with $SOCl_2$ in anhydrous CH_2Cl_2 at room temperature for 12 h under nitrogen atmosphere to afford 1-(2-chloro-2-phenylethyl)-3-iodo-1*H*-pyrazolo[3,4-*d*]pyrimidin-4-amine **111**. The last reaction was performed via a Suzuki cross-coupling in which compound **111** was reacted with an excess of the suitable boronic acid in the presence of

Cs_2CO_3 and $Pd(dppf)Cl_2$ in DME and H_2O at 90 °C for 14 h to give compounds **104a,b** (**Scheme 5**).

Scheme 5. Preparation of derivatives **104a,b.**

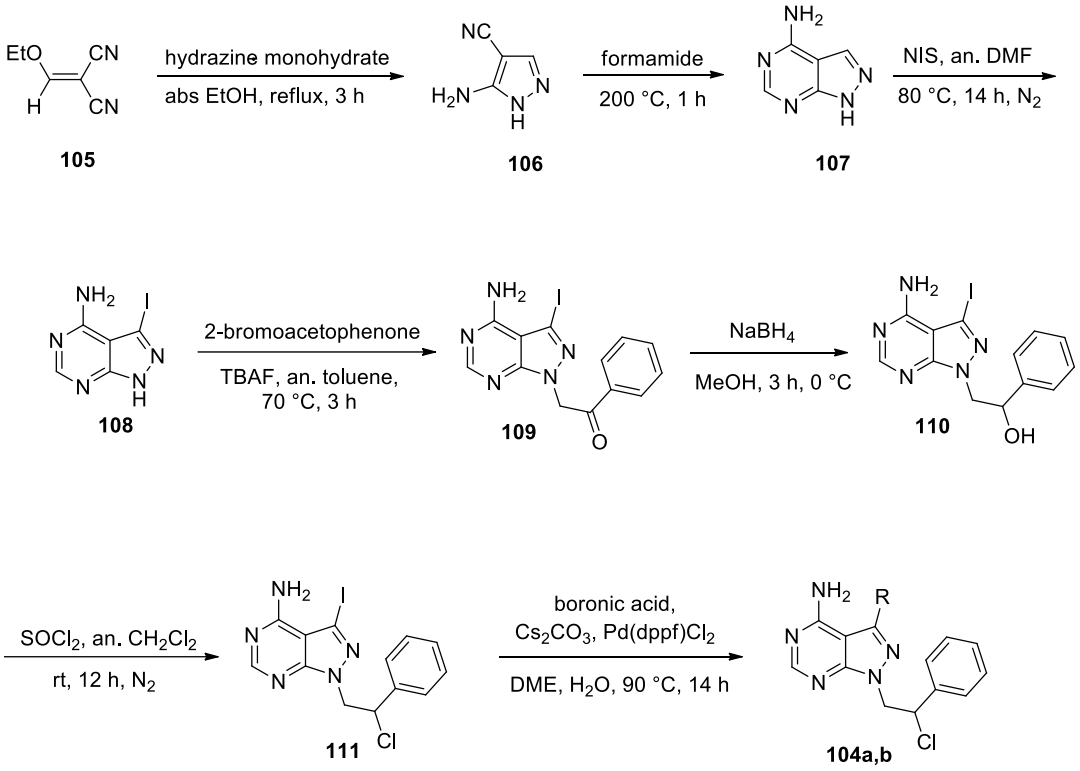

For the synthesis of compounds **104c,d** different attempts have been performed. I tried to perform the Suzuki reaction both on intermediate **110** and **111** with 4-nitrophenylboronic acid or 5-indolylboronic acid, but no reaction was successful (**Scheme 6**). Other attempts will be performed in the future.

Scheme 6. Attempts to obtain **104c,d.**

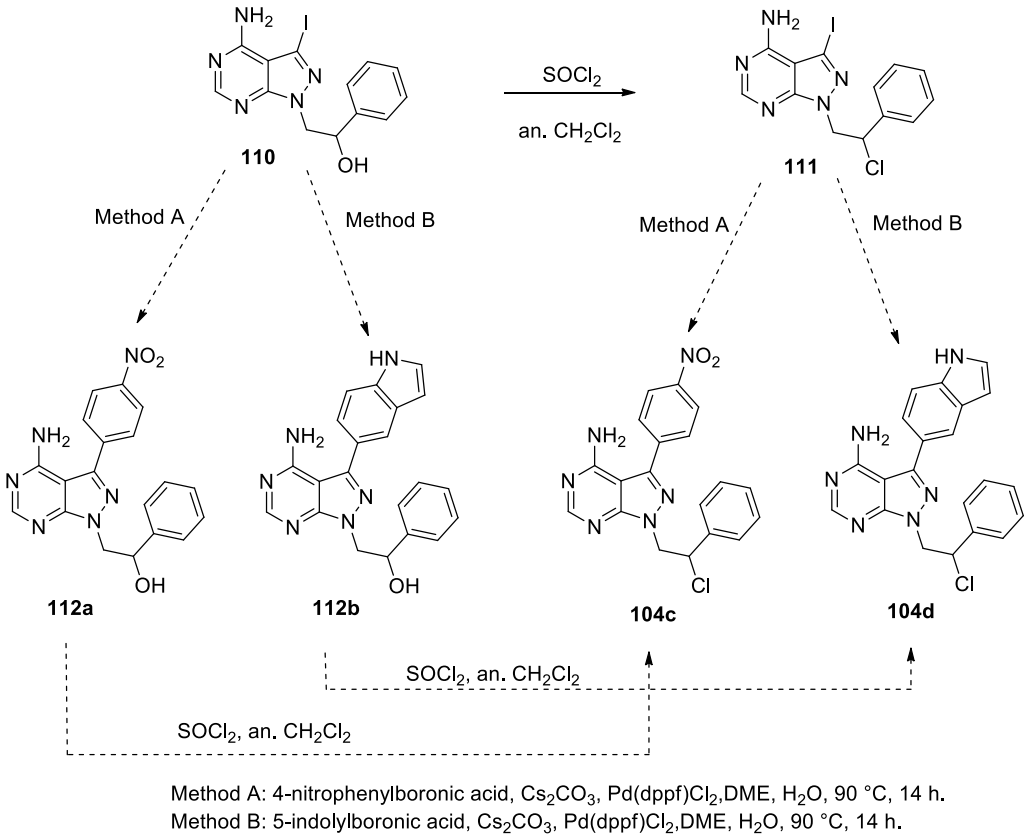

Method A: 4-nitrophenylboronic acid, Cs_2CO_3, $Pd(dppf)Cl_2$,DME, H_2O, 90 °C, 14 h.
Method B: 5-indolylboronic acid, Cs_2CO_3, $Pd(dppf)Cl_2$,DME, H_2O, 90 °C, 14 h.

For the synthesis of compounds **104e-j** a new approach has been used, since the methodology (Suzuki cross-coupling route) used for the previously synthesized compounds **104a,b** did not have good yields. The new route allowed savings in time and solvents and it is feasible thanks to the commercial availability of the acyl chlorides, that are the building blocks used to introduce substituents in C3. This new method could be used, in future, to attempt again the synthesis of compound **104c**, while, unfortunately, for compound **104d,** the appropriate acyl chloride is not available. The synthesis of 3-substituted pyrazolo[3,4-*d*]pyrimidines **104e-j** was performed using a three component one-pot synthesis.[430] Sodium hydride was added in small batches to a solution of malononitrile **113** in dry THF precooled at 0-5 °C; after 30 min, the suitable acyl chloride was added and the solution stirred at room temperature for 2-12 h. Then dimethylsulfate was added, and the solution was refluxed for 3-6 h. Finally, 2-hydrazino-1-phenylethanol **80c** dissolved in dry THF was added and the reaction was carried at reflux for 3-6 h to afford intermediates **114a-f**, purified by flash chromatography. Compounds **114a-f** were

suspended in formamide, and the mixture was heated at 190 °C for 3-4 h to afford the pyrazolo-pyrimidines **115a-f**, that were in turn reacted with thionyl chloride in dry CH_2Cl_2 at room temperature for 12 h under nitrogen atmosphere to give the final compounds **104e-j** (**Scheme 7**).

Scheme 7. Preparation of derivatives **104e-j.**

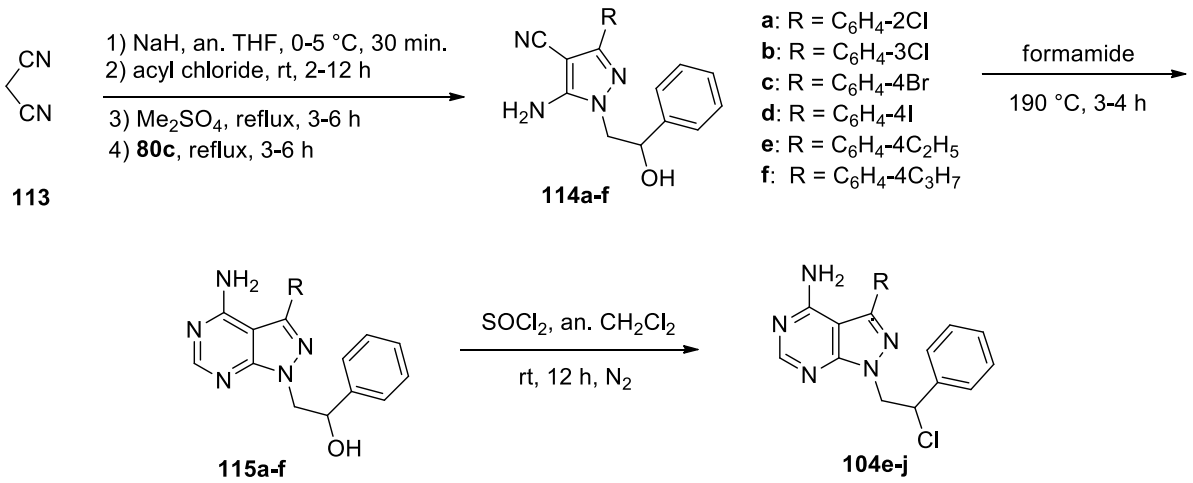

8.2.2 Biology

All the synthesized compounds **104a,b** and **104e-j** were tested in a cell-free assay to evaluate their affinity towards Fyn (**Table V**). In particular, compounds **104a** and **104g**, bearing a *p*-Br and a *p*-CH_2OH substituent, respectively, on the phenyl ring in C3 showed a good *in vitro* inhibitory effect, with K_i values of 1.17 and 1.8 μM, respectively.

Moreover, **104a,b** and **104e-j** were evaluated for their antiproliferative activity on different human lymphoma cell lines. Although the new compounds resulted less active in the cell-free assay than the previously reported derivatives, one of the most effective compounds, **104a** showed very promising IC_{50} values as antiproliferative agents on many of the tested cell lines. Also derivative **104j**, for which the enzymatic data is not available at the moment, is a quite potent antiproliferative agent on some of the tested lymphoma cell lines.

Table V. Enzymatic and cellular activities of compounds **104a,b** and **104e-j** toward isolated Fyn kinase.

Cpd	K_i (μM)	DOHH2 IC_{50} (μM)	FARAGE IC_{50} (μM)	SUDHL8 IC_{50} (μM)	SUDHL6 IC_{50} (μM)	HUT-78 IC_{50} (μM)	FEPD IC_{50} (μM)	H9 IC_{50} (μM)	HH IC_{50} (μM)
104a	1.8	2.438	7.019	6.14	9.282	4.497	10.84	3.417	2.399
104b	ND	ND	ND	ND	ND	ND	ND	ND	ND
104e	9.4	26.58	51.45	18.39	4292	210.9	38.86	38.86	1134
104f	6.92	27.35	30.9	13.69	38914	1677000	24.89	22.07	43.12
104g	1.17	10.99	13.61	11.85	45.64	21.05	21.7	21.7	12.44
104h	2.1	3.677	12.64	11.46	13.17	12.03	20.46	11.61	5.235
104i	5.75	21.18	22.74	17.47	29.68	58	21.53	24.17	21.08
104j	ND	4.382	29.36	6.717	31.11	9.899	29.15	4.735	48.53

ND = not determined

8.2.3 Conclusions

Because of its central role in AD pathogenesis and in various human cancers, Fyn kinase may be surely considered an interesting target for therapeutic intervention. In the present work, we synthesized a small library of new pyrazolo[3,4-*d*]pyrimidines bearing substituents in the C3 position of the heterocyclic scaffold. In particular, a differently decorated phenyl moiety has been introduced in this position, maintaining the primary amino group in C4 and the 2-chloro-2-phenylethyl chain in N1, how the most active compounds obtained in the previous studies. Compound **104a**, bearing a *p*CH_2OH group on the phenyl ring in C3, showed activity towards Fyn with K_i values in the micromolar range and a good activity towards different lymphoma cell lines, with IC_{50} values in the low micromolar range.

This study gave us the possibility to expand the SAR on this family of pyrazolo[3,4-*d*]pyrimidines and to identify a new active compound **104a**. At the moment, we are waiting for other biological results on **104a,g,h** and **j** that are being tested in an Alzheimer cell model and on different cancer cells.

CHAPTER 9. Discussion. Synthesis of Hck inhibitors as hits for the development of antileukemia and anti-HIV agents

9.1 Background

Several studies demonstrated that high levels of Hck are associated with drug resistance in chronic myeloid leukemia and, furthermore, that Hck activity is connected with HIV-1. In this context, we employed a structure-based drug design study with the aim of identifying novel Hck inhibitors. First, our in house library of pyrazolo[3,4-*d*]pyrimidines was analyzed to select the most promising binders of Hck for biological investigation. Later, the same computational methodology was applied to screen a library of commercially available compounds. For this aim, we used the crystal structure of Hck in complex with 4-amino-5-(4-methylphenyl)-7-(tert-butyl)-pyrazolo[3,4-*d*]pyrimidine (PP1, **7**), (2.0 Å resolution, PDB ID: 1QCF).[431]

From this *in silico* screening we identified some derivatives, both from our library and commercial, endowed with inhibitory activity against Hck in enzymatic assays. These findings demonstrated the suitability of the applied computational approach. The predicted binding modes for the best compounds **116** and **117** (K_i = 0.14 and 0.22 μM, respectively) are shown in **Fig. 32A,B**.

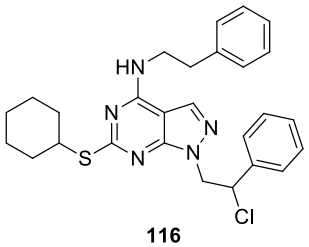

116

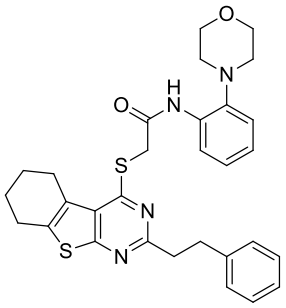

117

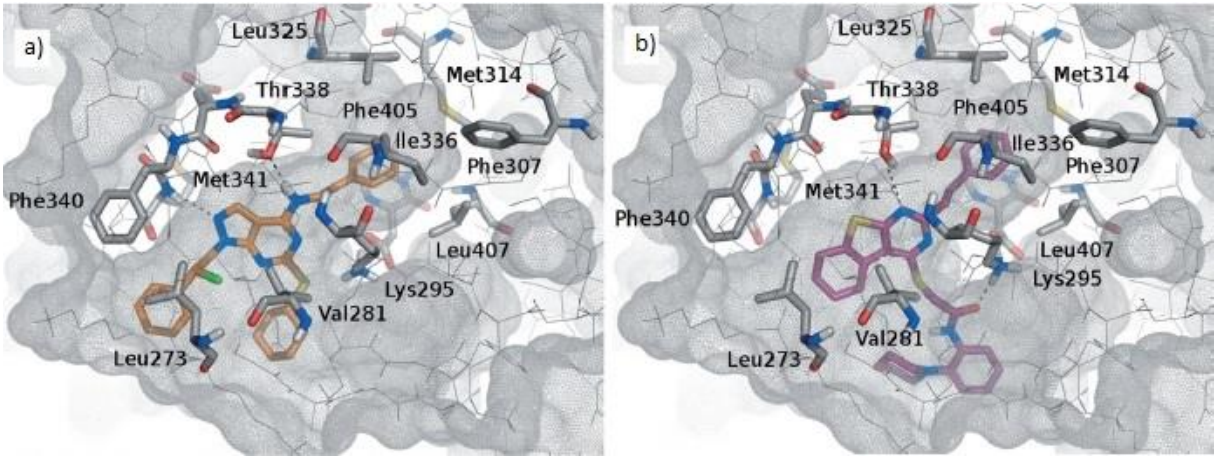

Fig. 32. Graphical representation of the predicted binding modes of compounds. **A. 116** (orange), **B. 117** (warm pink) in the ATP binding site of Hck.

Evaluation of these Hck inhibitors on the KU-812 leukemia cell line indicated weak activity for compound **117** (IC_{50} = 66.5 ± 11.8 µM), while **116** was almost inactive. On the other hand, because Hck was shown to be a novel target for HIV, compound **117** was tested for anti HIV-1 activity in primary monocyte-derived macrophages (MDM)[432,433] and data showed that it is able to block viral replication with an EC_{50} value of 12.9 µM without significant cytotoxicity. Furthermore, to assess its specificity against Hck, compound **117** was tested against a panel of kinases including other Src family members (Blk, Fgr, Fyn, c-Src, Lck, Lyn, Syk, and Yes), TK (Abl and Abl-T315I), as well as some kinases important for HIV-1 (CDK9, Fak, Itk, Jak3, Ron).[434–438] The percentage of residual enzymatic activity was measured for each kinase by using **117** at 10 µM, and the results are listed in **Table VI**. Remarkably, **117** proved to be more efficient against Hck than toward the other investigated kinases, confirming such a compound as a useful probe to study Hck function.[390]

Table VI. Residual kinase activity after treatment with **117**, expressed as percent of basal kinase activity.

Kinase	**Residual activity**
Hck(h)	38
Abl(h)	103
Abl(T315I)(h)	83
Blk(h)	100
CDK9/cyclin T1(h)	104
cSrc(h)	67
Fak(h)	101
Fgr(h)	105
Fyn(h)	93
Itk(h)	102
Jak3(h)	92
Lck(h)	120
Lyn(h)	91
Ron(h)	109
Syk(h)	77
Yes(h)	83

9.2 Project

Thanks to this study, we identified two new Hck inhibitors **116**, previously synthesized by my research group, and the commercial compound **117**. These molecules showed an inhibitory activity in the low micromolar concentration range in enzymatic assays. Moreover, **117** showed antiproliferative activity against the human leukemia cell line KU-812. Derivative **116** resulted inactive in cellular assays, maybe because its scarce pharmacokinetics properties. For these reasons, during my PhD course, I decided to synthesize a new generation of compound **118a-e** and **119a-c** in order to improve ADME properties and to expand SAR evaluations of these molecules.

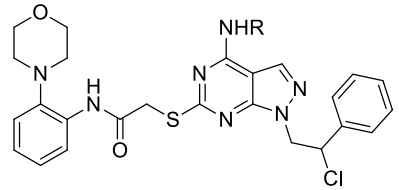

118a-e

NHR = aliphatic and aromatic amino groups

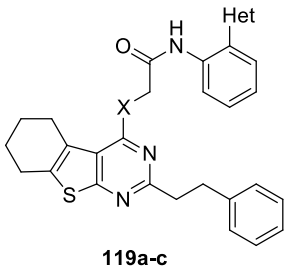

119a-c

X = NH, S
Het = nitrogen heterocycles

Compounds **118a-e**, maintain the pyrazolo[3,4-*d*]pyrimidine scaffold of compound **116**, but in C6 they bring a hydrophilic *N*-(2-morpholin-4-ylphenyl)thioacetamidic chain, analogously to compound **117**. Moreover, several aromatic and aliphatic amino groups were introduced in C4. Compounds **119a-c** conserve the nucleus of compound **117** and bring different chain in C4 on the basis of molecular modeling suggestions.

9.2.1 Chemistry

The synthesis of compounds **118a-e** was performed using a multistep convergent synthesis (**Scheme 8**). First, the intermediate 1-(2-hydroxy-2-phenyl-ethyl)-6-thioxo-1,5,6,7-tetrahydro-pyrazolo[3,4-*d*]pyrimidin-4-one **83c** and the building-block **120** have been synthesized and then these two intermediates were reacted together to obtain the final compounds **118a-e**.

Scheme 8. Simplified retrosynthesis to obtain compounds **118a-e.**

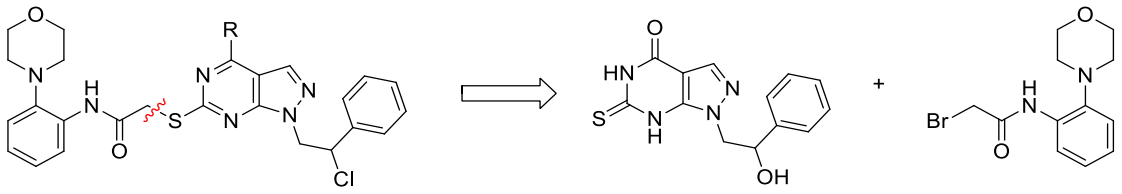

118a-e **83c** **120**

The building-block **120** was synthesized reacting 2-morpholinoaniline **121** with bromoacetyl chloride in Et_2O at room temperature for 4 h (**Scheme 9**).

Scheme 9. Synthesis of building-block **120.**

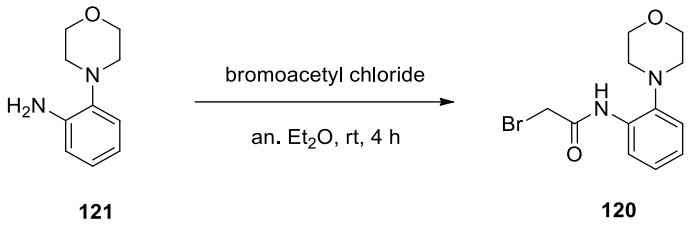

121 **120**

Afterwards, **83c** and **120** were reacted in anhydrous DMF at room temperature in presence of K_2CO_3 to obtain compound **122** with a good yield. This intermediate was treated with the Vilsmeier complex ($POCl_3$/DMF, 1:1) in CH_2Cl_2 to obtain the halogenated compound **123** and a little part of compound **118a**. The reaction of **123** with an excess of the appropriate amine in anhydrous toluene at room temperature for 48 h gave the desired compounds **118b-d** with a good yield. Compound **118e** was synthesized with the reaction between **123** and the 3-chloroaniline in absolute EtOH at reflux for 5 h (**Scheme 10**).

Scheme 10. Synthesis of compounds **118a-e.**

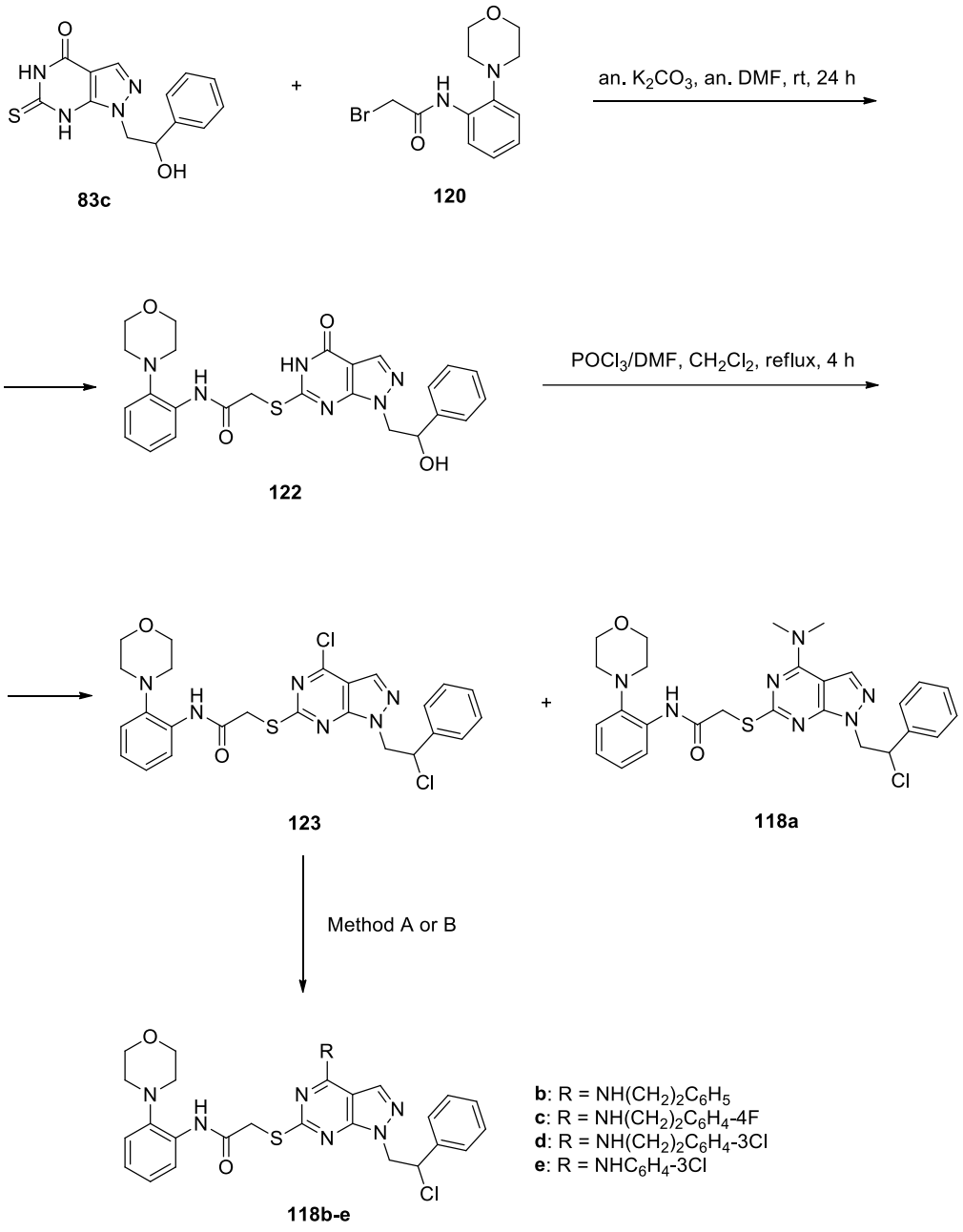

83c **120** **122** **123** **118a** **118b-e**

Method A: appropriate amine, an. toluene, rt, 48 h (to obtain **118b-d**).
Method B: 3-chloroaniline, abs EtOH, reflux, 5 h (to obtain **118e**).

Compounds **119a-c** were synthesized with three different multistep approaches. The three methods have in common only the first intermediate of the synthesis, the 2-phenethyl-5,6,7,8-tetrahydrobenzo[4,5]thieno[2,3-*d*]pyrimidin-4(3*H*)-one **125** that was synthesized reacting the ethyl 2-amino-4,5,6,7-tetrahydrobenzo[*b*]thiophene-3-carboxylate **124** with 3-phenylpropionitrile in the conditions reported by Pochetti *et al*. for the synthesis of an analogue compound (**Scheme 11**).[439] For the synthesis of compound **119a**, the intermediate **125** was treated with $POCl_3$ at 80 °C for 8 h to obtain the halogenated compound 4-chloro-2-phenethyl-5,6,7,8-tetrahydrobenzo[4,5]thieno[2,3-*d*]pyrimidine **126**.[440] This last was reacted with glycine ethyl ester hydrochloride, in the presence of triethylamine (TEA), in absolute EtOH at reflux for 48 h to give the ethyl 2-((2-phenethyl-5,6,7,8-tetrahydrobenzo[4,5]thieno[2,3-*d*]pyrimidin-4-yl)amino)acetate **127** in the same condition suggested by Fujita *et. al*. to obtain an analogue compound.[441] The ester derivative was treated with 1 N NaOH in absolute EtOH at room temperature for 12 h to obtain the acid **128**. Finally, the reaction between compound **128** and 2-morpholinoaniline in presence of PCl_3 in ACN at reflux for 8 h gave the final compound N-(2-morpholinophenyl)-2-((2-phenethyl-5,6,7,8-tetrahydrobenzo[4,5]thieno[2,3-*d*]pyrimidin-4-yl)amino)acetamide **119a** following the conditions reported by Lupea *et al*. (**Scheme 12**).[442]

Scheme 11. Synthesis of compound **125**.

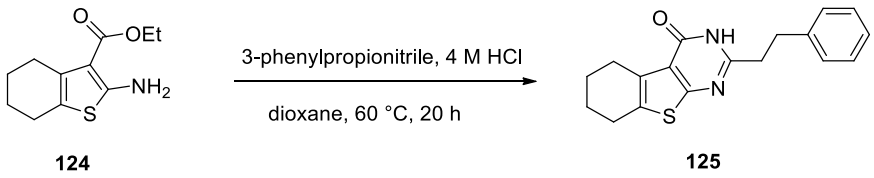

124 **125**

Scheme 12. Synthesis of compound **119a**.

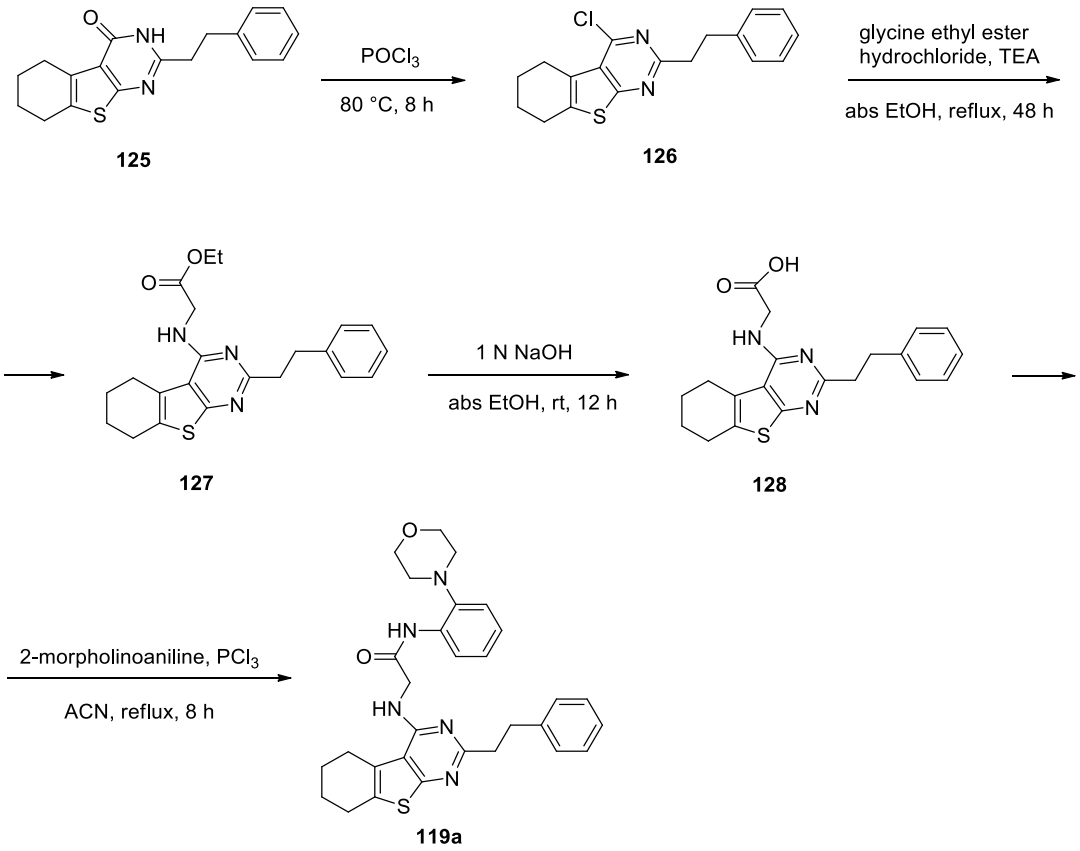

For the synthesis of compound **119b** a convergent approach was utilized. The intermediate **125** was reacted with phosphorus pentasulfide (P_2S_5) in anhydrous 1,4-dioxane at reflux for 8 h, under nitrogen atmosphere, to obtain compound **129.** At the same time, a Pd catalyzed hydrogenation was performed on 1-methyl-4-(2-nitrophenyl)piperazine to obtain 2-(4-methylpiperazin-1-yl)aniline **130**[443] which was in turn reacted with bromoacetyl chloride to obtain compound **131**. Finally, compounds **129** and **131** were reacted in presence of an. K_2CO_3 in an. DMF at room temperature, in nitrogen atmosphere for 4 h to obtain the final compound *N*-(2-(4-methylpiperazin-1-yl)phenyl)-2-((2-phenethyl-5,6,7,8-tetrahydrobenzo[4,5]thieno[2,3-*d*]pyrimidin-4-yl)thio)acetamide **119b** (**Scheme 13**).

Scheme 13. Synthesis of compound **119b**.

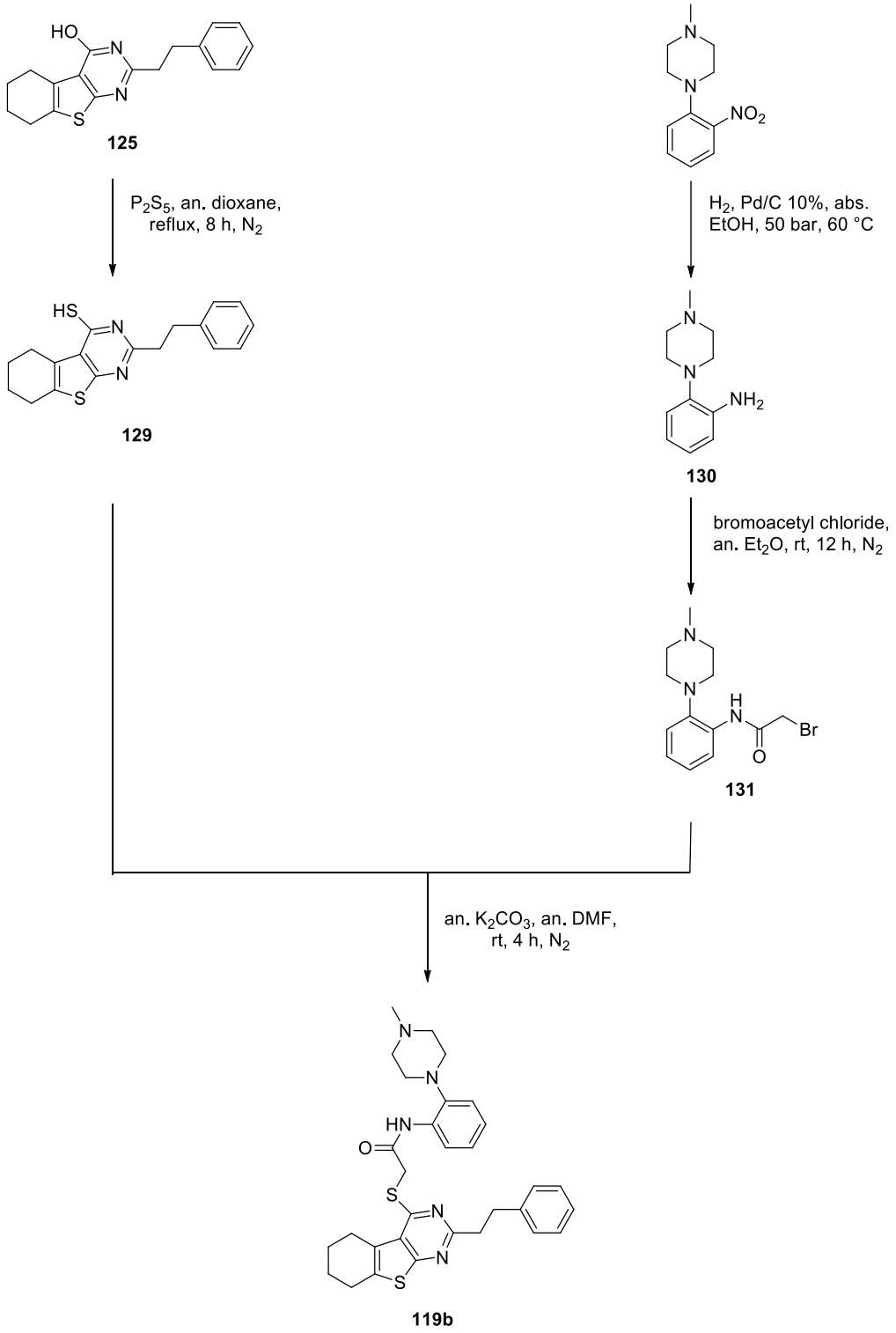

For the synthesis of compound **119c** the 3-methyl-1-(2-nitrophenyl)piperazine **132**, **(**obtained by reaction between 2-methylpiperazine and 1-bromo-2-nitrobenzene) was treated with di-*tert*-butyl dicarbonate (Boc_2O), in presence of TEA, in anhydrous CH_2Cl_2 at room temperature for 12 h to protect the amine group and the reaction gave compound **133**. This last was reduced utilizing a Pd catalyzed hydrogenation to obtain compound **134**. Derivative **134** was reacted with bromoacetyl chloride in anhydrous Et_2O at room temperature for 3 h under nitrogen atmosphere to obtain tert-butyl 4-(2-(2-bromoacetamido)phenyl)-2-methylpiperazine-1-carboxylate **135**. Finally, compound **135** was reacted with derivative **125** in presence of an. K_2CO_3 in anhydrous DMF at room temperature under nitrogen atmosphere for 12 h to give compound **136** which was deprotected using trifluoroacetic acid (TFA) in anhydrous CH_2Cl_2 at room temperature under nitrogen atmosphere to obtain *N*-(2-(3-methylpiperazin-1-yl)phenyl)-2-((2-phenethyl-5,6,7,8-tetrahydrobenzo[4,5]thieno[2,3-*d*]pyrimidin-4-yl)thio)acetamide **119c** (**Scheme 14**).

Scheme 14. Synthesis of compound **119c**.

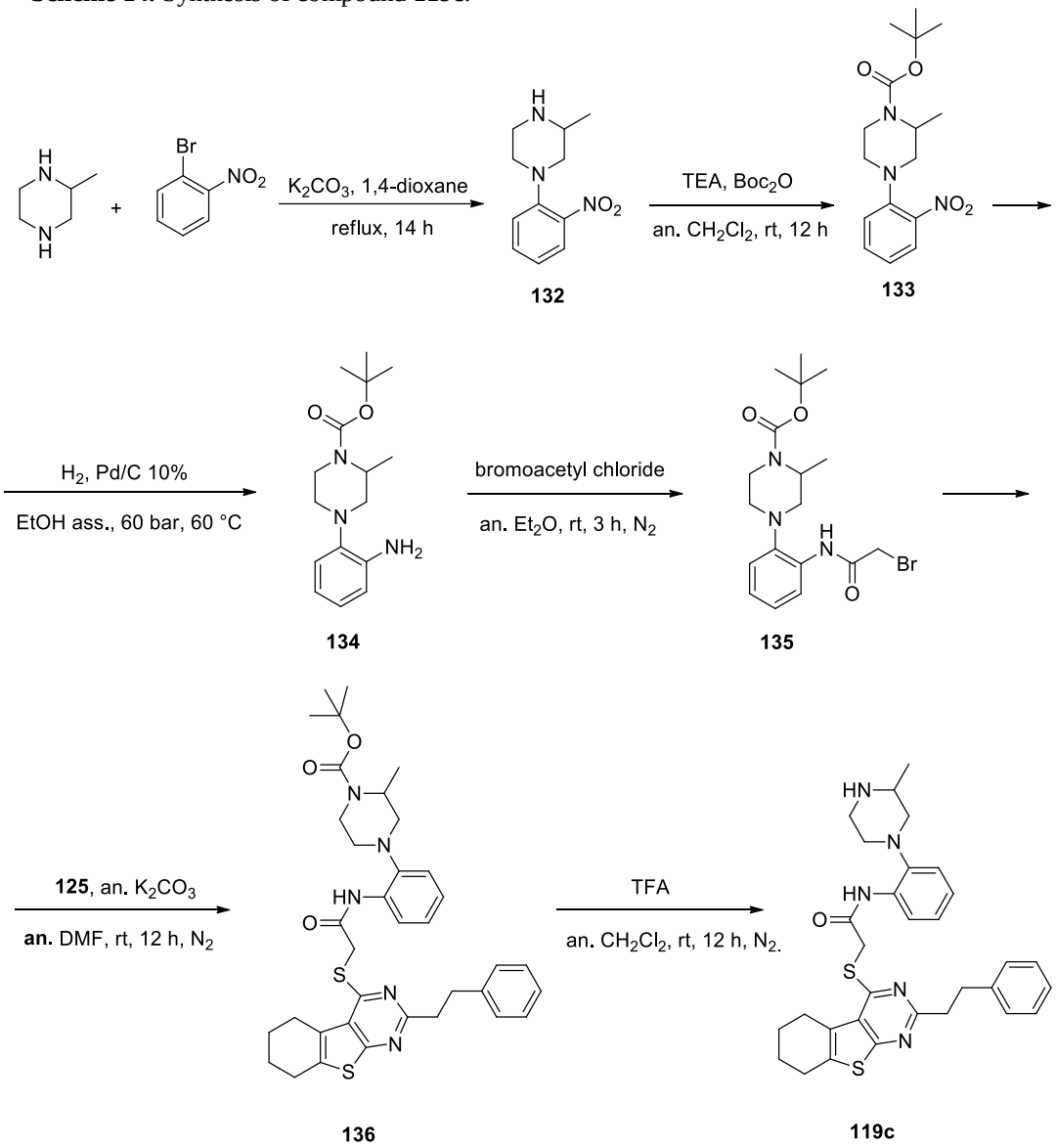

9.2.2 Conclusions

In this work, a structure-based computational study led to the identification of new ATP-competitive Hck inhibitors which show inhibitory activity toward isolated Hck in the sub-micromolar to low-micromolar concentration range and are endowed with an interesting antiproliferative activity profile against the human leukemia cell line KU-812. On the basis of these considerable results, during my PhD course I synthesized a second-generation compounds with the aim to improve the activity and SAR evaluations of this class of inhibitors. *In vitro* assays on these molecules are in progress. On the basis of their enzymatic activity, compounds will be tested on KU-812 cell lines. Enzymatic and cellular assays are in progress.

CHAPTER 10. Discussion. Synthesis of potential Sgk1 inhibitors

10.1 Background

As previously reported, Sgk1 has demonstrated to be involved in cancer development and resistance, and in the metabolic syndrome. For these reasons, starting from the high homology among kinases, an *in silico* screening was recently conducted, in collaboration with the University of Magna Graecia of Catanzaro, to assess if some members of the in house library of 4-amino-substituted pyrazolo[3,4-*d*]pyrimidines, active as Abl and Src inhibitors, were also active on Sgk1 and Akt through an ATP competitive mechanism. This study allowed us to identify different pyrazolo[3,4-*d*]pyrimidines endowed with a good activity toward Sgk1. In particular, SI113 is effective in inhibiting Sgk1 with an IC_{50} value of 600 nM and it is selective versus Akt[288] (**Fig. 33**).

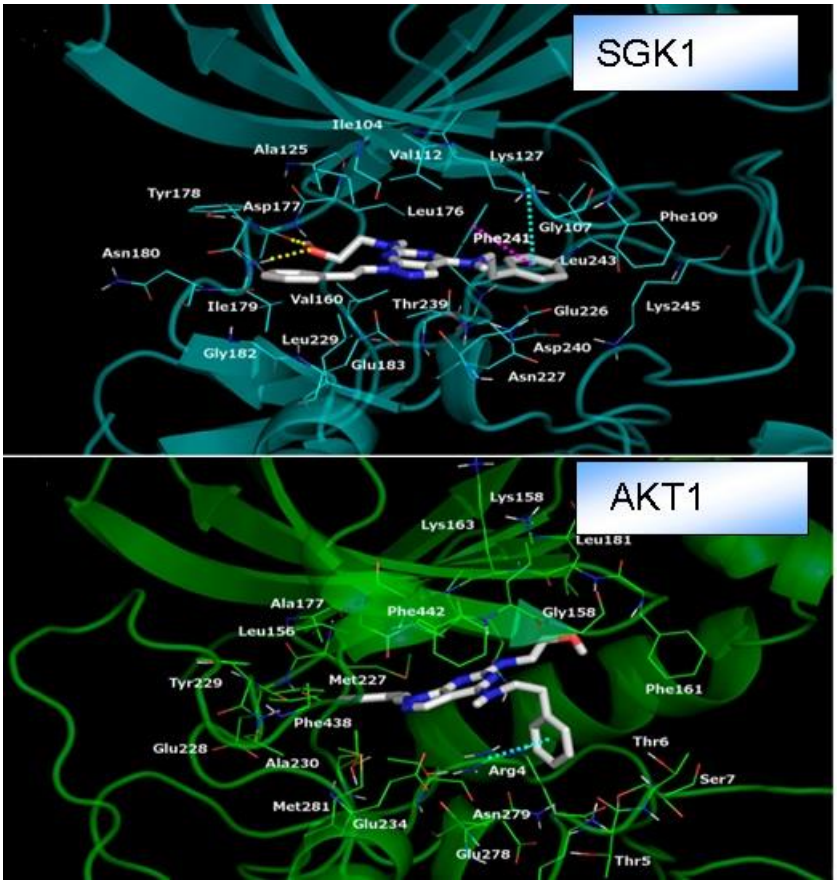

Fig. 33. Binding mode of SI113 into Sgk1 and Akt.

Furthermore, SI113 showed several biological activities: it inhibits tumour growth *in vitro* and *in vivo* in hepatocarcinoma models,[295] it reduces cell proliferation and potentiates paclitaxel effect in colon carcinoma cells,[290] potentiates radiotherapy effects in human GB multiforme cells[296] and induces apoptosis in endometrial cancer cells.[291]

10.2 Project

On the basis of these interesting results, during my PhD course I started a lead optimization study, synthesizing a library of SI113 derivates **137a-i**.

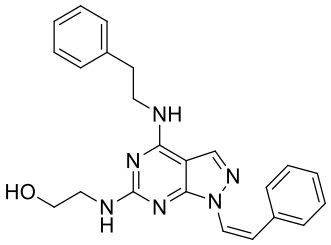

SI113

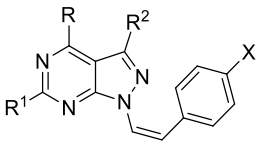

137a-e

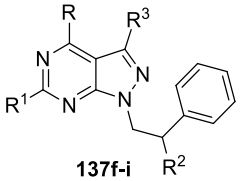

137f-i

a: R = NHC_3H_7; R^1 = H; R^2 = H; X = F
b: R = $NHCH_2C_6H_4$-4Cl; R^1 = H; R^2 = H; X = Cl
c: R = $NHCH_2C_6H_4$-3Cl; R^1 = H; R^2 = H; X = Br
d: R = 4-morpholinyl; R^1 = $NHCH_2CH_2OH$; R^2 = H; X = H
e: R = NH_2; R^1= H; R^2 = CCPh; X = H

f: R = NH_2; R^1 = H; R^2 = Cl; R^3 = CCPh
g: R = NHC_6H_4-3OH; R^1 = $SCH(CH_3)_2$; R^2 = Cl; R^3 = H
h: R = NHC_6H_4-3OH; R^1 = S-cyclopentyl; R^2 = Cl; R^3 = H
i: R = NHC_6H_4-3OH; R^1 = SCH_2CH_3; R^2 = CH_3; R^3 = H

10.2.1 Chemistry

For the synthesis of derivatives **137a-c**, the starting compounds **139a-c** were prepared from the appropriate hydrazino derivatives **138a-c**[410] and ethyl(ethoxymethylene)cyanoacetate. Intermediates **139a-c** were reacted with formamide for 8 h at 190 °C to give intermediates **140a-c** in high yields. Treatment of these compounds with an excess of the Vilsmeier complex ($POCl_3$/DMF, 1:1) for 8-12 h at reflux in $CHCl_3$ led to the formation of the halogenated derivatives **141a-c**. They were in turn treated with an excess of the appropriate amine in anhydrous toluene at room temperature for 24 h to afford compounds **142a-c**, which were

finally dehydrohalogenated by refluxing with NaOH for 5 h to give the N1-unsaturated derivatives **137a-c** (**Scheme 15**).

Scheme 15. Synthesis of compounds **169a-c**.

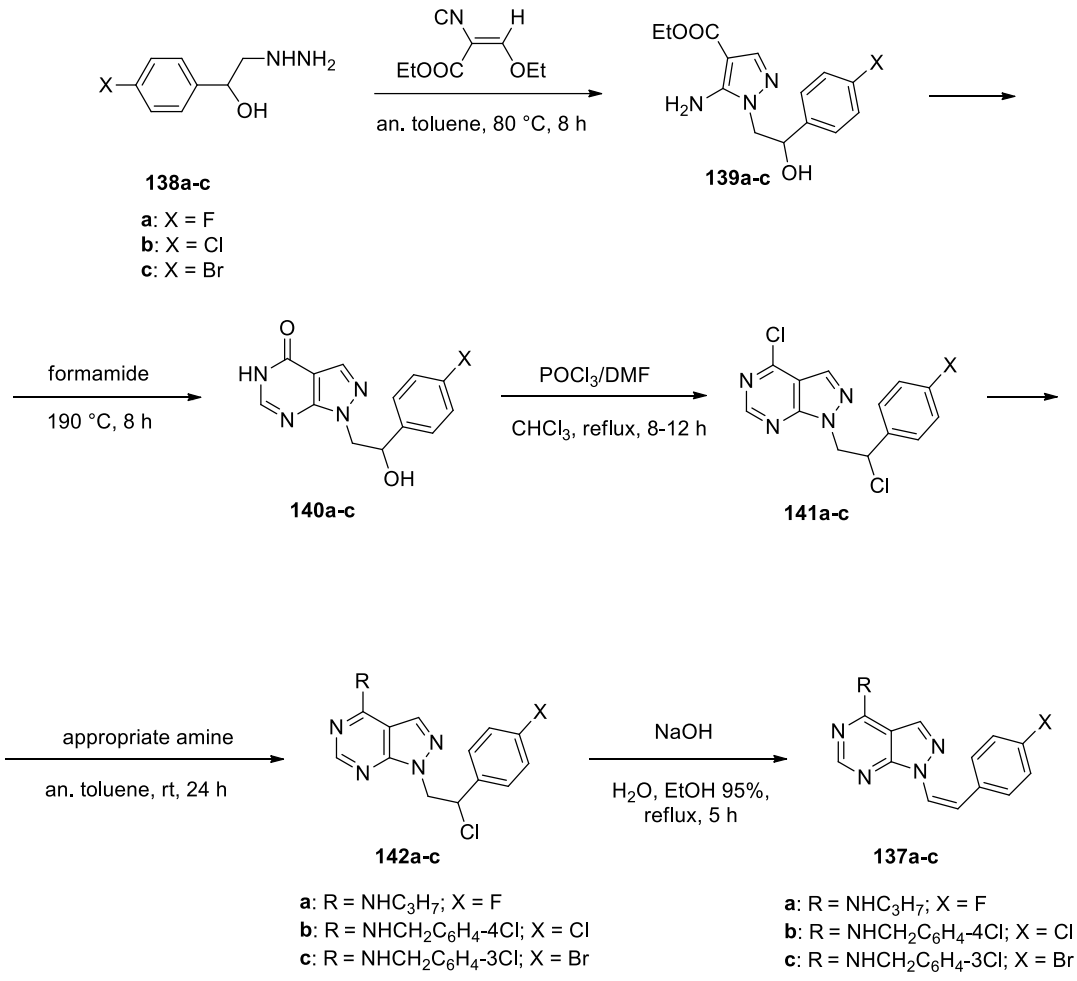

For the synthesis of the final compound **137d**, derivative **83c**, reported above, was alkylated on the thio group in position 6 with methyl iodide in anhydrous THF at reflux. The 6-thioalkyl derivative **143**, obtained from this reaction, was in turn treated with the Vilsmeier complex ($POCl_3$:DMF, 1:1) in $CHCl_3$ to afford the dihalogenated compound **144**, bearing the chlorine atom both at the position 4 of the pyrimidine nucleus and on the N1 side chain. Finally, the regioselective substitution of the C4 chlorine atom with an excess of morpholine in anhydrous toluene at room temperature for 24 h afforded compound **145** in good yields. Compound **145** was dehydrohalogenated by refluxing with NaOH to give the corresponding N1-unsaturated

derivative **146**. Then, the oxidation of the latter with 3-chloroperoxybenzoic acid in $CHCl_3$ gave the 6-methylsulfonyl derivative **147**. Finally, compound **137d** was obtained by nucleophilic substitution of the methylsulfonyl group of **147** with 2-aminoethanol in DMSO at 90 °C for 12 h (**Scheme 16**).

Scheme 16. Synthesis of compound **137d**.

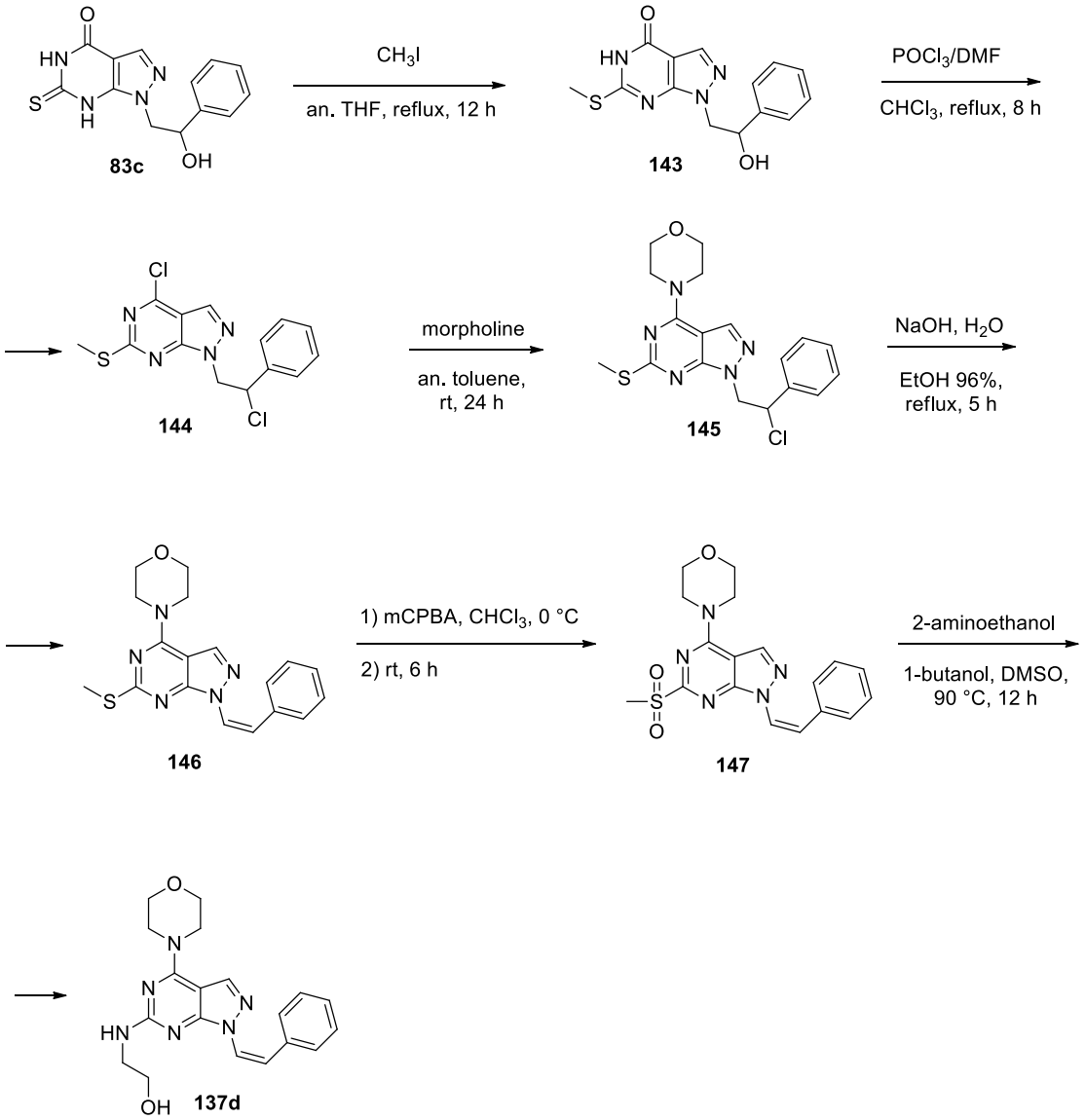

Compounds **137e,f** were synthesized reacting compound **110**, previously reported, with phenylacetylene in the presence of bis(triphenylphosphine)palladium(II) dichloride, CuI and Et_3N in THF (Sonogashira reaction conditions) at reflux for 14 h affording compound **148**. Treatment with $SOCl_2$ in anhydrous CH_2Cl_2 at room temperature for 12 h under nitrogen atmosphere gave compound **137e**. Finally, **137e** was reacted with NaOH in 96% EtOH at reflux for 5 h affording compound **137f** (**Scheme 17**).

Scheme 17. Synthesis of compounds **137e,f**.

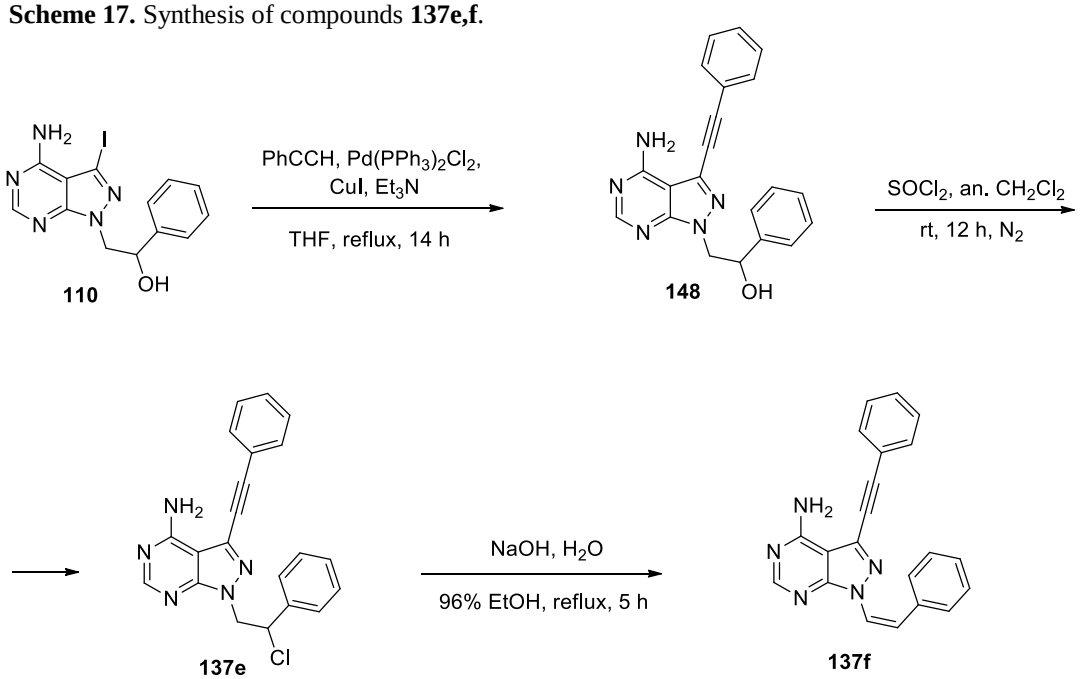

The synthesis of compound 137g,h started with the alkylation of the thio-group in position 6 of intermediate **83c** with 2-bromopropane or bromocyclopentane and an. K_2CO_3 in anhydrous DMF at room temperature for 8 h afforded derivatives **149a,b**. The suitable 4-chloro derivatives **150a,b**, obtained by treatment of **149a,b** with the Vilsmeier complex ($POCl_3$:DMF, 1:1), were reacted with 3-aminophenol in absolute EtOH at reflux for 3-5 h to give the desired compounds **137g,h** in good yields (**Scheme 18**).

Scheme 18. Synthesis of compounds **137g,h.**

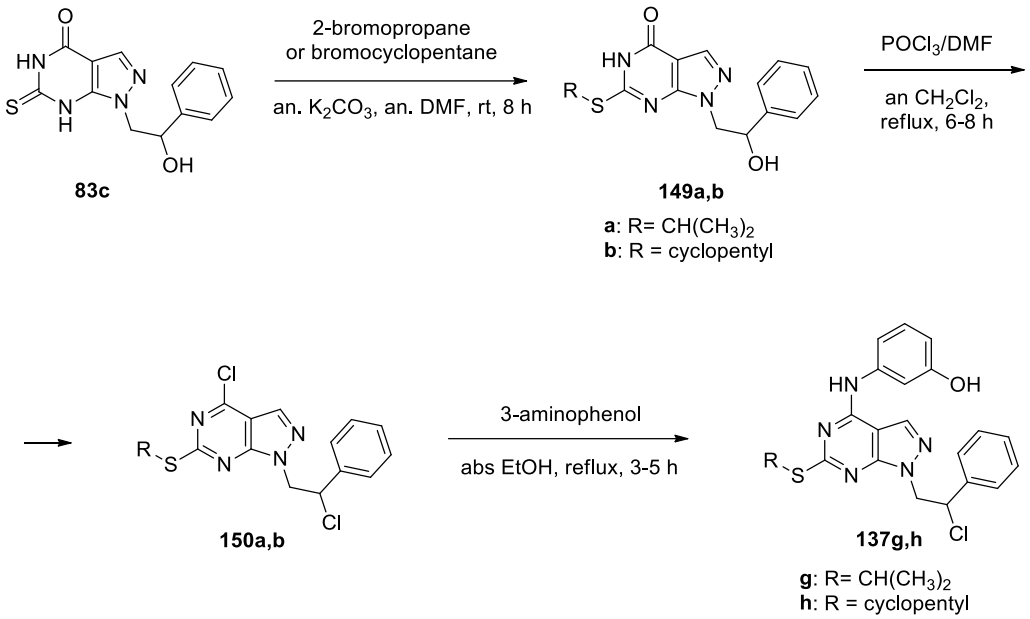

For the synthesis of compound **137i** (2-phenylpropyl)hydrazine **151** (prepared from 1-bromo-2-phenylpropane)[410] was reacted with ethyl(ethoxymethylene)cyanoacetate at reflux to afford the ethyl 5-amino-1*H*-pyrazole-4-carboxylate **152**. The latter was treated with benzoyl isothiocyanate in anhydrous THF at reflux for 12 h to give intermediate **153**. This compound was then cyclized to the pyrazolo[3,4-*d*]pyrimidinone **154** by treatment with 2 M NaOH at 100 °C for 10 min, followed by acidification with acetic acid. Alkylation of the thiocarbonyl group of derivative **154** with iodoethane afforded the 6-alkylthio derivative **155**, which was in turn treated with the Vilsmeier complex ($POCl_3$/DMF, 1:1) in CH_2Cl_2 at reflux for 6 h to obtain compound **156** bearing a chlorine atom in C4. Finally, the reaction of **156** with 3-aminophenol in absolute EtOH at reflux for 3-5 h gave the desired compound **137i** in good yield (**Scheme 19**).

Scheme 19. Synthesis of compound **137i**.

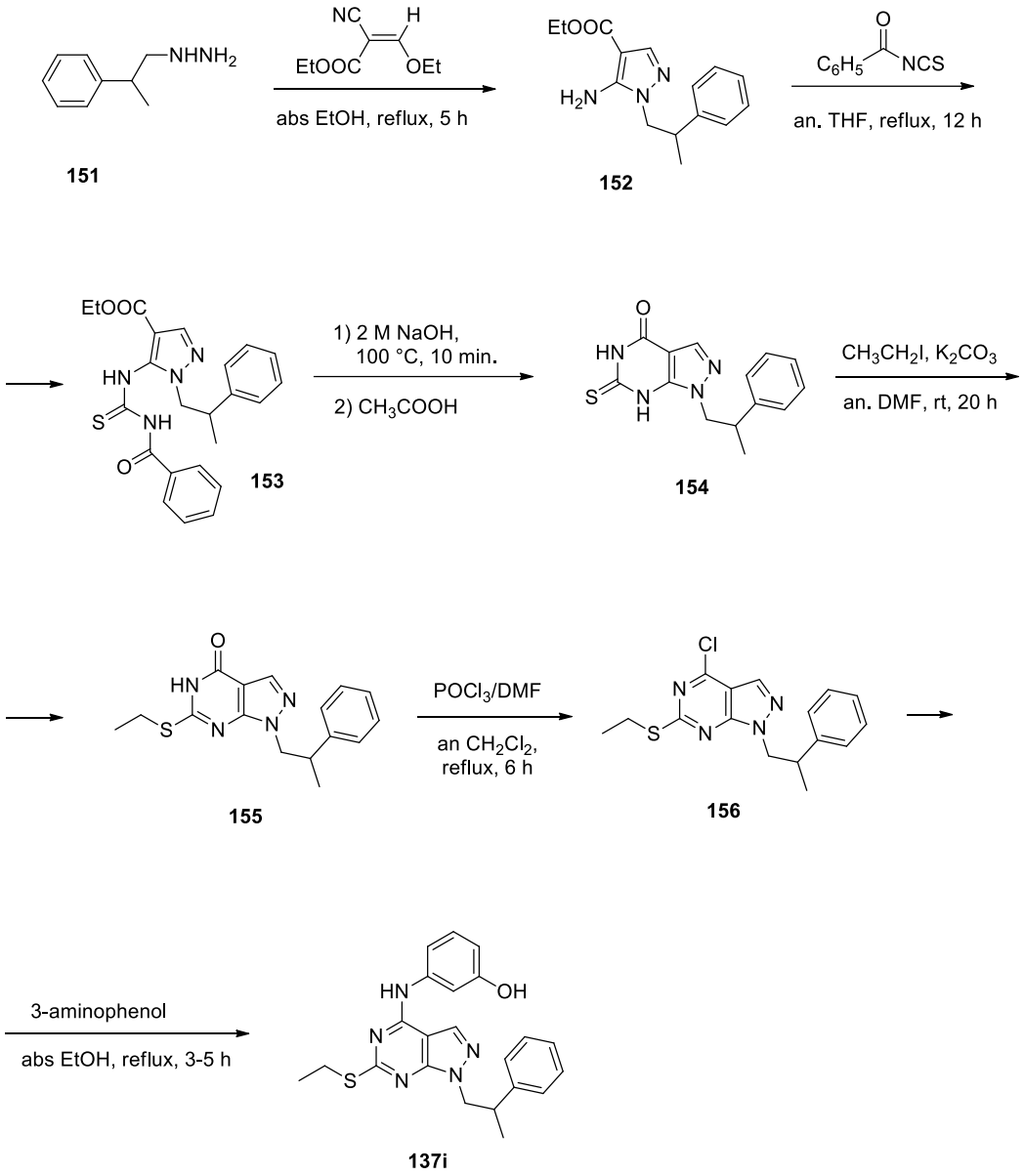

10.3 Conclusions

In conclusion, a new Sgk1 selective inhibitor has been identified following a multidisciplinary approach based on association of molecular modeling, organic synthesis, molecular biology, and cell biology skills. Thanks to this study, during my PhD course I synthesized nine potential Sgk1 inhibitors. Enzymatic assays of these compounds are in progress and, on the basis of the enzymatic results, we will orient future synthesis.

CHAPTER 11. Discussion. Water solubility enhancement of pyrazolo[3,4-*d*]pyrimidine derivatives via miniaturized polymer-drug microarrays

11.1 Background

The pyrazolo[3,4-*d*]pyrimidines are readily soluble in DMSO and other organic solvents, but the limited solubility in water adversely affects their bioavailability and efficacy. Thus, in order to avoid the use of toxic organic solvents for *in vitro* and *in vivo* tests, several strategies have been sought to improve the aqueous solubility and pharmacokinetics of pyrazolo[3,4-*d*]pyrimidine derivatives, including formation of complexes with cyclodextrins,[444] encapsulation into liposomes,[445] formulation with albumin into nanoparticles[446] and synthesis of prodrug derivatives.[447] However, one of the simplest and most promising methods is to create an amorphous solid dispersion where the drug is molecularly dispersed in an inert carrier, typically a hydrophilic polymer,[448–450] such that the resulting stabilised amorphous drug shows a higher water solubility compared to the crystal form.[451]

11.2 Project

For these reasons, during the four months that I spent at the School of Pharmacy at the University of Nottingham, under the supervision of Prof. Cameron Alexander, I have been developing a novel miniaturized printing technology as a screening method to evaluate drug-polymer compatibility.[452] Thanks to this work, I recently published a letter.[453]

This new technique represents an efficient method to evaluate pharmaceutical formulations, and uses nanogram quantities of materials, which results in about 6 order of magnitude lower amount of active pharmaceutical ingredient (API) compared to conventional methods. In this regard, routinely analytical techniques such as DSC and XRPD need milligrams of samples to evaluate drug−polymer blend stability.

I performed, for the first time, an efficient inkjet 2D printer-based screening process to identify the best polymeric carriers for aqueous solubilization of different pyrazolo[3,4-*d*]pyrimidine derivatives at minimal sample amounts. I demonstrated a complete miniaturized and fast analytical route to determine polymer-drug formulations for hit derivatives and validated this approach in a standard cytotoxicity screening. The initial work involved selection of five

previously reported pyrazolo[3,4-*d*]pyrimidines, S31,[454] SI162,[455] SI83,[456] SI91,[456] SI310[102] and synthesis of one new molecule, compound **137d**. These candidate drugs were combined with seven different commercially available hydrophilic polymers selected from those commonly used as pharmaceutical excipients.

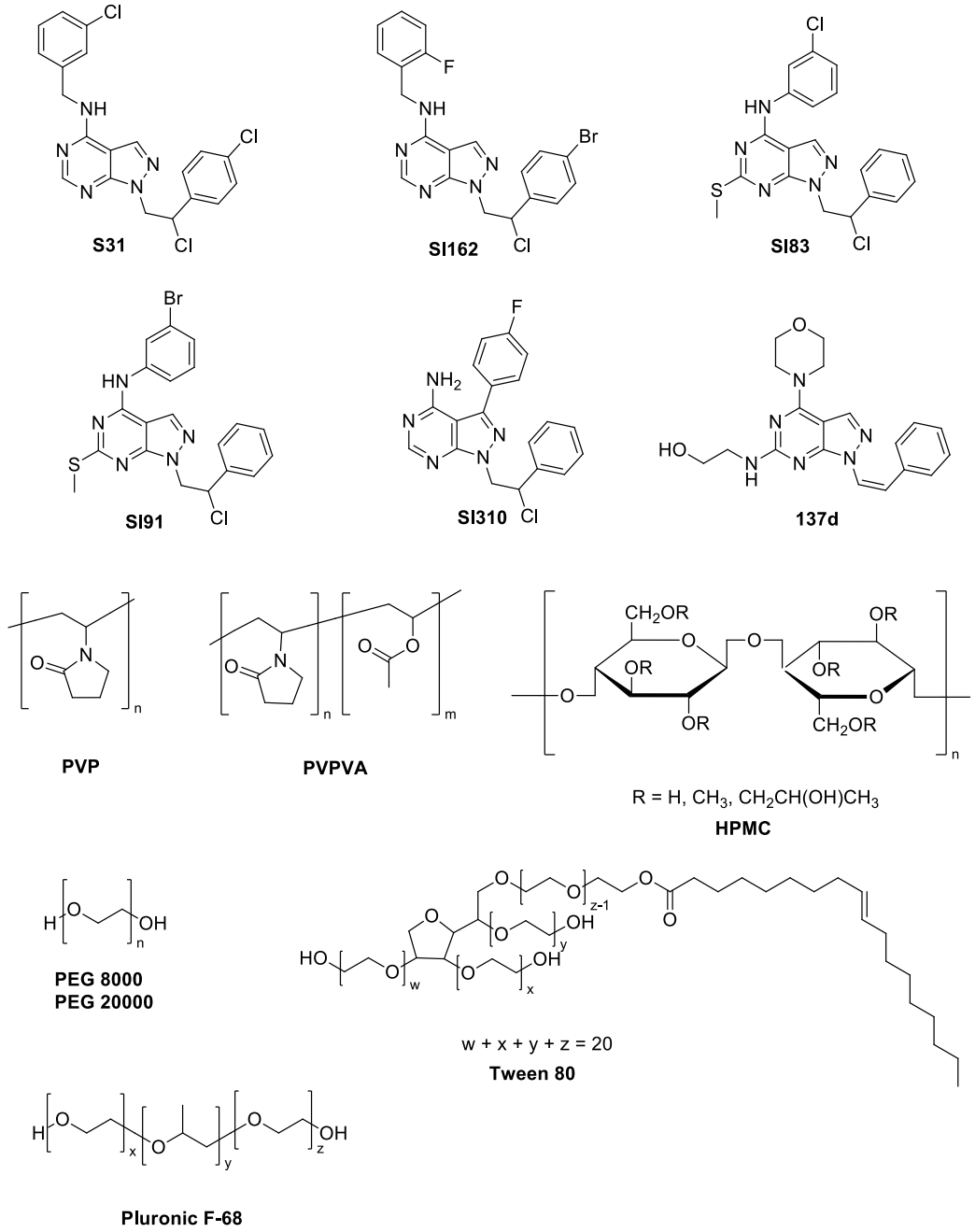

The initial drug and polymer stock solutions were prepared by dissolving the drugs in DMSO and the polymers in deionized (DI) water, in order to reach a final concentration of 10 and 1

mg/mL, respectively. Initially, a fixed volume of each drug solution was dispensed by a piezoelectric printer into a 96-well plate (each drug was formulated at drug/polymer ratio of 10/90% w/w), used as printer target as well as a storage platform.

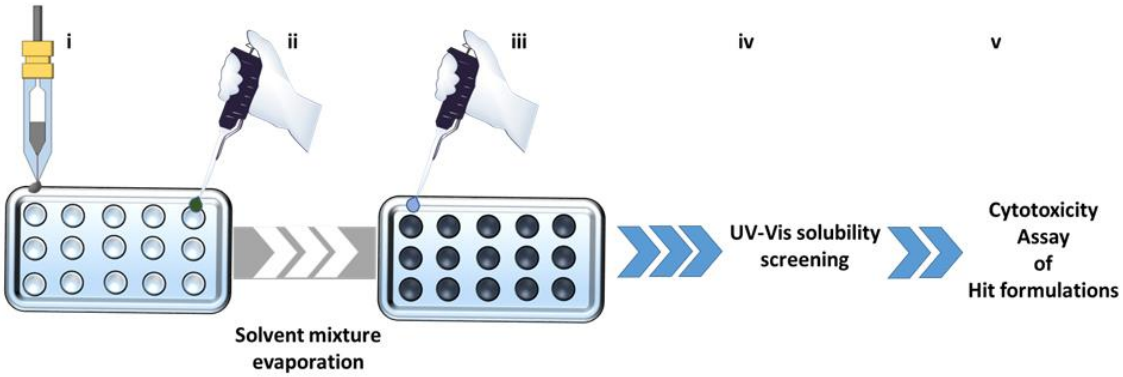

Fig. 34. i. High-throughput dispensing of DMSO drug solutions by an inkjet 2D printer; **ii.** Sequential addition of polymeric aqueous solutions and evaporation of water and DMSO; **iii.** Resuspension with water of the dry solid dispersions; **iv.** Evaluation of the apparent-solubility of the drugs in water from the polymeric matrixes via multiwell-reader UV-vis analysis; and **v.** MTT-cytotoxicity assessment of the hit formulations.

DMSO droplets with nominal volumes ranging from 250 to 280 pL were dispensed to obtain a final amount of drug of 5-6 µg (**Fig. 34i**). Subsequently (**Fig. 34ii**), the different polymer solutions were pipetted into the different wells, by using a pipet (drug controls were prepared by simply adding water rather than polymer solutions). The well plates were left inside the printer cage to allow the DMSO-water mixture to slowly evaporate overnight at room temperature (from previous experience, 24 the amount of DMSO dispensed, for each well in the present work, evaporates completely in the employed conditions). Subsequently, in order to remove any possible residual trapped solvent in the solid formulations, all the well plates were moved into a vacuum drying oven at room temperature for two days (**Fig. 34ii**).

Generally, to dispense the complete set of 6 pure drugs and to pipet the 7 polymers in triplicate, the entire process required around 40 minutes and around 15-18 µg per drug. The drug-polymer solid formulations were then analyzed for solubility by resuspension in 200 µL of DI water (**Fig. 34iii**). The quantitative determination of any UV-vis active molecule present in a solution (in this case the aromatic pyrazolo[3,4-*d*]pyrimidine derivatives) can be obtained by comparison with its calibration curve plotted using several solutions of known concentration.

However, due to the low solubility and stability in water and DMSO, respectively, of the whole set of drugs, it was not possible to determine quantitatively the amount of soluble component. To overcome this problem in a pragmatic manner, an analytic screening based on the variation of the absorbance between the free drug redissolved in water and its polymer formulation was developed (**Fig. 34iv**). This was achieved by normalizing the absorbance values of the drug/polymer dispersions against the absorbance of the free drug in water at the same maximum wavelength. The resulting values (ΔA%) were then used to compare the ability of the different polymers to solubilize the sample set of drugs. The absorbance (A_0) of the drugs alone in water was evaluated by using a UV-vis multiwell plate reader, which was able to measure the full wavelength-spectrum in the range between 200 to 1000 nm in less than 30 seconds per sample. As anticipated, no signals were observed from the presence of water-insoluble drugs. In parallel, the absorbance of the aqueous solutions of drug/polymer blends (A) was tested by using the absorbance of the polymer solutions as a blank. All the absorbance values were kept in the range $0 < A < 1$ where the Beer-Lambert law can be considered valid and, thus, the correlation between absorbance and drug concentration.

$$\Delta A\% = \frac{\Delta A}{A_0} \times 100 = \frac{(A - A_0)}{A_0} \times 100$$

It is apparent from these data that two surfactants (Pluronic F-68 and Tween 80) and the amphiphilic copolymer PVPVA showed notably higher ΔA% average values compared to the homopolymers (PEG 8000-20000, PVP and HPMC). Based on these data, ΔA% average values were calculated and used to rank the polymers in terms of drug apparent-solubility enhancement (**Fig. 35**). This was anticipated, since as a first assumption, the trend in solubilising hydrophobic drugs might be attributed to the presence of hydrophobic blocks in Pluronic F-68, Tween 80 and PVPVA, which could participate in associative interactions with the drugs. However, it is also interesting to highlight that, in this first-generation array, PEG chain length also affected the overall drug apparent-solubility **(Fig. 35**), which increased independently from the initial water solubility of the drugs.

After this first analytical screening, on the basis of the ΔA% average results, each drug was formulated with two of the best performing polymers from the initial set i.e. PVPVA, Pluronic F-68 and Tween 80.

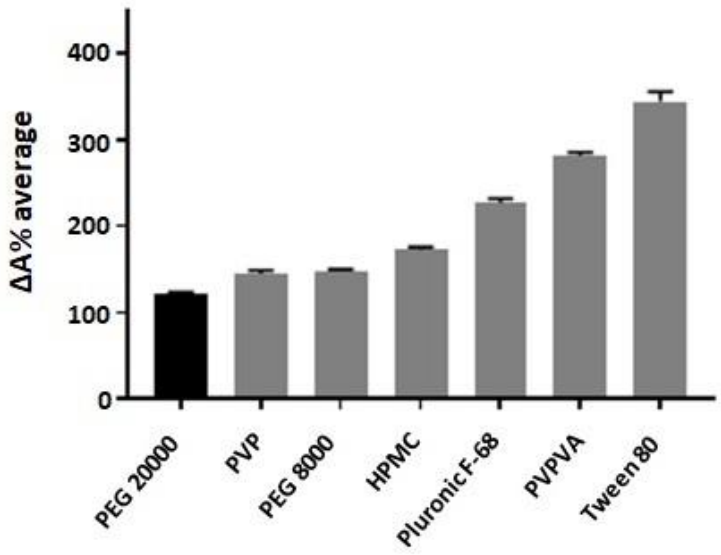

Fig. 35. ΔA% average of polymers ranked according to their water apparent-solubility enhancement (high ΔA% is related a high drug water solubility). Error bars show standard deviation (n = 3).

The anti-proliferative activity of the pyrazolo[3,4-*d*]pyrimidine derivatives alone or in combination with polymers was assessed against a human lung adenocarcinoma cell line (A549), due to its high cytosolic content of tyrosine and serine-threonine kinases (**Fig. 34v**). As shown in **Fig. 36**, none of the drugs formulated as aqueous suspensions was cytotoxic after 24 h treatment. Before screening the drug-polymer formulations, all the polymers were also tested at varying concentrations against the A549 cell line to evaluate their cytotoxicity and identify the least toxic polymer concentration, in order to avoid any effects of the polymer carrier on the final formulation killing activity.

The data showed that the polymers were essentially non-toxic to A549 cells up to concentrations of 200 µg/mL. Subsequent solid dispersion cytotoxicity assays were therefore performed at polymer carrier concentrations below the threshold level of 200 µg/mL.

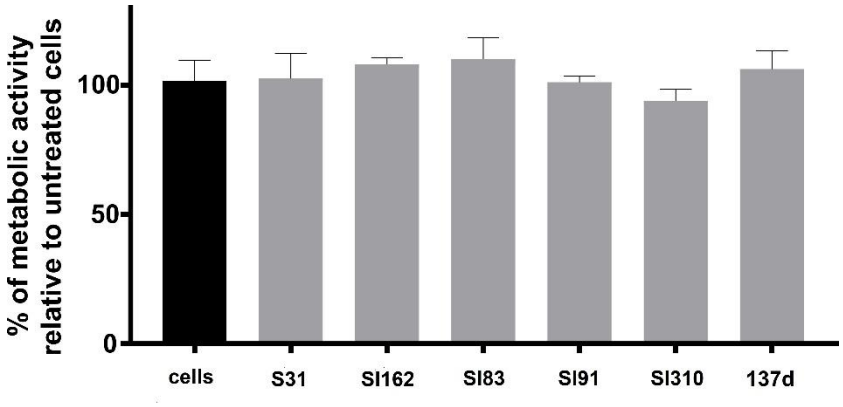

Fig. 36. Cytotoxicity of pure drug solutions (30 µg/mL) against human lung adenocarcinoma cell line (A549). Due to the low solubility of the whole set of drugs, no antiproliferative activity was shown in the high-throughput MTT assay adopted. Error bars show standard deviation (n = 4).

Printing of drugs into polymer dispersions at a level of 90% polymer and assays of these formulations with A549 cells showed growth inhibition of ~ 20-50% (**Fig. 37**), and more than the drugs alone at 30 µg/mL. These data also showed that compounds S31 and SI162 were the most active drug candidates (**Fig. 37**). This formulation process was also used to identify a pair of drugs to evaluate the combined effect of two more potent active principles in a single polymeric blend; thus S31 (15 µg/mL) and SI162 (15 µg/mL) were formulated with PVPVA (drugs/polymer ratio constant at 10/90% w/w). As shown in **Fig. 37** (red bar) a synergic effect of the combined formulation (S31 + SI162-PVPVA) was observed with respect to the single ones. In particular, a further 15-20% growth inhibition was reached (~60% of killing effect). This experimental evidence may facilitate both the future adoption of drug combinations in the field of kinase inhibitors and dosage of drugs with different nature and/or mechanisms of action in one single formulation. To further validate this methodology, traditional cell viability assays using DMSO drug solutions were also performed; formulations gave similar or more accurate cytotoxicity results than that obtained with DMSO. These latter results not only support the analytical evidence of an improved drug water solubility after formulation but also support the enhancement of availability conferred by solid dispersions.

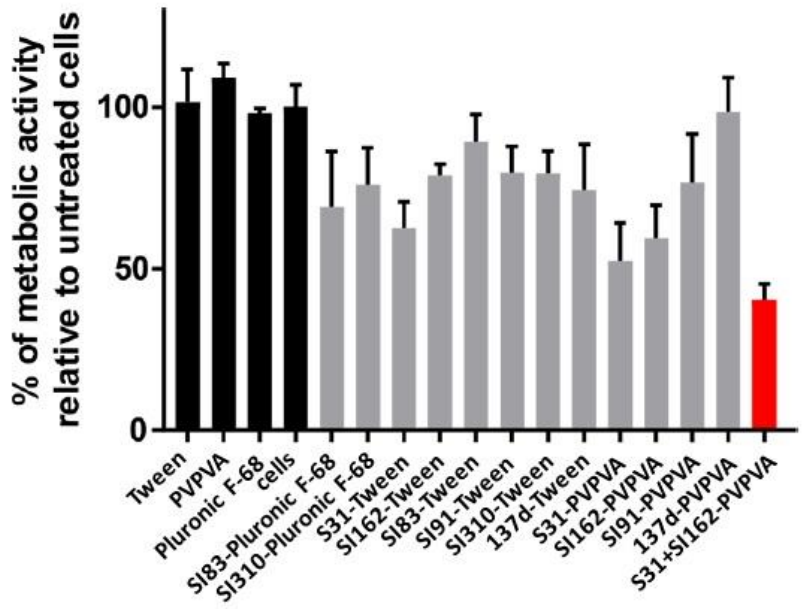

Fig. 37. Cytotoxicity of selected prescreened formulations. The final drug concentration reached in the formulations was around 30 µg/mL, equal to a loading in the polymer matrix of 10% w/w. As shown in **Fig.**, polymers alone showed no adverse activity against the selected cell type. Red bar: cytotoxicity of S31 + SI162-PVPVA at 30 µg/mL in drugs (15 µg/mL, 15 µg/mL of S31 + SI162). Error bars show standard deviation (*n* = 4).

In an attempt to shed some lights upon the interactions established between drug and polymer, some preliminary experiments were carried out using dynamic light scattering (DLS). This was carried out on just the most powerful single drug formulation (S31-PVPVA) resulting from the biological screening reported above (**Fig. 37**). PVPVA showed a poor correlation curve indicating a highly disperse preparation, and the resulting DLS traces could be interpreted as a mixture of small and large polymer micelles. A similar poor correlation curve accompanied by the presence of big aggregates was observed for the free form of S31 as would be expected from its low solubility. On the other hand, the S31-PVPVA formulation showed a single unimodal peak in the range of 1000 nm with a discrete dispersion (PDI of 0.4). As the only peak in this sample, this must be a mixture of both polymer and drug, hinting at a degree of interaction between the hydrophilic polymeric matrix and the hydrophobic drug (**Fig. 38**). The self-assembling of the S31-PVPVA blend into nanomicro structures might explain not only the higher apparent-solubility of the formulation, compared to the free drug, but also the enhanced biological activity, due to a higher bioavailability than the free drug. This result provides preliminary support for the effectiveness of the new method. However, a more rigorous study

would be needed to prove the exact nature of polymer-drug interactions and the features of any structure in particles of the final blend.

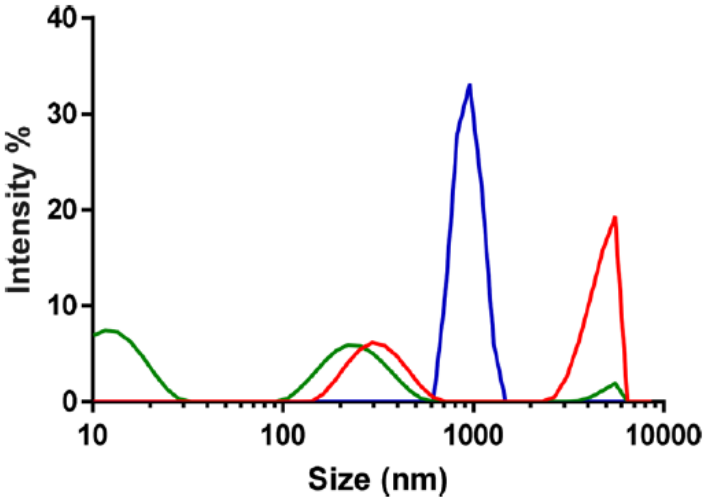

Fig. 38. DLS traces in DI water of untreated S31 (red), PVPVA (green) and S31-PVPVA (blue) as a formulation. Light scattering measurements were collected on suspensions prepared with a final concentration of 0.5 mg/mL in drug (concentration adopted due to instrumental detection limits.

It is worth remarking that the drugs alone have a really low water solubility, which reflects the neglectable availability in water (**Fig. 36**), while, by formulating the pyrazolo[3,4-*d*]pyrimidine derivatives as reported in the present method, the molecules become more soluble and can support a concentration around 30 μg/mL for the cell assays.[455]

11.3 Conclusions

In the present work, I have developed a new miniaturized screening process, based on an inkjet printing technologies, able to identify the best formulation to enhance the apparent water solubility of some pyrazolo[3,4-*d*]pyrimidine derivatives, active as kinase inhibitors. From the Δ A% as a single value for each combination drug-polymer or a Δ A% average value to rank the apparent-solubility enhancement, I have identified the best polymers able to solubilize the pyrazolo[3,4-*d*]pyrimidines in water. The low quantity of drugs used in the present experiments is one of the strongest points of the reported method. In fact, I have used in total less than 20 μg for each drug. This is crucial since the synthesis of these molecules encompasses difficult and timeconsuming synthetic steps with long workup procedures and high organic solvent

consumption. Moreover, with this strategy, it is possible to carry out biological tests for these drugs without direct drug dissolution in DMSO as required in previous work.[457] This method offers a powerful strategy to overcome the problem of the low solubility of this class of compounds and/or other systems involving different poorly water-soluble drugs. As a consequence, formulations can be readily identified for biological (*in vitro-in vivo*) studies and as a starting point for more detailed formulation work.

CHAPTER 12. Experimental section

Starting materials were purchased from Aldrich-Italia (Milan, Italy) and Alfa Aesar (Lancashire, UK). Melting points were determined with a Büchi 530 apparatus and are uncorrected. IR spectra were measured in KBr with a Perkin-Elmer 398 spectrophotometer. ^{1}H NMR spectra were recorded in a $(CD_3)_2SO$ or $CDCl_3$ solution on a Varian Gemini 200 (200 MHz) instrument. Chemical shifts are reported as δ (ppm) relative to TMS as the internal standard, *J* in Hz. ^{1}H patterns are described using the following abbreviations: s = singlet, d = doublet, dd = doublet of doublets, dt = doublet of triplets, t = triplet, q = quartet, quint = quintet, sex = sextet, sept = septet, m = multiplet, and br = broad. TLC was carried out using Merck TLC plates silica gel 60 F254. Chromatographic purifications were performed on columns packed with silica gel 60 Å, 220-440 mesh particle size, 35-75 μM, or using, for flash technique, the instrument Isolera™ One Biotage that works with cartridge Biotage® SNAP Ultra packed with Biotage® HP-Sphere™ spherical silica. Mass spectra (MS) data were obtained using an Agilent 1100 LC/MSD VL system (G1946C) with a 0.4 mL/min flow rate using a binary solvent system of 95:5 methanol/water. UV detection was monitored at 254 nm. MS were acquired in positive and negative modes, scanning over the mass range 50-1500. The following ion source parameters were used: drying gas flow, 9 mL/min; nebulizer pressure, 40 psig; drying gas temperature, 350 °C. Analyses for C, H, N, and S were within ± 0.4% of the theoretical value. All target compounds possessed a purity of ≥ 95% as verified by elemental analyses by comparison with the theoretical values.

General procedure for the synthesis of compounds 81a-c.

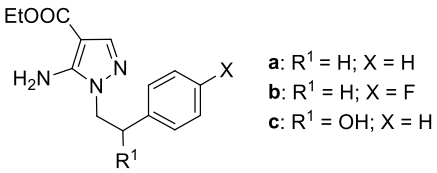

81a-c

The appropriate hydrazine derivatives **80a-c** (20 mmol) were added to a solution of ethyl(ethoxymethylene)cyanoacetate (3.38 g, 20 mmol) in anhydrous toluene (20 mL) and the mixture was heated at 80 °C for 8 h. The solution was concentrated under reduced pressure to half of the volume and allowed to cool to room temperature. The yellow pale solid was filtered and recrystallized from toluene to afford **81a-c** as white solids.

Ethyl 5-amino-1-phenylethyl-1H-pyrazole-4-carboxylate 81a.

Yield: 1.55 g, 60%

Mp: 85-86 °C

MW = 259.30

Anal. calcd for $C_{14}H_{17}N_3O_2$, C 64.85, H 6.61, N 16.21, found C 64.92, H 6.80, N 16.02. ^{1}H NMR ($(CD_3)_2SO$): δ 1.25 (t, *J* = 7.2, 3H, CH_3), 3.02 (t, *J* = 6.8, 2H, CH_2Ar), 4.03 (t, *J* = 6.8, 2H, CH_2N), 4.13 (q, *J* = 7.2, 2H, CH_2O), 4.30 (br s, 2H, NH_2 disappears with D_2O), 6.90-7.28 (m, 5H Ar), 7.59 (s, 1H, H-3).

IR (KBr): cm^{-1} 3428, 3296 (NH_2), 1685 (CO).

MS: m/z 259 $[M+1]^+$.

Ethyl 5-amino-1-(4-fluorophenethyl)-1H-pyrazole-4-carboxylate 81b.

Yield: 4.33 g, 78%

Mp: 129-131 °C

MW = 277.29

Anal. calcd for $C_{14}H_{16}N_3O_2$, C 60.64, H 5.82, N 15.15, found C 60.44, H 5.92, N 15.32. ^{1}H NMR ($(CD_3)_2SO$): δ 1.27 (t, *J* = 7.2 Hz, 3H, CH_3), 3.05 (t, *J* = 6.8 Hz, 2H, CH_2Ar), 4.05 (t,

J = 6.8 Hz, 2H, CH_2N), 4.16 (q, *J* = 7.2 Hz, 2H, CH_2O), 4.36 (s all., 2H, NH_2 disappears with D_2O), 6.94-7.35 (m, 4H Ar), 7.65 (s, 1H, H-3).
IR (KBr): cm^{-1} 3426, 3293 (NH_2), 1678 (CO).

Ethyl-5-amino-1-(2-hydroxy-2-phenylethyl)-1H-pyrazole-4-carboxylate 81c.

Yield: 4.40 g, 80%
Mp: 136-137 °C
MW = 275.30
Anal. calcd for $C_{14}H_{17}N_3O_3$, C 61.08, H 6.22, N 15.26, found C 61.07, H 6.22, N 15.31. ^1H NMR ($(CD_3)_2SO$): δ 1.33 (t, *J* = 7.0, 3H, CH_3), 3.53 (m, 1H, OH, disappears with D_2O), 3.92-4.20 (m, 2H, CH_2N), 4.25 (q, *J* = 7.0, 2H, CH_2O), 5.02-5.13 (m, 1H, CHOH), 5.30 (br s, 2H, NH_2, disappears with D_2O), 7.23-7.42 (m, 5H Ar), 7.58 (s, 1H, H-3).
IR (KBr): cm^{-1} 3470, 3330 (NH_2), 3300-3000 (OH), 1685 (CO).

General procedure for the synthesis of compounds 82a-c.

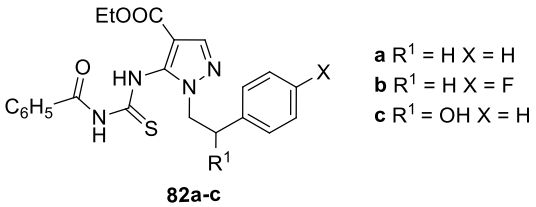

A suspension of the appropriate derivatives **81a-c** (10 mmol) and benzoyl isothiocyanate (1.7 g, 11 mmol) in anhydrous THF (20 mL) was refluxed for 18 h. The solvent was evaporated under reduced pressure, and the crude was crystallized as a white solid by adding Et_2O (30 mL).

Ethyl 5-{[(benzoylamino)carbonothioyl]amino}-1-(2-phenylethyl)-1H-pyrazole-4-carboxylate 82a.

Yield: 2.53 g, 60%
Mp: 168-169 °C
MW = 422.50

Anal. calcd for $C_{22}H_{22}N_4O_3S$, C 62.54, H 5.25, N 13.26, S 7.59, found C 62.50, H 5.41, N 13.02, S 7.50.

^{1}H NMR ($(CD_3)_2SO$): δ (t, *J* = 7.2, 3H, CH_3), 3.18 (t, *J* = 7.0, 2H, CH_2Ar), 4.10-4.30 (m, 4H, CH_2O + CH_2N), 6.97-7.90 (m, 10H Ar), 7.94 (s, 1H, H-3), 9.30 (s, 1H, NH, disappears with D_2O), 11.76 (s, 1H, NH, disappears with D_2O).

IR (KBr): cm^{-1} 3366, 3127 (NH), 1707 (COOEt), 1662 (CONH).

MS: m/z 423 $[M+1]^+$.

Ethyl 5-{[(benzoylamino)carbonothioyl]amino}-1-[2-(4-fluorophenyl)ethyl]-1H-pyrazole-4-carboxylate 82b.

Yield: 3.96 g, 90%

Mp: 185-187 °C

MW = 440.49

Anal. calcd for $C_{22}H_{21}N_4O_3FS$, C 59.99, H 4.81, N 12.72, S 7.28, found C 60.05, H 4.75, N 12.58, S 7.02.

^{1}H NMR ($(CD_3)_2SO$): δ 1.24 (t, *J* = 7.2 Hz, 3H, CH_3), 3.20 (t, *J* = 7.0 Hz, 2H, CH_2Ar), 4.12-4.34 (m, 4H, CH_2O + CH_2N), 7.00-7.98 (m, 9H Ar), 7.98 (s, 1H, H-3), 9.32 (s, 1H, NH, disappears with D_2O), 11.80 (s, 1H, NH, disappears with D_2O).

IR (KBr): cm^{-1} 3367, 3127 (NH), 1706 (COOEt), 1662 (CONH).

Ethyl 5-{[(benzoylamino)carbonothioyl]amino}-1-(2-hydroxy-2-phenethyl)-1H-pyrazole-4-carboxylate 82c.

Yield: 4.07 g, 93%

Mp: 171-172 °C

MW = 438.50

Anal. calcd for $C_{22}H_{22}N_4O_4S$, C 60.26, H 5.06, N 12.78, S 7.31, found C 60.22, H 5.20, N 12.95, S 7.50.

^{1}H NMR ($(CD_3)_2SO$): δ 1.29 (t, *J* = 7.0, 3H, CH_3), 3.97-4.20 (m, 5H, $2CH_2$ + OH, 1H disappears with D_2O), 4.58-4.68 (m, 1H, CHO), 7.05-7.98 (m, 10H Ar), 8.02 (s, 1H, H-3), 8.70 (s, 1H, NH, disappears with D_2O), 12.05 (s, 1H, NH, disappears with D_2O).

IR (KBr): cm^{-1} 3221(NH), 3190-2940 (OH), 1708 and 1671 (2 CO).

General procedure for the synthesis of compounds 83a-c.

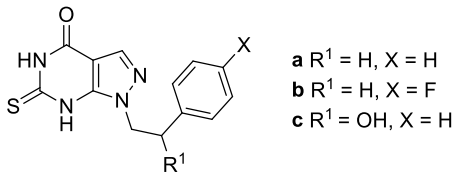

83a-c

A solution of **82a-c** (10 mmol) in 2 M NaOH (40 mL) was refluxed for 10 min and successively diluted with water (40 mL). The solution was acidified with glacial acetic acid. After 12 h of standing in a refrigerator, the crystallized solid was filtered and recrystallized from absolute EtOH to give a white solid.

1-Phenethyl-6-thioxo-1,5,6,7-tetrahydro-pyrazolo[3,4-d]pyrimidin-4-one 83a.

Yield: 1.50 g, 55%

Mp: 200-201 °C

MW = 272.33

Anal. calcd for $C_{13}H_{12}N_4OS$, C 57.34, H 4.44, N 20.57, S 11.77, found C 57.22, H 4.20, N 20.30, S 11.47.

^1H NMR ($(CD_3)_2SO$): δ 3.20 (t, *J* = 7.0, 2H, CH_2Ar), 4.20 (t, *J* = 7.0, 2H, CH_2N), 7.00-7.50 (m, 5H Ar), 7.95 (s, 1H, H-3), 9.25 (s, 1H, NH, disappears with D_2O).

IR (KBr): cm^{-1} 3400-3300 (NH + OH), 1660 (CO).

MS: m/z 272 $[M+1]^+$.

1-[2-(4-Fluorophenyl)ethyl]-6-thioxo-1,5,6,7-tetrahydro-4H-pyrazolo[3,4-d]pyrimidin-4-one 83b.

Yield: 1.83 g, 63%

Mp: 257-259 °C

MW = 290.32

Anal. calcd for $C_{13}H_{11}N_4OFS$, C 53.78, H 3.82, N 19.30, S 11.05, found C 54.04, H 4.04, N 19.54, S 11.36.

^{1}H NMR ($(CD_3)_2SO$): δ 3.22 (t, *J* = 7.0 Hz, 2H, CH_2Ar), 4.25 (t, *J* = 7.0 Hz, 2H, CH_2N), 7.06-7.51 (m, 4H Ar), 7.96 (s, 1H, H-3), 9.28 (s, 1H, NH, disappears with D_2O).

IR (KBr): cm^{-1} 3400-3300 (NH + OH), 1694 (CO).

1-(2-Hydroxy-2-phenyl-ethyl)-6-thioxo-1,5,6,7-tetrahydro-pyrazolo[3,4-d]pyrimidin-4-one 83c.

Yield: 2.3 g, 80%

Mp: 264-265 °C

MW = 288.32

Anal. calcd for $C_{13}H_{12}N_4O_2S$, C 54.16, H 4.20, N 19.43, S 11.12, found C 54.28, H 4.27, N 19.70, S 10.86.

^{1}H NMR ($(CD_3)_2SO$): δ 4.15-4.30 and 4.55-4.72 (2m, 2H, CH_2N), 4.85-5.00 (m, 1H, CHO), 5.66 (br s, 1H, OH, disappears with D_2O), 7.20-7.51 (m, 5H Ar), 8.02 (s, 1H, H-3), 12.20 (s, 1H, NH, disappears with D_2O), 13.40 (s, 1H, NH, disappears with D_2O).

IR (KBr): cm^{-1} 3362 (NH), 3242-2973 (OH), 1681 (CO).

General procedure for the synthesis of compounds 84a-c.

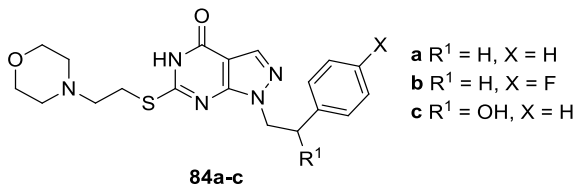

84a-c

a R^1 = H, X = H
b R^1 = H, X = F
c R^1 = OH, X = H

NaOH (0.4 g, 10 mmol) dissolved in absolute EtOH (5 mL) and 4-(2-chloroethyl)morpholine (2.24 g, 15 mmol) were added to a solution of intermediates **83a-c** (2.88 g, 10 mmol) in anhydrous DMF (5 mL). The solution was refluxed for 6 h. After cooling, the solvent was evaporated under reduced pressure, and the crude was poured into cold water. The white solid was filtered, washed with water, and recrystallized from absolute EtOH.

6-((2-Morpholinoethyl)thio)-1-phenethyl-1H-pyrazolo[3,4-d]pyrimidin-4(5H)-one 84a.

Yield: 1.97g, 51%

Mp: 197-198°C

MW = 385.48

Anal. calcd for $C_{19}H_{23}N_5O_2S$, C 56.56, H 5.50, N 17.36, S 7.95, found C 56.61, H 5.28, N 17.13, S 7.67.

^{1}H NMR ($CDCl_3$): δ 2.55-2.70 (m, 4H, $2CH_2N$ morph.), 2.80-2.84 (m, 2H, CH_2N), 3.17-3.24 (m, 4H, CH_2S + CH_2Ar), 3.80-3.85 (m, 4H, $2CH_2O$ morph.), 4.50 (t, *J* = 7.6 Hz, 2H, CH_2N pyraz.), 7.10-7.26 (m, 5H Ar), 8.02 (s, 1H, H-3).

IR (KBr): cm^{-1} 3500-2800 (NH), 1667 (CO).

1-(4-Fluorophenethyl)-6-((2-morpholinoethyl)thio)-1H-pyrazolo[3,4-d]pyrimidin-4(5H)-one 84b.

Yield: 3.47g, 86%

MW = 213-215 °C

MW = 403.48

Anal. calcd for $C_{19}H_{22}N_5O_2FS$, C 59.20, H 6.01, N 18.17, S 8.32, found C 59.27, H 6.14, N 17.99, S 8.23.

^{1}H NMR ($CDCl_3$): 2.42-2.68 (m, 4H, $2CH_2N$ morph.), 2.77-2.83 (m, 2H, CH_2N), 3.15-3.22 (m, 4H, CH_2S + CH_2Ar), 3.75-3.83 (m, 4H, $2CH_2O$ morph.), 4.45 (t, *J* = 7.6 Hz, 2H, CH_2N pyraz.), 7.08-7.23 (m, 4H Ar), 8.02 (s, 1H, H-3).

IR (KBr): cm^{-1} 3400-2800 (NH), 1667 (CO).

1-(2-Hydroxy-2-phenylethyl)-6-((2-morpholinoethyl)thio)-1H-pyrazolo[3,4-d]pyrimidin-4(5H)-one 84c.

Yield: 2.53 g, 63%

Mp: 201-202 °C

MW = 401.48

Anal. calcd for $C_{19}H_{23}N_5O_3S$, C 56.84, H 5.77, N 17.44, S 7.99, found C 56.68, H 5.55, N 17.48, S 8.00.

^{1}H NMR ($CDCl_3$): δ 2.36-2.50 (m, 4H, $2CH_2N$ morph.), 3.10-3.40 (m, 4H, CH_2S + $\underline{CH_2}CH_2S$), 3.45-3.56 (m, 4H, $2CH_2O$ morph.), 4.13-4.40 (m, 2H, CH_2N), 4.83-5.06 (m, 1H, CHO), 5.55 (d, 1H, OH disappears with D_2O), 7.10-7.28 (m, 5H Ar), 7.89 (s, 1H, H-3).

IR (KBr): cm^{-1} 3100-2850 (NH + OH), 1664 (CO).

MS: m/z 401 $[M+1]^+$.

General procedure for the synthesis of compounds 85a,b.

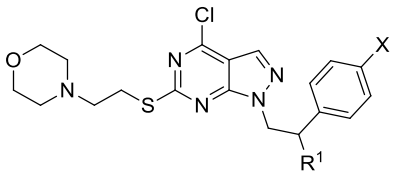

a R^1 = H, X = H
b R^1 = H, X = F

85a,b

The Vilsmeier complex, previously prepared from $POCl_3$ (3 g, 20 mmol) and anhydrous DMF (1.46 g, 20 mmol) was added to a suspension of intermediates **84a,b** (1 mmol) in $CHCl_3$ (10 mL). The mixture was refluxed for 8 h. The solution was washed with water (2 x 20 mL), dried ($MgSO_4$), and concentrated under reduced pressure. The yellow crude oil was purified by column chromatography (Silica gel 0.06-0200 mm, 40 Å) using Et_2O as the eluant, to afford the pure product as a yellow oil (**85a**), or as white solid (**85b**).

4-(2-((4-Chloro-1-phenethyl-1H-pyrazolo[3,4-d]pyrimidin-6-yl)thio)ethyl)morpholine 85a.

Yield: 0.32 g, 80%

MW = 403.93

Anal. calcd for $C_{19}H_{22}N_5OClS$, C 56.50, H 5.49, N 17.34, S 7.49, found C 56.43, H 5.52, N 17.14, S 7.77.

^{1}H NMR ($CDCl_3$): δ 2.51-2.90 (m, 6H, $2CH_2N$ morph. + CH_2N), 3.22 (t, *J* = 7.2 Hz, 2H, CH_2Ar), 3.30-3.40 (m, 2H, SCH_2), 3.68-3.88 (m, 4H, $2CH_2O$ morph.), 4.62 (t, *J* = 7.2 Hz, 2H, CH_2N pyraz.), 7.09-7.26 (m, 5H Ar), 8.01 (s, 1H, H-3).

4-(2-((4-Chloro-1-(4-fluorophenethyl)-1H-pyrazolo[3,4-d]pyrimidin-6-yl)thio)ethyl)morpholine 85b.

Yield: 0.36 g, 86%
Mp: 101-102 °C
MW = 421.92
Anal. calcd for $C_{19}H_{21}N_5OClFS$, C 54.09, H 5.02, N 16.60, S 7.60, found C 53.89, H 5.00, N 16.72, S 7.34.
^{1}H NMR ($CDCl_3$): 2.50-2.85 (m, 6H, $2CH_2N$ morph. + CH_2N), 3.24 (t, *J* = 7.2 Hz, 2H, CH_2Ar), 3.33-3.45 (m, 2H, SCH_2), 3.67-3.84 (m, 4H, $2CH_2O$ morph.), 4.61 (t, *J* = 7.2 Hz, 2H, CH_2N pyraz.), 7.00-7.33 (m, 4H Ar), 8.04 (s, 1H, H-3).

Synthesis of 4-(2-((4-chloro-1-(2-chloro-2-phenylethyl)-1*H*-pyrazolo[3,4-*d*]pyrimidin-6-yl)thio)ethyl)morpholine 85c.

The Vilsmeier complex, previously prepared from $POCl_3$ (12.27 g, 80 mmol) and anhydrous DMF (5.85 g, 80 mmol) was added to a suspension of intermediate **84c** (4.01 g, 10 mmol) in $CHCl_3$ (50 mL). The mixture was refluxed for 8 h. The solution was washed with 4 M NaOH (2 x 20 mL), then with water (20 mL), dried ($MgSO_4$), and concentrated under reduced pressure. The yellow crude oil was crystallized as a brown solid by adding absolute EtOH and standing in a refrigerator.

Yield: 3.29 g, 75%
Mp: 106-107 °C
MW = 438.37
Anal. calcd for $C_{19}H_{21}N_5Cl_2OS$, C 52.06, H 4.83, N 15.98, S 7.31, found C 52.00, H 4.91, N 16.01, S 7.52.
^{1}H NMR ($CDCl_3$): δ 2.81-3.12 (m, 4H, $2CH_2N$ morph.), 3.18-3.81 (m, 4H, CH_2S + CH_2CH_2S), 3.86-4.10 (m, 4H, $2CH_2O$ morph.), 4.60-4.78 and 5.12-5.30 (2m, 2H, CH_2N), 5.36-5.50 (m, 1H, CHCl), 7.16-7.50 (m, 5H Ar), 8.00 (s, 1H, H-3).
MS: m/z 438 $[M+1]^+$.

General procedure for the synthesis of compounds 78a-e.

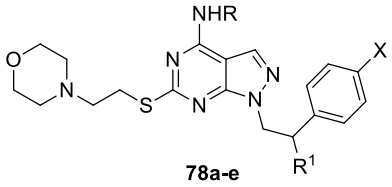

78a-e

a: R = C_6H_5, R^1 = H, X = H
b: R = C_6H_4-*m*F, R^1 = H, X = H
c: R = C_6H_4-*m*Br, R^1 = H, X = H
d: R = C_6H_4-*m*Cl, R^1 = H, X = F
e: R = C_6H_4-*m*Br, R^1 = Cl, X = H

The appropriate aniline (2 mmol) was added to a solution of the opportune intermediates **85a-e** (1 mmol) in absolute EtOH (5 mL), and the mixture was refluxed for 3-5 h. After cooling to room temperature, the solid was filtered, washed with water, and recrystallized from absolute EtOH.

6-((2-Morpholinoethyl)thio)-1-phenethyl-N-phenyl-1H-pyrazolo[3,4-d]pyrimidin-4-amine 78a.

Yield: 0.26 g, 57%
Mp: 177-180 °C
MW = 460.60
Anal. calcd for $C_{25}H_{28}N_6OS$, C 65.19, H 6.13, N 18.25, S 6.96, found C 62.25, H 6.37, N 17.96, S 7.36.
^{1}H NMR ($CDCl_3$): δ 2.53-2.55 (m, 4H, $2CH_2N$ morph.), 2.76 (t, *J* = 8.0 Hz, 2H, CH_2N), 3.18 (t, *J* = 7.0, 2H, CH_2Ar), 3.31 (t, *J* = 8.0 Hz, 2H, CH_2S), 3.69-3.71 (m, 4H, $2CH_2O$ morph.), 4.53 (t, *J* = 7.0, 2H, CH_2N pyraz.), 7.18-7.21 and 7.24-7.29 (2m, 10H, Ar), 7.84 (s, 1H, H-3).
IR (KBr): cm^{-1} 3435 (NH).

N-(3-fluorophenyl)-6-((2-morpholinoethyl)thio)-1-phenethyl-1H-pyrazolo[3,4-d]pyrimidin-4-amine 78b.

Yield: 0.25 g, 51%
Mp: 160-162 °C
MW = 478.59

Anal. calcd for $C_{25}H_{27}N_6FOS$, C 62.74, H 5.69, N 17.56, S 6.70, found C 62.97, H 5.66, N 17.56, S 6.63.

^{1}H NMR ($CDCl_3$): δ 2.55-2.57 (m, 4H, $2CH_2N$ morph.), 2.75 (t, *J* = 8.0 Hz, 2H, CH_2N), 3.19 (t, *J* = 7.0, 2H, CH_2Ar), 3.30 (t, *J* = 8.0 Hz, 2H, CH_2S), 3.71-3.74 (m, 4H, 2 CH_2O morph.), 4.54 (t, *J* = 7.0, 2H, CH_2N pyraz.), 7.24-7.26 and 7.28-7.33 (2 m, 10H, Ar), 7.87 (s, 1H, H-3).

IR (KBr): cm^{-1} 3310 (NH).

N-(3-bromophenyl)-6-((2-morpholinoethyl)thio)-1-phenethyl-1H-pyrazolo[3,4-d]pyrimidin-4-amine 78c.

Yied: 0.30 g, 55%

Mp: 140-141 °C

MW = 539.49

Anal. calcd for $C_{25}H_{27}N_6BrOS$, C 55.66, H 5.04, N 15.58, S 5.94, found C 55.72, H 5.34, N 15.24, S 5.38.

^{1}H NMR ($CDCl_3$): δ 2.50-2.52 (m, 4H, $2CH_2N$ morph.), 2.72 (t, *J* = 8.0 Hz, 2H, CH_2N), 3.17 (t, *J* = 7.0, 2H, CH_2Ar), 3.28 (t, *J* = 8.0 Hz, 2H, CH_2S), 3.66-3.69 (m, 4H, $2CH_2O$ morph.), 4.52 (t, *J* = 7.0, 2H, CH_2N pyraz.), 7.12-7.26 and 7.34-7.44 (2 m, 10H, Ar), 7.75 (s, 1H, H-3).

IR (KBr): cm^{-1} 3314 (NH).

N-(3-chlorophenyl)-1-(4-fluorophenethyl)-6-((2-morpholinoethyl)thio)-1H-pyrazolo[3,4-d]pyrimidin-4-amine 78d.

Yield: 0.16 g, 31%

Mp: 127-128 °C

MW = 513.03

Anal. calcd for $C_{25}H_{26}N_6OClFS$, C 58.53, H 5.11, N 16.38, S 6.25, found C 58.76, H 4.86, N 16.09, S 6.46.

^{1}H NMR ($CDCl_3$): 2.44-2.69 and 2.80-2.91 (2m, 6H, $2CH_2N$ morph. + CH_2N), 3.14 (t, *J* = 6.8 Hz, 2H, SCH_2), 3.37-3.54 and 3.70-3.82 (2m, 6H, CH_2Ar + $2CH_2O$ morph.), 4.49 (t, *J* = 6.8 Hz, 2H, CH_2N pyraz.), 6.87-6.92, 7.05-7.08 and 7.28-7.36 (3m, 9H, 8 Ar + H-3).

IR (KBr): cm^{-1} 3300-3100 (NH).

N-(3-bromophenyl)-1-(2-chloro-2-phenylethyl)-6-((2-morpholinoethyl)thio)-1H-pyrazolo[3,4-d]pyrimidin-4-amine 78e.

Yield: 0.35 g, 61%

Mp: 232-233 °C

MW = 573.94

Anal. calcd for $C_{25}H_{26}N_6BrClOS$, C 52.32, H 4.57, N 14.64, S 5.59, found C 52.12, H 4.52, N 14.55, S 5.52.

^{1}H NMR ($CDCl_3$): δ 2.90-3.99 (m, 12H, 4CH_2 morph. + CH_2N + CH_2S), 4.63-4.85 and 5.04-5.21 (2m, 2H, CH_2N pyraz.), 5.55-5.70 (m, 1H, CHCl), 7.03-8.52 (m, 10H, 9 Ar + H-3), 11.33 (s all., 1H, NH disappears with D_2O).

IR (KBr): cm^{-1} 3450 (NH).

General procedure for the synthesis of compounds 78f,g.

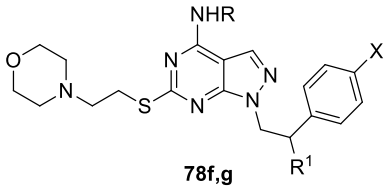

78f,g

f: R = $CH_2C_6H_4$-*o*F, R^1 = Cl, X = H

g: R = $CH_2C_6H_4$-*o*Cl, R^1 = Cl, X = H

The appropriate amine (40 mmol) was added to a solution of the intermediate **85c** (3.67 g, 10 mmol) in anhydrous toluene (20 mL), and the mixture was stirred at room temperature for 48 h. The organic phase was washed with water (20 mL), dried ($MgSO_4$), and concentrated under reduced pressure. The obtained crude oil was crystallized by adding a mixture of Et_2O/PE (bp 40-60 °C) (1:1).

1-(2-Chloro-2-phenylethyl)-N-(2-fluorobenzyl)-6-((2-morpholinoethyl)thio)-1H-pyrazolo[3,4-d]pyrimidin-4-amine 78f.

Yield: 0.27 g, 51%

Mp: 134-135 °C

MW = 527.06

Anal. calcd for $C_{26}H_{28}N_6ClFOS$, C 59.25, H 5.35, N 15.95, S 6.08, found C 59.60, H 5.58, N 15.62, S 5.94.

^{1}H NMR ($CDCl_3$): δ 2.53-2.55 (m, 4H, $2CH_2N$ morph.), 2.78 (t, *J* = 7.0 Hz, 2H, CH_2N), 3.28 (t, *J* = 7.0 Hz, 2H, CH_2S), 3.66-3.69 (m, 4H, $2CH_2O$ morph.), 4.52-4.57 (m, 4H, CH_2N pyraz. + CH_2Ar), 5.35-5.38 (m, 1H, CHCl), 7.12-7.21 (m, 9H, Ar), 7.70 (s, 1H, H-3).

IR (KBr): cm^{-1} 3250 (NH).

1-(2-Chloro-2-phenylethyl)-N-(2-chlorobenzyl)-6-((2-morpholinoethyl)thio)-1H-pyrazolo[3,4-d]pyrimidin-4-amine 78g.

Yield: 0.26 g, 48%

Mp: 121-122 °C

MW = 543.51

Anal. calcd for $C_{26}H_{28}N_6Cl_2OS$, C 57.46, H 5.19, N 15.46, S 5.90, found C 57.28, H 5.39, N 15.38, S 5.27.

^{1}H NMR ($CDCl_3$): δ 2.51-2.53 (m, 4H, $2CH_2N$ morph.), 2.77 (t, *J* = 7.2 Hz, 2H, CH_2N), 3.28 (t, *J* = 7.2 Hz, 2H, CH_2S), 3.66-3.69 (m, 4H, 2 CH_2O morph.), 4.51-4.55 (m, 4H, CH_2N pyraz. + CH_2Ar), 5.34-5.37 (m, 1H, CHCl), 7.10-7.18 (m, 9H, Ar), 7.69 (s, 1H, H-3).

IR (KBr): cm^{-1} 3268 (NH).

Synthesis of 1-(2-hydroxy-2-phenylethyl)-6-{[2-(4-methylpiperazin-1-yl)ethyl]thio}-1*H*-pyrazolo[3,4-*d*]pyrimidin-4-ol 86.

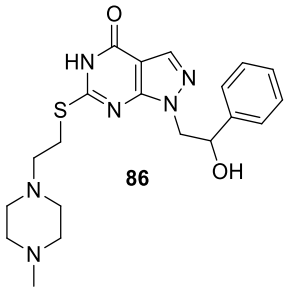

86

A suspension of **83c** (1.01 g, 3.5 mmol), 1-(2-chloroethyl)-4-methylpiperazine (0.73 g, 4.2 mmol), KOH (0.42 g, 7 mmol) and KI (0.062 g, 0.35 mmol) in absolute EtOH (50 mL) was stirred at 80 °C for 12 h. The solvent was evaporated under reduced pressure to obtain a crude,

which was purified by column chromatography using a mixture of CH_2Cl_2/MeOH (8:2) as the eluent to afford compound **86**.

Yield: 0.8 g, 55%

Mp: 251.0-253.0 °C

MW = 414.52

Anal. calcd for $C_{20}H_{26}N_6O_2S$, C 57.95, H 6.32, N 20.27, S 7.74, found C 57.89, H 6.15, N 20.40, S 7.90.

^{1}H NMR ($CDCl_3$): δ (ppm) 2.5 (s, 3H, CH_3), 2.55-3.40 (m, 12H, $4CH_2$ piperaz. + $\underline{CH_2}CH_2S$ + CH_2S), 4.20-4.25 and 4.25-4.45 (2m, 2H, CH_2N), 5.07 (br s, 1H, OH, disappears with D_2O), 5.60-5.80 (m, 1H, CHO), 7.20-7.40 (m, 5H Ar), 7.98 (s, 1H, H-3).

IR (cm^{-1}): 3332 (NH), 3087-2831 (OH), 1679 (CO).

Synthesis of 2-(methylthio)-7*H*-pyrrolo[2,3-*d*]pyrimidin-4-ol 97.

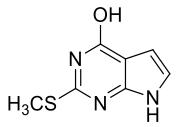

97

Chloroacetaldehyde (50% aqueous solution, 1 mL, 7.87 mmol) was added to a suspension of intermediate **96** (0.5 g, 3.18 mmol) and sodium acetate (0.88 g, 10.69 mmol) in water (12.5 mL) and the mixture was heated at 80 °C for 2 min in a microwave oven (open vessel mode, 100 W). After cooling to room temperature, acetone (3 mL) was added and the obtained solid was filtered. Grey solid constituted by a mixture of the C4 keto enolic forms.

Yield: 0.41 g, 71%

Mp: 265-267 °C

MW = 181.21

Anal. calcd for $C_7H_7N_3OS$, C 46.39, H 3.89, N 23.19, S 17.69, found C 46.51, H 3.96, N 23.15, S 17.68.

^{1}H NMR ($(CD_3)_2SO$): δ 3.26 (s, 3H, SCH_3), 7.61-7.65 (m, 1H, H-5), 7.75-7.90 (m, 1H, H-6), 9.59 (br s, 1H disappears wih D_2O), 9.92 (br s, 1H disappears with D_2O).
IR (KBr): cm^{-1} 3330-2900 (OH), 3220 (NH), 1667 (CO).
MS: m/z $[M+1]^+$ 182.

Synthesis of 4-chloro-2-(methylthio)-7*H*-pyrrolo[2,3-*d*]pyrimidine 98.

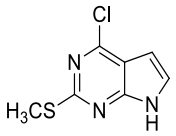

98

$POCl_3$ (5 mL, 53.7 mmol) and TEA (0.2 mL, 1.43 mmol) were added to intermediate **97** (0.10 g, 0.55 mmol); the mixture was heated at 130 °C for 4 h and then cooled to room temperature. The excess of $POCl_3$ was removed by distillation under reduced pressure. Ice was then carefully added to the residue and the suspension was extracted with Et_2O (3 x 20 mL). The organic phase was washed with water (10 mL), dried on $MgSO_4$, filtered and concentrated under reduced pressure. The crude was purified by column chromatography (Florisil®, 100-200 mesh), using Et_2O as the eluent to afford the pure product **98**.

Yield: 84 mg, 77%
Mp: 207-209 °C
MW = 199.66
Anal. calcd for $C_7H_6N_3ClS$, C 42.11, H 3.03, N 21.05, S 16.06, found C 42.29, H 3.38, N 21.14, S 16.36.
^{1}H NMR ($(CD_3)_2SO$): δ 2.67 (s, 3H, SCH_3), 6.56-6.59 (m, 1H, H-5), 7.21-7.23 (m, 1H, H-6)
IR (KBr): cm^{-1} 3412 (NH), 3122 (CH), 1614 (CC).
MS: m/z $[M+1]^+$ 201.

Synthesis of 2-(4-chloro-2-(methylthio)-7*H*-pyrrolo[2,3-*d*]pyrimidin-7-yl)-1-phenylethanone 99.

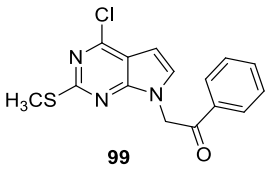

99

Sodium hydride (60% dispersion in mineral oil, 0.04 g, 1 mmol) was added in small portions at 0 °C to a solution of intermediate **98** (0.2 g, 1 mmol) in anhydrous DMF and the mixture was stirred at room temperature for 20 min. Then 2-bromo-1-phenylethanone (0.3 g, 1 mmol) was added dropwise at 0 °C and the reaction was stirred at room temperature for 18 h. Then the mixture was poured into water (20 mL) and extracted with ethylacetate (3 x 10 mL); the organic phases were washed with water (2 x 10 mL), dried on $MgSO_4$, filtered and concentrated under reduced pressure. The crude was purified by column chromatography (Silica gel 220-440 mesh), using CH_2Cl_2 as the eluent to afford the pure product as a white solid.

Yield: 0.15 g, 47%

Mp: 157-159 °C

MW = 317.79

Anal. calcd for $C_{15}H_{12}N_3OClS$, C 56.69, H 3.81, N 13.22, S 10.09, found C 56.65, H 3.83, N 12.97, S 10.07.

^{1}H NMR ($CDCl_3$): δ 2.65 (s, 3H, SCH_3), 5.65 (s, 2H, CH_2N), 6.60 (d, J = 3.6, 1H, H-5), 7.11 (d, J = 3.6, 1H, H-6), 7.52-7.56, 7.64-7.67 and 8.03-8.05 (3m, 5H Ar).

IR (KBr): cm^{-1} 1694 (CO).

MS: m/z [M+1]$^+$ 319.

Synthesis of 2-(4-chloro-2-(methylthio)-7*H*-pyrrolo[2,3-*d*]pyrimidin-7-yl)-1-phenylethanol 100.

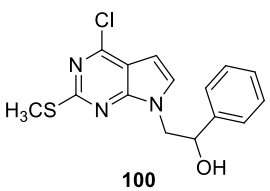

100

A solution of sodium borohydride (0.26 g, 6.9 mmol) in water (1 mL) was slowly added at 0 °C to a solution of intermediate **99** (0.31 g, 1 mmol) in THF (6 mL), and the reaction was stirred at room temperature for 3 h. Then the mixture was poured in water (20 mL) and extracted with Et_2O (3 x 10 mL); the organic phases were washed with water (2 x 10 mL), dried on $MgSO_4$, filtered and concentrated under reduced pressure to obtain an oil which crystallized by adding a 1:1 mixture of Et_2O and PE (bp 40-60 °C) to give a white solid.

Yield: 0.22 g, 69%
Mp: 157-159 °C
MW = 319.81
Anal. calcd for $C_{15}H_{14}N_3OClS$, C 56.33, H 4.41, N 13.14, S 10.03, found C 56.08, H 4.73, N 13.04, S 9.98.
^{1}H NMR ($CDCl_3$): δ 2.65 (s, 3H, SCH_3), 3.91 (br s, 1H, OH disappears with D_2O), 4.32-4.64 (m, 2H, CH_2N), 5.10-5.25 (m, 1H, CHOH), 6.48 (d, J = 3.6, 1H, H-5), 7.03 (d, J = 3.6, 1H, H-6), 7.23-7.47 (m, 5H Ar).
IR (KBr): cm^{-1} 3500-3200 (OH).
MS: m/z $[M+1]^+$ 321.

Synthesis of 4-chloro-7-(2-chloro-2-phenylethyl)-2-(methylthio)-7*H*-pyrrolo[2,3-*d*]pyrimidine 101.

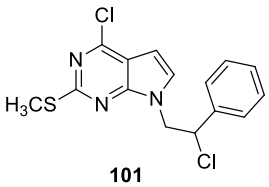

101

The Vilsmeier complex, previously prepared from $POCl_3$ (1.65 mL, 17.6 mmol) and DMF (1.28 g, 17.6 mmol) was added to a suspension of intermediate **100** (0.56 g, 1.76 mmol) in CH_2Cl_2 (10 mL). The mixture was refluxed for 8 h. After cooling to room temperature, the mixture was washed with water (2 x 20 mL), dried on $MgSO_4$, filtered, and concentrated under reduced pressure. The crude oil was purified by column chromatography (Silica gel 220-440 mesh), using Et_2O as the eluent, to afford the pure product as a white solid.

Yield: 0.31 g, 92%

Mp: 87-88 °C

MW = 338.25

Anal. calcd for $C_{15}H_{13}N_3Cl_2S$, C 53.26, H 3.87, N 12.42, S 9.48, found C 53.23, H 3.81, N 12.18, S 9.15.

^{1}H NMR ($CDCl_3$): δ 2.65 (s, 3H, SCH_3), 4.66-4.80 (m, 2H, CH_2N), 5.29-5.34 (m, 1H, CHCl), 6.47 (d, J = 3.6, 1H, H-5), 6.99 (d, J = 3.6, 1H, H-6), 7.22-7.50 (m, 5H Ar).

MS: m/z $[M+1]^+$ 339.

General procedure for the synthesis of compounds 95a,b.

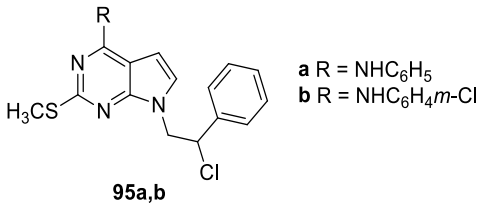

95a,b

The appropriate aniline (2 mmol) was added to a solution of **101** (0.33 g, 1 mmol) in absolute EtOH (10 mL) and the reaction mixture was stirred at reflux for 5 h. After cooling, a solid precipitated which was filtered, washed with water and recrystallized from absolute EtOH (10 mL) to give the final products as white solids.

7-(2-Chloro-2-phenylethyl)-2-(methylthio)-N-phenyl-7H-pyrrolo[2,3-d]pyrimidin-4-amine 95a.

Yield: 0.26 g, 66%

Mp: 157-159 °C

MW = 394.92

Anal. calcd for $C_{21}H_{19}N_4ClS$, C 63.87, H 4.85, N 14.19, S 8.12, found C 63.81, H 4.62, N 14.38, S 7.99.

^{1}H NMR ($CDCl_3$): δ 2.65 (s, 3H, SCH_3), 4.72-5.22 (m, 2H, CH_2N), 5.39-5.66 (m, 1H, CHCl), 7.00-7.76 (m, 12H, H-5 + H-6 + 10Ar), 8.40 (br s, 1H, NH disappears with D_2O).

^{13}C NMR (MeOD): δ 168.96, 150.48, 146.94, 141.15, 138.23, 129.39, 129.08, 128.86, 127.54, 124.04, 123.66, 120.80, 101.88, 100.01, 60.17, 53.07, 14.82.

IR (KBr): cm^{-1} 3000-2830 (NH).

MS: m/z $[M+1]^+$ 396.

7-(2-Chloro-2-phenylethyl)-N-(3-chlorophenyl)-2-(methylthio)-7H-pyrrolo[2,3-d]pyrimidin-4-amine 95b.

Yield: 0.26 g, 61%

Mp: 147-149 °C

MW = 429.37

Anal. calcd for $C_{21}H_{18}N_4Cl_2S$, C 58.74, H 4.23, N 13.05, S 7.47, found C 58.76, H 4.37, N 13.25, S 7.11.

^{1}H NMR ($CDCl_3$): δ 2.66 (s, 3H, SCH_3), 4.64-5.23 (m, 2H, CH_2N), 5.41-5.67 (m, 1H, CHCl), 7.00-7.81 (m, 11H, H-5 + H- 6 + 9Ar), 9.76 (br s, 1H, NH disappears with D_2O).

^{13}C NMR (MeOD): δ 168.96, 150.48, 146.94, 144.13, 138.23, 134.43, 130.17, 129.39, 128.86, 127.54, 124.04, 122.58, 120.89, 120.18, 101.88, 100.01, 60.17, 53.07,14.82.

IR (KBr): cm^{-1} 3000-2800 (NH).

MS: m/z $[M+1]^+$ 430.

Synthesis of N-benzyl-7-(2-chloro-2-phenylethyl)-2-(methylthio)-7*H*-pyrrolo[2,3-*d*]pyrimidin-4-amine 95c.

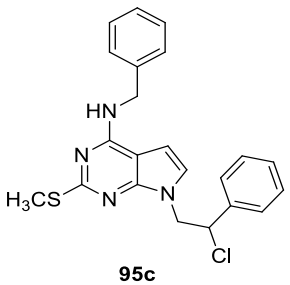

95c

Benzylamine (0.4 g, 4 mmol) was added to a solution of intermediate **101** (0.3 g, 1 mmol) in anhydrous toluene (5 mL) and the mixture was stirred at room temperature for 24 h. Then, the organic phase was washed with water (2 x 10 mL), dried on $MgSO_4$, and concentrated under

reduced pressure. The crude oil was purified by column chromatography (Silica gel 220-440 mesh), using Et_2O as the eluent. The obtained oil crystallized as a yellow solid by adding a 1:1 mixture of Et_2O and PE (bp 40-60 °C).

Yield: 0.33 g, 81%

Mp: 106-107 °C

MW = 408.95

Anal. calcd for $C_{22}H_{21}N_4ClS$, C 64.61, H 5.18, N 13.70, S 7.84, found C 64.38, H 5.08, N 13.87, S 7.78.

^1H NMR ($CDCl_3$): δ 2.65 (s, 3H, SCH_3), 4.65-4.71 (m, 4H, CH_2N + CH_2Ar), 5.05 (br s, 1H, NH disappears with D_2O), 5.33-5.35 (m, 1H, CHCl), 6.45 (d, J = 3.6, 1H, H-5), 6.96 (d, J = 3.6, 1H, H-6), 7.18-7.50 (m, 10H Ar).

^{13}C NMR (MeOD): δ 169.80, 153.68, 148.47, 139.85, 138.23, 129.39, 128.86, 128.43, 127.59, 127.54, 126.92, 124.04, 103.94, 100.01, 60.17, 53.07, 43.38, 14.82.

IR (KBr): cm^{-1} 3100-2900 (NH).

MS: m/z $[M+1]^+$ 410.

Synthesis of 4-chloro-7-(4-fluorobenzyl)-2-(methylthio)-7*H*-pyrrolo[2,3-*d*]pyrimidine 102.

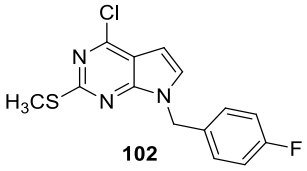

102

Sodium hydride (60% dispersion in mineral oil, 0.1 g, 2.5 mmol) was slowly added to a solution of **98** (0.19 g, 1 mmol) in anhydrous ACN (5 mL) and the mixture was stirred at room temperature for 20 min. Then 4-fluorobenzyl chloride (0.14 g, 1 mmol) solved in anhydrous ACN (5 mL) was added dropwise. The mixture was heated at 50 °C for 2 h, then cooled to room temperature and filtered to eliminate the little amount of solid obtained. Then the solution was evaporated under reduced pressure and the crude was purified by column chromatography (Florisil®, 100-200 mesh), using Et_2O as the eluent to afford the pure compound **102** as light yellow solid.

Yield: 0.11 g, 36%

Mp: 99-100 °C

MW = 307.77

Anal. calcd for $C_{14}H_{11}N_3ClFS$, C 54.63, H 3.60, N 13.65, S 10.42, found C 54.41, H 3.69, N 13.42, S 10.15.

^{1}H NMR ($CDCl_3$): δ 2.65 (s, 3H, SCH_3), 5.36 (s, 2H, CH_2N), 6.53 (d, J = 3.6, 1H, H-5), 6.96-7.04 and 7.14-7.24 (2m, 5H, 4Ar + H-6).

MS: m/z $[M+1]^+$ 309.

General procedure for the synthesis compounds 95d-j.

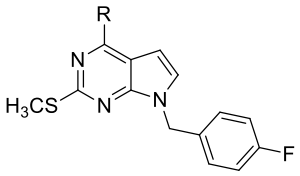

95d-j

d R = nC_4H_9
e R = 1-pyrrolidino
f R = 1-piperidino
g R = 4-morpholino
h R = $NHCH_2C_6H_5$
i R = $NHCH_2CH_2C_6H_5$
j R = $NHCH_2CH_2C_6H_4$-*p*Cl

The suitable amine (5 mmol) was added to a solution **102** (0.31 g, 1 mmol) in DMSO (5 mL) and the mixture was heated at 90-130 °C (the temperature depending on the boiling point of the amine) for 3-5. Then the mixture was cooled to room temperature, poured in ice-water (50 mL), extracted with CH_2Cl_2 (3 x 20 mL), dried on $MgSO_4$, filtered and concentrated under reduced pressure. The crude was purified by column chromatography (Florisil®, 100-200 mesh), using $CHCl_3$ as the eluent to afford the pure products.

4-Butyl-7-(4-fluorobenzyl)-2-(methylthio)-7H-pyrrolo[2,3-d]pyrimidine 95d.

Yield: 0.14 g, 42%,

Mp: 99-100 °C

MW = 329.43

Anal. calcd for $C_{18}H_{21}N_4FS$, C 62.76, H 6.15, N 16.27, S 9.31, found C 62.58, H 6.45, N 16.21, S 9.08.

^{1}H NMR ($CDCl_3$): δ 0.89 (t, J = 7.2, 3H, CH_3), 1.37 (sx, J = 7.2, 2H, $CH_2\underline{CH_2}CH_3$), 1.59 (quint, J = 7.2, 2H, $\underline{CH_2}CH_2CH_3$), 2.52 (s, 3H, SCH_3), 3.53 (q, J = 7.2, 2H, CH_2NH), 5.04 (br s, 1H,

NH disappears with D_2O), 5.21 (s, 2H, CH_2N), 6.22 (d, *J* = 3.6, 1H, H-5), 6.65 (d, *J* = 3.6, 1H, H-6), 6.84-6.94 and 7.07-7.21 (2m,
4H Ar).

^{13}C NMR (MeOD): δ 170.01, 162.67, 154.48, 147.83, 132.42, 130.45, 125.95, 115.11, 103.01, 101.64, 50.49, 43.71, 30.87, 20.23, 14.82, 14.02.

IR (KBr): cm^{-1} 3382 (NH).

MS: m/z $[M+1]^+$ 345.

7-(4-Fluorobenzyl)-2-(methylthio)-4-(pyrrolidin-1-yl)-7H-pyrrolo[2,3-d]pyrimidine 95e.

Yield: 0.18 g, 52%,

Mp: 149-150 °C

MW = 342.43

Anal. calcd for $C_{18}H_{19}N_4FS$, C 63.13, H 5.59, N 16.36, S 9.36, found C 63.25, H 5.69, N 16.27, S 9.06.

^1H NMR ($CDCl_3$): δ 1.86-2.00 (m, 4H, $2CH_2$ pyrr.), 2.51 (s, 3H, SCH_3), 3.66-3.78 (m, 4H, $2CH_2N$ pyrr.), 5.22 (s, 2H, CH_2N), 6.39 (d, *J* = 3.4, 1H, H-5), 6.61 (d, *J* = 3.4, 1H, H-6), 6.83-6.96 and 7.07-7.21 (2m, 4H Ar).

^{13}C NMR (MeOD): δ 167.66, 162.67, 155.30, 151.11, 132.42, 130.45, 123.66, 115.11, 110.00, 101.76, 65.59, 50.49, 45.92, 14.82.

MS: m/z $[M+1]^+$ 343.

7-(4-Fluorobenzyl)-2-(methylthio)-4-(piperidin-1-yl)-7H-pyrrolo[2,3-d]pyrimidine 95f.

Yield: 0.16 g, 46%,

Mp: 73-74 °C

MW = 356.46

Anal. calcd for $C_{19}H_{21}N_4FS$, C 64.02, H 5.94, N 15.72, S 9.00, found C 64.24, H 5.94, N 15.70, S 9.07.

^1H NMR ($CDCl_3$): δ 1.51-1.72 (m, 6H, $3CH_2$ pip.), 2.50 (s, 3H, SCH_3), 3.74-3.88 (m, 4H, $2CH_2N$ pip.), 5.23 (s, 2H, CH_2N), 6.34 (d, *J* = 3.6, 1H, H-5), 6.65 (d, *J* = 3.6, 1H, H-6), 6.83-6.98 and 7.08-7.21 (2m, 4H Ar).

^{13}C NMR (MeOD): δ 167.66, 162.67, 155.30, 151.11, 132.42, 130.45, 123.66, 115.11, 110.00, 101.76, 50.49, 48.07, 25.08, 23.42, 14.82.
MS: m/z $[M+1]^+$ 357.

4-(7-(4-Fluorobenzyl)-2-(methylthio)-7H-pyrrolo[2,3-d]pyrimidin-4-yl)morpholine 95g.

Yield: 0.18 g, 51%
Mp: 115-116 °C
MW = 358.43
Anal. calcd for $C_{18}H_{19}N_4FSO$, C 60.32, H 5.34, N 15.63, S 8.95, found C 60.15, H 5.44, N 15.63, S 8.70.
^{1}H NMR ($CDCl_3$): δ 2.50 (s, 3H, SCH_3), 3.75 (t, J = 5.4, 4H, 2 CH_2N morph.), 3.87 (t, J = 5.4, 4H, 2CH_2O morph.), 5.24 (s, 2H, CH_2N), 6.33 (d, J = 3.6, 1H, H-5), 6.69 (d, J = 3.6, 1H, H-6), 6.84-6.98 and 7.06-7.23 (2m, 4H Ar).
^{13}C NMR (MeOD): δ 168.25, 162.67, 153.43, 151.84, 132.42, 130.45, 123.66, 115.11, 108.99, 101.76, 50.49, 49.09, 26.01, 14.82.
MS: m/z $[M+1]^+$ 359.

N-benzyl-7-(4-fluorobenzyl)-2-(methylthio)-7H-pyrrolo[2,3-d]pyrimidin-4-amine 95h.

Yield: 0.14 g, 36%
Mp: 95-96 °C
MW = 378.47
Anal. calcd for $C_{21}H_{19}N_4FS$, C 66.64, H 5.06, N 14.80, S 8.47, found C 66.52, H 5.18, N 14.64, S 8.17.
^{1}H NMR ($CDCl_3$): δ 2.51 (s, 3H, SCH_3), 4.76 (d, J = 5.8, 2H, CH_2NH), 5.22 (s, 2H, CH_2N), 6.17 (d, J = 3.6, 1H, H-5), 6.62 (d, J = 3.4, 1H, H-6), 6.83-6.97 and 7.07-7.38 (2m, 9H Ar), 7.73 (br s, 1H, NH disappears with D_2O).
^{13}C NMR (MeOD): δ 169.91, 162.67, 153.45, 147.86, 139.85, 132.42, 130.45, 128.43, 127.59, 126.92, 125.95, 115.11, 103.57, 101.64, 50.49, 43.38, 14.82.
IR (KBr): cm^{-1} 3228 (NH).
MS: m/z $[M+1]^+$ 379.

7-(4-Fluorobenzyl)-2-(methylthio)-N-phenethyl-7H-pyrrolo[2,3-d]pyrimidin-4-amine 95i.

Yield: 0.15 g, 37%

Mp: 61-68 °C

MW = 392.49

Anal. calcd for $C_{22}H_{21}N_4FS$, C 67.32, H 5.39, N 14.27, S 8.17, found C 67.34, H 5.60, N 14.36, S 8.00.

^{1}H NMR ($CDCl_3$): δ 2.56 (s, 3H, SCH_3), 2.92 (t, J = 6.8, 2H, CH_2Ar), 3.81 (q, J = 6.8, 2H, CH_2NH), 5.07 (br s, 1H, NH disappears with D_2O), 5.21 (s, 2H, CH_2N), 6.15 (d, J = 3.4, 1H, H-5), 6.64 (d, J = 3.4, 1H, H-6), 6.83-6.98 and 7.06-7.33 (2m, 9H Ar).

^{13}C NMR (MeOD): δ 170.01, 162.67, 154.48, 147.83, 139.08, 132.42, 130.45, 129.19, 128.83, 126.13, 125.95, 115.11, 103.01, 101.64, 50.49, 43.75, 35.64, 14.82.

IR (KBr): cm^{-1} 3317 (NH).

MS: m/z $[M+1]^+$ 393.

N-(4-chlorophenethyl)-7-(4-fluorobenzyl)-2-(methylthio)-7H-pyrrolo[2,3-d]pyrimidin-4-amine 95j.

Yield: 0.13 g, 31%

Mp: 141-143 °C

MW = 426.94

Anal. calcd for $C_{22}H_{20}N_4ClFS$, C 61.89, H 4.72, N 13.12, S 7.51, found C 61.67, H 4.57, N 13.10, S 7.33.

^{1}H NMR ($CDCl_3$): δ 2.55 (s, 3H, SCH_3), 2.90 (t, J = 6.8, 2H, CH_2Ar), 3.83 (q, J = 6.8, 2H, $\underline{CH_2}NH$), 5.15 (br s, 1H, NH disappears with D_2O), 5.25 (s, 2H, CH_2N), 6.18 (d, J = 3.4, 1H, H-5), 6.67 (d, J = 3.4, 1H, H-6), 6.85-7.01 and 7.10-7.37 (2m, 8H Ar).

^{13}C NMR (MeOD): δ 170.01, 162.67, 154.48, 147.83, 136.26, 132.64, 132.42, 130.45, 130.05, 129.35, 125.95, 115.11, 103.01, 101.64, 50.49, 43.75, 35.64, 14.82.

MS: m/z $[M+1]^+$ 428.

Synthesis of 5-amino-1*H*-pyrazolo-4-carbonitrile 106.

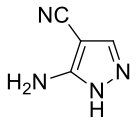

106

To a solution of **105** (4 g, 32.75 mmol) in absolute EtOH (20 mL), hydrazine monohydrate (1.65 mL, 34.06 mmol) was added, and the reaction mixture was stirred at reflux for 3 h.
The ethanol was evaporated under reduced pressure. Cold water was added, the crude product was collected by filtration, washed with water (3 x 40 mL) and dried in the vacuum drying oven at 70 °C to give **106** as a brown solid.

Yield: 2.87 g, 81%
Mp: 172-174 °C
MW = 108.10
Anal. calcd for $C_4H_4N_4$, C 44.44, H 3.73, N 51.83, found C 44.74, H 4.01, N 51.85.
^{1}H NMR ($(CD_3)_2SO$): δ 6.26 (s all., 2H, NH_2, disappears with D_2O), 7.57 (s, 1H, CH), 11.98 (s all., 1H, NH, disappears with D_2O).
IR (KBr): cm^{-1} 3420, 3416 (NH_2), 1645 (CN).

Synthesis of 1*H*-pyrazolo[3,4-*d*]pyrimidin-4-amine 107.

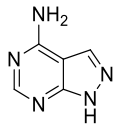

107

A solution of **106** (400 mg, 3.7 mmol) and formamide (5 mL, 125.8 mmol) was stirred at 200 °C for 1 h. After cooling to room temperature, water was added (20 mL) and the obtained solid was filtered. The crude product was suspended in hot water (40 mL) and conc. HCl (5 mL), then charcoal (600 mg) was added and the mixture was boiled for 15 min. After charcoal

filtration, conc. NH_3 was added and the precipitated solid was filtered, giving compound **107** as a white solid.

Yield: 0.40 g

Mp: 353-356 °C

MW = 135.13

Anal. calcd for $C_5H_5N_5$, C 44.44, H 3.73, N 51.83, found C 44.39, H 3.43, N 51.66. ^{1}H NMR ($(CD_3)_2SO$): δ 7.52 (s all., 2H, NH_2), 8.07 (s, 1H, H-3), 8.13 (s, 1H, H-6), 13.22 (s, 1H, NH).

IR (KBr): cm^{-1} 3401, 3360 (NH_2).

Synthesis of 3-iodo-1*H*-pyrazolo[3,4-*d*]pyrimidin-4-amine 108.

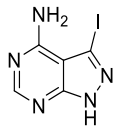

108

N-iodosuccinimide (2 g, 8.9 mmol) was added to a solution of 1*H*-pyrazolo[3,4-*d*]pyrimidin-4-amine **107** (800 mg, 5.9 mmol) in dry DMF (5 mL) and the mixture was heated at 80 °C for 14 h under nitrogen atmosphere. After cooling to room temperature, water was added (20 mL) and the precipitated solid was filtered and washed with water (50 mL). The crude product was recrystallized from absolute EtOH to give compound **108** as a light-yellow solid.

Yield: 1.97 g, 85%

Mp: 272-275 °C

MW = 261.02

Anal. calcd for $C_5H_4N_5I$, C 23.01, H 1.54, N 26.83, found C 22.72, H 1.81, N 26.61. ^{1}H NMR ($CDCl_3$): δ 8.15 (s, 1H, H-6), 9.18 (s all., 2H, NH_2, disappears with D_2O).

IR (KBr): cm^{-1} 3410, 3381 (NH_2).

Synthesis of 2-(4-amino-3-iodo-1*H*-pyrazolo[3,4-*d*]pyrimidin-1-yl)-1-phenylethanone 109.

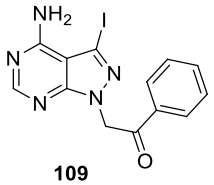

109

A solution of TBAF 1 M in THF (7.05 mL, 7.05 mmol) was added to a solution of 3-iodo-1*H*-pyrazolo[3,4-*d*]pyrimidin-4-amine **108** (1.84 g, 7.05 mmol) in anhydrous toluene (40 mL), and the mixture was heated at 70 °C for 1 h. 2-Bromoacetophenone (1.7 g, 8.46 mmol) was added and the reaction was stirred at 70 °C for 2 h. After cooling to room temperature, toluene was evaporated, ethyl acetate (AcOEt) (50 mL) was added and the precipitated solid was filtered and washed with water (2 x 20 mL) and Et_2O (3 x 15 mL). The crude product was recrystallized from absolute EtOH, to give compound **109** as a white solid.

Yield: 1.26 g, 47%

Mp: 227-231 °C

MW = 379.16

Anal. calcd for $C_{13}H_{10}N_5IO$, C 41.18, H 2.66, N 18.47, found C 41.27, H 2.91, N 18.13. ^{1}H NMR ($(CD_3)_2SO$): δ 6.01 (s, 2H, CH_2), 7.74-7.56 (m, 5H Ar), 8.18 (s, 1H, H-6).

Synthesis of 2-(4-amino-3-iodo-1*H*-pyrazolo[3,4-*d*]pyrimidin-1-yl)-1-phenylethanol 110.

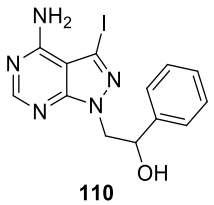

110

To a solution of **109** (600 mg, 1.58 mmol) in MeOH (150 mL), $NaBH_4$ (1.08 g, 28.48 mmol) was added and the mixture was stirred at 0 °C for 3 h. Water (40 mL) was added and the mixture was stirred for other 10 minutes. MeOH was evaporated then the suspension was extracted with CH_2Cl_2 (3 x 50 mL), the organic solution was washed with water (100 mL), dried ($MgSO_4$),

filtered, and concentrated under reduced pressure. The crude oil was purified by column chromatography (Silica gel 220-440 mesh, 60 Å) using CH_2Cl_2/MeOH (95:5) as the eluant to afford the pure product **110**.

Yield: 0.19 g, 31%
Mp: 186-188 °C
MW = 381.17
Anal. calcd for $C_{13}H_{12}N_5IO$, C 40.96, H 3.17, N 18.37, found C 40.89, H 3.32, N 18.58. ^1H NMR ($CDCl_3$): δ 4.65-4.63 (m, 2H, CH_2N), 5.30-5.25 (m, 1H, CHO), 6.75 (s all., 1H, OH), 7.51-7.29 (m, 5H Ar), 8.34 (s, 1H, H-6).
IR (KBr): cm^{-1} 3465, 3294 (NH_2), 3055 (OH).

Synthesis of 1-(2-chloro-2-phenylethyl)-3-iodo-1*H*-pyrazolo[3,4-*d*]pyrimidin-4-amine 111.

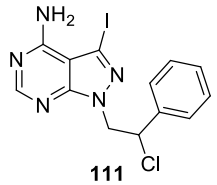

111

$SOCl_2$ (230 μL, 3.2 mmol) was added dropwise to a solution of the intermediate **110** (370 mg, 0.97 mmol) in dry CH_2Cl_2 (15 mL), and the reaction was stirred at room temperature for 12 h under nitrogen atmosphere. Water (10 mL) and 1 N NaOH (2 mL) were added with caution and the aqueous phase was extracted with CH_2Cl_2 (3 x 15 mL). Then the organic phase was washed with water (30 mL), saturated NaCl solution (30 mL), dried (Na_2SO_4) and concentrated under reduced pressure. The crude product was purified by column chromatography (Silica gel 220-440 mesh) using CH_2Cl_2/MeOH (95:5) as the eluant to afford the pure product **111**.

Yield: 0.13 g, 33%
Mp: 204-209 °C
MW = 399.62

Anal. calcd for $C_{13}H_{11}N_5ICl$, C 39.07, H 2.27, N 17.53, found C 38.89, H 2.89, N 17.62.
^{1}H NMR ($CDCl_3$): δ 5.06-4.69 (m, 2H, CH_2N), 5.57-5.50 (m, 1H, CHO), 6.43 (s all., 2H, NH_2), 7.57-7.29 (m, 5H Ar), 8.34 (s, 1H, H-6).
IR (KBr): cm^{-1} 3452, 3301 (NH_2).

General procedure for the synthesis of compounds 104a,b.

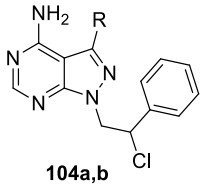

104a,b

a: R = C_6H_4-*p*CH_2OH
b: R = C_6H_4-*p*OH

To a solution of **111** (50 mg, 0.125 mmol) in DME (2 mL) and H_2O (0.3 mL), the appropriate boronic acid (0.5 mmol) was added, then Cs_2CO_3 (122 mg, 0.375 mmol) and Pd(dppf)Cl_2 (5 mg, 0.0125 mmol) were added and the mixture was stirred at 90° C for 14 h. The cooled mixture was extracted with AcOEt (3 x 5 mL). The organic layers were washed with water (30 mL), dried ($MgSO_4$), filtered, and concentrated under reduced pressure. The crude product was purified by column chromatography (Silica gel 220-440 mesh) using AcOEt/*n*-Hexane (95:5) as the eluant to afford the pure products **104a,b**.

(4-(4-Amino-1-(2-chloro-2-phenylethyl)-1H-pyrazolo[3,4-d]pyrimidin-3-yl)phenyl)methanol 104a.

Yield: 27 mg, 57%
Mp: 220-238 °C
MW = 379.84
Anal. calcd for $C_{20}H_{18}N_5ClO$, C 63.24, H 4.78, N 18.44, found C 63.27, H 5.11, N 18.09.
^{1}H NMR ($CDCl_3$): δ 4.82-4.80 (m, 2H, CH_2Ar), 8.38 (s, 1H, H-6), 7.78-7.25 (m, 9H Ar), 5.62-5.59 (m, 1H, OH), 5.55-5.47 (m, 1H, CH), 5.08-5.03 (m, 2H, CH_2N),
IR (KBr): cm^{-1} 3500, 3319 (NH_2), 3083 (OH).

4-(4-Amino-1-(2-chloro-2-phenylethyl)-1H-pyrazolo[3,4-d]pyrimidin-3-yl)phenol 104b.

Yield: 28 mg, 62%

Mp: 274-278 °C

MW = 365.82

Anal. calcd for $C_{19}H_{16}N_5ClO$, C 62.38, H 4.41, N 19.14, found C 62.54, H 4.68, N 18.94. ^1H NMR ($CDCl_3$): 4.68-4.82 and 4.89-5.04 (2m, 2H, CH_2N), 5.61-5.75 (m, 1H, CH), 6.88-7.52 (m, 9H Ar), 8.21 (s, 1H, H-6).

IR (KBr): cm^{-1} 3479, 3302 (NH_2), 3061 (OH).

General procedure for the synthesis of compounds 114a-f.

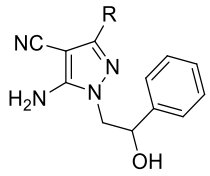

114a-f

a: R = C_6H_4-2Cl
b: R = C_6H_4-3Cl
c: R = C_6H_4-4Br
d: R = C_6H_4-4I
e: R = C_6H_4-4C_2H_5
f: R = C_6H_4-4C_3H_7

A 60% sodium hydride dispersion in mineral oil (1.21 g, 30.3 mmol) was added in small batches to a solution of malononitrile (1.00 g, 15.1 mmol) in anhydrous THF (25 mL) precooled at 0-5 °C. After 30 min at 0-5 °C, the suitable acyl chloride (15.1 mmol) was added dropwise. The orange solution was stirred at room temperature for 2-12 h, then dimethylsulfate (1.75 mL, 18.2 mmol) was slowly added and the solution was refluxed for 3-6 h. Finally, 2-hydrazino-1-phenylethanol **80c** (4.62 g, 30.2 mmol) dissolved in anhydrous THF (2 mL) was added and the reaction was refluxed for 3-6 h. After cooling to room temperature, water (25 mL) and conc. NH_3 (5 mL) were added under stirring. After 15 min, THF was removed under reduced pressure and the aqueous phase was extracted with CH_2Cl_2 (3 × 30 mL). Organic phases were washed with water (15 mL) and saturated NaCl solution (15 mL), dried (Na_2SO_4), and evaporated under reduced pressure. The crude was purified by flash chromatography (Isolera^{TM} One Biotage) using Et_2O/PE as the eluent, with a gradient elution (2:8 → 9:1) to afford compounds **104a-f**.

5-Amino-3-(2-chlorophenyl)-1-(2-hydroxy-2-phenylethyl)-1H-pyrazole-4-carbonitrile 114a.

Yield: 1.9 g, 37%

Mp: 131-134 °C

MW = 338.79

Anal. calcd for $C_{18}H_{15}N_4ClO$, C 63.81, H 4.46, N 16.54, found C 63.79, H 4.58, N 16.73. ^{1}H NMR ($CDCl_3$): δ 4.20-4.11 (m, 2H, CH_2N), 5.19-5.16 (m, 1H, CHO), 7.48-7.29 (m, 9H Ar). IR (KBr): cm^{-1} 3450-2800 (OH), 3426, 3327 (NH_2), 2216 (CN).

5-Amino-3-(3-chlorophenyl)-1-(2-hydroxy-2-phenylethyl)-1H-pyrazole-4-carbonitrile 114b.

Yield: 2.0 g, 39%

Mp: 172-180 °C

MW = 338.79

Anal. calcd for $C_{18}H_{15}ClN_4O$, C 63.81, H 4.46, N 16.54, found C 63.86, H 4.56, N 16.83. ^{1}H NMR ($CDCl_3$): δ 4.21-4.09 (m, 2H, CH_2N), 5.16-5.12 (m, 1H, CHO), 7.46-7.27 (m, 9H Ar). IR (KBr): cm^{-1} 3450-2900 (OH), 3407, 3327 (NH_2), 2218 (CN).

5-Amino-3-(4-bromophenyl)-1-(2-hydroxy-2-phenylethyl)-1H-pyrazole-4-carbonitrile 114c.

Yield: 2.4 g, 41%

Mp: 185.7-188.4 °C

MW = 383.24

Anal. calcd for $C_{18}H_{15}BrN_4O$, C 56.41, H 3.95, N 14.62, found C 56.52, H 4.01, N 14.25. ^{1}H NMR ($CDCl_3$): δ 4.07-4.38 (m, 2H, CH_2N), 5.20-5.25 (m, 1H, CHO), 7.28-7.82 (m, 9H Ar). IR (KBr): cm^{-1} 3398 (OH), 3329 (NH_2), 2194 (CN).

5-Amino-1-(2-hydroxy-2-phenylethyl)-3-(4-iodophenyl)-1H-pyrazole-4-carbonitrile 114d.

Yield: 2.4 g, 41%

Mp: 173.4-177.2 °C

MW = 430.24

Anal. calcd for $C_{18}H_{15}IN_4O$, C 50.25, H 3.51, N 13.02, found C 50.55, H 3.56, N 13.30. ^{1}H NMR ($CDCl_3$): δ 4.06-4.37 (m, 2H, CH_2N), 5.19-5.23 (m, 1H, CHO), 7.29-7.77 (m, 9H Ar). IR (KBr): cm^{-1} 3500-2800 (OH), 3398, 3329 (NH_2), 2195 (CN).

5-Amino-3-(4-ethylphenyl)-1-(2-hydroxy-2-phenylethyl)-1H-pyrazole-4-carbonitrile 114e.

Yield: 2.2 g, 44%

Mp: 160.6-163.5 °C

MW = 332.40

Anal. calcd for $C_{20}H_{20}N_4O$, C 72.27, H 6.06, N 16.86, found C 72.14, H 6.14, N 16.55. ^{1}H NMR ($CDCl_3$): δ 1.28-1.32 (m, 3H, CH_3), 2.69-2.73 (m, 2H, $CH_3\underline{CH_2}$), 4.03-4.16 (m, 2H, CH_2N), 5.09-5.13 (m, 1H, CHO), 7.27-7.43 and 7.81-7.84 (2m, 9H Ar).

IR (KBr): cm^{-1} 3500-2800 (OH), 3393, 3320 (NH_2), 2216 (CN).

5-Amino-1-(2-hydroxy-2-phenylethyl)-3-(4-propylphenyl)-1H-pyrazole-4-carbonitrile 114f.

Yield: 2.5 g, 48%

Mp: 106.7-109.3 °C

MW = 346.43

Anal. calcd for $C_{21}H_{22}N_4O$, C 72.81, H 6.40, N 16.17, found C 72.68, H 6.72, N 16.45. ^{1}H NMR ($CDCl_3$): δ 0.94-1.01 (m, 3H, CH_3), 1.63-1.70 (m, 2H, $CH_3\underline{CH_2}$), 2.60-2.68 (m, 2H, $CH_3CH_2\underline{CH_2}$) 4.12-4.30 (m, 2H, CH_2N), 5.22-5.28 (m, 1H, CHO), 7.24-7.83 (m, 9H Ar).

General procedure for the synthesis of compounds 115a-f.

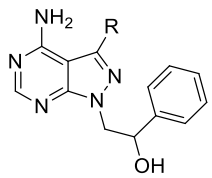

115a-f

a: R = C_6H_4-2Cl
b: R = C_6H_4-3Cl
c: R = C_6H_4-4Br
d: R = C_6H_4-4I
e: R = C_6H_4-4C_2H_5
f: R = C_6H_4-4C_3H_7

A suspension of the suitable intermediate **114a-f** (3 mmol) in formamide (18 mL, 450 mmol) was heated at 190 °C for 3-4 h and then poured into water (40 mL). The crude solid was filtered,

washed with water, suspended in EtOH, and boiled with charcoal for 10 min. The solid dissolved at the EtOH boiling point. After charcoal filtration, compounds **115a-f** precipitated as pure solids.

2-[4-Amino-3-(2-chlorophenyl)-1H-pyrazolo[3,4-d]pyrimidin-1-yl]-1-phenylethanol 115a.

Yield: 0.5 g, 46%
Mp: 126-129 °C
MW = 365.82
Anal. calcd for $C_{19}H_{16}N_5ClO$, C 62.38, H 4.41, N 19.14, found C 62.77, H 4.45, N 19.47. ^{1}H NMR ($CDCl_3$): δ 4.76-4.74 (m, 2H, CH_2N), 5.38-5.26 (m, 1H, CHO), 7.53-7.29 (m, 9H Ar), 8.35 (s, 1H, H-6).
IR (KBr): cm^{-1} 3600-2800 (OH), 3319, 3183 (NH_2).

2-[4-Amino-3-(3-chlorophenyl)-1H-pyrazolo[3,4-d]pyrimidin-1-yl]-1-phenylethanol 115b.

Yield: 0.55 g, 50%
Mp: 84-89 °C
MW = 365.82
Anal. calcd for $C_{19}H_{16}N_5ClO$, C 62.38, H 4.41, N 19.14, found C 62.19, H 4.78, N 19.13. ^{1}H NMR ($CDCl_3$): δ 4.73-4.70 (m, 2H, CH_2N), 5.39-5.26 (m, 1H, CHO), 7.53-7.29 (m, 9H Ar), 8.37 (s, 1H, H-6).
IR (KBr): cm^{-1} 3550-2800 (OH), 3319, 3180 (NH_2).

2-[4-Amino-3-(4-bromophenyl)-1H-pyrazolo[3,4-d]pyrimidin-1-yl]-1-phenylethanol 115c.

Yield: 0.8 g, 65%
Mp: 198.2-201.0 °C
MW = 410.27
Anal. calcd for $C_{19}H_{16}BrN_5O$, C 55.62, H 3.95, N 17.07, found C 55.81, H 4.06, N 16.74. ^{1}H NMR ($CDCl_3$): δ 3.63-3.88 and 4.70-4.87 (2m, 2H, CH_2N), 5.29-5.39 (m, 1H, CHO), 7.28-7.77 (m, 9H Ar), 8.35 (s, 1H, H-6).

IR (KBr): cm^{-1} 3500-2900 (OH), 3406, 3293 (NH_2).

2-[4-Amino-3-(4-iodophenyl)-1H-pyrazolo[3,4-d]pyrimidin-1-yl]-1-phenylethanol 115d.

Yield: 0.6 g, 44%

Mp: 218.0-220.0 °C

MW = 457.27

Anal. calcd for $C_{19}H_{16}IN_5O$, C 49.91, H 3.53, N 15.32, found C 50.13, H 3.53, N 15.27. ^{1}H NMR ($CDCl_3$): δ 4.56-4.87 (m, 2H, CH_2N), 5.23-5.40 (m, 1H, CHO), 7.29-7.46 and 7.81-8.00 (2m, 9H Ar), 8.32 (s, 1H, H-6).

2-[4-Amino-3-(4-ethylphenyl)-1H-pyrazolo[3,4-d]pyrimidin-1-yl]-1-phenylethanol 115e.

Yield: 0.65 g, 60%

Mp: 53.6-59.2 °C

MW = 359.42

Anal. calcd for $C_{21}H_{21}N_5O$, C 70.17, H 5.89, N 19.48, found C 70.05, H 6.18, N 19.77. ^{1}H NMR ($(CD_3)_2SO$): δ 1.20-1.28 (m, 3H, CH_3), 2.46-2.70 (m, 2H $CH_3\underline{CH_2}$) 4.27-4.61 (m, 2H, CH_2N), 5.09-5.23 (m, 1H, CHO), 7.28-7.59 (m, 9H Ar), 8.21 (s, 1H, H-6).

IR (KBr): cm^{-1} 3600-2800 (OH), 3468, 3303 (NH_2).

2-[4-Amino-3-(4-propylphenyl)-1H-pyrazolo[3,4-d]pyrimidin-1-yl]-1-phenylethanol 115f.

Yield: 0.5 g, 45%

Mp: 57.3-58.4 °C

MW = 373.45

Anal. calcd for $C_{22}H_{23}N_5O$, C 70.76, H 6.21, N 18.75, found C 70.62, H 6.40, N 18.64. ^{1}H NMR ($CDCl_3$): δ 0.98-1.05 (m, 3H, CH_3), 1.62-1.83 (m, 2H, $CH_3\underline{CH_2}$), 2.67-2.77 (m, 2H, $CH_3CH_2\underline{CH_2}$) 4.68-4.71 (m, 2H, CH_2N), 5.26-5.37 (m, 1H, CHO), 7.29-7.62 (m, 9H Ar), 8.31 (s, 1H, H-6).

General procedure for the synthesis of compounds 104e-j.

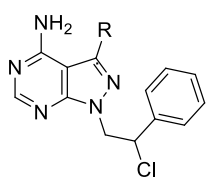

104e-j

e: R = C_6H_4-2Cl
f: R = C_6H_4-3Cl
g: R = C_6H_4-4Br
h: R = C_6H_4-4I
i: R = C_6H_4-4C_2H_5
j: R = C_6H_4-4C_3H_7

$SOCl_2$ (80 μL, 1.1 mmol) was added dropwise to a solution of the suitable intermediate **115a-f** (0.5 mmol) in anhydrous CH_2Cl_2 (5 mL), and the reaction was stirred at room temperature for 12 h under nitrogen atmosphere. Water (5 mL) and 1 N NaOH (1 mL) were added with caution, and the aqueous phase was extracted with CH_2Cl_2 (2 × 5 mL). Then the organic phase was washed with water (5 mL) and saturated NaCl solution (5 mL), dried (Na_2SO_4), and concentrated under reduced pressure. The crude was purified by column chromatography using CH_2Cl_2/MeOH (98:2) as the eluent to afford compounds **104e-j**.

3-(2-Chlorophenyl)-1-(2-chloro-2-phenylethyl)-1H-pyrazolo[3,4-d]pyrimidin-4-amine 104e.

Yield: 75 mg, 39%

Mp: 181-184 °C

MW = 384.26

Anal. calcd for $C_{19}H_{15}N_5Cl_2$, C 59.39, H 3.93, N 18.23, found C 59.60, H 3.95, N 17.93. ^{1}H NMR ($(CD_3)_2SO$): δ 4.95-4.78 and 5.13-4.96 (2m, 2H, CH_2N), 5.76-5.62 (m, 1H, CHCl), 7.60-7.33 (m, 9H Ar), 8.23 (s, 1H, H-6).

IR (KBr): cm^{-1} 3496, 3296 (NH_2).

3-(3-Chlorophenyl)-1-(2-chloro-2-phenylethyl)-1H-pyrazolo[3,4-d]pyrimidin-4-amine 104f.

Yield: 80 mg, 42%

Mp: 162-163 °C

MW = 384.26

Anal. calcd for $C_{19}H_{15}Cl_2N_5$, C 59.39, H 3.93, N 18.23, found C 59.54, H 4.00, N 18.46. ^{1}H NMR ($(CD_3)_2SO$): δ 4.88-4.76 and 5.12-4.98 (2m, 2H, CH_2N), 5.79-5.71 (m, 1H, CHCl), 7.66-7.36 (m, 9H Ar), 8.28 (s, 1H, H-6).
IR (KBr): cm^{-1} 3473, 3294 (NH_2).

3-(4-Bromophenyl)-1-(2-chloro-2-phenylethyl)-1H-pyrazolo[3,4-d]pyrimidin-4-amine 104g.

Yield: 0.2 g, 42%
Mp: 195.5-199.4 °C
MW = 428.71
Anal. calcd for $C_{19}H_{15}BrClN_5$, C 53.23, H 3.53, N 16.34, found C 53.12, H 3.57, N 16.11. ^{1}H NMR ($(CD_3)_2SO$): δ 4.74-4.89 and 4.92-5.12 (2m, 2H, CH_2N), 5.68-5.88 (m, 1H, CHCl), 7.36-7.75 (m, 9H Ar), 8.26 (s, 1H, H-6).
IR (KBr): cm^{-1} 3455, 3061 (NH_2).

1-(2-Chloro-2-phenylethyl)-3-(4-iodophenyl)-1H-pyrazolo[3,4-d]pyrimidin-4-amine 104h.

Yield: 0.1 g, 53%
Mp: 214.8-218.4 °C
MW = 475.71
Anal. calcd for $C_{19}H_{15}ClIN_5$, C 47.97, H 3.18, N 14.72, found C 47.99, H 3.35, N 14.66. ^{1}H NMR ($(CD_3)_2SO$): δ 4.76-4.89 and 4.98-5.13 (2m, 2H, CH_2N), 5.63-5.87 (m, 1H, CHCl), 7.38-7.55 and 7.89-7.94 (2m, 9H Ar), 8.28 (s, 1H, H-6).

1-(2-Chloro-2-phenylethyl)-3-(4-ethylphenyl)-1H-pyrazolo[3,4-d]pyrimidin-4-amine 104i.

Yield: 0.1 g, 53%
Mp: 228.0-229.1 °C
MW = 377.87
Anal. calcd for $C_{21}H_{20}ClN_5$, C 66.75, H 5.33, N 18.53, found C 66.91, H 5.40, N 18.56. ^{1}H NMR ($(CD_3)_2SO$): δ 1.21-1.28 (m, 3H, CH_3), 2.68-2.71 (m, 2H $CH_3\underline{CH_2}$) 4.77-4.91 and 4.99-5.11 (2m, 2H, CH_2N), 5.69-5.87 (m, 1H, CHCl), 7.37-7.60 (m, 9H Ar), 8.27 (s, 1H, H-6).

1-(2-Chloro-2-phenylethyl)-3-(4-propylphenyl)-1H-pyrazolo[3,4-d]pyrimidin-4-amine 104j.

Yield: 0.09 g, 46%

Mp: 190.0-192.3 °C

MW = 391.90

Anal. calcd for $C_{22}H_{22}ClN_5$, C 67.42, H 5.66, N 17.87, found C 67.63, H 5.36, N 17.60. ^{1}H NMR ($(CD_3)_2SO$): δ 0.90-0.97 (m, 3H, CH_3), 1.59-1.67 (m, 2H, $CH_3\underline{CH_2}$), 2.60-2.63 (m, 2H, $CH_3CH_2\underline{CH_2}$) 4.76-4.89 and 4.94-5.09 (2m, 2H, CH_2N), 5.63-5.87 (m, 1H, CHCl), 7.35-7.66 (m, 9H Ar), 8.27 (s, 1H, H-6).

Synthesis of 2-bromo-*N*-(2-morpholinophenyl)acetamide 120.

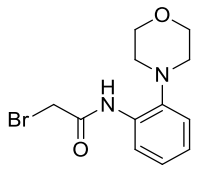

120

To a solution of bromoacetyl chloride (500 µL, 5 mmol) in Et_2O, a solution of 2-morpholinoaniline **121** (891 mg, 5 mmol) in Et_2O (50 mL) was added dropwise, then the suspension was stirred at room temperature for 4 h. The solvent was evaporated, then 1 N NaOH (50 mL) was added and the suspension was extracted with CH_2Cl_2 (3 x 75 mL), washed with water (100 mL), dried (Na_2SO_4) and concentrated under reduced pressure. The crude was crystallized as a white solid by adding Et_2O (20 mL).

Yield: 1.17 g, 78%

Mp: 140-142 °C

MW = 299.16

Anal. calcd for $C_{12}H_{15}N_2O_2Br$, C 48.18, H 5.05, N 9.36, found C 47.86, H 5.50, N 9.13. ^{1}H NMR ($CDCl_3$): δ 3.22-3.31 (m, 4H, $2CH_2N$ morph), 3.54-3.76 (2m, 4H, $2CH_2O$ morph), 4.30 (s, 2H, CH_2Br), 6.66-6.96 (2m, 2H Ar), 7.32-7.36 (m, 1H Ar), 8.14-8.16 (m, 1H Ar).

IR (KBr): cm^{-1} 3268 (NH), 1670 (CO).

Synthesis of 2-((1-(2-hydroxy-2-phenylethyl)-4-oxo-4,5-dihydro-1*H*-pyrazolo[3,4-*d*]pyrimidin-6-yl)thio)-*N*-(2-morpholinophenyl)acetamide 122.

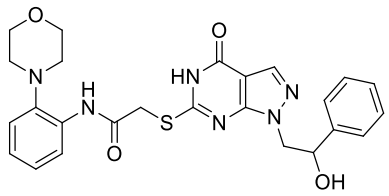

122

To a suspension of **83c** (288 mg, 1 mmol), **122** (300 mg, 1.14 mmol) and anhydrous K_2CO_3 (138 mg, 1 mmol) in anhydrous DMF (2 mL), the mixture was stirred at room temperature for 24 h. Cold water was added to obtain a white solid that was filtered, washed with water (10 mL) and recrystallized from AcOEt.

Yield: 0.23 g, 46%

Mp: 193-194 °C

MW = 506.58

Anal. calcd for $C_{25}H_{26}N_6O_4S$, C 59.27, H 5.17, N 16.59, S 6.33, found C 59.27, H 5.52, N 16.35, S 5.94.

^{1}H NMR ($CDCl_3$): δ 3.35-3.70 (m, 4H, $2CH_2N$ morph), 3.82-4.00 and 4.55-4.65 (2m, 4H, $2CH_2O$ morph), 4.83-5.10 (m, 4H, SCH_2 + CH_2N pyraz.), 5.56-5.61 (m, 1H, CHCl), 6.45 (s all, 1H, NH disappears with D_2O), 7.28-7.50 and 7.80-7.82 (2m, 9H Ar), 8.06 (s, 1H, H-3).

IR (KBr): cm^{-1} 3500-3030 (OH), 3322 (NH), 1704 (CO), 1685 (CO).

General procedure for the synthesis of compounds 123 and 118a.

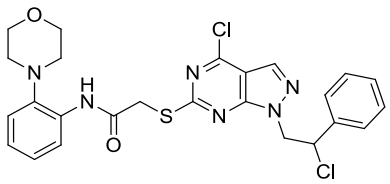

123

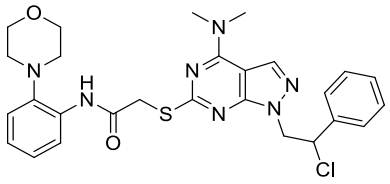

118a

The Vilsmeier complex, previously prepared from $POCl_3$ (4.6 g, 30 mmol) and anhydrous DMF (2.19 g, 30 mmol) was added to a suspension of **122** (506 mg, 1 mmol) in CH_2Cl_2 (10 mL). The mixture was refluxed for 4 h. After cooling at room temperature, 1 M NaOH was added (150 mL) and the suspension was extracted with CH_2Cl_2 (3 x 20 mL), washed with water (2 x 20 mL), dried ($MgSO_4$), filtered and concentrated under reduced pressure. The yellow crude oil was purified by column chromatography (Silica gel 0.06-0200 mm, 40 Å) using Et_2O as the eluant, to afford compound **123** and **118a**.

2-((4-Chloro-1-(2-chloro-2-phenylethyl)-4,5-dihydro-1H-pyrazolo[3,4-d]pyrimidin-6-yl)thio)-N-(2-morpholinophenyl)acetamide 123.

Yield: 0.24 g, 44%
Mp: 107-118 °C
MW = 543.47
Anal. calcd for $C_{25}H_{24}N_6Cl_2O_2S$, C 55.25, H 4.45, N 15.46, S 5.90, found C 55.55, H 4.48, N 15.06, S 6.32.
^{1}H NMR ($CDCl_3$): δ 3.35-3.70 (m, 4H, $2CH_2N$ morph), 3.82-4.00 and 4.55-4.65 (2m, 4H, $2CH_2O$ morph), 4.83-5.10 (m, 4H, SCH_2 + CH_2N pyraz.), 5.56-5.61 (m, 1H, CHCl), 7.28-7.50 and 7.80-7.82 (2m, 9H Ar), 8.06 (s, 1H, H-3).
IR (KBr): cm^{-1} 3011 (NH), 1730 (CO).

2-((1-(2-Chloro-2-phenylethyl)-4-(dimethylamino)-4,5-dihydro-1H-pyrazolo[3,4-d]pyrimidin-6-yl)thio)-N-(2-morpholinophenyl)acetamide 118a.

Yield: 0.15 g, 28%
Mp: 197-201 °C
MW = 552.09
Anal. calcd for $C_{27}H_{30}N_7O_2ClS$, C 58.74, H 5.48, N 17.76, S 5.81, found C 58.74, H 5.49, N 17.52, S 5.32.
^{1}H NMR ($CDCl_3$): δ 2.55-2.70 (m, 4H, $2CH_2N$ morph), 3.20-3.40 (s, 6H, $2CH_3$), 3.65-3.75 (2m, 4H, $2CH_2O$ morph), 3.98 (s, 2H, SCH_2), 4.58-4.63 and 4.82-4.88 (2m, 2H, CH_2N pyraz.), 5.44-

5.46 (m, 1H, CHCl), 6.99-7.14, 7.26-7.43 and 7.82-7.84 (m, 8H Ar), 7.84 (s, 1H, H-3), 8.48-8.50 (d, *J* = 8.0, 1H Ar), 9.53 (s, 1H, NH).
IR (KBr): cm^{-1} 3280 (NH), 1677 (CO).

General procedure for the synthesis of compounds 118b-d.

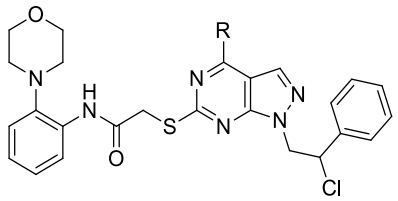

118b-d

b: R = $NH(CH_2)_2C_6H_5$
c: R = $NH(CH_2)_2C_6H_4$-4F
d: R = $NH(CH_2)_2C_6H_4$-3Cl

To a solution of **123** (543 mg, 1 mmol) in anhydrous toluene (5 mL), the appropriate amine (4 mmol) was added and the reaction was stirred at room temperature for 48 h. The solution was washed with water (2 x 10 mL), dried ($MgSO_4$), filtered and concentrated under reduced pressure. The crude oil was purified by column chromatography (Florisil®, 100-200 mesh), using Et_2O as the eluent to obtain compounds **118b-d** which crystallized by adding a 1:1 mixture of Et_2O and PE (bp 40-60 °C) to give a white solid.

2-((1-(2-Chloro-2-phenylethyl)-4-(phenethylamino)-4,5-dihydro-1H-pyrazolo[3,4-d]pyrimidin-6-yl)thio)-N-(2-morpholinophenyl)acetamide 118b.

Yield: 0.32 g, 51%
Mp: 128-132 °C
MW = 628.19
Anal. calcd for $C_{33}H_{34}N_7O_2ClS$, C 63.09, H 5.46, N 15.61, S 5.10, found C 62.85, H 5.72, N 15.48, S 4.85.
^{1}H NMR ($CDCl_3$): δ 2.80-3.10 (m, 2H, CH_2Ar), 3.40-3.50 and 3.52-3.62 (2m, 4H, $2CH_2N$ morph), 3.80-3.96 (m, 4H, $2CH_2O$ morph), 4.55-4.57 (m, 2H, $\underline{CH_2}NH$), 4.69-4.73 and 4.87-5.01 (2m, 4H, SCH_2 + CH_2N pyraz.), 5.54-5.58 (m, 1H, CHCl), 7.23-7.41 (m, 15H, 14Ar + H-3), 7.91 (s all., 1H, NH).
IR (KBr): cm^{-1} 3247 (NH), 3176 (NH), 1621 (CO).

2-((1-(2-Chloro-2-phenylethyl)-4-((4-fluorophenethyl)amino)-4,5-dihydro-1H-pyrazolo[3,4-d]pyrimidin-6-yl)thio)-N-(2-morpholinophenyl)acetamide 118c.

Yield: 0.25 g, 39%

Mp: 130-132 °C

MW = 646.18

Anal. calcd for $C_{33}H_{33}N_7O_2ClFS$, C 61.34, H 5.15, N 15.17, S 4.96, found C 61.42, H 5.33, N 14.91, S 4.74.

^{1}H NMR ($CDCl_3$): δ 2.80-3.05 (m, 2H, CH_2Ar), 3.44-3.48 and 3.53-3.56 (2m, 4H, $2CH_2N$ morf), 3.82-3.85 (2m, 4H, $2CH_2O$ morph), 4.53 (m, 2H, $\underline{CH_2}NH$), 4.52-4.56 and 4.83-4.96 (2m, 4H, SCH_2 + CH_2N pyraz.), 5.56-5.60 (m, 1H, CHCl), 6.97-7.01, 7.15-7.19, 7.26-7.36 and 7.40-7.42 (4m, 13H, 12Ar + H-3), 7.7-7.73 (m, 1H Ar).

IR (KBr): cm^{-1} 3249 (NH), 3178 (NH), 1615 (CO).

2-((1-(2-Chloro-2-phenylethyl)-4-((3-chlorophenethyl)amino)-4,5-dihydro-1H-pyrazolo[3,4-d]pyrimidin-6-yl)thio)-N-(2-morpholinophenyl)acetamide 118d.

Yield: 0.29 g, 44%

Mp: 118-124 °C

MW = 662.63

Anal. calcd for $C_{33}H_{33}N_7O_2Cl_2S$, C 59.81, H 5.02, N 14.80, S 4.84, found C 59.55, H 4.95, N 14.51, S 4.72.

^{1}H NMR ($CDCl_3$): δ 2.94-2.98 (t, *J* = 6.8, 2H, CH_2Ar), 3.45-3.48 and 3.54-3.56 (2m, 4H, $2CH_2N$ morph), 3.82-3.85 (m, 4H, $2CH_2O$ morph), 4.53 (m, 2H, $\underline{CH_2}NH$), 4.70-4.75 and 4.83-4.96 (2m, 4H, SCH_2 + CH_2N pyraz.), 5.57-5.59 (m, 1H, CHCl), 7.08-7.10 and 7.22-7.36 (2m, 13H, 12Ar + H-3), 7.41-7.42 (m, 1H Ar).

IR (KBr): cm^{-1} 3300-3100 (NH), 1621 (CO).

Synthesis of 2-((1-(2-chloro-2-phenylethyl)-4-((3-chlorophenyl)amino)-4,5-dihydro-1*H*-pyrazolo[3,4-*d*]pyrimidin-6-yl)thio)-*N*-(2-morpholinophenyl)acetamide 118e.

A solution of **123** (543 mg, 1 mmol) and 3-chloroaniline (255 mg, 2 mmol) in absolute EtOH was refluxed for 5 h. After cooling at room temperature, the solvent was evaporated under reduced pressure, then water was added (20 mL) and the suspension was extracted with CH_2Cl_2 (3 x 20 mL); washed with water (20 mL), dried ($MgSO_4$), filtered and concentred under reduced pressure. The crude oil was crystallized by adding a 1:1 mixture of Et_2O and PE (bp 40-60 °C) and finally the solid was recrystallized from absolute EtOH to obtain compound **118e** as a white solid.

Yield: 0.27 g, 42%
Mp: 153-157 °C
MW = 634.58
Anal. calcd for $C_{31}H_{29}N_7O_2Cl_2S$, C 58.67, H 4.61, N 15.45, S 5.05, found C 58.76, H 4.88, N 15.17, S 4.74.
^{1}H NMR ($CDCl_3$): δ 3.40-3.44 and 3.52-3.56 (2m, 4H, $2CH_2N$ morph), 3.80-3.84 (m, 4H, $2CH_2O$ morph), 4.67-4.73 and 4.80-4.99 (2m, 4H, SCH_2 + CH_2N pyraz.), 5.55-5.57 (m, 1H, CHCl), 7.15-7.41 (m, 14H, 13Ar + H-3).
IR (KBr): cm^{-1} 3286 (NH), 1634 (CO).

Synthesis of 2-phenethyl-5,6,7,8-tetrahydrobenzo[4,5]thieno[2,3-*d*]pyrimidin-4(3*H*)-one 125.

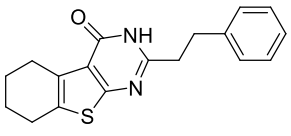

125

To a solution of **124** (451 mg, 2 mmol) in 4 M HCl in dioxane (10 mL), 3-phenylproprionitrile (1.31 mL, 10 mmol) was added and the suspension was stirred at 60 °C for 20 h. The solvent was evaporated under reduced pressure, water was added (50 mL) and the suspension was extracted with AcOEt (3 x 50 mL), washed with saturated NaCl solution (50 mL), dried

(Na_2SO_4), filtered and evaporated under reduced pressure. The brown oil crystallized by adding a 1:1 mixture of Et_2O and *n*-hexane to give a white solid.

Yield: 0.61 g, 99%

Mp: 234-235 °C

MW = 310.41

Anal. calcd for $C_{18}H_{18}N_2SO$, C 69.65, H 5.84, N 9.02, S 10.33, found C 69.57, H 6.09, N 8.95, S 10.10.

^1H NMR ($CDCl_3$): δ 1.80-1.95 (m, 4H, CH_2-6 and CH_2-7), 2.77-2.83 (m, 2H, CH_2-9), 3.04-3.06 (m, 4H, CH_2-5 and CH_2-8), 3.12-3.14 (m, 2H, CH_2-10), 7.25-7.27 (m, 5H Ar), 12.35 (s all., 1H, NH).

IR (KBr): cm^{-1} 1663 (CO), 1594 (NH).

Synthesis of 4-chloro-2-phenethyl-5,6,7,8-tetrahydrobenzo[4,5]thieno[2,3-*d*]pyrimidine 126.

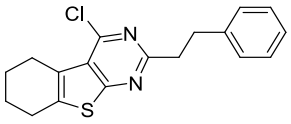

126

A suspension of **125** (100 mg, 0.32 mmol) and $POCl_3$ (1 mL, 10.73 mmol) was heated at 80 °C for 8 h. $POCl_3$ was evaporated under reduced pressure, then a solution of $NaHCO_3$ was added until pH ~ 7 (5 mL) and the suspension was extracted with AcOEt (3 × 10 mL), washed with water (10 mL), dried (Na_2SO_4), filtered and evaporated under reduced pressure. The brown oil crystallized by adding a mixture of Et_2O and PE (bp 40-60 °C) to give a white solid.

Yield: 65 mg, 62%

Mp: 83-87 °C

MW = 328.86

Anal. calcd for $C_{18}H_{17}N_2SCl$, C 65.74, H 5.21, N 8.52, S 9.75, found C 65.96, H 5.24, N 8.70, S 9.43.

^{1}H NMR ($CDCl_3$): δ 1.81-1.98 (m, 4H, CH_2-6 and CH_2-7), 2.67-2.98 (m, 2H, CH_2-9), 3.04-3.18 (m, 6H, CH_2-5, CH_2-8 and CH_2-10), 7.21-7.32 (m, 5H Ar).

Synthesis of ethyl 2-((2-phenethyl-5,6,7,8-tetrahydrobenzo[4,5]thieno[2,3-*d*]pyrimidin-4-yl)amino)acetate 127.

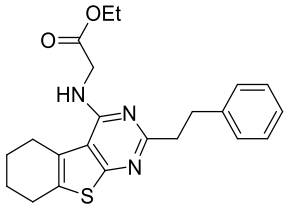

127

A solution of glycine ethyl ester hydrochloride (216 mg, 1.55 mmol) and TEA (628 μL, 4.50 mmol) in absolute EtOH (15 mL) was stirred at room temperature for 5 min. **126** (443 mg, 1.35 mmol) was added and the reaction was refluxed for 12 h. The solvent was evaporated under reduced pressure then water was added (50 mL) and the suspension was extracted with AcOEt (3 x 50 mL), washed with saturated NaCl solution (50 mL), dried (Na_2SO_4), filtered and evaporated under reduced pressure. The oil crystallized by adding a 1:1 mixture of Et_2O and PE (bp 40-60 °C) to give a white solid.

Yield: 0.38 g, 71%

Mp: 128-129 °C

MW = 395.52

Anal. calcd for $C_{22}H_{25}N_3SO_2$, C 66.81, H 6.37, N 10.62, S 8.11, found C 66.55, H 6.27, N 10.50, S 8.00.

^{1}H NMR ($CDCl_3$): δ 1.35 (t, *J* = 7.2 Hz, 3H, CH_3), 1.93-1.99 (m, 4H, CH_2-6 and CH_2-7), 2.88-2.96 (m, 2H, CH_2-9), 2.98-3.06 (m, 2H, CH_2-10), 3.18-3.23 (m, 4H, CH_2-5 and CH_2-8), 4.28-4.32 and 4.34-4.36 (2m, 4H, CH_2 N + CH_2O), 7.15-7.32 (m, 5H Ar).

IR (KBr): cm^{-1} 3340 (NH), 1741 (CO), 1580 (NH).

Synthesis of 2-((2-phenethyl-5,6,7,8-tetrahydrobenzo[4,5]thieno[2,3-*d*]pyrimidin-4-yl)amino)acetic acid 128.

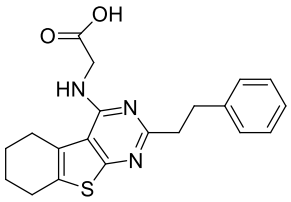

128

To a suspension of **127** (313 mg, 0.79 mmol) in absolute EtOH, a solution 1 N NaOH in absolute EtOH (6.7 mL) was added and the reaction was stirred at room temperature for 12 h. The solvent was evaporated under reduced pressure, water was added, then 1 N HCl was added until pH ~ 2. Compound **128** precipitated as a white solid and was filtered and washed with cold water.

Yield: 98%

Mp: 208-210 °C

MW = 367.47

Anal. calcd for $C_{20}H_{21}N_3SO_2$, C 65.37, H 5.76, N 11.44, S 8.73, found C 65.36, H 6.08, N 11.23, S 8.81.

^{1}H NMR ($(CD_3)_2SO$): δ 1.84-1.94 (m, 4H, CH_2-6 and CH_2-7), 2.50-2.52 (m, 2H, CH_2-9), 2.70-2.76 (m, 2H, CH_2-10), 2.83-3.03 (m, 4H, CH_2-5 and CH_2-8), 4.08 (d, *J* = 5.0 Hz, 2H, CH_2N), 7.16-7.25 (m, 5H Ar).

IR (KBr): cm^{-1} 3417 (NH), 1721 (CO), 1579 (NH).

Synthesis of N^1-(2-morpholinophenyl)-N^2-(2-phenethyl-5,6,7,8-tetrahydrobenzo[4,5]thieno[2,3-*d*]pyrimidin-4-yl)ethane-1,2-diamine 119a.

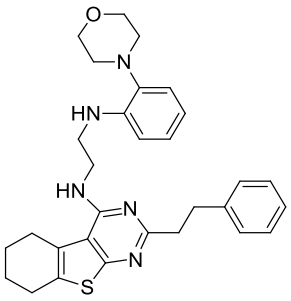

119a

To a suspension of **128** (100 mg, 0.27 mmol) and 2-morpholinoaniline (49 mg, 0.27 mmol) in ACN (2 mL) PCl_3 was added dropwise (7.15 µL, 0.082 mmol) and the reaction was refluxed for 8 h. Then, $NaHCO_3$ (50 mL) was added and the suspension was extracted with CH_2Cl_2 (3 x 50 mL), washed with water (50 mL), dried (Na_2SO_4), filtered and evaporated under reduced pressure. The crude was purified by flash chromatography (Isolera™ One Biotage) using CH_2Cl_2/MeOH as the eluent, with a gradient elution to afford compounds **119a**.

Yield: 50 mg, 35%

Mp: 147-154 °C

MW = 527.68

Anal. calcd for $C_{30}H_{33}N_5O_2S$, C 68.28, H 6.30, N 13.27, S 6.08, found C 68.25, H 6.29, N 13.05, S 6.08.

^{1}H NMR ($CDCl_3$): δ 1.96-1.98 (m, 4H, CH_2-6 and CH_2-7), 2.68-2.72, 2.84-2.92 and 3.08-3.22 (3m, 12H, CH_2-5, CH_2-8, CH_2-9, CH_2-10, CH_2-11 and CH_2-14), 3.48-3.57 (m, 4H, CH_2-12 and CH_2-13), 4.43 (d, *J* = 4.4 Hz, 2H, $\underline{CH_2}NH$), 6.25 (s all., 1H, $\underline{NH}CH_2$), 7.12-7.22 (m, 8H Ar), 8.48 (d, *J* = 6 Hz, 1H Ar), 9.12 (s all., 1H, NHCO).

Synthesis of 2-phenethyl-5,6,7,8-tetrahydrobenzo[4,5]thieno[2,3-*d*]pyrimidine-4-thiol 129.

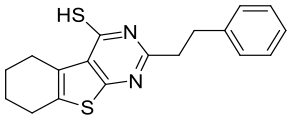

129

To a solution of **125** (310 mg, 1 mmol) in anhydrous dioxane (10 mL), P_2S_5 (108 µL, 1 mmol) was added and the reaction was refluxed for 8 h under nitrogen atmosphere. The reaction was poured in water (50 mL) to obtain a white solid. The suspension was heated at 100 °C for 1 h to obtain a solution, after cooling at room temperature, the reaction was extracted with AcOEt (3 x 100 mL), the organic phase was washed with saturated NaCl solution (150 mL), dried (Na_2SO_4), filtered and evaporated under reduced pressure. Et_2O was added and the solid was filtered to obtain the pure compound **129**.

Yield: 0.33 g, quantitative

Mp: 228-231 °C

MW = 326.48

Anal. calcd for $C_{18}H_{18}N_2S_2$, C 66.22, H 5.56, N 8.58, S 19.64, found C 66.03, H 5.63, N 8.25, S 19.68.

^{1}H NMR ($(CD_3)_2SO$): δ 1.65-1.83 (m, 4H, CH_2-6 and CH_2-7), 2.65-2.81 (m, 2H, CH_2-9), 2.76-3.01 (m, 4H, CH_2-5 and CH_2-8), 3.08-3.21 (m, 2H, CH_2-10), 7.19-7.29 (m, 5H Ar).

IR (KBr): cm^{-1} 3200-2900 (SH), 1525 (NH).

Synthesis of 2-(4-methylpiperazin-1-yl)aniline 130.

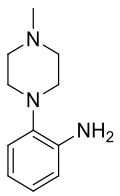

130

To obtain **130**, a Pd catalyzed hydrogenation was performed on 1-methyl-4-(2-nitrophenyl)piperazine (1.15 g, 5.19 mmol), then the solvent was evaporated under reduced pressure to give a white solid.

Yield: 0.96 g, 97%

Mp: 101-103 °C

MW = 191.27

Anal. calcd for $C_{11}H_{17}N_3$, C 69.07, H 8.96, N 21.97, found C 69.00, H 9.09, N 21.70. ^{1}H NMR ($CDCl_3$): δ 2.42 (s, 3H, CH_3), 2.51-2.65 (m, 4H, 2$\underline{CH_2}$NCH_3), 2.98-3.02 (t, *J* = 4.8 Hz, 4H, 2CH_2N), 3.99 (s all, 2H, NH_2), 6.74-6.81 and 6.93-7.07 (2m, 4H Ar).

IR (KBr): cm^{-1} 3389, 3293 (NH_2), 1503 (NH).

Synthesis of 2-bromo-*N*-(2-(4-methylpiperazin-1-yl)phenyl)acetamide 131.

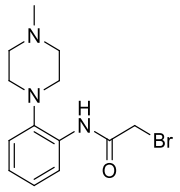

131

To a solution of bromoacetyl chloride (247 mg, 1.57 mmol), in anhydrous Et_2O (4 mL), a solution of **130** (130 µL, 1.31 mmol) in anhydrous Et_2O (15 mL) was added dropwise and the reaction was stirred at room temperature for 12 h under nitrogen atmosphere. 1 N NaOH was added and the reaction was extracted with AcOEt (3 × 15 mL) and CH_2Cl_2 (3 × 15 mL), the organic phase was washed with saturated NaCl solution (100 mL), dried (Na_2SO_4), filtered and evaporated under reduced pressure. The crude was purified by column chromatography (Silica gel 220-440 mesh, 60 Å), using AcOEt/MeOH (MeOH 30→40%) as the eluent.

Yield: 0.14 g, 34%

Mp: 108-113 °C

MW = 312.21

Anal. calcd for $C_{13}H_{18}N_3OBr$, C 50.01, H 5.81, N 13.46, found C 50.20, H 5.80, N 13.16.
^{1}H NMR ($CDCl_3$): δ 2.43 (s, 3H, CH_3), 3.62-3.78 (m, 4H, 2$\underline{CH_2}$NCH$_3$), 2.95-3.00 (t, *J* = 4.6 Hz, 4H, 2CH_2N), 4.26 (s, 2H, CH_2Br), 7.16-7.23 1(m, 3H Ar), 8.38-8.42 (m, 1H Ar).
IR (KBr): cm^{-1} 3317 (NH), 1669 (CO), 1528 (NH).

Synthesis of *N*-(2-(4-methylpiperazin-1-yl)phenyl)-2-((2-phenethyl-5,6,7,8-tetrahydrobenzo[4,5]thieno[2,3-*d*]pyrimidin-4-yl)thio)acetamide 119b.

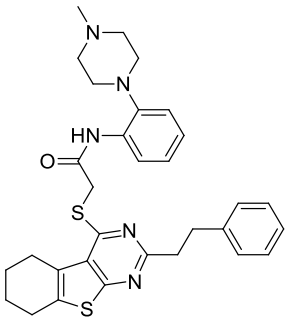

119b

To a solution of **129** (70 mg, 0.214 mmol) and **131** (74 mg, 0.236 mmol) in anhydrous DMF, anhydrous K_2CO_3 (445 mg, 0.322 mmol) was added and the reaction was stirred at room temperature for 4 h under nitrogen atmosphere. The solvent was evaporated under reduced pressure, then, water (10 mL) was added and the suspension was extracted with CH_2Cl_2 (3 x 10 mL). The organic phase was washed with saturated NaCl solution (15 mL), dried (Na_2SO_4), filtered and evaporated under reduced pressure. The crude oil was purified by column chromatography (Silica gel 220-440 mesh, 60 Å), using AcOEt/MeOH (95:5) as the eluent. A mixture of Et_2O and PE (bp 40-60 °C) was added and the solid was filtered to obtain the pure compound **119b**.

Yield: 75 mg, 63%
Mp: 124-126 °C
MW = 557.78
Anal. calcd for $C_{31}H_{35}N_5OS_2$, C 66.75, H 6.32, N 12.56, S 11.50, found C 66.85, H 6.38, N 12.35, S 11.34.

^{1}H NMR ($CDCl_3$): δ 1.94-1.99 (m, 4H, CH_2-6 and CH_2-7), 2.06 (s, 3H, CH_3), 2.60-2.68, 2.82-2.88 and 3.04-3.19 (3 m, 16 H, CH_2-5, CH_2-8 + 8H piperaz + CH_2CH_2Ar), 4.14 (s, 2H, CH_2S), 7.07-7.14 (m, 8H Ar), 8.41-8.44 (m, 1H Ar), 9 (s all., 1H, NH).
IR (KBr): cm^{-1} 3292 (NH), 1680 (CO), 1522 (NH).

Synthesis of 3-methyl-1-(2-nitrophenyl)piperazine 132.

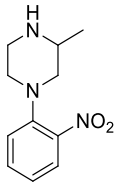

132

To a suspension of 1-bromo-2-nitrobenzene (1.5 g, 7.42 mmol) in dioxane (30 mL), 2-methylpiperazine (1.12 g, 11.14 mmol) and K_2CO_3 (5.13 g, 37.1 mmol) were added and the reaction was refluxed for 14 h. The suspension was filtered and washed with AcOEt (3 × 10 mL). The solution was evaporated under reduced pressure and the crude was purified by flash chromatography (Isolera^{TM} One Biotage), using AcOEt/MeOH as the eluent, with a gradient elution to afford compounds **132** as an orange oil.

Yield: 1.64 g, quantitative
MW = 221.26
Anal. calcd for $C_{11}H_{15}N_3O_2$, C 59.71, H 6.83, N 18.99, found C 59.99, H 7.02, N 18.65.
^{1}H NMR ($CDCl_3$): δ 1.12 (d, *J* = 6.2 Hz, 3H, CH_3), 2.31 (s all., 1H, NH), 2.57(t, *J* = 11.2 Hz, 1H piperaz), 2.82-2.95 and 3.06-3.19 (2m, 6H piperaz), 7.05-7.18 (m, 2H Ar, H_B and H_D), 7.49 (dt, *J* = 6.4 Hz, *J* = 1.6 Hz, 1H Ar, H_C), 7.78 (dd, *J* = 6.4 Hz, *J* = 1.6 Hz, 1H Ar, H_A).
IR (KBr): cm^{-1} 1604, 1342 (ν_{sim} and ν_{as} NO_2).

Synthesis of tert-butyl 2-methyl-4-(2-nitrophenyl)piperazine-1-carboxylate 133.

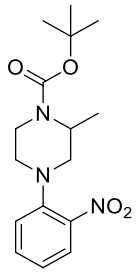

133

To a solution of **132** (538 mg, 2.43 mmol) in anhydrous CH_2Cl_2 (10 mL), TEA (474 µL, 3.40 mmol) and Boc_2O (636 mg, 2.91 mmol) were added and the reaction was stirred at room temperature for 12 h. The solution was washed with $NaHCO_3$ (2 × 10 mL), then was extracted with CH_2Cl_2 (10 mL), the organic phase was washed with saturated NaCl solution (10 mL), dried (Na_2SO_4), filtered and evaporated under reduced pressure to obtain **133** as an orange oil.

Yield: 0.78 g, quantitative

MW = 321.37

Anal. calcd for $C_{16}H_{23}N_3O_4$, C 59.80, H 7.21, N 13.08, found C 59.49, H 7.35, N 13.29. ^{1}H NMR ($CDCl_3$): δ 1.3 (d, *J* = 6.8 Hz, 3H, $CH\underline{CH_3}$), 1.49 (s, 9H, $3CH_3$ *t*But), 2.85 (dt, *J* = 16.0 Hz, *J* = 4 Hz, 1H piperaz), 3.02-3.41, 3.82-3.96 and 4.22-4.40 (3m, 6H piperaz), 7.07-7.17 (m, 2H Ar, H_B and H_D), 7.51 (t, *J* = 9.6 Hz, 1H Ar, H_C), 7.72 (d, *J* = 9.6 Hz, 1H Ar, H_A).

IR (KBr): cm^{-1} 1693 (CO), 1524, 1365 (ν_{sim} and ν_{as} NO_2).

Synthesis of tert-butyl 4-(2-aminophenyl)-2-methylpiperazine-1-carboxylate 134.

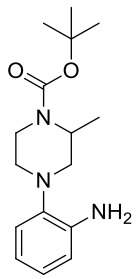

134

To obtain **134**, a Pd catalyzed hydrogenation was performed on **133** (800 mg, 2.49 mmol), then the solvent was evaporated under reduced pressure to give a red oil which was purified by column chromatography (Silica gel 220-440 mesh, 60 Å), using CH_2Cl_2 as the eluent to give a brown solid.

.

Yield: 0.50 g, 69%

Mp: 119-122 °C

MW = 291.39

Anal. calcd for $C_{16}H_{25}N_3O_2$, C 65.95, H 8.65, N 14.42, found C 65.82, H 8.69, N 14.71. ^{1}H NMR ($CDCl_3$): δ 1.40 (d, *J* = 6.6 Hz, 3H, CH<u>CH_3</u>), 1.51 (s, 9H, $3CH_3$ *t*But), 2.63-3.18, 3.21-3.39, 3.94-4.07 and 4.28-4.42 (4m, 7H piperaz), 6.81-6.85 and 6.98-6.99 (2m, 4H Ar).

IR (KBr): cm^{-1} 3429, 3345 (NH_2), 1686 (CO).

Synthesis of tert-butyl 4-(2-(2-bromoacetamido)phenyl)-2-methylpiperazine-1-carboxylate 135.

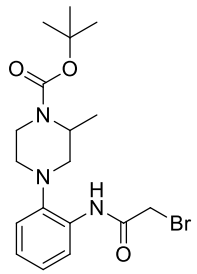

135

To a solution of **134** (210 mg, 0.721 mmol) and bromoacetyl chloride (78 µL, 0.937 mmol) in anhydrous Et_2O (7 mL), the reaction was stirred at room temperature for 3 h under nitrogen atmosphere. 1 N NaOH was added and the suspension was extracted with CH_2Cl_2 (3 x 20 mL), dried (Na_2SO_4) and evaporated under reduced pressure to obtain **135** as a white solid.

Yield: 0.28 g, 95%

Mp: 145-148 °C

MW = 412.32

Anal. calcd for $C_{18}H_{26}N_3O_3Br$, C 52.43, H 6.36, N 10.19, found C 52.34, H 6.50, N 10.26. ^{1}H NMR ($CDCl_3$): δ 1.45 (d, *J* = 6.4 Hz, 3H, CH$\underline{CH_3}$), 1.52 (s, 9H, $3CH_3$ *t*But), 2.58-3.01, 3.11-3.21, 3.30-3.57 and 3.90-4.18 (4m, 6H piperaz), 4.27 (s, 2H, CH_2Br), 4.38-4.58 (m, 1H piperaz), 7.15-7.22 (m, 3H Ar), 8.38-8.42 (m, 1H Ar), 9.65 (s all, 1H, NH).
IR (KBr): cm^{-1} 3295 (NH), 1696 (CO estere), 1681 (CO ammide), 1531 (NH).

Synthesis of tert-butyl 2-methyl-4-(2-(2-((2-phenethyl-5,6,7,8-tetrahydrobenzo[4,5] thieno[2,3-*d*]pyrimidin-4-yl)thio)acetamido)phenyl)piperazine-1-carboxylate 136.

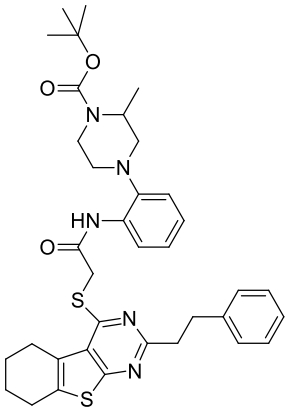

136

To a suspension of **135** (84 mg, 0.203 mmol) and **125** (60.5 mg, 0.185 mmol) in the presence of anhydrous K_2CO_3 (38.4 mg, 0.277 mmol) in anhydrous DMF (5 mL), the reaction was stirred at room temperature for 12 h under nitrogen atmosphere. The solvent was evaporated under reduced pressure, H_2O (10 mL) was added and the suspension was extracted with CH_2Cl_2 (3 x 10 mL), the organic phase was washed with saturated NaCl solution (15 mL), dried (Na_2SO_4), filtered and evaporated under reduced pressure. The crude oil was purified by column chromatography (Silica gel 220-440 mesh, 60 Å), using Et_2O/PE (1:1) as the eluent to afford **136** as a white solid.

Yield: 0.11 g, 90%
Mp: 156-157 °C
MW = 657.89

Anal. calcd for $C_{36}H_{43}N_5O_3S_2$, C 65.72, H 6.59, N 10.65, S 9.75, found C 65.57, H 6.69, N 10.79, S 9.48.

^{1}H NMR ($CDCl_3$): δ 1.12 (d, *J* = 6.6 Hz, 3H, CH$\underline{CH_3}$), 1.48 (s, 9H, 3CH_3 *t*But), 1.85-2.01, 3.38-3.31 and 3.45-3.41 (3m, 18H, 6H piperaz + CH_2CH_2Ar + 8H pyrano), 4.18 (s, 2H, CH_2Br), 4.21-4.28 (m, 1H piperaz), 7.07-7.20 (m, 8H Ar), 8.48 (d, *J* = 8.6 Hz, 1H Ar), 9.57 (s all, 1H, NH).

IR (KBr): cm^{-1} 3315 (NH), 1692 (CO ester), 1591 (CO amide), 1519 (NH).

Synthesis of *N*-(2-(3-methylpiperazin-1-yl)phenyl)-2-((2-phenethyl-5,6,7,8-tetrahydrobenzo[4,5]thieno[2,3-*d*]pyrimidin-4-yl)thio)acetamide 119c.

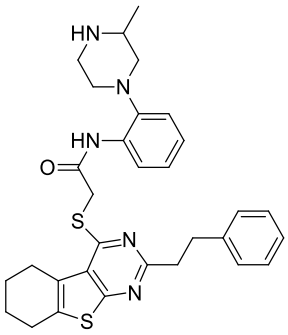

119c

To a solution of **136** (100 mg, 0.15 mmol) in anhydrous CH_2Cl_2 (10 mL), TFA (70 µL, 0.9 mmol) was added dropwise and the reaction was stirred at room temperature for 12 h under nitrogen atmosphere. TFA was evaporated and 1 N NaOH was added, the suspension was extracted with CH_2Cl_2 (3 x 10 mL), the organic phase was washed with saturated NaCl solution (15 mL), dried (Na_2SO_4), filtered and evaporated under reduced pressure. Et_2O (10 mL) was added and then evaporated to obtain **119c** as a white solid.

Yield: 62 mg, 75%

Mp: 57-65 °C

MW = 557.78

Anal. calcd for $C_{31}H_{35}N_5OS_2$, C 66.75, H 6.32, N 12.56, S 11.50, found C 66.72, H 6.56, N 12.48, S 11.14.

^{1}H NMR ($CDCl_3$): δ 0.75 (d, *J* = 6 Hz, 3H, CH_3), 1.94-2.01 (m, 4H, CH_2-6 and CH_2-7), 2.19-3.21 (m, 15H, 7H piperaz, + CH_2CH_2Ar + CH_2-5 and CH_2-8), 4.12 (d, *J* = 5.2 Hz, 2H, CH_2S), 7.07-7.18 (m, 8H Ar), 8.5 (d, *J* = 8 Hz, 1H Ar), 9.62 (s, 1H, NH).
IR (KBr): cm^{-1} 3285 (NH), 1679 (CO), 1518 (NH).

General procedure for the synthesis of compounds 139a-c.

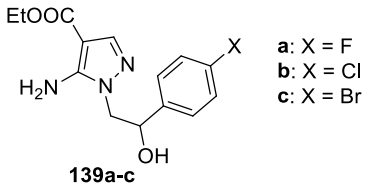

a: X = F
b: X = Cl
c: X = Br

139a-c

The appropriate hydrazine **138a-c** (20 mmol) was added to a solution of ethyl(ethoxymethylene)cyanoacetate (3.38 g, 20 mmol) in anhydrous toluene (20 mL) and the mixture was heated at 80 °C for 8 h. The solution was concentrated under reduced pressure to half of the volume and allowed to cool to room temperature. The yellow pale solid was filtered and recrystallized from toluene to afford **139a-c** as white solids.

Ethyl 5-amino-1-(2-(4-fluorophenyl)-2-hydroxyethyl)-1H-pyrazole-4-carboxylate 139a.

Yield: 4.11 g, 70%
Mp: 163-164 °C
MW = 293.29
Anal. calcd for $C_{14}H_{16}N_3O_3F$, C 57.33, H 5.50, N 14.33, found C 57.31, H 5.72, N 14.25.
^{1}H NMR ($CDCl_3$): δ 1.33 (t, *J* = 7.0, 3H, CH_3), 3.73 (s all, 1H, OH, disappears with D_2O), 3.90-4.15 (m, 2H, CH_2N), 4.29 (q, *J* = 7.0, 2H, CH_2O), 5.01-5.18 (m, 1H, CHO), 5.36 (s all, 2H, NH_2, disappears with D_2O), 7.03-7.40 (m, 4H Ar), 7.55 (s, 1H, H-3).
IR (KBr) cm^{-1}: 3448, 3446 (NH_2), 3300-3000 (OH), 1685 (CO).

Ethyl 5-amino-1-(2-(4-chlorophenyl)-2-hydroxyethyl)-1H-pyrazole-4-carboxylate 139b.

Yield: 4.65 g, 75%

Mp: 168-169 °C

MW = 309.75

Anal. calcd for $C_{14}H_{16}N_3O_3Cl$, C 54.29, H 5.21, N 13.57, found C 54.27, H 5.16, N 13.48. ^{1}H NMR ($CDCl_3$): δ 1.38 (t, *J* = 7.0, 3H, CH_3), 3.56 (s all., 1H, OH, disappears with D_2O), 3.91-4.19 (m, 2H, CH_2N), 4.28 (q, *J* = 7.0, 2H, CH_2O), 5.05-5.18 (m, 1H, CHO), 5.33 (s all., 2H, NH_2, disappears with D_2O), 7.25-7.46 (m, 4H Ar), 7.59 (s, 1H, H-3).

IR (KBr) cm^{-1}: 3412, 3291 (NH_2), 3219-3100 (OH), 1689 (C=O).

Ethyl 5-amino-1-(2-(4-bromophenyl)-2-hydroxyethyl)-1H-pyrazole-4-carboxylate 139c.

Yield: 4.60 g, 65%

Mp: 164-165 °C

MW = 354.20

Anal. calcd for $C_{14}H_{16}N_3O_3Br$, C 47.47, H 4.55, N 11.86, found C 47.50, H 4.60, N 11.90. ^{1}H NMR ($CDCl_3$): δ 1.28 (t, *J* = 7.2, 3H, CH_3), 3.84-4.13 (m, 2H, CH_2N), 4.21 (q, *J* = 7.2, 2H, CH_2O), 5.03-5.12 (m, 1H, CHO), 7.14-7.24 and 7.37-7.47 (2m, 4H Ar), 7.55 (s, 1H, H-3).

IR (KBr) cm^{-1}: 3411, 3291 (NH_2), 3157-2900 (OH), 1689 (C=O).

General procedure for the synthesis of compounds 140a-c.

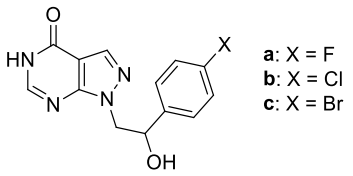

140a-c

To a suspension of the appropriate intermediates **139a-c** (10 mmol) in formamide (10 g, 333 mmol), the reaction was heated at 190 °C for 8 h. After cooling to room temperature, water was added (300 ml) and the obtained solid was filtered. The solid was solubilized in 2 M NaOH then charcoal (600 mg) was added and the mixture was boiled for 10 min. After charcoal filtration, acetic acid was added until pH 4 and the precipitated solid was filtered, washed with water and recrystallized from absolute EtOH.

1-(2-(4-Fluorophenyl)-2-hydroxyethyl)-1H-pyrazolo[3,4-d]pyrimidin-4(5H)-one 140a.

Yield: 2.0 g, 73%

Mp: 281-282 °C

MW = 274.25

Anal. calcd for $C_{13}H_{11}N_4O_2F$, C 56.93, H 4.04, N 20.43, found C 56.90, H 4.19, N 20.41. ^{1}H NMR ($CDCl_3$): δ 4.22-4.35 and 4.39-4.54 (2m, 2H, CH_2N), 5.02-5.17 (m, 1H, CHO), 5.72 (s all., 1H, OH, disappears with D_2O), 7.03-7.19 and 7.24-7.38 (2m, 4H Ar), 8.02 (s, 1H, H-3), 8.07 (s, 1H, H-6), 12.13 (s all., 1H, NH, disappears with D_2O).

IR (KBr): cm^{-1} 3387 (NH), 3168-2900 (OH), 1737 (C=O).

1-(2-(4-Chlorophenyl)-2-hydroxyethyl)-1H-pyrazolo[3,4-d]pyrimidin-4(5H)-one 140b.

Yield: 2.27 g, 78%

Mp: 259-260 °C

MW = 290.71

Anal. calcd for $C_{13}H_{11}N_4O_2Cl$, C 53.71, H 3.81, N 19.27, found C 53.60, H 3.77, N 19.01. ^{1}H NMR ($CDCl_3$): δ 4.20-4.52 (m, 2H, CH_2N), 4.97-5.17 (m, 1H, CHO), 5.94 (s all., 1H, OH, disappears with D_2O), 7.20-7.42 (m, 4H Ar), 8.03 (s, 1H, H-3), 8.07 (s, 1H, H-6), 12.14 (s all., 1H, NH, disappears with D_2O).

IR (KBr): cm^{-1} 3390 (NH), 3200-2800 (OH), 1740 (C=O).

1-(2-(4-Bromophenyl)-2-hydroxyethyl)-1H-pyrazolo[3,4-d]pyrimidin-4(5H)-one 140c.

Yield: 2.35 g, 70%

Mp: 269-270 °C

MW = 335.16

Anal. calcd for $C_{13}H_{11}N_4O_2Br$, C 46.59, H 3.31, N 16.72, found C 46.71, H 3.13, N 16.85. ^{1}H NMR ($CDCl_3$): δ 4.14-4.43 (m, 2H, CH_2N), 4.90-5.07 (m, 1H, CHO), 5.68 (s all., 1H, OH, disappears with D_2O), 7.07-7.21 and 7.31-7.44 (2m, 4H Ar), 7.94 (s, 1H, H-3), 7.98 (s, 1H, H-6), 12.04 (s all., 1H, NH, disappears with D_2O).

IR (KBr): cm^{-1} 3274 (NH), 2900-3100 (OH), 1694 (C=O).

General procedure for the synthesis of compounds 141a-c.

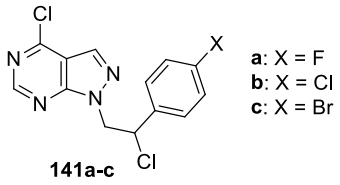

141a-c

a: X = F
b: X = Cl
c: X = Br

The Vilsmeier complex, previously prepared from $POCl_3$ (15.33 g, 100 mmol) and anhydrous DMF (7.31 g, 100 mmol) was added to a suspension of appropriate intermediate **140a-c** (10 mmol) in $CHCl_3$ (50 mL). The mixture was refluxed for 8-12 h. The solution was washed with water (2 x 20 mL), dried ($MgSO_4$), and concentrated under reduced pressure. The crude oil was purified by column chromatography (Florisil®, 100-200 mesh) using Et_2O.

4-Chloro-1-(2-chloro-2-(4-fluorophenyl)ethyl)-1H-pyrazolo[3,4-d]pyrimidine 141a.

Yield: 2.33 g, 75%

Mp: 128-129 °C

MW = 311.14

Anal. calcd for $C_{13}H_9N_4Cl_2F$, C 50.18, H 2.92, N 18.01, found C 50.05, H 2.86, N 17.84. ^{1}H NMR ($CDCl_3$): δ 4.73-4.88 and 4.92-5.08 (2m, 2H, CH_2N), 5.38-5.54 (m, 1H, CHCl), 6.84-7.06 and 7.18-7.45 (2m, 4H Ar), 8.10 (s, 1H, H-3), 8.68 (s, 1H, H-6).

4-Chloro-1-(2-chloro-2-(4-chlorophenyl)ethyl)-1H-pyrazolo[3,4-d]pyrimidine 141b.

Yield: 2.29 g, 70%

Mp: 118-119 °C

MW = 327.60

Anal. calcd for $C_{13}H_9N_4Cl_3$, C 47.66, H 2.77, N 17.10, found C 47.78, H 2.86, N 17.25. ^{1}H NMR ($CDCl_3$): δ 4.72-4.85 and 4.91-5.05 (2m, 2H, CH_2N), 5.38-5.50 (m, 1H, CHCl), 7.16-7.36 (m, 4H Ar), 8.10 (s, 1H, H-3), 8.69 (s, 1H, H-6).

1-(2-(4-Bromophenyl)-2-chloroethyl)-4-chloro-1H-pyrazolo[3,4-d]pyrimidine 141c.

Yield: 2.23 g, 60%

Mp: 108-109 °C

MW = 372.05

Anal. calcd for $C_{13}H_9N_4Cl_2Br$, C 41.97, H 2.44, N 15.06, found C 41.96, H 2.40, N 15.23. ^{1}H NMR ($CDCl_3$): δ 4.82-4.87 and 4.90-5.05 (2m, 2H, CH_2N), 5.46-5.50 (m, 1H, CHCl), 7.24-7.30 and 7.35-7.46 (2m, 4H Ar), 8.15 (s, 1H, H-3), 8.74 (s, 1H, H-6).

General procedure for the synthesis of compounds 142a-c.

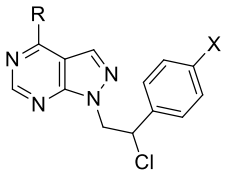

142a-c

a: R = NHC_3H_7; X = F
b: R = $NHCH_2C_6H_4$-4Cl; X = Cl
c: R = $NHCH_2C_6H_4$-3Cl; X = Br

To a solution of **141a-c** (10 mmol) in anhydrous toluene (20 mL), the appropriate amine (40 mmol) was added and the reaction was stirred at room temperature for 24 h. The solution was washed with water (20 mL), dried ($MgSO_4$), and concentrated under reduced pressure. The oil was crystallized by adding a 1:1 mixture of Et_2O/PE (bp 40-60 °C).

1-(2-Chloro-2-(4-fluorophenyl)ethyl)-N-propyl-1H-pyrazolo[3,4-d]pyrimidin-4-amine 142a.

Yield: 2.17 g, 65%

Mp: 139-140 °C

MW = 333.79

Anal. calcd for $C_{16}H_{17}N_5ClF$, C 57.57, H 5.13, N 20.98, found C 57.76, H 5.21, N 21.20. ^{1}H NMR ($CDCl_3$): δ 0.97 (t, *J* = 7.2, 3H, CH_3), 1.59-1.76 (m, 2H, $\underline{CH_2}CH_3$), 3.51 (q, *J* = 7.2, 2H, $\underline{CH_2}NH$), 4.60-4.75 and 4.81-4.94 (2m, 2H, CH_2N), 5.38-5.52 (m, 1H, CHCl), 5.73 (s all., 1H, NH disappears with D_2O), 6.90-7.00 and 7.23-7.44 (2m, 4H Ar), 7.81 (s, 1H, H-3), 8.27 (s, 1H, H-6).

IR (KBr): cm^{-1} 3227 (NH).

1-(2-Chloro-2-(4-chlorophenyl)ethyl)-N-(4-chlorobenzyl)-1H-pyrazolo[3,4-d]pyrimidin-4-amine 142b.

Yield: 3.25 g, 75%

Mp: 153-157 °C

MW = 432.73

Anal. calcd for $C_{20}H_{16}N_5Cl_3$, C 55.51, H 3.73, N 16.18, found C 55.72, H 4.03, N 15.90. ^{1}H NMR ($CDCl_3$): δ 4.62-4.84 (m, 4H, CH_2N +CH_2Ar), 5.38-5.50 (m, 1H, CHCl), 7.16-7.36 (m, 8H Ar), 7.76 (s, 1H, H-3), 8.31 (s, 1H, H-6).

IR (KBr): cm^{-1} 3201 (NH).

1-(2-(4-Bromophenyl)-2-chloroethyl)-N-(3-chlorobenzyl)-1H-pyrazolo[3,4-d]pyrimidin-4-amine 142c.

Yield: 2.86 g, 60%

Mp: 142-143 °C

MW = 477.18

Anal. calcd for $C_{20}H_{16}N_5BrCl_2$, C 50.34, H 3.38, N 14.68, found C 50.37, H 3.69, N 14.36. ^{1}H NMR ($CDCl_3$): δ 4.43-4.85 (m, 4H, CH_2N + CH_2Ar), 5.43-5.59 (m, 1H, CHCl), 7.01-7.49 (m, 8H Ar), 7.80 (s, 1H, H-3), 8.41 (s, 1H, H-6).

IR (KBr): cm^{-1} 3243 (NH).

General procedure for the synthesis of compounds 137a-c.

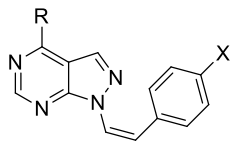

a: R = NHC_3H_7; X = F
b: R = $NHCH_2C_6H_4$-4Cl; X = Cl
c: R = $NHCH_2C_6H_4$-3Cl; X = Br

137a-c

To a solution of NaOH (0.3 g, 7.5 mmol), a solution of the appropriate **142a-c** (1 mmol) in EtOH 95% was added and the reaction was refluxed for 5 h. After cooling to room temperature, the precipitated solid was filtered, washed with water and recrystallized from absolute EtOH.

1-(4-Fluorostyryl)-N-propyl-1H-pyrazolo[3,4-d]pyrimidin-4-amine 137a.

Yield: 0.18 g, 61%

Mp: 232-235 °C

MW = 297.33

Anal. calcd for $C_{16}H_{16}N_5F$, C 64.63, H 5.42, N 23.55, found C 64.83, H 6.00, N 23.63. ^{1}H NMR ($CDCl_3$): δ 0.93 (t, J = 7, 3H, CH_3), 1.58 (quint, J = 7, 2H, $\underline{CH_2}CH_3$), 3.42 (t, J = 7, 3H, CH_2N), 6.99-7.40 (m, 5H, 4Ar + CH=), 7.70 (d, J_{trans} = 14.4, 1H, CH=), 7.99 (s, 1H, H-3), 8.76 (s, 1H, H-6).

IR (KBr): cm^{-1} 3216 (NH), 1662 (C=C).

N-(4-chlorobenzyl)-1-(4-chlorostyryl)-1H-pyrazolo[3,4-d]pyrimidin-4-amine 137b.

Yield: 0.21 g, 58%

Mp: 238-240 °C

MW = 369.27

Anal. calcd for $C_{20}H_{15}N_5Cl_2$, C 60.62, H 3.82, N 17.67, found C 60.54, H 4.10, N 17.39. ^{1}H NMR ($CDCl_3$): δ 4.65-4.80 (m, 2H, CH_2Ar), 7.16-7.40 (m, 9H, 8Ar + CH=), 7.69 (d, J_{trans} = 14.3, 1H, CH=) 7.78 (s, 1H, H-3), 8.30 (s, 1H, H-6).

IR (KBr): cm^{-1} 3203 (NH), 1658 (C=C).

1-(4-Bromostyryl)-N-(3-chlorobenzyl)-1H-pyrazolo[3,4-d]pyrimidin-4-amine 137c.

Yield: 0.22 g, 51%

Mp: 222-223 °C

MW = 440.72

Anal. calcd for $C_{20}H_{15}N_5ClBr$, C 54.50, H 3.43, N 15.89, found C 54.39, H 3.65, N 15.73. ^{1}H NMR ($CDCl_3$): δ 4.60-4.67 (m, 2H, CH_2Ar), 7.20-7.43 (m, 9H, 8Ar + CH=), 7.70 (m, 1H, CH=) 7.81 (s, 1H, H-3), 8.31 (s, 1H, H-6).

IR (KBr): cm^{-1} 3234 (NH), 1659 (C=C).

Synthesis of 1-(2-hydroxy-2-phenylethyl)-6-(methylthio)-1*H*-pyrazolo[3,4-*d*]pyrimidin-4(5*H*)-one 143.

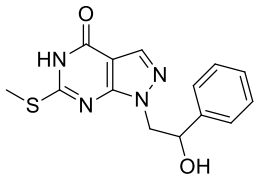

143

A solution of **83c** (10 mmol) and methyl iodide (7.10 g, 50 mmol) in anhydrous THF (20 mL) was refluxed for 12 h. After cooling at room temperature, the solvent was removed under reduced pressure. $CHCl_3$ was added and the precipitated solid was filtered and recrystallization from absolute EtOH.

Yield: 2.17 g, 72%

Mp: 207-209 °C

MW = 302.35

Anal. calcd for $C_{14}H_{14}N_4O_2S$, C 55.61, H 4.67, N 18.53, S 10.61, found C 55.46, H 4.34, N 18.71, S 10.31.

^{1}H NMR ($CDCl_3$): δ 2.52 (s, 3H, SCH_3), 4.27-4.50 (m, 2H, CH_2N), 5.04-5.18 (m, 1H, CHO), 5.68 (d, 1H, OH), 7.20-7.42 (m, 5H Ar), 7.97 (s, 1H, H-3).

IR (KBr): cm^{-1} 3544 (NH), 1678 (C=O).

Synthesis of 4-chloro-1-(2-chloro-2-phenylethyl)-6-(methylthio)-1*H*-pyrazolo[3,4-*d*]pyrimidine 144.

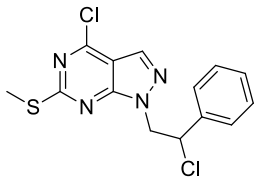

144

The Vilsmeier complex, previously prepared from $POCl_3$ (6.13 g, 40 mmol) and anhydrous DMF (2.92 g, 40 mmol) was added to a suspension of **143** (3.02 g, 10 mmol) in $CHCl_3$ (20 mL). The mixture was refluxed for 8 h. The solution was washed with water (2 x 20 mL), dried

($MgSO_4$), filtered, and concentrated under reduced pressure. The crude oil was purified by column chromatography (Silica gel 0.06-0200 mm, 40 Å), using a mixture of Et_2O/PE (bp 40-60 °C) (1:1) as the eluant to afford the pure product **144**.

Yield: 2.2 g, 65%

Mp: 95-96 °C

MW = 339.24

Anal. calcd for $C_{14}H_{12}N_4SCl_2$, C 49.57, H 3.57, N 16.52, S 9.45, found C 49.92, H 3.44, N 16.89, S 9.40.

^{1}H NMR ($CDCl_3$): δ (s, 3H, CH_3S), 4.77-5.05 (m, 2H, CH_2N), 5.45-5.56 (m, 1H, CHCl), 7.29-7.46 (m, 5H Ar), 8.02 (s, 1H, H-3).

Synthesis of 1-(2-chloro-2-phenylethyl)-6-(methylthio)-4-morpholin-4-yl-1*H*-pyrazolo[3,4-*d*]pyrimidine 145.

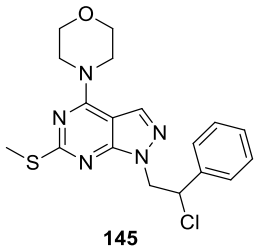

145

To a solution of **144** (3.39 g, 10 mmol) in anhydrous toluene (20 mL), morpholine (3.48 g, 40 mmol) was added and the reaction mixture was stirred at room temperature for 24 h. The mixture was washed with water, the organic phase was dried ($MgSO_4$) and evaporated under reduced pressure; the residue oil crystallized by adding PE (bp 40-60 °C) (10 mL), to give the desired products.

Yield: 2.92 g, 75%

Mp: 116-117 °C

MW = 389.90

Anal. calcd for $C_{18}H_{20}N_5OSCl$, C 55.45, H 5.17, N 17.96, S 8.22, found C 55.48, H 5.32, N 18.19, S 8.09.

^{1}H NMR ($CDCl_3$): δ 2.57 (s, 3H, CH_3), 3.77-3.87 and 3.89-3.98 (2m, 8H, 4CH_2morph.), 4.71-4.98 (m, 2H, CH_2N), 5.51-5.61 (m, 1H, CHCl), 7.26-7.49 (m, 5H Ar), 7.82 (s, 1H, H-3).

Synthesis of 6-(methylthio)-4-morpholin-4-yl-1-(-2-phenylvinyl)-1*H*-pyrazolo[3,4-*d*]pyrimidine 146.

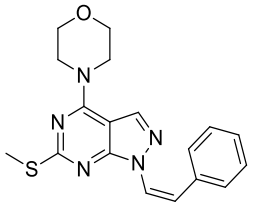

146

A solution of NaOH (300 mg, 7.5 mmol) in water (2.15 mL) was added to a suspension of **145** (390 mg, 1 mmol), in 96% EtOH (12 mL), and the mixture was refluxed for 5 h. After cooling, the white solid was filtered, washed with water, and recrystallized from absolute EtOH.

Yield: 0.26 g, 75%

Mp: 161-162 °C

MW = 353.44

Anal. calcd for $C_{18}H_{19}N_5OS$, C 61.17, H 5.42, N 19.81, S 9.07, found C 61.25, H 5.48, N 19.81, S 8.88.

^{1}H NMR ($CDCl_3$): δ 2.63 (s, 3H, CH_3S), 3.80-3.89 and 3.91-3.99 (2m, 8H, 4CH_2 morph.), 7.21-7.55 (m, 6H, 5H Ar + CH=), 7.95 (s, 1H, H-3), 8.01 (d, J_{trans} =14.6, 1H, CH=).

IR cm^{-1}: 1658 (C=C).

Synthesis of 6-(methylsulfonyl-4-morpholin-4-yl-1-(2-phenylvinyl)-1*H*-pyrazolo[3,4-*d*]pyrimidine 147.

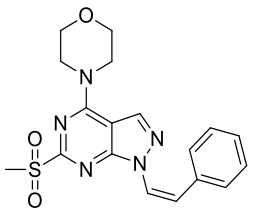

147

3-Chloroperoxybenzoic acid (2 mmol of 77% suspension in mineral oil) was added portion wise to a solution of **146** (350 mg, 1 mmol) in $CHCl_3$ (10 mL) at 0 °C. The mixture was stirred at room temperature for 6 h; the organic phase was washed with saturated $NaHCO_3$ solution (2 x 20 mL), then with water (20 mL), dried ($MgSO_4$), and evaporated under reduced pressure. The crude oil crystallized by adding a mixture of Et_2O/PE (bp 40-60 °C) (1:1).

Yield: 0.34 g, 87%

Mp: 215-216 °C (dec.)

MW = 385.44

Anal. calcd for $C_{18}H_{19}N_5O_3S$, C 56.09, H 4.97, N 18.17, S 8.32, found C 56.18, H 5.07, N 17.86, S 8.64.

^1H NMR ($CDCl_3$): 3.41 (s, 3H, SO_2CH_3), 3.86-3.97 and 4.02-4.16 (2m, 8H, $4CH_2$ morph.), 7.27-7.59 (m, 6H, 5Ar + CH=), 8.04 (d, J_{trans} = 14.4, 1H, CH=), 8.16 (s, 1H, H-3).

IR cm^{-1}: 1658 (C=C), 1315, 1128 (SO_2).

MS: *m/z* 385 $[M+1]^+$.

Synthesis of 2-{[4-morpholin-4-yl-1-(2-phenylvinyl)-1*H*-pyrazolo[3,4-*d*]pyrimidin-6-yl]amino} ethanol 137d.

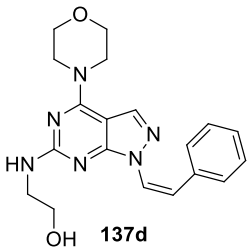

137d

2-Aminoethanol (180 mg, 3 mmol) was added to a suspension of **147** (385 mg, 1 mmol) in 1-butanol (16 mL) and DMSO (4 mL), and the mixture was heated at 90 °C for 12 h. After cooling, 1-butanol was removed under reduced pressure; then water was added, and the solution was extracted with AcOEt (2 x 20 mL); the organic phase was washed with water (20 mL), dried ($MgSO_4$), and evaporated under reduced pressure. The white solid was filtered and recrystallized from absolute EtOH.

Yield: 0.25 g, 68%

Mp: 177-178 °C

MW = 366.42

Anal. calcd for $C_{19}H_{22}N_6O_2$, C 62.28, H 6.05, N 22.94, found C 62.23, H 6.19, N 23.25. ^{1}H NMR ($CDCl_3$): δ 3.70 (q, J = 4.0, 2H, CH_2), 3.81-3.96 (m, 10H, 4CH_2 morph. + CH_2), 4.06 (br s, 1H, disappears with D_2O), 5.52 (br s, 1H, disappears with D_2O), 7.19-7.52 (m, 6H, 5H Ar + CH=), 7.87 (s, 1H, H-3), 7.88 (d, J_{trans} = 14.4, 1H, CH=).

IR cm^{-1}: 3250-3150 (OH + NH), 1656 (C=C).

MS: m/z 366 $[M+1]^+$.

Synthesis of 2-[4-amino-3-(phenylethynyl)-1*H*-pyrazolo[3,4-*d*]pyrimidin-1-yl]-1-phenylethanol 148.

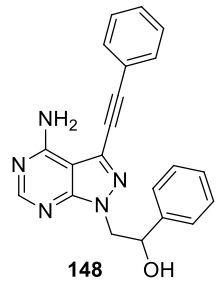

148

To a solution of **110** (100 mg, 0.26 mmol) in THF (5 mL), phenylacetylene (35 mg, 0.34 mmol) was added, then $Pd(PPh)_3Cl_2$ (9 mg, 0.0079 mmol), CuI (3 mg, 0.016 mmol) and Et_3N (50 mg, 0.52 mmol) were added and the mixture was refluxed for 14 h. The cooled mixture was filtered and the solution was evaporated under reduced pressure. The crude product was purified by column chromatography using AcOEt/n-hexane (8:2) as the eluent to afford the pure product **148**.

Yield: 42 mg, 45%

Mp: 188-190 °C

MW = 355.39

Anal. calcd for $C_{21}H_{17}N_5O$, C 70.97, H 4.82, N 19.71, found C 70.88, H 4.96, N 19.41. ^{1}H NMR ($(CD_3)_2SO$): δ 4.32-4.37 and 4.47-4.53 (2m, 2H, CH_2N), 5.61-5.62 (m, 1H, CHO), 6.22 (s all., 2H, NH_2), 7.23-7.74 (m, 10H Ar), 8.23 (s, 1H, H-6).

Synthesis of 1-(2-chloro-2-phenylethyl)-3-(phenylethynyl)-1*H*-pyrazolo[3,4-*d*]pyrimidin-4-amine 137e.

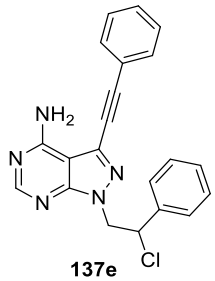

137e

$SOCl_2$ (150 µL, 2.01 mmol) was added dropwise to a solution of the intermediate **148** (150 mg, 0.40 mmol) in dry CH_2Cl_2 (5 mL), and the reaction was stirred at room temperature for 12 h under nitrogen atmosphere. Ice and 1 N NaOH were added with caution and the aqueous phase was extracted with CH_2Cl_2. Then the organic phase was washed with water, dried (Na_2SO_4) and concentrated under reduced pressure to give a white solid. The crude product was purified by column chromatography using CH_2Cl_2/CH_3OH (95:5) as the eluent to afford the pure product **137e**.

Yield: 69 mg, 43%

Mp: 186-187 °C

MW = 373.84

Anal. calcd for $C_{21}H_{16}N_5Cl$, C 67.47, H 4.31, N 18.73, found C 67.54, H 4.16, N 18.75. ^{1}H NMR ($(CD_3)_2SO$): δ 4.74-5.11 (m, 2H, CH_2N), 5.57-5.50 (m, 1H, CHCl), 6.82 (s all., 2H, NH_2), 7.39-7.77 (m, 10H Ar), 8.29 (s, 1H, H-6).

Synthesis of 3-(phenylethynyl)-1-(-2-phenylvinyl)-1*H*-pyrazolo[3,4-*d*]pyrimidin-4-amine 137f.

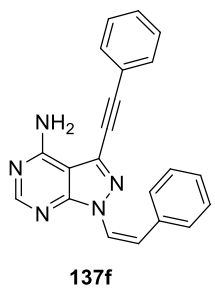

137f

A solution of NaOH (48 mg, 1.2 mmol) in water (360 µL) was added to a suspension of **137e** (60 mg, 0.16 mmol), in 96% EtOH (4 mL), and the mixture was refluxed for 5 h. After cooling, the white solid was filtered, washed with water, and recrystallized from absolute EtOH to obtain compound **137f**.

Yield: 22 mg, 35%

Mp: 245-252 °C

MW = 337.38

Anal. calcd for $C_{21}H_{15}N_5$, C 74.76, H 4.48, N 20.76, found C 74.57, H 4.23, N 20.93. ^{1}H NMR ($(CD_3)_2SO$): δ 7.16 (s all., 2H, NH_2), 7.33-7.82 (m, 10H Ar), 8.04-8.12 (m, 2H, CH=CH), 8.38 (s, 1H, H-6).

Synthesis of 1-(2-hydroxy-2-phenylethyl)-6-(isopropylthio)-1*H*-pyrazolo[3,4-*d*]pyrimidin-4(5*H*)-one 149a.

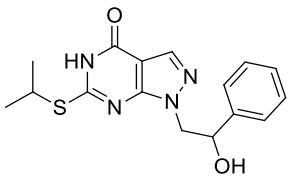

149a

A mixture of **83c** (2.88 g, 10 mmol), 2-bromopropane (1.25 g, 10.14 mmol) and anhydrous K_2CO_3 (1.38 g, 10 mmol) in anhydrous DMF (10 mL) was stirred at room temperature for 8 h. The mixture was poured in cold water; the white solid obtained was filtered, washed with water and recrystallized from absolute EtOH to afford **149a** as a white solid.

Yield: 1.22 g, 37%

Mp: 194-195 °C

MW= 330.41

Anal. calcd for $C_{16}H_{18}N_4O_2S$, C 58.16, H 5.49, N 16.96, S 9.70, found C 58.37, H 5.22, N 16.88, S 9.82.

^{1}H NMR ($(CD_3)_2SO$): δ 1.44 (d, J = 6.2, 6H, $2CH_3$), 3.90 (d, 1H, OH, disappears with D_2O),

3.98 (sept, J = 6.2, 1H, CHS), 4.38-4.48 and 4.50-4.58 (2m, 2H, CH_2N), 5.19-5.22 (m, 1H, CHOH), 7.24-7.37 (m, 5H Ar), 8.06 (s, 1H, H-3), 11.06 (br s, 1H, NH disappears with D_2O).
IR (KBr): cm^{-1} 3300-3100 (NH + OH), 1704 (CO).

Synthesis of 6-(cyclopentylthio)-1-(2-hydroxy-2-phenylethyl)-1*H*-pyrazolo[3,4-*d*]pyrimidin-4(5*H*)-one 149b.

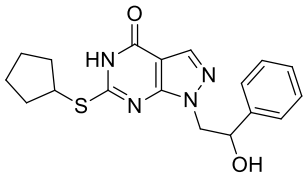

149b

A mixture of **83c** (2.88 g, 10 mmol), bromocyclopentane (1.5 g, 10.14 mmol) and anhydrous K_2CO_3 (1.38 g, 10 mmol) in anhydrous DMF (10 mL) was stirred at room temperature for 8 h. The mixture was poured into cold water, the white solid was filtered, washed with water, and recrystallized from absolute EtOH to afford **149b** as a white solid.

Yield: 1.96 g, 55%
Mp: 213-214 °C
MW = 356.44
Anal. calcd for $C_{18}H_{20}N_4O_2S$, C 60.65, H 5.66, N 15.72, S 9.00, found C 60.31, H 5.82, N 15.70, S 8.90.
^{1}H NMR ($(CD_3)_2SO$): δ 1.42-1.74 and 1.94-2.27 (2m, 8H, $4CH_2$ cyclopentyl) 3.76-3.97 (m, 1H, CHS), 4.17-4.42 (m, 2H, CH_2N), 4,92-5.12 (m, 1H, CHOH), 5.57 (d, 1H, OH disappears with D_2O), 7.03-7.28 (m, 5H, Ar), 7.87 (s, 1H, H-3), 12.19 (br s, 1H, NH disappears with D_2O).
IR (KBr): cm^{-1} 3150-2850 (NH+OH), 1703 (CO).

General procedure for the synthesis of compounds 150a,b.

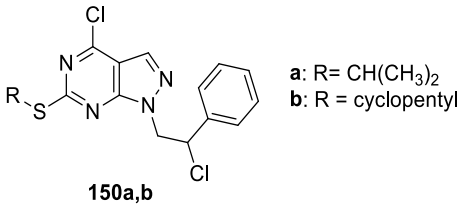

150a,b

The Vilsmeier complex, previously prepared from $POCl_3$ (1.22 g, 8 mmol) and anhydrous DMF (580 mg, 8 mmol) was added to a suspension of **149a,b** (1 mmol) in CH_2Cl_2 (10 mL). The mixture was refluxed for 6-8 h. The solution was washed with water (2 x 10 mL), dried ($MgSO_4$), filtered, and concentrated under reduced pressure. The crude oil was purified by column chromatography (Florisil, 100-200 mesh), using Et_2O as the eluent, to afford the pure products.

4-Chloro-1-(2-chloro-2-phenylethyl)-6-(isopropylthio)-1H-pyrazolo[3,4-d]pyrimidine 150a.

Yield: 0.27 g, 74%

Mp: 67-68 °C

MW = 367.29

Anal. calcd for $C_{16}H_{16}N_4Cl_2S$, C 52.32, H 4.39, N 15.25, S 8.73, found C 52.37, H 4.29, N 15.33, S 8.90.

^{1}H NMR ($(CD_3)_2SO$): δ 1.45 (d, J = 6.2, 3H, CH_3), 1.49 (d, J = 6.2, 3H, CH_3), 4.00 (sept, J = 6.2, 1H, CHS), 4.74-4.82 and 4.88-4.97 (2m, 2H, CH_2N), 5.45-5.55 (m, 1H, CHCl), 7.21-7.50 (m, 5H, Ar), 8.00 (s, 1H, H-3).

4-Chloro-1-(2-chloro-2-phenylethyl)-6-(cyclopentylthio)-1H-pyrazolo[3,4-d]pyrimidine 150b.

Yield: 0.25 g, 63%

Mp: 70-71 °C

MW = 393.33

Anal. calcd for $C_{18}H_{18}N_4Cl_2S$, C 54.96, H 4.61, N 14.24, S 8.15, found C 54.88, H 4.73, N

14.31, S 8.24.

^{1}H NMR ($(CD_3)_2SO$): δ 1.54-1.85 and 2.10-2.32 (2m, 8H, $4CH_2$ cyclopentyl), 3.93-4.07 (m, 1H, CHS), 4.67-4.80 and 4.82-4.97 (2m, 2H, CH_2N), 5.38-5.50 (m, 1H, CHCl), 7.19-7.42 (m, 5H, Ar), 7.94 (s, 1H, H-3).

General procedure for the synthesis of compounds 137g,h.

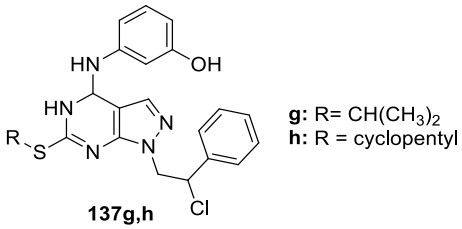

137g,h

The 3-aminophenol (545 mg, 5 mmol) was added to a solution of the suitable 4-chloro derivative **150a,b** (1 mmol) in absolute EtOH (10 mL), and the mixture was refluxed for 3-5 h. After cooling to room temperature, the solvent was evaporated under reduced pressure and the crude was solved in AcOEt (10 mL), washed with 0.1 N HCl solution (2 x 10 mL), 1 N NaOH solution (10 mL) and saturated NaCl solution (2 x 10 mL), dried ($MgSO_4$), filtered, and concentrated under reduced pressure to give a brown oil which crystallized at 4 °C by adding a 1:1 mixture of Et_2O/PE (bp 40−60 °C). The solid obtained was purified by column chromatography (Silica gel 0.06-0200 mm, 40 Å) using CH_2Cl_2 as the eluent.

3-((1-(2-Chloro-2-phenylethyl)-6-(isopropylthio)-4,5-dihydro-1H-pyrazolo[3,4-d]pyrimidin-4-yl)amino)phenol 137g.

Yield: 339 mg, 77%

Mp: 198-199 °C.

MW = 439.96

Anal. calcd for $C_{22}H_{22}N_5OClS$, C 60.06, H 5.04, N 15.92, S 7.29, found C 60.17, H 4.94, N 16.21, S 7.38.

^{1}H NMR ($(CD_3)_2SO$): δ 1.46 (d, J = 6.0 Hz, 3H, CH_3), 1.49 (d, J = 6.0 Hz, 3H, CH_3), 3.97-4.07 (m, 1H, SCH), 4.70-4.75 and 4.83-4.88 (2m, 2H, CH_2N) 5.48-5.51 (m, 1H, CHCl), 6.78-6.80,

6.94-7.02 and 7.21-7.41 (3m, 10H, 9 Ar + H-3).
IR (KBr): cm^{-1} 3300-3100 (NH + OH).
MS: m/z 441 $[M + 1]^+$.

3-((1-(2-Chloro-2-phenylethyl)-6-(cyclopentylthio)-4,5-dihydro-1H-pyrazolo[3,4-d]pyrimidin-4-yl)amino)phenol 137h.

Yield: 359 mg, 77%
Mp: 160-161 °C
MW = 466.00
Anal. calcd for $C_{24}H_{24}N_5OClS$, C 61.86, H 5.19, N 15.03, S 6.88, found C 61.95, H 4.97, N 15.18, S 7.01.
^1H NMR ($(CD_3)_2SO$): δ 1.62-2.24 (m, 8H, $4CH_2$ cyclopent), 4.03-4.22 (m, 1H, SCH), 4.75-4.95 (m, 2H, CH_2N), 5.45-5.56 (m, 1H, CHCl), 6.80-7.60 (m, 9H Ar), 8.06 (s, 1H H-3), 10.20 (br s, 1H, disappears with D_2O).
IR (KBr): cm^{-1} 3500-3000 (NH + OH).
MS: m/z 467 $[M + 1]^+$.

Synthesis of ethyl 5-amino-1-(2-phenylpropyl)-1*H*-pyrazole-4-carboxylate 152.

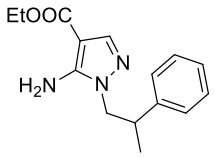

152

A solution of (2-phenylpropyl)hydrazine **151** (1.50 g, 10 mmol) and ethyl(ethoxymethylene)cyanoacetate (1.69 g, 10 mmol) in absolute EtOH was refluxed for 5 h. The solvent was evaporated under reduced pressure and the crude was purified by column chromatography (Florisil 100-200 mesh) using Et_2O as the eluent, to afford the pure product **152** as a yellow oil.

Yield: 1.65 g, 60%

Mp: 85-86 °C

MW = 273.33

Anal. calcd for $C_{15}H_{19}N_3O_2$, C 65.91, H 7.01, N 15.37, found C 65.90, H 6.99, N 15.25.

^{1}H NMR ($CDCl_3$): δ 1.06-1.20 (m, 6H, $2CH_3$), 3.24-3.26 (m, 1H, $CHCH_3$), 3.78-3.83 and 3.89-3.91 (2m, 2H, CH_2N), 4.10 (q, J = 7.0, 2H, CH_2O), 4.79 (br s, 2H, NH_2 disappears with D_2O), 7.00-7.16 (m, 5H Ar), 7.55 (s, 1H, H-3).

IR (KBr): cm^{-1} 3398, 3291 (NH_2), 1681 (CO).

MS: m/z 273 $[M+1]^+$.

Synthesis of ethyl-5-{[(benzoylamino)carbonothioyl]amino}-1-(2-phenylpropyl)-1*H*-pyrazole-4-carboxylate 153.

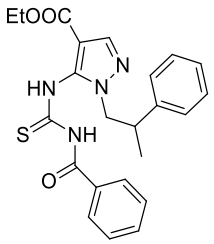

153

A suspension of **152** (2.73 g, 10 mmol) and benzoyl isothiocyanate (1.7 g, 11 mmol) in anhydrous THF (20mL) was refluxed for 12 h. The solvent was evaporated under reduced pressure, and the crude was crystallized as a white solid by adding Et_2O (30 mL).

Yield: 2.75 g, 73%

Mp: 112-113 °C

MW = 436.53

Anal. calcd for $C_{23}H_{24}N_4O_3S$, C 63.28, H 5.54, N 12.83, S 7.35, found C 63.35, H 5.48, N 12.86, S 7.51.

^{1}H NMR ($CDCl_3$): δ 1.21-1.29 (m, 6H, $2CH_3$), 3.43-3.49 (m, 1H, $CHCH_3$), 4.17-4.22 (m, 4H, CH_2N + CH_2O), 7.07-7.89 (m 10H Ar), 7.93 (s, 1H, H-3), 9.19 (br s, 1H, NH disappears with D_2O), 11.60 (br s, 1H, NH disappears with D_2O).

IR (KBr): cm^{-1} 3384, 3129 (NH), 1696 (COOEt), 1666 (CONH).

MS: m/z 437 $[M+1]^+$.

Synthesis of 1-(2-phenylpropyl)-6-thioxo-1,5,6,7-tetrahydro-pyrazolo[3,4-*d*]pyrimidin-4-one 154.

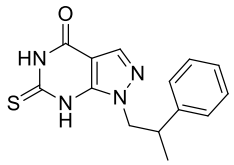

154

A solution of **153** (4.38 g, 10 mmol) in 2 M NaOH (40 mL) was boiled for 10 min and successively diluted with water (40 mL). The solution was acidified with glacial acetic acid. After 12 h of standing in a refrigerator, the crystallized solid was filtered and recrystallized from absolute EtOH to give a white solid.

Yield: 1.72 g, 60%

Mp: 192-193 °C (dec)

MW = 286.35

Anal. calcd for $C_{14}H_{14}N_4OS$, C 58.72, H 4.93, N 19.57, S 11.20, found C 58.83, H 4.98, N 19.78, S 11.45.

^{1}H NMR ($CDCl_3$): δ 1.22-1.60 (m, 3H, CH_3), 3.36-3.42 (m, 1H, $CHCH_3$), 4.26-4.32 and 4.45-4.51 (2m, 2H, CH_2N), 7.12-7.31 (m 5H Ar), 7.82 (s, 1H, H-3), 10.49 (br s, 1H disappears with D_2O).

IR (KBr): cm^{-1} 3455-2867 (NH + OH), 1677 (CO).

MS: m/z 286 $[M+1]^+$.

Synthesis of 6-(ethylthio)-1-(2-phenylpropyl)-1,5-dihydro-4*H*pyrazolo[3,4-*d*]pyrimidin-4-one 155.

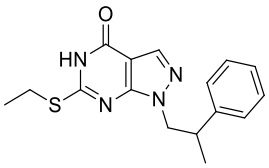

155

A mixture of **154** (286 mg, 1 mmol), iodoethane (172 mg, 1.1 mmol), and K_2CO_3 (138 mg, 1 mmol) in anhydrous DMF (2 mL) was stirred at room temperature for 20 h. The mixture was poured into cold water (50 mL). The obtained solid was filtered, washed with water, and recrystallized from absolute EtOH.

Yield: 192 mg, 61%
Mp: 155-156 °C
MW = 314.41
Anal. calcd for $C_{16}H_{18}N_4OS$, C 61.12, H 5.77, N 17.82, S 10.20, found C 61.09, H 5.77, N 17.86, S 10.10.
^{1}H NMR ($CDCl_3$): δ 1.22 (d, *J* = 7.0 Hz, 3H, CH_3CH), 1.36 (t, *J* = 7.2, 3H, SCH_2CH_3), 3.17 (q, *J* = 7.2 Hz, 2H, SCH_2), 3.40-3.50 (m, 1H, $CHCH_3$), 4.26-4.50 (m, 2H, CH_2N), 7.07-7.30 (m, 5H Ar), 7.94 (s, 1H, H-3), 12.10 (br s, 1H, NH disappears with D_2O).
IR (KBr): cm^{-1} 3110-2800 (NH), 1681 (CO).
MS: m/z 315 $[M + 1]^+$.

Synthesis of 4-chloro-6-(ethylthio)-1-(2-phenylpropyl)-1*H*-pyrazolo[3,4-*d*]-pyrimidine 156.

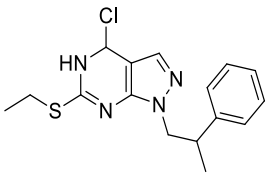

156

The Vilsmeier complex, previously prepared from $POCl_3$ (0.74 mL, 8 mmol) and anhydrous DMF (590 mg, 8 mmol) was added to a suspension of **155** (300 mg, 1 mmol) in CH_2Cl_2 (10 mL). The mixture was refluxed for 6 h. The solution was washed with water (2 x 10 mL), dried ($MgSO_4$), filtered, and concentrated under reduced pressure. The crude oil was purified by column chromatography (Florisil, 100-200 mesh), using Et_2O as the eluent, to afford the pure product.

Yield: 300 mg, 90%
Mp: 161-163 °C

MW = 332.85

Anal. calcd for $C_{16}H_{17}N_4ClS$, C 57.73, H 5.15, N 16.83, S 9.63, found C 57.67, H 5.00, N 16.77, S 9.55.

^{1}H NMR ($CDCl_3$): δ 1.31 (d, *J* = 7.2 Hz, 3H, CH_3CH), 1.47 (t, *J* = 7.4 Hz, 3H, SCH_2CH_3), 3.21 (q, *J* = 7.4 Hz, 2H, SCH_2), 3.48-3.63 (m, 1H, $CHCH_3$), 4.42-4.66 (m, 2H, CH_2N), 7.12-7.31 (m, 5H Ar), 8.01 (s, 1H, H-3).

MS: m/z 334 $[M + 1]^+$.

Synthesis of 3-{[6-(ethylthio)-1-(2-phenylpropyl)-1*H*-pyrazolo[3,4-*d*]-pyrimidin-4-yl]amino}phenol 137i.

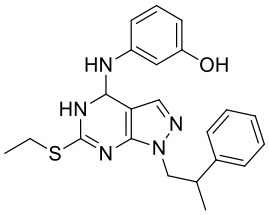

137i

The 3-aminophenol (545 mg, 5 mmol) was added to a solution of **156** (330 mg, 1 mmol) in absolute EtOH (10 mL), and the mixture was refluxed for 3-5 h. After cooling to room temperature, the solvent was evaporated under reduced pressure and the crude was solved in AcOEt (10 mL), washed with 0.1 N HCl solution (2 x 10 mL), 1 N NaOH solution (10 mL) and saturated NaCl solution (2 x 10 mL), dried ($MgSO_4$), filtered, and concentrated under reduced pressure to give a brown oil which crystallized at 4 °C by adding a 1:1 mixture of Et_2O/PE (bp 40−60 °C). The solid obtained was purified by column chromatography (Silica gel 0.06-0200 mm, 40 Å) using CH_2Cl_2 as the eluent.

Yield: 296 mg, 73%

Mp: 184-186 °C

MW = 405.52

Anal. calcd for $C_{22}H_{23}N_5OS$, C 65.16, H 5.72, N 17.27, S 7.91, found C 65.35, H 5.69, N 17.11, S 7.67.

^{1}H NMR ($CDCl_3$): δ 1.22 (d, *J* = 6.8 Hz, 3H, CH_3CH), 1.44 (t, *J* = 7.6 Hz, 3H, SCH_2CH_3), 3.19 (q, *J* = 7.6 Hz, 2H, SCH_2), 3.46-3.52 (m, 1H, $CHCH_3$), 4.36-4.89 (m, 2H, CH_2N), 6.82-6.84,

6.93-6.95, 6.99-7.05 and 7.16-7.24 (4m, 10H, 9 Ar + H-3).

IR (KBr): cm^{-1} 3200-2900 (NH + OH).

MS: m/z 407 $[M + 1]^+$.

BIBLIOGRAPHY

(1) Adams, J. A. Kinetic and Catalytic Mechanisms of Protein Kinases. *Chem. Rev.* **2001**, *101*, 2271–2290.

(2) Manning, G.; Whyte, D. B.; Martinez, R.; Hunter, T.; Sudarsanam, S. The Protein Kinase Complement of the Human Genome. *Science* **2002**, *298*, 1912–1934.

(3) Krebs, E. G. Nobel Lecture. Protein Phosphorylation and Cellular Regulation I. *Biosci. Rep.* **1993**, *13*, 127–142.

(4) Taylor, S. S.; Kornev, A. P. Protein Kinases: Evolution of Dynamic Regulatory Proteins. *Trends Biochem. Sci.* **2011**, *36*, 65–77.

(5) Manning, B. D. Challenges and Opportunities in Defining the Essential Cancer Kinome. *Sci. Signal.* **2009**, *2*, 15.

(6) Wu, P.; Nielsen, T. E.; Clausen, M. H. FDA-Approved Small-Molecule Kinase Inhibitors. *Trends Pharmacol. Sci.* **2015**, *36*, 422–439.

(7) Wu, P.; Nielsen, T. E.; Clausen, M. H. Small-Molecule Kinase Inhibitors: An Analysis of FDA-Approved Drugs. *Drug Discov. Today* **2016**, *21*, 5–10.

(8) Hanks, S. K.; Quinn, A. M. Protein Kinase Catalytic Domain Sequence Database: Identification of Conserved Features of Primary Structure and Classification of Family Members. *Methods Enzymol.* **1991**, *200*, 38–62.

(9) Cowan-Jacob, S. W. Structural Biology of Protein Tyrosine Kinases. *Cell. Mol. Life Sci.* **2006**, *63*, 2608–2625.

(10) Hubbard, S. R.; Till, J. H. Protein Tyrosine Kinase Structure and Function. *Annu. Rev. Biochem.* **2000**, *69*, 373–398.

(11) Weinstein, I. B.; Joe, A. Oncogene Addiction. *Cancer Res.* **2008**, *68*, 3077–3080.

(12) Schlessinger, J.; Ullrich, A. Growth Factor Signaling by Receptor Tyrosine Kinases. *Neuron* **1992**, *9*, 383–391.

(13) Yarden, Y.; Ullrich, A. Growth Factor Receptor Tyrosine Kinases. *Annu. Rev. Biochem.* **1988**, *57*, 443–478.

(14) Tsygankov, A. Y. Non-Receptor Protein Tyrosine Kinases. *Front. Biosci. A J. Virtual Libr.* **2003**, *8*, 595-635.

(15) Edelman, A. M.; Blumenthal, D. K.; Krebs, E. G. Protein Serine/threonine Kinases. *Annu. Rev. Biochem.* **1987**, *56*, 567–613.

(16) Capra, M.; Nuciforo, P. G.; Confalonieri, S.; Quarto, M.; Bianchi, M.; Nebuloni, M.; Boldorini, R.; Pallotti, F.; Viale, G.; Gishizky, M. L.; *et al*. Frequent Alterations in the Expression of Serine/threonine Kinases in Human Cancers. *Cancer Res.* **2006**, *66*, 8147–8154.

(17) Hunter, T. Signaling--2000 and Beyond. *Cell* **2000**, *100*, 113–127.

(18) Josso, N.; di Clemente, N. Serine/threonine Kinase Receptors and Ligands. *Curr. Opin. Genet. Dev.* **1997**, *7*, 371–377.

(19) Ingley, E. Src Family Kinases: Regulation of Their Activities, Levels and Identification of New Pathways. *Biochim. Biophys. Acta* **2008**, *1784*, 56–65.

(20) Boggon, T. J.; Eck, M. J. Structure and Regulation of Src Family Kinases. *Oncogene* **2004**, *23*, 7918–7927.

(21) Roskoski, R. J. Src Protein-Tyrosine Kinase Structure, Mechanism, and Small Molecule Inhibitors. *Pharmacol. Res.* **2015**, *94*, 9–25.

(22) Resh, M. D. Fatty Acylation of Proteins: New Insights into Membrane Targeting of Myristoylated and Palmitoylated Proteins. *Biochim. Biophys. Acta* **1999**, *1451*, 1–16.

(23) Gil-Henn, H.; Elson, A. Tyrosine Phosphatase-Epsilon Activates Src and Supports the Transformed Phenotype of Neu-Induced Mammary Tumor Cells. *J. Biol. Chem.* **2003**, *278*, 15579–15586.

(24) Finn, R. S. Targeting Src in Breast Cancer. *Ann. Oncol.* **2008**, *19*, 1379–1386.

(25) Guarino, M. Src Signaling in Cancer Invasion. *J. Cell. Physiol.* **2010**, *223*, 14–26.

(26) Warmuth, M.; Damoiseaux, R.; Liu, Y.; Fabbro, D.; Gray, N. SRC Family Kinases: Potential Targets for the Treatment of Human Cancer and Leukemia. *Curr. Pharm. Des.* **2003**, *9*, 2043–2059.

(27) Hanahan, D.; Weinberg, R. A. The Hallmarks of Cancer. *Cell* **2000**, *100*, 57–70.

(28) Martin, G. S. The Road to Src. *Oncogene* **2004**, *23*, 7910–7917.

(29) Irby, R. B.; Mao, W.; Coppola, D.; Kang, J.; Loubeau, J. M.; Trudeau, W.; Karl, R.; Fujita, D. J.; Jove, R.; Yeatman, T. J. Activating SRC Mutation in a Subset of Advanced Human Colon Cancers. *Nat. Genet.* **1999**, *21*, 187–190.

(30) Irby, R. B.; Yeatman, T. J. Role of Src Expression and Activation in Human Cancer. *Oncogene* **2000**, *19*, 5636–5642.

(31) Louis, D. N.; Ohgaki, H.; Wiestler, O. D.; Cavenee, W. K.; Burger, P. C.; Jouvet, A.; Scheithauer, B. W.; Kleihues, P. The 2007 WHO Classification of Tumours of the

Central Nervous System. *Acta Neuropathol*. **2007**, *114*, 97–109.

(32) Luo, J. W.; Wang, X.; Yang, Y.; Mao, Q. Role of Micro-RNA (miRNA) in Pathogenesis of Glioblastoma. *Eur. Rev. Med. Pharmacol. Sci.* **2015**, *19*, 1630–1639.

(33) Omuro, A.; DeAngelis, L. M. Glioblastoma and Other Malignant Gliomas: A Clinical Review. *JAMA* **2013**, *310*, 1842–1850.

(34) Wick, W.; Weller, M.; Weiler, M.; Batchelor, T.; Yung, A. W. K.; Platten, M. Pathway Inhibition: Emerging Molecular Targets for Treating Glioblastoma. *Neuro. Oncol.* **2011**, *13*, 566–579.

(35) Alifieris, C.; Trafalis, D. T. Glioblastoma Multiforme: Pathogenesis and Treatment. *Pharmacol. Ther.* **2015**, *152*, 63–82.

(36) Ahluwalia, M. S.; de Groot, J.; Liu, W. M.; Gladson, C. L. Targeting SRC in Glioblastoma Tumors and Brain Metastases: Rationale and Preclinical Studies. *Cancer Lett.* **2010**, *298*, 139–149.

(37) Du, J.; Bernasconi, P.; Clauser, K. R.; Mani, D. R.; Finn, S. P.; Beroukhim, R.; Burns, M.; Julian, B.; Peng, X. P.; Hieronymus, H.; *et al*. Bead-Based Profiling of Tyrosine Kinase Phosphorylation Identifies SRC as a Potential Target for Glioblastoma Therapy. *Nat. Biotechnol.* **2009**, *27*, 77–83.

(38) Parsons, S. J.; Parsons, J. T. Src Family Kinases, Key Regulators of Signal Transduction. *Oncogene* **2004**, *23*.

(39) Couto, M.; García, M. F.; Alamón, C.; Cabrera, M.; Cabral, P.; Merlino, A.; Teixidor, F.; Cerecetto, H.; Viñas, C. Discovery of Potent EGFR Inhibitors through the Incorporation of a 3D-Aromatic-Boron-Rich-Cluster into the 4-Anilinoquinazoline Scaffold: Potential Drugs for Glioma Treatment. *Chem. - A Eur. J.* **2017**.

(40) Yamaguchi, K.; Kugimiya, T.; Miyazaki, T. Substance P Receptor in U373 MG Human Astrocytoma Cells Activates Mitogen-Activated Protein Kinases ERK1/2 through Src. *Brain Tumor Pathol.* **2005**, *22*, 1–8.

(41) Ding, Q.; Stewart, J. J.; Olman, M. A.; Klobe, M. R.; Gladson, C. L. The Pattern of Enhancement of Src Kinase Activity on Platelet-Derived Growth Factor Stimulation of Glioblastoma Cells Is Affected by the Integrin Engaged. *J. Biol. Chem.* **2003**, *278*, 39882–39891.

(42) Vignaroli, G.; Iovenitti, G.; Zamperini, C.; Coniglio, F.; Calandro, P.; Molinari, A.; Fallacara, A. L.; Sartucci, A.; Calgani, A.; Colecchia, D.; *et al*. Prodrugs of Pyrazolo[3,4-

d]pyrimidines: From Library Synthesis to Evaluation as Potential Anticancer Agents in an Orthotopic Glioblastoma Model. *J. Med. Chem.* **2017**, *60*, 6305–6320.

(43) Maris, J. M.; Hogarty, M. D.; Bagatell, R.; Cohn, S. L. Neuroblastoma. *Lancet* **2007**, *369*, 2106–2120.

(44) Brodeur, G. M.; Nakagawara, A. Molecular Basis of Clinical Heterogeneity in Neuroblastoma. *Am. J. Pediatr. Hematol. Oncol.* **1992**, *14*, 111–116.

(45) Mullassery, D.; Losty, P. D. Neuroblastoma. *Paediatr. Child Health* **2016**, *26*, 68–72.

(46) Bolen, J. B.; Rosen, N.; Israel, M. A. Increased pp60c-Src Tyrosyl Kinase Activity in Human Neuroblastomas Is Associated with Amino-Terminal Tyrosine Phosphorylation of the Src Gene Product. *Proc. Natl. Acad. Sci. U. S. A.* **1985**, *82*, 7275–7279.

(47) Kratimenos, P.; Koutroulis, I.; Syriopoulou, V.; Michailidi, C.; Delivoria-Papadopoulos, M.; Klijanienko, J.; Theocharis, S. FAK-Src-Paxillin System Expression and Disease Outcome in Human Neuroblastoma. *Pediatr. Hematol. Oncol.* **2017**, *34*, 221–230.

(48) Tintori, C.; Fallacara, A. L.; Radi, M.; Zamperini, C.; Dreassi, E.; Crespan, E.; Maga, G.; Schenone, S.; Musumeci, F.; Brullo, C.; *et al*. Combining X-Ray Crystallography and Molecular Modeling toward the Optimization of Pyrazolo[3,4-*d*]pyrimidines as Potent c-Src Inhibitors Active *in Vivo* against Neuroblastoma. *J. Med. Chem.* **2015**, *58*, 347–361.

(49) Kratimenos, P.; Koutroulis, I.; Marconi, D.; Syriopoulou, V.; Delivoria-Papadopoulos, M.; Chrousos, G. P.; Theocharis, S. Multi-Targeted Molecular Therapeutic Approach in Aggressive Neuroblastoma: The Effect of Focal Adhesion Kinase-Src-Paxillin System. *Expert Opin. Ther. Targets* **2014**, *18*, 1395–1406.

(50) Rossi, A.; Caracciolo, V.; Russo, G.; Reiss, K.; Giordano, A. Medulloblastoma: From Molecular Pathology to Therapy. *Clin. Cancer Res.* **2008**, *14*, 971–976.

(51) Kumar, V.; Kumar, V.; McGuire, T.; Coulter, D. W.; Sharp, J. G.; Mahato, R. I. Challenges and Recent Advances in Medulloblastoma Therapy. *Trends Pharmacol. Sci.* **2017**, *38*, 1061–1084.

(52) Packer, R. J.; Gajjar, A.; Vezina, G.; Rorke-Adams, L.; Burger, P. C.; Robertson, P. L.; Bayer, L.; LaFond, D.; Donahue, B. R.; Marymont, M. H.; *et al*. Phase III Study of Craniospinal Radiation Therapy Followed by Adjuvant Chemotherapy for Newly Diagnosed Average-Risk Medulloblastoma. *J. Clin. Oncol.* **2006**, *24*, 4202–4208.

(53) Gajjar, A.; Chintagumpala, M.; Ashley, D.; Kellie, S.; Kun, L. E.; Merchant, T. E.; Woo,

S.; Wheeler, G.; Ahern, V.; Krasin, M. J.; *et al*. Risk-Adapted Craniospinal Radiotherapy Followed by High-Dose Chemotherapy and Stem-Cell Rescue in Children with Newly Diagnosed Medulloblastoma (St Jude Medulloblastoma-96): Long-Term Results from a Prospective, Multicentre Trial. *Lancet. Oncol.* **2006**, *7*, 813–820.

(54) Nieder, C.; Mehta, M. P.; Jalali, R. Combined Radio- and Chemotherapy of Brain Tumours in Adult Patients. *Clin. Oncol. (R. Coll. Radiol).* **2009**, *21*, 515–524.

(55) Sikkema, A. H.; Diks, S. H.; den Dunnen, W. F. A.; ter Elst, A.; Scherpen, F. J. G.; Hoving, E. W.; Ruijtenbeek, R.; Boender, P. J.; de Wijn, R.; Kamps, W. A.; *et al.* Kinome Profiling in Pediatric Brain Tumors as a New Approach for Target Discovery. *Cancer Res.* **2009**, *69*, 5987–5995.

(56) Rossi, A.; Schenone, S.; Angelucci, A.; Cozzi, M.; Caracciolo, V.; Pentimalli, F.; Puca, A.; Pucci, B.; La Montagna, R.; Bologna, M.; *et al*. New Pyrazolo[3,4-*d*]pyrimidine Derivative Src Kinase Inhibitors Lead to Cell Cycle Arrest and Tumor Growth Reduction of Human Medulloblastoma Cells. *FASEB J.* **2010**, *24*, 2881–2892.

(57) Cancer Incidence in Five Continents. Volume VIII., *IARC Sci. Publ.* **2002**, *155*, 1–781.

(58) Labianca, R.; Beretta, G. D.; Kildani, B.; Milesi, L.; Merlin, F.; Mosconi, S.; Pessi, M. A.; Prochilo, T.; Quadri, A.; Gatta, G.; *et al*. Colon Cancer. *Crit. Rev. Oncol. Hematol.* **2010**, *74*, 106–133.

(59) Chen, J.; Elfiky, A.; Han, M.; Chen, C.; Saif, M. W. The Role of Src in Colon Cancer and Its Therapeutic Implications. *Clin. Colorectal Cancer* **2014**, *13*, 5–13.

(60) Martinez-Perez, J.; Lopez-Calderero, I.; Saez, C.; Benavent, M.; Limon, M. L.; Gonzalez-Exposito, R.; Soldevilla, B.; Riesco-Martinez, M. C.; Salamanca, J.; Carnero, A.; *et al*. Prognostic Relevance of Src Activation in Stage II-III Colon Cancer. *Hum. Pathol.* **2017**, *67*, 119–125.

(61) Malek, R. L.; Irby, R. B.; Guo, Q. M.; Lee, K.; Wong, S.; He, M.; Tsai, J.; Frank, B.; Liu, E. T.; Quackenbush, J.; *et al*. Identification of Src Transformation Fingerprint in Human Colon Cancer. *Oncogene* **2002**, *21*, 7256–7265.

(62) Laghi, L.; Bianchi, P.; Orbetegli, O.; Gennari, L.; Roncalli, M.; Malesci, A. Lack of Mutation at Codon 531 of SRC in Advanced Colorectal Cancers from Italian Patients. *Br. J. Cancer*. **2001**, *84*, 196–198.

(63) Sirvent, A.; Bénistant, C.; Pannequin, J.; Veracini, L.; Simon, V.; Bourgaux, J.-F.; Hollande, F.; Cruzalegui, F.; Roche, S. Src Family Tyrosine Kinases-Driven Colon

Cancer Cell Invasion Is Induced by Csk Membrane Delocalization. *Oncogene* **2010**, *29*, 1303–1315.

(64) Yeatman, T. J. A Renaissance for SRC. *Nat. Rev. Cancer* **2004**, *4*, 470–480.

(65) Song, N.; Qu, X.; Liu, S.; Zhang, S.; Liu, J.; Qu, J.; Zheng, H.; Liu, Y.; Che, X. Dual Inhibition of MET and SRC Kinase Activity as a Combined Targeting Strategy for Colon Cancer. *Exp. Ther. Med.* **2017**, *14*, 1357–1366.

(66) Verbeek, B. S.; Vroom, T. M.; Adriaansen-Slot, S. S.; Ottenhoff-Kalff, A. E.; Geertzema, J. G.; Hennipman, A.; Rijksen, G. C-Src Protein Expression Is Increased in Human Breast Cancer. An Immunohistochemical and Biochemical Analysis. *J. Pathol.* **1996**, *180*, 383–388.

(67) Elsberger, B. Translational Evidence on the Role of Src Kinase and Activated Src Kinase in Invasive Breast Cancer. *Crit. Rev. Oncol. Hematol.* **2014**, *89*, 343–351.

(68) Nicholson, R. I.; Gee, J. M.; Harper, M. E. EGFR and Cancer Prognosis. *Eur. J. Cancer* **2001**, *37*, 9-15.

(69) Biscardi, J. S.; Ishizawar, R. C.; Silva, C. M.; Parsons, S. J. Tyrosine Kinase Signalling in Breast Cancer: Epidermal Growth Factor Receptor and c-Src Interactions in Breast Cancer. *Breast Cancer Res*. **2000**, *2*, 203–210.

(70) Ishizawar, R.; Parsons, S. J. C-Src and Cooperating Partners in Human Cancer. *Cancer Cell* **2004**, *6*, 209–214.

(71) Maa, M. C.; Leu, T. H.; McCarley, D. J.; Schatzman, R. C.; Parsons, S. J. Potentiation of Epidermal Growth Factor Receptor-Mediated Oncogenesis by c-Src: Implications for the Etiology of Multiple Human Cancers. *Proc. Natl. Acad. Sci. U. S. A.* **1995**, *92*, 6981–6985.

(72) Roche, S.; Fumagalli, S.; Courtneidge, S. A. Requirement for Src Family Protein Tyrosine Kinases in G2 for Fibroblast Cell Division. *Science* **1995**, *269*, 1567–1569.

(73) Wilson, L. K.; Luttrell, D. K.; Parsons, J. T.; Parsons, S. J. pp60c-Src Tyrosine Kinase, Myristylation, and Modulatory Domains Are Required for Enhanced Mitogenic Responsiveness to Epidermal Growth Factor Seen in Cells Overexpressing c-Src. *Mol. Cell. Biol.* **1989**, *9*, 1536–1544.

(74) Belsches-Jablonski, A. P.; Biscardi, J. S.; Peavy, D. R.; Tice, D. A.; Romney, D. A.; Parsons, S. J. Src Family Kinases and HER2 Interactions in Human Breast Cancer Cell Growth and Survival. *Oncogene* **2001**, *20*, 1465–1475.

(75) Ishizawar, R. C.; Miyake, T.; Parsons, S. J. C-Src Modulates ErbB2 and ErbB3 Heterocomplex Formation and Function. *Oncogene* **2007**, *26*, 3503–3510.

(76) Sam, M. R.; Elliott, B. E.; Mueller, C. R. A Novel Activating Role of SRC and STAT3 on HGF Transcription in Human Breast Cancer Cells. *Mol. Cancer*. **2007**, *6*, 69.

(77) Lengyel, E.; Prechtel, D.; Resau, J. H.; Gauger, K.; Welk, A.; Lindemann, K.; Salanti, G.; Richter, T.; Knudsen, B.; Vande Woude, G. F.; *et al*. C-Met Overexpression in Node-Positive Breast Cancer Identifies Patients with Poor Clinical Outcome Independent of Her2/neu. *Int. J. cancer* **2005**, *113*, 678–682.

(78) Lindemann, K.; Resau, J.; Nahrig, J.; Kort, E.; Leeser, B.; Annecke, K.; Welk, A.; Schafer, J.; Vande Woude, G. F.; Lengyel, E.; *et al*. Differential Expression of c-Met, Its Ligand HGF/SF and HER2/neu in DCIS and Adjacent Normal Breast Tissue. *Histopathology* **2007**, *51*, 54–62.

(79) Biscardi, J. S.; Belsches, A. P.; Parsons, S. J. Characterization of Human Epidermal Growth Factor Receptor and c-Src Interactions in Human Breast Tumor Cells. *Mol. Carcinog.* **1998**, *21*, 261–272.

(80) Mayer, E. L.; Krop, I. E. Advances in Targeting SRC in the Treatment of Breast Cancer and Other Solid Malignancies. *Clin Cancer Res.* **2010**, *16*, 3526–3532.

(81) Guy, C. T.; Muthuswamy, S. K.; Cardiff, R. D.; Soriano, P.; Muller, W. J. Activation of the c-Src Tyrosine Kinase Is Required for the Induction of Mammary Tumors in Transgenic Mice. *Genes Dev.* **1994**, *8*, 23–32.

(82) Ocana, A.; Gil-Martin, M.; Martin, M.; Rojo, F.; Antolin, S.; Guerrero, A.; Trigo, J. M.; Munoz, M.; Pandiella, A.; Diego, N. G.; *et al*. A Phase I Study of the SRC Kinase Inhibitor Dasatinib with Trastuzumab and Paclitaxel as First Line Therapy for Patients with HER2-Overexpressing Advanced Breast Cancer. GEICAM/2010-04 Study. *Oncotarget* **2017**, *8*, 73144–73153.

(83) Lutz, M. P.; Esser, I. B.; Flossmann-Kast, B. B.; Vogelmann, R.; Lührs, H.; Friess, H.; Büchler, M. W.; Adler, G. Overexpression and Activation of the Tyrosine Kinase Src in Human Pancreatic Carcinoma. *Biochem. Biophys. Res. Commun.* **1998**, *243*, 503–508.

(84) Trevino, J. G.; Summy, J. M.; Lesslie, D. P.; Parikh, N. U.; Hong, D. S.; Lee, F. Y.; Donato, N. J.; Abbruzzese, J. L.; Baker, C. H.; Gallick, G. E. Inhibition of SRC Expression and Activity Inhibits Tumor Progression and Metastasis of Human Pancreatic Adenocarcinoma Cells in an Orthotopic Nude Mouse Model. *Am. J. Pathol.*

2006, *168*, 962–972.

(85) Nagaraj, N. S.; Smith, J. J.; Revetta, F.; Washington, M. K.; Merchant, N. B. Targeted Inhibition of SRC Kinase Signaling Attenuates Pancreatic Tumorigenesis. *Mol. Cancer Ther.* **2010**, *9*, 2322–2332.

(86) MacMillan-Crow, L. A.; Greendorfer, J. S.; Vickers, S. M.; Thompson, J. A. Tyrosine Nitration of c-SRC Tyrosine Kinase in Human Pancreatic Ductal Adenocarcinoma. *Arch. Biochem. Biophys.* **2000**, *377*, 350–356.

(87) Duxbury, M. S.; Ito, H.; Zinner, M. J.; Ashley, S. W.; Whang, E. E. Inhibition of SRC Tyrosine Kinase Impairs Inherent and Acquired Gemcitabine Resistance in Human Pancreatic Adenocarcinoma Cells. *Clin. Cancer Res.* **2004**, *10*, 2307–2318.

(88) Ischenko, I.; Camaj, P.; Seeliger, H.; Kleespies, A.; Guba, M.; De Toni, E. N.; Schwarz, B.; Graeb, C.; Eichhorn, M. E.; Jauch, K.-W.; *et al*. Inhibition of Src Tyrosine Kinase Reverts Chemoresistance toward 5-Fluorouracil in Human Pancreatic Carcinoma Cells: An Involvement of Epidermal Growth Factor Receptor Signaling. *Oncogene* **2008**, *27*, 7212–7222.

(89) Trevino, J. G.; Pillai, S.; Kunigal, S.; Singh, S.; Fulp, W. J.; Centeno, B. A.; Chellappan, S. P. Nicotine Induces Inhibitor of Differentiation-1 in a Src-Dependent Pathway Promoting Metastasis and Chemoresistance in Pancreatic Adenocarcinoma. *Neoplasia* **2012**, *14*, 1102–1114.

(90) Chou, T. C.; Talalay, P. Quantitative Analysis of Dose-Effect Relationships: The Combined Effects of Multiple Drugs or Enzyme Inhibitors. *Adv. Enzyme Regul.* **1984**, *22*, 27–55.

(91) Kopetz, S.; Lesslie, D. P.; Dallas, N. A.; Park, S. I.; Johnson, M.; Parikh, N. U.; Kim, M. P.; Abbruzzese, J. L.; Ellis, L. M.; Chandra, J.; *et al*. Synergistic Activity of the SRC Family Kinase Inhibitor Dasatinib and Oxaliplatin in Colon Carcinoma Cells Is Mediated by Oxidative Stress. *Cancer Res.* **2009**, *69*, 3842–3849.

(92) Cardin, D. B.; Goff, L. W.; Chan, E.; Whisenant, J. G.; Dan Ayers, G.; Takebe, N.; Arlinghaus, L. R.; Yankeelov, T. E.; Berlin, J.; Merchant, N. Dual Src and EGFR Inhibition in Combination with Gemcitabine in Advanced Pancreatic Cancer: Phase I Results : A Phase I Clinical Trial. *Invest. New Drugs* **2017**.

(93) Pan, C. C.; Kumar, S.; Shah, N.; Hoyt, D. G.; Hawinkels, L. J. A. C.; Mythreye, K.; Lee, N. Y. Src-Mediated Post-Translational Regulation of Endoglin Stability and Function Is

Critical for Angiogenesis. *J. Biol. Chem.* **2014**, *289*, 25486–25496.

(94) Bengoetxea, H.; Argandoña, E. G.; Lafuente, J. V. Effects of Visual Experience on Vascular Endothelial Growth Factor Expression during the Postnatal Development of the Rat Visual Cortex. *Cereb. Cortex* **2008**, *18*, 1630–1639.

(95) Mukhopadhyay, D.; Tsiokas, L.; Zhou, X. M.; Foster, D.; Brugge, J. S.; Sukhatme, V. P. Hypoxic Induction of Human Vascular Endothelial Growth Factor Expression through c-Src Activation. *Nature* **1995**, *375*, 577–581.

(96) Schenone, S.; Manetti, F.; Botta, M. SRC Inhibitors and Angiogenesis. *Curr. Pharm. Des.* **2007**, *13* (21), 2118–2128.

(97) Kypta, R. M.; Hemming, A.; Courtneidge, S. A. Identification and Characterization of p59fyn (a Src-like Protein Tyrosine Kinase) in Normal and Polyoma Virus Transformed Cells. *EMBO J.* **1988**, *7*, 3837–3844.

(98) Goel, R. K.; Lukong, K. E. Understanding the Cellular Roles of Fyn-Related Kinase (FRK): Implications in Cancer Biology. *Cancer Metastasis Rev.* **2016**, *35*, 179–199.

(99) Saito, Y. D.; Jensen, A. R.; Salgia, R.; Posadas, E. M. Fyn: A Novel Molecular Target in Cancer. *Cancer* **2010**, *116*, 1629–1637.

(100) Ahrendsen, J. T.; Macklin, W. Signaling Mechanisms Regulating Myelination in the Central Nervous System. *Neurosci. Bull.* **2013**, *29*, 199–215.

(101) Nygaard, H. B. Targeting Fyn Kinase in Alzheimer's Disease. *Biol. Psychiatry* **2017**.

(102) Tintori, C.; La Sala, G.; Vignaroli, G.; Botta, L.; Fallacara, A. L.; Falchi, F.; Radi, M.; Zamperini, C.; Dreassi, E.; Dello Iacono, L.; *et al*. Studies on the ATP Binding Site of Fyn Kinase for the Identification of New Inhibitors and Their Evaluation as Potential Agents against Tauopathies and Tumors. *J. Med. Chem.* **2015**, *58*, 4590–4609.

(103) Couronne, L.; Palomero, T.; Khiabanian, H.; Kim, M.-Y.; Ambesi, A.; Carpenter, Z.; Abate, F.; Allegretta, M.; Lossos, I. S.; Nicolas, C.; *et al*. Activating Mutations In Fyn Kinase In Peripheral T-Cell Lymphomas. *Blood* **2013**, *122*, 811 LP-811.

(104) Schenone, S.; Brullo, C.; Musumeci, F.; Biava, M.; Falchi, F.; Botta, M. Fyn Kinase in Brain Diseases and Cancer: The Search for Inhibitors. *Curr. Med. Chem.* **2011**, *18*, 2921–2942.

(105) Miyamoto, Y.; Tamano, M.; Torii, T.; Kawahara, K.; Nakamura, K.; Tanoue, A.; Takada, S.; Yamauchi, J. Data Supporting the Role of Fyn in Initiating Myelination in the Peripheral Nervous System. *Data Br.* **2016**, *7*, 1098–1105.

(106) Thomas, S. M.; Brugge, J. S. Cellular Functions Regulated by Src Family Kinases. *Annu. Rev. Cell Dev. Biol.* **1997**, *13*, 513–609.

(107) Goldsmith, J. F.; Hall, C. G.; Atkinson, T. P. Identification of an Alternatively Spliced Isoform of the Fyn Tyrosine Kinase. *Biochem. Biophys. Res. Commun.* **2002**, *298*, 501–504.

(108) Schenone, S.; Manetti, F.; Botta, M. Synthetic SRC-Kinase Domain Inhibitors and Their Structural Requirements. *Anticancer. Agents Med. Chem.* **2007**, *7*, 660–680.

(109) Salmond, R. J.; Filby, A.; Qureshi, I.; Caserta, S.; Zamoyska, R. T-Cell Receptor Proximal Signaling via the Src-Family Kinases, Lck and Fyn, Influences T-Cell Activation, Differentiation, and Tolerance. *Immunol. Rev.* **2009**, *228*, 9–22.

(110) Levi, M.; Shalgi, R. The Role of Fyn Kinase in the Release from Metaphase in Mammalian Oocytes. *Mol. Cell. Endocrinol.* **2010**, *314*, 228–233.

(111) Vatish, M.; Yamada, E.; Pessin, J. E.; Bastie, C. C. Fyn Kinase Function in Lipid Utilization: A New Upstream Regulator of AMPK Activity? *Arch. Physiol. Biochem.* **2009**, *115*, 191–198.

(112) Chin, J.; Palop, J. J.; Puoliväli, J.; Massaro, C.; Bien-Ly, N.; Gerstein, H.; Scearce-Levie, K.; Masliah, E.; Mucke, L. Fyn Kinase Induces Synaptic and Cognitive Impairments in a Transgenic Mouse Model of Alzheimer's Disease. *J. Neurosci. Off. J. Soc. Neurosci.* **2005**, *25*, 9694–9703.

(113) Bhaskar, K.; Hobbs, G. A.; Yen, S.-H.; Lee, G. Tyrosine Phosphorylation of Tau Accompanies Disease Progression in Transgenic Mouse Models of Tauopathy. *Neuropathol. Appl. Neurobiol.* **2010**, *36*, 462–477.

(114) Knox, R.; Jiang, X. Fyn in Neurodevelopment and Ischemic Brain Injury. *Dev. Neurosci.* **2015**, *37*, 311–320.

(115) Sperber, B. R.; Boyle-Walsh, E. A.; Engleka, M. J.; Gadue, P.; Peterson, A. C.; Stein, P. L.; Scherer, S. S.; McMorris, F. A. A Unique Role for Fyn in CNS Myelination. *J. Neurosci. Off. J. Soc. Neurosci.* **2001**, *21*, 2039–2047.

(116) Macurek, L.; Dráberová, E.; Richterová, V.; Sulimenko, V.; Sulimenko, T.; Dráberová, L.; Marková, V.; Dráber, P. Regulation of Microtubule Nucleation from Membranes by Complexes of Membrane-Bound Gamma-Tubulin with Fyn Kinase and Phosphoinositide 3-Kinase. *Biochem. J.* **2008**, *416*, 421–430.

(117) Belkadi, A.; LoPresti, P. Truncated Tau with the Fyn-Binding Domain and without the

Microtubule-Binding Domain Hinders the Myelinating Capacity of an Oligodendrocyte Cell Line. *J. Neurochem.* **2008**, *107*, 351–360.

(118) Lau, D. H. W.; Hogseth, M.; Phillips, E. C.; O'Neill, M. J.; Pooler, A. M.; Noble, W.; Hanger, D. P. Critical Residues Involved in Tau Binding to Fyn: Implications for Tau Phosphorylation in Alzheimer's Disease. *Acta Neuropathol. Commun*. **2016**, *4*, 49.

(119) Trepanier, C. H.; Jackson, M. F.; MacDonald, J. F. Regulation of NMDA Receptors by the Tyrosine Kinase Fyn. *FEBS J.* **2012**, *279*, 12–19.

(120) Tezuka, T.; Umemori, H.; Akiyama, T.; Nakanishi, S.; Yamamoto, T. PSD-95 Promotes Fyn-Mediated Tyrosine Phosphorylation of the N-Methyl-D-Aspartate Receptor Subunit NR2A. *Proc. Natl. Acad. Sci. U. S. A.* **1999**, *96*, 435–440.

(121) Kalia, L. V; Salter, M. W. Interactions between Src Family Protein Tyrosine Kinases and PSD-95. *Neuropharmacology* **2003**, *45*, 720–728.

(122) Salter, M. W.; Kalia, L. V. Src Kinases: A Hub for NMDA Receptor Regulation. *Nat. Rev. Neurosci.* **2004**, *5*, 317–328.

(123) Chen, M.; Hou, X.; Zhang, G. Tyrosine Kinase and Tyrosine Phosphatase Participate in Regulation of Interactions of NMDA Receptor Subunit 2A with Src and Fyn Mediated by PSD-95 after Transient Brain Ischemia. *Neurosci. Lett.* **2003**, *339*, 29–32.

(124) Nada, S.; Shima, T.; Yanai, H.; Husi, H.; Grant, S. G. N.; Okada, M.; Akiyama, T. Identification of PSD-93 as a Substrate for the Src Family Tyrosine Kinase Fyn. *J. Biol. Chem.* **2003**, *278*, 47610–47621.

(125) Jurd, R.; Tretter, V.; Walker, J.; Brandon, N. J.; Moss, S. J. Fyn Kinase Contributes to Tyrosine Phosphorylation of the GABA(A) Receptor gamma2 Subunit. *Mol. Cell. Neurosci.* **2010**, *44*, 129–134.

(126) Bourgin, C.; Murai, K. K.; Richter, M.; Pasquale, E. B. The EphA4 Receptor Regulates Dendritic Spine Remodeling by Affecting beta1-Integrin Signaling Pathways. *J. Cell Biol.* **2007**, *178*, 1295–1307.

(127) Isosaka, T.; Hattori, K.; Yagi, T. NMDA-Receptor Proteins Are Upregulated in the Hippocampus of Postnatal Heterozygous Reeler Mice. *Brain Res.* **2006**, *1073–1074*, 11–19.

(128) Ramseger, R.; White, R.; Kroger, S. Transmembrane Form Agrin-Induced Process Formation Requires Lipid Rafts and the Activation of Fyn and MAPK. *J. Biol. Chem.* **2009**, *284*, 7697–7705.

(129) Isosaka, T.; Hattori, K.; Kida, S.; Kohno, T.; Nakazawa, T.; Yamamoto, T.; Yagi, T.; Yuasa, S. Activation of Fyn Tyrosine Kinase in the Mouse Dorsal Hippocampus Is Essential for Contextual Fear Conditioning. *Eur. J. Neurosci.* **2008**, *28*, 973–981.

(130) Isosaka, T.; Kida, S.; Kohno, T.; Hattori, K.; Yuasa, S. Hippocampal Fyn Activity Regulates Extinction of Contextual Fear. *Neuroreport* **2009**, *20*, 1461–1465.

(131) Jin, D.-Z.; Mao, L.-M.; Wang, J. Q. An Essential Role of Fyn in the Modulation of Metabotropic Glutamate Receptor 1 in Neurons. *eNeuro* **2017**, *4*.

(132) Scheltens, P.; Blennow, K.; Breteler, M. M. B.; de Strooper, B.; Frisoni, G. B.; Salloway, S.; Van der Flier, W. M. Alzheimer's Disease. *Lancet* **2016**, *388*, 505–517.

(133) Khanahmadi, M.; Farhud, D. D.; Malmir, M. Genetic of Alzheimer's Disease: A Narrative Review Article. *Iran. J. Public Health*. **2015**, *44*, 892–901.

(134) Zou, Z.; Liu, C.; Che, C.; Huang, H. Clinical Genetics of Alzheimer's Disease. *Biomed Res. Int.* **2014**, *2014*, 291862.

(135) Reitz, C.; Brayne, C.; Mayeux, R. Epidemiology of Alzheimer Disease. *Nat. Rev. Neurol.* **2011**, *7*, 137–152.

(136) Glenner, G. G.; Wong, C. W. Alzheimer's Disease and Down's Syndrome: Sharing of a Unique Cerebrovascular Amyloid Fibril Protein. *Biochem. Biophys. Res. Commun.* **1984**, *122*, 1131–1135.

(137) Hardy, J.; Selkoe, D. J. The Amyloid Hypothesis of Alzheimer's Disease: Progress and Problems on the Road to Therapeutics. *Science* **2002**, *297*, 353–356.

(138) Mohamed, T.; Shakeri, A.; Rao, P. P. N. Amyloid Cascade in Alzheimer's Disease: Recent Advances in Medicinal Chemistry. *Eur. J. Med. Chem.* **2016**, *113*, 258–272.

(139) Mufson, E. J.; Counts, S. E.; Perez, S. E.; Ginsberg, S. D. Cholinergic System during the Progression of Alzheimer's Disease: Therapeutic Implications. *Expert Rev. Neurother*. **2008**, *8*, 1703–1718.

(140) Lloret, A.; Badia, M.-C.; Giraldo, E.; Ermak, G.; Alonso, M.-D.; Pallardo, F. V; Davies, K. J. A.; Vina, J. Amyloid-Beta Toxicity and Tau Hyperphosphorylation Are Linked via RCAN1 in Alzheimer's Disease. *J. Alzheimers. Dis.* **2011**, *27*, 701–709.

(141) Wang, X.; Wang, W.; Li, L.; Perry, G.; Lee, H.; Zhu, X. Oxidative Stress and Mitochondrial Dysfunction in Alzheimer's Disease. *Biochim. Biophys. Acta* **2014**, *1842*, 1240–1247.

(142) Crews, L.; Masliah, E. Molecular Mechanisms of Neurodegeneration in Alzheimer's

Disease. *Hum. Mol. Genet.* **2010**, *19*, 12-20.

(143) Lee, G.; Thangavel, R.; Sharma, V. M.; Litersky, J. M.; Bhaskar, K.; Fang, S. M.; Do, L. H.; Andreadis, A.; Van Hoesen, G.; Ksiezak-Reding, H. Phosphorylation of Tau by Fyn: Implications for Alzheimer's Disease. *J. Neurosci. Off. J. Soc. Neurosci.* **2004**, *24*, 2304–2312.

(144) Ho, G. J.; Hashimoto, M.; Adame, A.; Izu, M.; Alford, M. F.; Thal, L. J.; Hansen, L. A.; Masliah, E. Altered p59Fyn Kinase Expression Accompanies Disease Progression in Alzheimer's Disease: Implications for Its Functional Role. *Neurobiol. Aging* **2005**, *26*, 625–635.

(145) Williamson, R.; Scales, T.; Clark, B. R.; Gibb, G.; Reynolds, C. H.; Kellie, S.; Bird, I. N.; Varndell, I. M.; Sheppard, P. W.; Everall, I.; *et al*. Rapid Tyrosine Phosphorylation of Neuronal Proteins Including Tau and Focal Adhesion Kinase in Response to Amyloid-β Peptide Exposure: Involvement of Src Family Protein Kinases. *J. Neurosci.* **2002**, *22*, 10–20.

(146) Peña, F.; Ordaz, B.; Balleza-Tapia, H.; Bernal-Pedraza, R.; Márquez-Ramos, A.; Carmona-Aparicio, L.; Giordano, M. Beta-Amyloid Protein (25-35) Disrupts Hippocampal Network Activity: Role of Fyn-Kinase. *Hippocampus* **2010**, *20*, 78–96.

(147) Haass, C.; Mandelkow, E. Fyn-Tau-Amyloid: A Toxic Triad. *Cell* **2010**, *142*, 356–358.

(148) Ittner, L. M.; Ke, Y. D.; Delerue, F.; Bi, M.; Gladbach, A.; van Eersel, J.; Wölfing, H.; Chieng, B. C.; Christie, M. J.; Napier, I. A.; *et al*. Dendritic Function of Tau Mediates Amyloid-Beta Toxicity in Alzheimer's Disease Mouse Models. *Cell* **2010**, *142*, 387–397.

(149) Ittner, A.; Chua, S. W.; Bertz, J.; Volkerling, A.; van der Hoven, J.; Gladbach, A.; Przybyla, M.; Bi, M.; van Hummel, A.; Stevens, C. H.; *et al*. Site-Specific Phosphorylation of Tau Inhibits Amyloid-Beta Toxicity in Alzheimer's Mice. *Science* **2016**, *354*, 904–908.

(150) Lauren, J.; Gimbel, D. A.; Nygaard, H. B.; Gilbert, J. W.; Strittmatter, S. M. Cellular Prion Protein Mediates Impairment of Synaptic Plasticity by Amyloid-Beta Oligomers. *Nature* **2009**, *457*, 1128–1132.

(151) Kostylev, M. A.; Kaufman, A. C.; Nygaard, H. B.; Patel, P.; Haas, L. T.; Gunther, E. C.; Vortmeyer, A.; Strittmatter, S. M. Prion-Protein-Interacting Amyloid-Beta Oligomers of High Molecular Weight Are Tightly Correlated with Memory Impairment in Multiple

Alzheimer Mouse Models. *J. Biol. Chem.* **2015**, *290*, 17415–17438.

(152) Barry, A. E.; Klyubin, I.; Mc Donald, J. M.; Mably, A. J.; Farrell, M. A.; Scott, M.; Walsh, D. M.; Rowan, M. J. Alzheimer's Disease Brain-Derived Amyloid-Beta-Mediated Inhibition of LTP *in Vivo* Is Prevented by Immunotargeting Cellular Prion Protein. *J. Neurosci.* **2011**, *31*, 7259–7263.

(153) Um, J. W.; Nygaard, H. B.; Heiss, J. K.; Kostylev, M. A.; Stagi, M.; Vortmeyer, A.; Wisniewski, T.; Gunther, E. C.; Strittmatter, S. M. Alzheimer Amyloid-Beta Oligomer Bound to Postsynaptic Prion Protein Activates Fyn to Impair Neurons. *Nat. Neurosci.* **2012**, *15*, 1227–1235.

(154) Haas, L. T.; Salazar, S. V; Kostylev, M. A.; Um, J. W.; Kaufman, A. C.; Strittmatter, S. M. Metabotropic Glutamate Receptor 5 Couples Cellular Prion Protein to Intracellular Signalling in Alzheimer's Disease. *Brain* **2016**, *139*, 526–546.

(155) Sharma, S.; Moon, C. S.; Khogali, A.; Haidous, A.; Chabenne, A.; Ojo, C.; Jelebinkov, M.; Kurdi, Y.; Ebadi, M. Biomarkers in Parkinson's Disease (Recent Update). *Neurochem. Int.* **2013**, *63*, 201–229.

(156) Mhyre, T. R.; Boyd, J. T.; Hamill, R. W.; Maguire-Zeiss, K. A. Parkinson's Disease. *Subcell. Biochem.* **2012**, *65*, 389–455.

(157) Kalia, L. V; Lang, A. E. Parkinson's Disease. *Lancet* **2015**, *386*, 896–912.

(158) Nakamura, T.; Yamashita, H.; Takahashi, T.; Nakamura, S. Activated Fyn Phosphorylates Alpha-Synuclein at Tyrosine Residue 125. *Biochem. Biophys. Res. Commun.* **2001**, *280*, 1085–1092.

(159) Ellis, C. E.; Schwartzberg, P. L.; Grider, T. L.; Fink, D. W.; Nussbaum, R. L. Alpha-Synuclein Is Phosphorylated by Members of the Src Family of Protein-Tyrosine Kinases. *J. Biol. Chem.* **2001**, *276*, 3879–3884.

(160) Dunah, A. W.; Sirianni, A. C.; Fienberg, A. A.; Bastia, E.; Schwarzschild, M. A.; Standaert, D. G. Dopamine D1-Dependent Trafficking of Striatal N-Methyl-D-Aspartate Glutamate Receptors Requires Fyn Protein Tyrosine Kinase but Not DARPP-32. *Mol. Pharmacol.* **2004**, *65*, 121–129.

(161) Panicker, N.; Saminathan, H.; Jin, H.; Neal, M.; Harischandra, D. S.; Gordon, R.; Kanthasamy, K.; Lawana, V.; Sarkar, S.; Luo, J.; *et al*. Fyn Kinase Regulates Microglial Neuroinflammatory Responses in Cell Culture and Animal Models of Parkinson's Disease. *Neurosci*. **2015**, *35*, 10058–10077.

(162) Sanz-Blasco, S.; Bordone, M. P.; Damianich, A.; Gomez, G.; Bernardi, M. A.; Isaja, L.; Taravini, I. R.; Hanger, D. P.; Avale, M. E.; Gershanik, O. S.; *et al*. The Kinase Fyn As a Novel Intermediate in L-DOPA-Induced Dyskinesia in Parkinson's Disease. *Mol. Neurobiol.* **2017**.

(163) Kawakami, T.; Kawakami, Y.; Aaronson, S. A.; Robbins, K. C. Acquisition of Transforming Properties by FYN, a Normal SRC-Related Human Gene. *Proc. Natl. Acad. Sci. U. S. A.* **1988**, *85*, 3870–3874.

(164) Twamley-Stein, G. M.; Pepperkok, R.; Ansorge, W.; Courtneidge, S. A. The Src Family Tyrosine Kinases Are Required for Platelet-Derived Growth Factor-Mediated Signal Transduction in NIH 3T3 Cells. *Proc. Natl. Acad. Sci. U. S. A.* **1993**, *90*, 7696–7700.

(165) Yasunaga, M.; Yagi, T.; Hanzawa, N.; Yasuda, M.; Yamanashi, Y.; Yamamoto, T.; Aizawa, S.; Miyauchi, Y.; Nishikawa, S. Involvement of Fyn Tyrosine Kinase in Progression of Cytokinesis of B Lymphocyte Progenitor. *J. Cell Biol.* **1996**, *132*, 91–99.

(166) Paszek, M. J.; Zahir, N.; Johnson, K. R.; Lakins, J. N.; Rozenberg, G. I.; Gefen, A.; Reinhart-King, C. A.; Margulies, S. S.; Dembo, M.; Boettiger, D.; *et al*. Tensional Homeostasis and the Malignant Phenotype. *Cancer Cell* **2005**, *8*, 241–254.

(167) Bouton, A. H.; Riggins, R. B.; Bruce-Staskal, P. J. Functions of the Adapter Protein Cas: Signal Convergence and the Determination of Cellular Responses. *Oncogene* **2001**, *20*, 6448–6458.

(168) Liu, G.; Beggs, H.; Jurgensen, C.; Park, H.-T.; Tang, H.; Gorski, J.; Jones, K. R.; Reichardt, L. F.; Wu, J.; Rao, Y. Netrin Requires Focal Adhesion Kinase and Src Family Kinases for Axon Outgrowth and Attraction. *Nat. Neurosci.* **2004**, *7*, 1222–1232.

(169) Miyake, I.; Hakomori, Y.; Misu, Y.; Nakadate, H.; Matsuura, N.; Sakamoto, M.; Sakai, R. Domain-Specific Function of ShcC Docking Protein in Neuroblastoma Cells. *Oncogene* **2005**, *24*, 3206–3215.

(170) Garcia, S.; Dales, J.-P.; Charafe-Jauffret, E.; Carpentier-Meunier, S.; Andrac-Meyer, L.; Jacquemier, J.; Andonian, C.; Lavaut, M.-N.; Allasia, C.; Bonnier, P.; *et al*. Overexpression of c-Met and of the Transducers PI3K, FAK and JAK in Breast Carcinomas Correlates with Shorter Survival and Neoangiogenesis. *Int. J. Oncol.* **2007**, *31*, 49–58.

(171) Elias, D.; Ditzel, H. J. Fyn Is an Important Molecule in Cancer Pathogenesis and Drug

Resistance. *Pharmacol. Res.* **2015**, *100*, 250–254.

(172) Zhang, S.; Fan, G.; Hao, Y.; Hammell, M.; Wilkinson, J. E.; Tonks, N. K. Suppression of Protein Tyrosine Phosphatase N23 Predisposes to Breast Tumorigenesis via Activation of FYN Kinase. *Genes Dev.* **2017**, *31*, 1939–1957.

(173) Huang, R. Y.-J.; Wang, S.-M.; Hsieh, C.-Y.; Wu, J.-C. Lysophosphatidic Acid Induces Ovarian Cancer Cell Dispersal by Activating Fyn Kinase Associated with p120-Catenin. *Int. J. Cancer* **2008**, *123*, 801–809.

(174) Yang, J.; Wang, Y.; Zeng, Z.; Qiao, L.; Zhuang, L.; Gao, Q.; Ma, D.; Huang, X. Smad4 Deletion in Blood Vessel Endothelial Cells Promotes Ovarian Cancer Metastasis. *Int. J. Oncol.* **2017**, *50*, 1693–1700.

(175) Posadas, E. M.; Al-Ahmadie, H.; Robinson, V. L.; Jagadeeswaran, R.; Otto, K.; Kasza, K. E.; Tretiakov, M.; Siddiqui, J.; Pienta, K. J.; Stadler, W. M.; *et al*. FYN Is Overexpressed in Human Prostate Cancer. *BJU Int.* **2009**, *103*, 171–177.

(176) Gururajan, M.; Cavassani, K. A.; Sievert, M.; Duan, P.; Lichterman, J.; Huang, J.-M.; Smith, B.; You, S.; Nandana, S.; Chu, G. C.-Y.; *et al*. SRC Family Kinase FYN Promotes the Neuroendocrine Phenotype and Visceral Metastasis in Advanced Prostate Cancer. *Oncotarget* **2015**.

(177) Posadas, E. M.; Ahmed, R. S.; Karrison, T.; Szmulewitz, R. Z.; O'Donnell, P. H.; Wade, J. L.; Shen, J.; Gururajan, M.; Sievert, M.; Stadler, W. M. Saracatinib as a Metastasis Inhibitor in Metastatic Castration-Resistant Prostate Cancer: A University of Chicago Phase 2 Consortium and DOD/PCF Prostate Cancer Clinical Trials Consortium Study. *Prostate*. **2016**, *76*, 286–293.

(178) Huang, J.; Asawa, T.; Takato, T.; Sakai, R. Cooperative Roles of Fyn and Cortactin in Cell Migration of Metastatic Murine Melanoma. *J. Biol. Chem.* **2003**, *278*, 48367–48376.

(179) Huang, C.; Sheng, Y.; Jia, J.; Chen, L. Identification of Melanoma Biomarkers Based on Network Modules by Integrating the Human Signaling Network with Microarrays. *J. Cancer Res. Ther.* **2014**, *10*, 114-124.

(180) Li, X.; Yang, Y.; Hu, Y.; Dang, D.; Regezi, J.; Schmidt, B. L.; Atakilit, A.; Chen, B.; Ellis, D.; Ramos, D. M. Alphavbeta6-Fyn Signaling Promotes Oral Cancer Progression. *J. Biol. Chem.* **2003**, *278*, 41646–41653.

(181) Lewin, B.; Siu, A.; Baker, C.; Dang, D.; Schnitt, R.; Eisapooran, P.; Ramos, D. M.

Expression of Fyn Kinase Modulates EMT in Oral Cancer Cells. *Anticancer Res.* **2010**, *30*, 2591–2596.

(182) Lee, C.; Ramos, D. M. Regulation of Multicellular Spheroids by MAPK and FYN Kinase. *Anticancer Res.* **2016**, *36*, 3833–3838.

(183) Lu, K. V.; Zhu, S.; Cvrljevic, A.; Huang, T. T.; Sarkaria, S.; Ahkavan, D.; Dang, J.; Dinca, E. B.; Plaisier, S. B.; Oderberg, I.; *et al*. Fyn and SRC Are Effectors of Oncogenic Epidermal Growth Factor Receptor Signaling in Glioblastoma Patients. *Cancer Res.* **2009**, *69*, 6889–6898.

(184) Comba, A.; Kadiyala, P.; Argento, A. E.; Patel, P.; Nunez, F. J.; Saxena, M.; Castro, M. G.; Lowenstein, P. R. CSIG-39. Fyn, An Oncogene That Reduces Glioblastoma Survival Yet Sensitizes to Chemo-radiotherapy. *Neuro. Oncol.* **2017**, *19*, vi58.

(185) Chen, Z. Y.; Cai, L.; Bie, P.; Wang, S. G.; Jiang, Y.; Dong, J. H.; Li, X. W. Roles of Fyn in Pancreatic Cancer Metastasis. *J. Gastroenterol. Hepatol.* **2010**, *25*, 293–301.

(186) Je, D. W.; O, Y. M.; Ji, Y. G.; Cho, Y.; Lee, D. H. The Inhibition of SRC Family Kinase Suppresses Pancreatic Cancer Cell Proliferation, Migration, and Invasion. *Pancreas* **2014**, *43*, 768–776.

(187) Jiang, P.; Li, Z.; Tian, F.; Li, X.; Yang, J. Fyn/heterogeneous Nuclear Ribonucleoprotein E1 Signaling Regulates Pancreatic Cancer Metastasis by Affecting the Alternative Splicing of Integrin beta1. *Int. J. Oncol.* **2017**, *51*, 169–183.

(188) Menges, C. W.; Chen, Y.; Mossman, B. T.; Chernoff, J.; Yeung, A. T.; Testa, J. R. A Phosphotyrosine Proteomic Screen Identifies Multiple Tyrosine Kinase Signaling Pathways Aberrantly Activated in Malignant Mesothelioma. *Genes Cancer* **2010**, *1*, 493–505.

(189) Eguchi, R.; Kubo, S.; Takeda, H.; Ohta, T.; Tabata, C.; Ogawa, H.; Nakano, T.; Fujimori, Y. Deficiency of Fyn Protein Is Prerequisite for Apoptosis Induced by Src Family Kinase Inhibitors in Human Mesothelioma Cells. *Carcinogenesis* **2012**, *33*, 969–975.

(190) Meyn, M. A. 3rd; Wilson, M. B.; Abdi, F. A.; Fahey, N.; Schiavone, A. P.; Wu, J.; Hochrein, J. M.; Engen, J. R.; Smithgall, T. E. Src Family Kinases Phosphorylate the Bcr-Abl SH3-SH2 Region and Modulate Bcr-Abl Transforming Activity. *J. Biol. Chem.* **2006**, *281*, 30907–30916.

(191) Grosso, S.; Puissant, A.; Dufies, M.; Colosetti, P.; Jacquel, A.; Lebrigand, K.; Barbry, P.; Deckert, M.; Cassuto, J. P.; Mari, B.; *et al*. Gene Expression Profiling of Imatinib

and PD166326-Resistant CML Cell Lines Identifies Fyn as a Gene Associated with Resistance to BCR-ABL Inhibitors. *Mol. Cancer Ther.* **2009**, *8*, 1924–1933.

(192) Ban, K.; Gao, Y.; Amin, H. M.; Howard, A.; Miller, C.; Lin, Q.; Leng, X.; Munsell, M.; Bar-Eli, M.; Arlinghaus, R. B.; *et al*. BCR-ABL1 Mediates up-Regulation of Fyn in Chronic Myelogenous Leukemia. *Blood*. **2008**, *111*, 2904–2908.

(193) Gao, Y.; Howard, A.; Ban, K.; Chandra, J. Oxidative Stress Promotes Transcriptional up-Regulation of Fyn in BCR-ABL1-Expressing Cells. *J. Biol. Chem.* **2009**, *284*, 7114–7125.

(194) Juric, D.; Lacayo, N. J.; Ramsey, M. C.; Racevskis, J.; Wiernik, P. H.; Rowe, J. M.; Goldstone, A. H.; O'Dwyer, P. J.; Paietta, E.; Sikic, B. I. Differential Gene Expression Patterns and Interaction Networks in BCR-ABL-Positive and -Negative Adult Acute Lymphoblastic Leukemias. *J. Clin. Oncol.* **2007**, *25*, 1341–1349.

(195) Singh, M. M.; Howard, A.; Irwin, M. E.; Gao, Y.; Lu, X.; Multani, A.; Chandra, J. Expression and Activity of Fyn Mediate Proliferation and Blastic Features of Chronic Myelogenous Leukemia. *PLoS One* **2012**, *7*, e51611.

(196) Chougule, R. A.; Kazi, J. U.; Ronnstrand, L. FYN Expression Potentiates FLT3-ITD Induced STAT5 Signaling in Acute Myeloid Leukemia. *Oncotarget* **2016**, *7*, 9964–9974.

(197) Poh, A. R.; O'Donoghue, R. J. J.; Ernst, M. Hematopoietic Cell Kinase (HCK) as a Therapeutic Target in Immune and Cancer Cells. *Oncotarget*. **2015**, *6*, 15752–15771.

(198) Musumeci, F.; Schenone, S.; Brullo, C.; Desogus, A.; Botta, L.; Tintori, C. Hck Inhibitors as Potential Therapeutic Agents in Cancer and HIV Infection. *Curr. Med. Chem.* **2015**, *22*, 1540–1564.

(199) Cohen, J. The Immunopathogenesis of Sepsis. *Nature* **2002**, *420*, 885–891.

(200) Suen, P. W.; Ilic, D.; Caveggion, E.; Berton, G.; Damsky, C. H.; Lowell, C. A. Impaired Integrin-Mediated Signal Transduction, Altered Cytoskeletal Structure and Reduced Motility in Hck/Fgr Deficient Macrophages. *J. Cell Sci.* **1999**, *112*, 4067–4078.

(201) Roversi, F. M.; Pericole, F. V.; Machado-Neto, J. A.; da Silva Santos Duarte, A.; Longhini, A. L.; Corrocher, F. A.; Palodetto, B.; Ferro, K. P.; Rosa, R. G.; Baratti, M. O.; *et al*. Hematopoietic Cell Kinase (HCK) Is a Potential Therapeutic Target for Dysplastic and Leukemic Cells due to Integration of erythropoietin/PI3K Pathway and Regulation of Erythropoiesis: HCK in erythropoietin/PI3K Pathway. *Biochim. Biophys. Acta* **2017**, *1863*, 450–461.

(202) Emert-Sedlak, L. A.; Narute, P.; Shu, S. T.; Poe, J. A.; Shi, H.; Yanamala, N.; Alvarado, J. J.; Lazo, J. S.; Yeh, J. I.; Johnston, P. A.; *et al*. Effector Kinase Coupling Enables High-Throughput Screens for Direct HIV-1 Nef Antagonists with Antiretroviral Activity. *Chem. Biol.* **2013**, *20*, 82–91.

(203) Sicheri, F.; Moarefi, I.; Kuriyan, J. Crystal Structure of the Src Family Tyrosine Kinase Hck. *Nature* **1997**, *385*, 602–609.

(204) Alvarado, J. J.; Betts, L.; Moroco, J. A.; Smithgall, T. E.; Yeh, J. I. Crystal Structure of the Src Family Kinase Hck SH3-SH2 Linker Regulatory Region Supports an SH3-Dominant Activation Mechanism. *J. Biol. Chem.* **2010**, *285*, 35455–35461.

(205) Robbins, S. M.; Quintrell, N. A.; Bishop, J. M. Myristoylation and Differential Palmitoylation of the HCK Protein-Tyrosine Kinases Govern Their Attachment to Membranes and Association with Caveolae. *Mol. Cell. Biol.* **1995**, *15*, 3507–3515.

(206) Lock, P.; Ralph, S.; Stanley, E.; Boulet, I.; Ramsay, R.; Dunn, A. R. Two Isoforms of Murine Hck, Generated by Utilization of Alternative Translational Initiation Codons, Exhibit Different Patterns of Subcellular Localization. *Mol. Cell. Biol.* **1991**, *11*, 4363–4370.

(207) Möhn, H.; Le Cabec, V.; Fischer, S.; Maridonneau-Parini, I. The Src-Family Protein-Tyrosine Kinase p59hck Is Located on the Secretory Granules in Human Neutrophils and Translocates towards the Phagosome during Cell Activation. *Biochem. J.* **1995**, *309*, 657–665.

(208) Carréno, S.; Caron, E.; Cougoule, C.; Emorine, L. J.; Maridonneau-Parini, I. p59Hck Isoform Induces F-Actin Reorganization to Form Protrusions of the Plasma Membrane in a Cdc42- and Rac-Dependent Manner. *J. Biol. Chem.* **2002**, *277*, 21007–21016.

(209) Willman, C. L.; Stewart, C. C.; Longacre, T. L.; Head, D. R.; Habbersett, R.; Ziegler, S. F.; Perlmutter, R. M. Expression of the c-Fgr and Hck Protein-Tyrosine Kinases in Acute Myeloid Leukemic Blasts Is Associated with Early Commitment and Differentiation Events in the Monocytic and Granulocytic Lineages. *Blood* **1991**, *77*, 726–734.

(210) Ziegler, S. F.; Wilson, C. B.; Perlmutter, R. M. Augmented Expression of a Myeloid-Specific Protein Tyrosine Kinase Gene (Hck) after Macrophage Activation. *J. Exp. Med.* **1988**, *168*, 1801–1810.

(211) Marks, D. C.; Csar, X. F.; Wilson, N. J.; Novak, U.; Ward, A. C.; Kanagasundarum, V.; Hoffmann, B. W.; Hamilton, J. A. Expression of a Y559F Mutant CSF-1 Receptor in M1

Myeloid Cells: A Role for Src Kinases in CSF-1 Receptor-Mediated Differentiation. *Mol. cell Biol. Res. Commun.* **1999**, *1*, 144–152.

(212) Guiet, R.; Poincloux, R.; Castandet, J.; Marois, L.; Labrousse, A.; Le Cabec, V.; Maridonneau-Parini, I. Hematopoietic Cell Kinase (Hck) Isoforms and Phagocyte Duties - from Signaling and Actin Reorganization to Migration and Phagocytosis. *Eur. J. Cell Biol.* **2008**, *87*, 527–542.

(213) Kloog, Y.; Mor, A. Cytotoxic-T-Lymphocyte Antigen 4 Receptor Signaling for Lymphocyte Adhesion Is Mediated by C3G and Rap1. *Mol. Cell. Biol.* **2014**, *34*, 978–988.

(214) Asai, T.; Morrison, S. L. The SRC Family Tyrosine Kinase HCK and the ETS Family Transcription Factors SPIB and EHF Regulate Transcytosis across a Human Follicle-Associated Epithelium Model. *J. Biol. Chem.* **2013**, *288*, 10395–10405.

(215) Page, T. H.; Smolinska, M.; Gillespie, J.; Urbaniak, A. M.; Foxwell, B. M. J. Tyrosine Kinases and Inflammatory Signalling. *Curr. Mol. Med.* **2009**, *9*, 69–85.

(216) Smolinska, M. J.; Page, T. H.; Urbaniak, A. M.; Mutch, B. E.; Horwood, N. J. Hck Tyrosine Kinase Regulates TLR4-Induced TNF and IL-6 Production via AP-1. *J. Immunol.* **2011**, *187*, 6043–6051.

(217) Gong, J.; Yan, J.; Gu, H.; Kong, X.; Cao, K. Expressing Murine p56Hck(ca) Promotes HeLa Cells' Motility and Invasion via Triggering Redistribution of F-Actin and Microtubules. *Mol. Biol. Rep.* **2012**, *39*, 6521–6527.

(218) Awad, R.; Marion, S.; Isabel, A.; Anne, C.; Philippe, F.; Pierre, G.; Jean-Baptiste, R.; Jean-Philippe, K. The SH3 Regulatory Domain of the Hematopoietic Cell Kinase Hck Binds ELMO via Its Polyproline Motif. *FEBS Open Bio*. **2015**, *5*, 99–106.

(219) Danhauser-Riedl, S.; Warmuth, M.; Druker, B. J.; Emmerich, B.; Hallek, M. Activation of Src Kinases p53/56lyn and p59hck by p210bcr/abl in Myeloid Cells. *Cancer Res.* **1996**, *56*, 3589–3596.

(220) Stephen, A. G.; Esposito, D.; Bagni, R. K.; McCormick, F. Dragging Ras Back in the Ring. *Cancer Cell* **2014**, *25*, 272–281.

(221) Stanglmaier, M.; Warmuth, M.; Kleinlein, I.; Reis, S.; Hallek, M. The Interaction of the Bcr-Abl Tyrosine Kinase with the Src Kinase Hck Is Mediated by Multiple Binding Domains. *Leukemia* **2003**, *17*, 283–289.

(222) Chen, S.; O'Reilly, L. P.; Smithgall, T. E.; Engen, J. R. Tyrosine Phosphorylation in the

SH3 Domain Disrupts Negative Regulatory Interactions within the c-Abl Kinase Core. *J. Mol. Biol.* **2008**, *383*, 414–423.

(223) Klejman, A.; Schreiner, S. J.; Nieborowska-Skorska, M.; Slupianek, A.; Wilson, M.; Smithgall, T. E.; Skorski, T. The Src Family Kinase Hck Couples BCR/ABL to STAT5 Activation in Myeloid Leukemia Cells. *EMBO J.* **2002**, *21*, 5766–5774.

(224) Chatain, N.; Ziegler, P.; Fahrenkamp, D.; Jost, E.; Moriggl, R.; Schmitz-Van de Leur, H.; Müller-Newen, G. Src Family Kinases Mediate Cytoplasmic Retention of Activated STAT5 in BCR-ABL-Positive Cells. *Oncogene* **2013**, *32*, 3587–3597.

(225) Lakshmikuttyamma, A.; Pastural, E.; Takahashi, N.; Sawada, K.; Sheridan, D. P.; DeCoteau, J. F.; Geyer, C. R. Bcr-Abl Induces Autocrine IGF-1 Signaling. *Oncogene* **2008**, *27*, 3831–3844.

(226) Baruzzi, A.; Iacobucci, I.; Soverini, S.; Lowell, C. A.; Martinelli, G.; Berton, G. C-Abl and Src-Family Kinases Cross-Talk in Regulation of Myeloid Cell Migration. *FEBS Lett.* **2010**, *584*, 15–21.

(227) Pene-Dumitrescu, T.; Peterson, L. F.; Donato, N. J.; Smithgall, T. E. An Inhibitor-Resistant Mutant of Hck Protects CML Cells against the Antiproliferative and Apoptotic Effects of the Broad-Spectrum Src Family Kinase Inhibitor A-419259. *Oncogene* **2008**, *27*, 7055–7069.

(228) Pene-Dumitrescu, T.; Smithgall, T. E. Expression of a Src Family Kinase in Chronic Myelogenous Leukemia Cells Induces Resistance to Imatinib in a Kinase-Dependent Manner. *J. Biol. Chem.* **2010**, *285*, 21446–21457.

(229) Hu, Y.; Liu, Y.; Pelletier, S.; Buchdunger, E.; Warmuth, M.; Fabbro, D.; Hallek, M.; Van Etten, R. A.; Li, S. Requirement of Src Kinases Lyn, Hck and Fgr for BCR-ABL1-Induced B-Lymphoblastic Leukemia but Not Chronic Myeloid Leukemia. *Nat. Genet.* **2004**, *36*, 453–461.

(230) Mitina, O.; Warmuth, M.; Krause, G.; Hallek, M.; Obermeier, A. Src Family Tyrosine Kinases Phosphorylate Flt3 on Juxtamembrane Tyrosines and Interfere with Receptor Maturation in a Kinase-Dependent Manner. *Ann. Hematol.* **2007**, *86*, 777–785.

(231) Saito, Y.; Kitamura, H.; Hijikata, A.; Tomizawa-Murasawa, M.; Tanaka, S.; Takagi, S.; Uchida, N.; Suzuki, N.; Sone, A.; Najima, Y.; *et al.* Identification of Therapeutic Targets for Quiescent, Chemotherapy-Resistant Human Leukemia Stem Cells. *Sci. Transl. Med.* **2010**, *2*, 17ra9.

(232) Lopez, S.; Voisset, E.; Tisserand, J. C.; Mosca, C.; Prebet, T.; Santamaria, D.; Dubreuil, P.; De Sepulveda, P. An Essential Pathway Links FLT3-ITD, HCK and CDK6 in Acute Myeloid Leukemia. *Oncotarget* **2016**, *7*, 51163–51173.

(233) Yang, C.; Lu, P.; Lee, F. Y.; Chadburn, A.; Barrientos, J. C.; Leonard, J. P.; Ye, F.; Zhang, D.; Knowles, D. M.; Wang, Y. L. Tyrosine Kinase Inhibition in Diffuse Large B-Cell Lymphoma: Molecular Basis for Antitumor Activity and Drug Resistance of Dasatinib. *Leukemia* **2008**, *22*, 1755–1766.

(234) Hausherr, A.; Tavares, R.; Schäffer, M.; Obermeier, A.; Miksch, C.; Mitina, O.; Ellwart, J.; Hallek, M.; Krause, G. Inhibition of IL-6-Dependent Growth of Myeloma Cells by an Acidic Peptide Repressing the gp130-Mediated Activation of Src Family Kinases. *Oncogene* **2007**, *26*, 4987–4998.

(235) Kaposi's Sarcoma and Pneumocystis Pneumonia among Homosexual Men--New York City and California. *MMWR. Morb. Mortal. Wkly. Rep.* **1981**, *30*, 305–308.

(236) Sepkowitz, K. A. AIDS — The First 20 Years. *N. Engl. J. Med.* **2001**, *344*, 1764–1772.

(237) Rom, W. N.; Markowitz, S. B. *Environmental and Occupational Medicine*; Lippincott Williams & Wilkins, **2007**.

(238) Nordqvist, C. HIV / AIDS : Causes , Symptoms and Treatments http://www.medicalnewstoday.com/articles/17131.php.

(239) Seitz, R. Human Immunodeficiency Virus (HIV). *Transfusion Medicine and Hemotherapy*. **2016**, *45*, 203–222.

(240) Klasse, P. J. The Molecular Basis of HIV Entry. *Cell. Microbiol*. **2012**, *14*, 1183–1192.

(241) Haseltine, W. A. Molecular Biology of the Human Immunodeficiency Virus Type 1. *FASEB J.* **1991**, *5*, 2349–2360.

(242) Lamers, S. L.; Fogel, G. B.; Singer, E. J.; Salemi, M.; Nolan, D. J.; Huysentruyt, L. C.; McGrath, M. S. HIV-1 Nef in Macrophage-Mediated Disease Pathogenesis. *Int. Rev. Immunol.* **2012**, *31*, 432–450.

(243) Abraham, L.; Fackler, O. T. HIV-1 Nef: A Multifaceted Modulator of T Cell Receptor Signaling. *Cell Commun. Signal.* **2012**, *10*, 39.

(244) Nazari-Shafti, T. Z.; Freisinger, E.; Roy, U.; Bulot, C. T.; Senst, C.; Dupin, C. L.; Chaffin, A. E.; Srivastava, S. K.; Mondal, D.; Alt, E. U.; *et al*. Mesenchymal Stem Cell Derived Hematopoietic Cells Are Permissive to HIV-1 Infection. *Retrovirology* **2011**, *8*, 3.

(245) Alvarado, J. J.; Tarafdar, S.; Yeh, J. I.; Smithgall, T. E. Interaction with the Src Homology (SH3-SH2) Region of the Src-Family Kinase Hck Structures the HIV-1 Nef Dimer for Kinase Activation and Effector Recruitment. *J. Biol. Chem.* **2014**, *289*, 28539–28553.

(246) Choi, H.-J.; Smithgall, T. E. Conserved Residues in the HIV-1 Nef Hydrophobic Pocket Are Essential for Recruitment and Activation of the Hck Tyrosine Kinase. *J. Mol. Biol.* **2004**, *343*, 1255–1268.

(247) Lee, C. H.; Leung, B.; Lemmon, M. A.; Zheng, J.; Cowburn, D.; Kuriyan, J.; Saksela, K. A Single Amino Acid in the SH3 Domain of Hck Determines Its High Affinity and Specificity in Binding to HIV-1 Nef Protein. *EMBO J.* **1995**, *14*, 5006–5015.

(248) Briggs, S. D.; Sharkey, M.; Stevenson, M.; Smithgall, T. E. SH3-Mediated Hck Tyrosine Kinase Activation and Fibroblast Transformation by the Nef Protein of HIV-1. *J. Biol. Chem.* **1997**, *272*, 17899–17902.

(249) Trible, R. P.; Emert-Sedlak, L.; Wales, T. E.; Ayyavoo, V.; Engen, J. R.; Smithgall, T. E. Allosteric Loss-of-Function Mutations in HIV-1 Nef from a Long-Term Non-Progressor. *J. Mol. Biol.* **2007**, *374*, 121–129.

(250) Kim, M.-O.; Suh, H.-S.; Si, Q.; Terman, B. I.; Lee, S. C. Anti-CD45RO Suppresses Human Immunodeficiency Virus Type 1 Replication in Microglia: Role of Hck Tyrosine Kinase and Implications for AIDS Dementia. *J. Virol.* **2006**, *80*, 62–72.

(251) Shinya, E.; Shimizu, M.; Owaki, A.; Paoletti, S.; Mori, L.; De Libero, G.; Takahashi, H. Hemopoietic Cell Kinase (Hck) and p21-Activated Kinase 2 (PAK2) Are Involved in the down-Regulation of CD1a Lipid Antigen Presentation by HIV-1 Nef in Dendritic Cells. *Virology* **2016**, *487*, 285–295.

(252) Malim, M. H.; Emerman, M. HIV-1 Accessory Proteins--Ensuring Viral Survival in a Hostile Environment. *Cell Host Microbe* **2008**, *3*, 388–398.

(253) Marcsisin, S. R.; Narute, P. S.; Emert-Sedlak, L. A.; Kloczewiak, M.; Smithgall, T. E.; Engen, J. R. On the Solution Conformation and Dynamics of the HIV-1 Viral Infectivity Factor. *J. Mol. Biol.* **2011**, *410*, 1008–1022.

(254) Firestone, G. L.; Giampaolo, J. R.; O'Keeffe, B. A. Stimulus-Dependent Regulation of Serum and Glucocorticoid Inducible Protein Kinase (SGK) Transcription, Subcellular Localization and Enzymatic Activity. *Cell. Physiol. Biochem.* **2003**, *13*, 1–12.

(255) Mora, A.; Komander, D.; van Aalten, D. M. F.; Alessi, D. R. PDK1, the Master Regulator

of AGC Kinase Signal Transduction. *Semin. Cell Dev. Biol.* **2004**, *15*, 161–170.

(256) Frödin, M.; Antal, T. L.; Dümmler, B. A.; Jensen, C. J.; Deak, M.; Gammeltoft, S.; Biondi, R. M. A Phosphoserine/threonine-Binding Pocket in AGC Kinases and PDK1 Mediates Activation by Hydrophobic Motif Phosphorylation. *EMBO J.* **2002**, *21*, 5396–5407.

(257) Bruhn, M. A.; Pearson, R. B.; Hannan, R. D.; Sheppard, K. E. Second AKT: The Rise of SGK in Cancer Signalling. *Growth Factors* **2010**, *28*, 394–408.

(258) Lang, F.; Bohmer, C.; Palmada, M.; Seebohm, G.; Strutz-Seebohm, N.; Vallon, V. (Patho)physiological Significance of the Serum- and Glucocorticoid-Inducible Kinase Isoforms. *Physiol. Rev.* **2006**, *86*, 1151–1178.

(259) Park, J.; Leong, M. L.; Buse, P.; Maiyar, A. C.; Firestone, G. L.; Hemmings, B. A. Serum and Glucocorticoid-Inducible Kinase (SGK) Is a Target of the PI 3-Kinase-Stimulated Signaling Pathway. *EMBO J.* **1999**, *18*, 3024–3033.

(260) Chen, S.; Bhargava, A.; Mastroberardino, L.; Meijer, O. C.; Wang, J.; Buse, P.; Firestone, G. L.; Verrey, F.; Pearce, D. Epithelial Sodium Channel Regulated by Aldosterone-Induced Protein Sgk. *Pro. Nat. Acad. Sci. U. S. A.* **1999**, *96*, 2514–2519.

(261) Perrotti, N.; He, R. A.; Phillips, S. A.; Haft, C. R.; Taylor, S. I. Activation of Serum- and Glucocorticoid-Induced Protein Kinase (Sgk) by Cyclic AMP and Insulin. *J. Biol. Chem.* **2001**, *276*, 9406–9412.

(262) Menniti, M.; Iuliano, R.; Amato, R.; Boito, R.; Corea, M.; Le Pera, I.; Gulletta, E.; Fuiano, G.; Perrotti, N. Serum and Glucocorticoid-Regulated Kinase Sgk1 Inhibits Insulin-Dependent Activation of Phosphomannomutase 2 in Transfected COS-7 Cells. *Am. J. Physiol. Cell Physiol.* **2005**, *288*, 148-55.

(263) Faletti, C. J.; Perrotti, N.; Taylor, S. I.; Blazer-Yost, B. L. Sgk: An Essential Convergence Point for Peptide and Steroid Hormone Regulation of ENaC-Mediated Na+ Transport. *Am. J. Physiol. Cell Physiol.* **2002**, *282*, C494-500.

(264) Amato, R.; Menniti, M.; Agosti, V.; Boito, R.; Costa, N.; Bond, H. M.; Barbieri, V.; Tagliaferri, P.; Venuta, S.; Perrotti, N. IL-2 Signals through Sgk1 and Inhibits Proliferation and Apoptosis in Kidney Cancer Cells. *J. Mol. Med.* **2007**, *85*, 707–721.

(265) Boini, K. M.; Bhandaru, M.; Mack, A.; Lang, F. Steroid Hormone Release as Well as Renal Water and Electrolyte Excretion of Mice Expressing PKB/SGK-Resistant GSK3. *Pflugers Arch.* **2008**, *456*, 1207–1216.

(266) Waldegger, S.; Klingel, K.; Barth, P.; Sauter, M.; Rfer, M. L.; Kandolf, R.; Lang, F. H-Sgk Serine-Threonine Protein Kinase Gene as Transcriptional Target of Transforming Growth Factor Beta in Human Intestine. *Gastroenterology* **1999**, *116*, 1081–1088.

(267) Mizuno, H.; Nishida, E. The ERK MAP Kinase Pathway Mediates Induction of SGK (Serum- and Glucocorticoid-Inducible Kinase) by Growth Factors. *Genes Cells* **2001**, *6*, 261–268.

(268) Maiyar, A. C.; Huang, A. J.; Phu, P. T.; Cha, H. H.; Firestone, G. L. p53 Stimulates Promoter Activity of the Sgk. Serum/glucocorticoid-Inducible Serine/threonine Protein Kinase Gene in Rodent Mammary Epithelial Cells. *J. Biol. Chem.* **1996**, *271*, 12414–12422.

(269) Waldegger, S.; Barth, P.; Raber, G.; Lang, F. Cloning and Characterization of a Putative Human Serine/threonine Protein Kinase Transcriptionally Modified during Anisotonic and Isotonic Alterations of Cell Volume. *Proc. Natl. Acad. Sci. U. S. A.* **1997**, *94*, 4440–4445.

(270) Leong, M. L. L.; Maiyar, A. C.; Kim, B.; O'Keeffe, B. A.; Firestone, G. L. Expression of the Serum- and Glucocorticoid-Inducible Protein Kinase, Sgk, Is a Cell Survival Response to Multiple Types of Environmental Stress Stimuli in Mammary Epithelial Cells. *J. Biol. Chem.* **2003**, *278*, 5871–5882.

(271) Imaizumi, K.; Tsuda, M.; Wanaka, A.; Tohyama, M.; Takagi, T. Differential Expression of Sgk mRNA, a Member of the Ser/Thr Protein Kinase Gene Family, in Rat Brain after CNS Injury. *Brain Res. Mol. Brain Res.* **1994**, *26*, 189–196.

(272) Fillon, S.; Klingel, K.; Wärntges, S.; Sauter, M.; Gabrysch, S.; Pestel, S.; Tanneur, V.; Waldegger, S.; Zipfel, A.; Viebahn, R.; *et al*. Expression of the Serine/Threonine Kinase hSGK1 in Chronic Viral Hepatitis. *Cell. Physiol. Biochem.* **2002**, *12*, 47–54.

(273) Zhou, R.; Snyder, P. M. Nedd4-2 Phosphorylation Induces Serum and Glucocorticoid-Regulated Kinase (SGK) Ubiquitination and Degradation. *J. Biol. Chem.* **2005**, *280*, 4518–4523.

(274) Hong, F.; Larrea, M. D.; Doughty, C.; Kwiatkowski, D. J.; Squillace, R.; Slingerland, J. M. mTOR-Raptor Binds and Activates SGK1 to Regulate p27 Phosphorylation. *Mol. Cell* **2008**, *30*, 701–711.

(275) Hayashi, M.; Tapping, R. I.; Chao, T. H.; Lo, J. F.; King, C. C.; Yang, Y.; Lee, J. D. BMK1 Mediates Growth Factor-Induced Cell Proliferation through Direct Cellular

Activation of Serum and Glucocorticoid-Inducible Kinase. *J. Biol. Chem.* **2001**, *276*, 8631–8634.

(276) Meng, F.; Yamagiwa, Y.; Taffetani, S.; Han, J.; Patel, T. IL-6 Activates Serum and Glucocorticoid Kinase via p38alpha Mitogen-Activated Protein Kinase Pathway. *Am. J. Physiol. Cell Physiol.* **2005**, *289*, 971-81.

(277) Castel, P.; Scaltriti, M. The Emerging Role of Serum/glucocorticoid-Regulated Kinases in Cancer. *Cell Cycle*. **2017**, *16*, 5–6.

(278) Mikosz, C. A.; Brickley, D. R.; Sharkey, M. S.; Moran, T. W.; Conzen, S. D. Glucocorticoid Receptor-Mediated Protection from Apoptosis Is Associated with Induction of the Serine/threonine Survival Kinase Gene, Sgk-1. *J. Biol. Chem.* **2001**, *276*, 16649–16654.

(279) Wu, W.; Chaudhuri, S.; Brickley, D. R.; Pang, D.; Karrison, T.; Conzen, S. D. Microarray Analysis Reveals Glucocorticoid-Regulated Survival Genes That Are Associated with Inhibition of Apoptosis in Breast Epithelial Cells. *Cancer Res.* **2004**, *64*, 1757–1764.

(280) Amato, R.; D'Antona, L.; Porciatti, G.; Agosti, V.; Menniti, M.; Rinaldo, C.; Costa, N.; Bellacchio, E.; Mattarocci, S.; Fuiano, G.; *et al*. Sgk1 Activates MDM2-Dependent p53 Degradation and Affects Cell Proliferation, Survival, and Differentiation. *J. Mol. Med.* **2009**, *87*, 1221–1239.

(281) Amato, R.; Scumaci, D.; D'Antona, L.; Iuliano, R.; Menniti, M.; Di Sanzo, M.; Faniello, M. C.; Colao, E.; Malatesta, P.; Zingone, A.; *et al*. Sgk1 Enhances RANBP1 Transcript Levels and Decreases Taxol Sensitivity in RKO Colon Carcinoma Cells. *Oncogene* **2013**, *32*, 4572–4578.

(282) Murray, J. T.; Campbell, D. G.; Morrice, N.; Auld, G. C.; Shpiro, N.; Marquez, R.; Peggie, M.; Bain, J.; Bloomberg, G. B.; Grahammer, F.; *et al*. Exploitation of KESTREL to Identify NDRG Family Members as Physiological Substrates for SGK1 and GSK3. *Biochem. J.* **2004**, *384*, 477–488.

(283) Sahin, P.; McCaig, C.; Jeevahan, J.; Murray, J. T.; Hainsworth, A. H. The Cell Survival Kinase SGK1 and Its Targets FOXO3a and NDRG1 in Aged Human Brain. *Neuropathol. Appl. Neurobiol.* **2013**, *39*, 623–633.

(284) Li, Y.; Pan, P.; Qiao, P.; Liu, R. Downregulation of N-Myc Downstream Regulated Gene 1 Caused by the Methylation of CpG Islands of NDRG1 Promoter Promotes

Proliferation and Invasion of Prostate Cancer Cells. *Int. J. Oncol.* **2015**, *47*, 1001–1008.

(285) Liu, W.; Yue, F.; Zheng, M.; Merlot, A.; Bae, D.-H.; Huang, M.; Lane, D.; Jansson, P.; Lui, G. Y. L.; Richardson, V.; *et al*. The Proto-Oncogene c-Src and Its Downstream Signaling Pathways Are Inhibited by the Metastasis Suppressor, NDRG1. *Oncotarget* **2015**, *6*, 8851–8874.

(286) Broggini, T.; Wustner, M.; Harms, C.; Stange, L.; Blaes, J.; Thome, C.; Harms, U.; Mueller, S.; Weiler, M.; Wick, W.; *et al*. NDRG1 Overexpressing Gliomas Are Characterized by Reduced Tumor Vascularization and Resistance to Antiangiogenic Treatment. *Cancer Lett.* **2016**, *380*, 568–576.

(287) Yan, X.; Chua, M.-S.; Sun, H.; So, S. N-Myc down-Regulated Gene 1 Mediates Proliferation, Invasion, and Apoptosis of Hepatocellular Carcinoma Cells. *Cancer Lett.* **2008**, *262*, 133–142.

(288) Ortuso, F.; Amato, R.; Artese, A.; D'antona, L.; Costa, G.; Talarico, C.; Gigliotti, F.; Bianco, C.; Trapasso, F.; Schenone, S.; *et al*. In Silico Identification and Biological Evaluation of Novel Selective Serum/Glucocorticoid-Inducible Kinase 1 Inhibitors Based on the Pyrazolo-Pyrimidine Scaffold. *J. Chem. Inf. Model.* **2014**, *54*, 1828–1832.

(289) Isikbay, M.; Otto, K.; Kregel, S.; Kach, J.; Cai, Y.; Vander Griend, D. J.; Conzen, S. D.; Szmulewitz, R. Z. Glucocorticoid Receptor Activity Contributes to Resistance to Androgen-Targeted Therapy in Prostate Cancer. *Horm. Cancer* **2014**, *5*, 72–89.

(290) D'Antona, L.; Amato, R.; Talarico, C.; Ortuso, F.; Menniti, M.; Dattilo, V.; Iuliano, R.; Gigliotti, F.; Artese, A.; Costa, G.; *et al.* SI113, a Specific Inhibitor of the Sgk1 Kinase Activity That Counteracts Cancer Cell Proliferation. *Cell. Physiol. Biochem.* **2015**, *35*, 2006–2018.

(291) Conza, D.; Mirra, P.; Cali, G.; Tortora, T.; Insabato, L.; Fiory, F.; Schenone, S.; Amato, R.; Beguinot, F.; Perrotti, N.; *et al*. The SGK1 Inhibitor SI113 Induces Autophagy, Apoptosis, and Endoplasmic Reticulum Stress in Endometrial Cancer Cells. *J. Cell. Physiol.* **2017**, *232*, 3735–3743.

(292) Sommer, E. M.; Dry, H.; Cross, D.; Guichard, S.; Davies, B. R.; Alessi, D. R. Elevated SGK1 Predicts Resistance of Breast Cancer Cells to Akt Inhibitors. *Biochem. J.* **2013**, *452*, 499–508.

(293) Abbruzzese, C.; Mattarocci, S.; Pizzuti, L.; Mileo, A. M.; Visca, P.; Antoniani, B.; Alessandrini, G.; Facciolo, F.; Amato, R.; D'Antona, L.; *et al*. Determination of SGK1

mRNA in Non-Small Cell Lung Cancer Samples Underlines High Expression in Squamous Cell Carcinomas. *J. Exp. Clin. Cancer Res.* **2012**, *31*, 4.

(294) Chung, E. J.; Sung, Y. K.; Farooq, M.; Kim, Y.; Im, S.; Tak, W. Y.; Hwang, Y. J.; Kim, Y. Il; Han, H. S.; Kim, J. C.; *et al.* Gene Expression Profile Analysis in Human Hepatocellular Carcinoma by cDNA Microarray. *Mol. Cells* **2002**, *14*, 382–387.

(295) Talarico, C.; D'Antona, L.; Scumaci, D.; Barone, A.; Gigliotti, F.; Fiumara, C. V.; Dattilo, V.; Gallo, E.; Visca, P.; Ortuso, F.; *et al*. Preclinical Model in HCC: The SGK1 Kinase Inhibitor SI113 Blocks Tumor Progression *in Vitro* and *in Vivo* and Synergizes with Radiotherapy. *Oncotarget* **2015**, *6*, 37511–37525.

(296) Talarico, C.; Dattilo, V.; D'Antona, L.; Barone, A.; Amodio, N.; Belviso, S.; Musumeci, F.; Abbruzzese, C.; Bianco, C.; Trapasso, F.; *et al*. SI113, a SGK1 Inhibitor, Potentiates the Effects of Radiotherapy, Modulates the Response to Oxidative Stress and Induces Cytotoxic Autophagy in Human Glioblastoma Multiforme Cells. *Oncotarget* **2016**, *7*, 15868–15884.

(297) Catalogna, G.; Talarico, C.; Dattilo, V.; Gangemi, V.; Calabria, F.; D'Antona, L.; Schenone, S.; Musumeci, F.; Bianco, C.; Perrotti, N.; *et al*. The SGK1 Kinase Inhibitor SI113 Sensitizes Theranostic Effects of the $^{64}CuCl_2$ in Human Glioblastoma Multiforme Cells. *Cell. Physiol. Biochem.* **2017**, *43*, 108–119.

(298) Dattilo, V.; D'Antona, L.; Talarico, C.; Capula, M.; Catalogna, G.; Iuliano, R.; Schenone, S.; Roperto, S.; Bianco, C.; Perrotti, N.; *et al*. SGK1 Affects RAN/RANBP1/RANGAP1 via SP1 to Play a Critical Role in Pre-miRNA Nuclear Export: A New Route of Epigenomic Regulation. *Scientific Reports*. **2017**, *7*, 45361.

(299) Sherk, A. B.; Frigo, D. E.; Schnackenberg, C. G.; Bray, J. D.; Laping, N. J.; Trizna, W.; Hammond, M.; Patterson, J. R.; Thompson, S. K.; Kazmin, D.; *et al*. Development of a Small Molecule Serum and Glucocorticoid-Regulated Kinase 1 Antagonist and Its Evaluation as a Prostate Cancer Therapeutic. *Cancer Res*. **2008**, *68*, 7475–7483.

(300) Szmulewitz, R. Z.; Chung, E.; Al-Ahmadie, H.; Daniel, S.; Kocherginsky, M.; Razmaria, A.; Zagaja, G. P.; Brendler, C. B.; Stadler, W. M.; Conzen, S. D. Serum/glucocorticoid-Regulated Kinase 1 Expression in Primary Human Prostate Cancers. *Prostate* **2012**, *72*, 157–164.

(301) Liu, W.; Wang, X.; Liu, Z.; Wang, Y.; Yin, B.; Yu, P.; Duan, X.; Liao, Z.; Chen, Y.; Liu, C.; *et al*. SGK1 Inhibition Induces Autophagy-Dependent Apoptosis via the mTOR-

Foxo3a Pathway. *Br. J. Cancer* **2017**, *117*, 1139.

(302) Liang, X.; Lan, C.; Zhou, J.; Fu, W.; Long, X.; An, Y.; Jiao, G.; Wang, K.; Li, Y.; Xu, J.; *et al*. Development of a New Analog of SGK1 Inhibitor and Its Evaluation as a Therapeutic Molecule of Colorectal Cancer. *J. Cancer*. **2017**, *8*, 2256–2262.

(303) Salker, M. S.; Christian, M.; Steel, J. H.; Nautiyal, J.; Lavery, S.; Trew, G.; Webster, Z.; Al-Sabbagh, M.; Puchchakayala, G.; Föller, M.; *et al*. Deregulation of the Serum- and Glucocorticoid-Inducible Kinase SGK1 in the Endometrium Causes Reproductive Failure. *Nat. Med.* **2011**, *17*, 1509.

(304) Salis, O.; Bedir, A.; Gulten, S.; Okuyucu, A.; Kulcu, C.; Alacam, H. Cytotoxic Effect of Fluvastatin on MCF-7 Cells Possibly through a Reduction of the mRNA Expression Levels of SGK1 and CAV1. *Cancer Biother. Radiopharm.* **2014**, *29*, 368–375.

(305) Castel, P.; Ellis, H.; Bago, R.; Toska, E.; Razavi, P.; Carmona, F. J.; Kannan, S.; Verma, C. S.; Dickler, M.; Chandarlapaty, S.; *et al*. PDK1-SGK1 Signaling Sustains AKT-Independent mTORC1 Activation and Confers Resistance to PI3Kα Inhibition. *Cancer Cell*. **2016**, *30*, 229–242.

(306) Shi, G.; Wang, Q.; Zhou, X.; Li, J.; Liu, H.; Gu, J.; Wang, H.; Wu, Y.; Ding, L.; Ni, S.; *et al*. Response of Human Non-Small-Cell Lung Cancer Cells to the Influence of Wogonin with SGK1 Dynamics. *Acta Biochim. Biophys. Sin.* **2017**, *49*, 1045.

(307) Won, M.; Park, K. A.; Byun, H. S.; Kim, Y.-R.; Choi, B. L.; Hong, J. H.; Park, J.; Seok, J. H.; Lee, Y.-H.; Cho, C.-H.; *et al*. Protein Kinase SGK1 Enhances MEK/ERK Complex Formation through the Phosphorylation of ERK2: Implication for the Positive Regulatory Role of SGK1 on the ERK Function during Liver Regeneration. *J. Hepatol.* **2009**, *51*, 67–76.

(308) Salis, O.; Okuyucu, A.; Bedir, A.; Gor, U.; Kulcu, C.; Yenen, E.; Kilic, N. Antimetastatic Effect of Fluvastatin on Breast and Hepatocellular Carcinoma Cells in Relation to SGK1 and NDRG1 Genes. *Tumour Biol.* **2016**, *37*, 3017–3024.

(309) Kulkarni, S.; Goel, S.; Sengupta, S.; Cochran, B. H. A Large-Scale RNAi Screen Identifies SGK1 as a Key Survival Kinase for GBM Stem Cells. *Mol. Cancer Res.* **2017**.

(310) Boini, K. M.; Nammi, S.; Grahammer, F.; Osswald, H.; Kuhl, D.; Lang, F. Role of Serum- and Glucocorticoid-Inducible Kinase SGK1 in Glucocorticoid Regulation of Renal Electrolyte Excretion and Blood Pressure. *Kidney Blood Press. Res.* **2008**, *31*, 280–289.

(311) von Wowern, F.; Berglund, G.; Carlson, J.; Mansson, H.; Hedblad, B.; Melander, O. Genetic Variance of SGK-1 Is Associated with Blood Pressure, Blood Pressure Change over Time and Strength of the Insulin-Diastolic Blood Pressure Relationship. *Kidney Int.* **2005**, *68*, 2164–2172.

(312) Schwab, M.; Lupescu, A.; Mota, M.; Mota, E.; Frey, A.; Simon, P.; Mertens, P. R.; Floege, J.; Luft, F.; Asante-Poku, S.; *et al.* Association of SGK1 Gene Polymorphisms with Type 2 Diabetes. *Cell. Physiol. Biochem.* **2008**, *21*, 151–160.

(313) Lang, F.; Huang, D. Y.; Vallon, V. SGK, Renal Function and Hypertension. *J. Nephrol.* **2010**, *23*, 124-129.

(314) Schernthaner-Reiter, M. H.; Kiefer, F.; Zeyda, M.; Stulnig, T. M.; Luger, A.; Vila, G. Strong Association of Serum- and Glucocorticoid-Regulated Kinase 1 with Peripheral and Adipose Tissue Inflammation in Obesity. *Int. J. Obes.* **2015**, *39*, 1143–1150.

(315) Petersen, K. F.; Shulman, G. I. Etiology of Insulin Resistance. *Am. J. Med.* **2006**, *119*, S10-6.

(316) Li, P.; Pan, F.; Hao, Y.; Feng, W.; Song, H.; Zhu, D. SGK1 Is Regulated by Metabolic-Related Factors in 3T3-L1 Adipocytes and Overexpressed in the Adipose Tissue of Subjects with Obesity and Diabetes. *Diabetes Res. Clin. Pract.* **2013**, *102*, 35–42.

(317) Zuccotto, F.; Ardini, E.; Casale, E.; Angiolini, M. Through The "gatekeeper Door": Exploiting the Active Kinase Conformation. *J. Med. Chem.* **2010**, *53*, 2681–2694.

(318) Hassan, A. Q.; Sharma, S. V; Warmuth, M. Allosteric Inhibition of BCR-ABL. *Cell Cycle* **2010**, *9*, 3710–3714.

(319) Ma, J.; Huang, H.; Chen, S.; Chen, Y.; Xin, X.; Lin, L.; Ding, J.; Liu, H.; Meng, L. PH006, a Novel and Selective Src Kinase Inhibitor, Suppresses Human Breast Cancer Growth and Metastasis *in Vitro* and *in Vivo*. *Breast Cancer Res. Treat.* **2011**, *130*, 85–96.

(320) Huang, H.; Ma, J.; Shi, J.; Meng, L.; Jiang, H.; Ding, J.; Liu, H. Discovery of Novel Purine Derivatives with Potent and Selective Inhibitory Activity against c-Src Tyrosine Kinase. *Bioorg. Med. Chem.* **2010**, *18*, 4615–4624.

(321) Fallah-Tafti, A.; Foroumadi, A.; Tiwari, R.; Shirazi, A. N.; Hangauer, D. G.; Bu, Y.; Akbarzadeh, T.; Parang, K.; Shafiee, A. Thiazolyl N-Benzyl-Substituted Acetamide Derivatives: Synthesis, Src Kinase Inhibitory and Anticancer Activities. *Eur. J. Med. Chem.* **2011**, *46*, 4853–4858.

(322) Naing, A.; Cohen, R.; Dy, G. K.; Hong, D. S.; Dyster, L.; Hangauer, D. G.; Kwan, R.; Fetterly, G.; Kurzrock, R.; Adjei, A. A. A Phase I Trial of KX2-391, a Novel Non-ATP Competitive Substrate-Pocket- Directed SRC Inhibitor, in Patients with Advanced Malignancies. *Invest. New Drugs* **2013**, *31*, 967–973.

(323) Antonarakis, E. S.; Heath, E. I.; Posadas, E. M.; Yu, E. Y.; Harrison, M. R.; Bruce, J. Y.; Cho, S. Y.; Wilding, G. E.; Fetterly, G. J.; Hangauer, D. G.; *et al*. A Phase 2 Study of KX2-391, an Oral Inhibitor of Src Kinase and Tubulin Polymerization, in Men with Bone-Metastatic Castration-Resistant Prostate Cancer. *Cancer Chemother. Pharmacol.* **2013**, *71*, 883–892.

(324) Moroco, J. A.; Baumgartner, M. P.; Rust, H. L.; Choi, H. G.; Hur, W.; Gray, N. S.; Camacho, C. J.; Smithgall, T. E. A Discovery Strategy for Selective Inhibitors of c-Src in Complex with the Focal Adhesion Kinase SH3/SH2-Binding Region. *Chem. Biol. Drug Des*. **2015**, *86*, 144–155.

(325) Cox, K. J.; Shomin, C. D.; Ghosh, I. Tinkering Outside the Kinase ATP Box: Allosteric (Type IV) and Bivalent (Type V) Inhibitors of Protein Kinases. *Future Med. Chem.* **2011**, *3*, 29–43.

(326) Parang, K.; Till, J. H.; Ablooglu, A. J.; Kohanski, R. A.; Hubbard, S. R.; Cole, P. A. Mechanism-Based Design of a Protein Kinase Inhibitor. *Nat. Struct. Biol.* **2001**, *8*, 37–41.

(327) Gower, C. M.; Chang, M. E. K.; Maly, D. J. Bivalent Inhibitors of Protein Kinases. *Crit. Rev. Biochem. Mol. Biol.* **2014**, *49*, 102–115.

(328) Lavogina, D.; Enkvist, E.; Uri, A. Bisubstrate Inhibitors of Protein Kinases: From Principle to Practical Applications. *ChemMedChem* **2010**, *5*, 23–34.

(329) Brandvold, K. R.; Santos, S. M.; Breen, M. E.; Lachacz, E. J.; Steffey, M. E.; Soellner, M. B. Exquisitely Specific Bisubstrate Inhibitors of c-Src Kinase. *ACS Chem. Biol.* **2015**, *10*, 1387–1391.

(330) Musumeci, F.; Schenone, S.; Brullo, C.; Botta, M. An Update on Dual Src/Abl Inhibitors. *Future Med. Chem.* **2012**, *4*, 799–822.

(331) Hanke, J. H.; Gardner, J. P.; Dow, R. L.; Changelian, P. S.; Brissette, W. H.; Weringer, E. J.; Pollok, B. A.; Connelly, P. A. Discovery of a Novel, Potent, and Src Family-Selective Tyrosine Kinase Inhibitor. Study of Lck- and FynT-Dependent T Cell Activation. *J. Biol. Chem.* **1996**, *271*, 695–701.

(332) Tatton, L.; Morley, G. M.; Chopra, R.; Khwaja, A. The Src-Selective Kinase Inhibitor PP1 Also Inhibits Kit and Bcr-Abl Tyrosine Kinases. *J. Biol. Chem.* **2003**, *278*, 4847–4853.

(333) Kong, L.; Deng, Z.; Shen, H.; Zhang, Y. Src Family Kinase Inhibitor PP2 Efficiently Inhibits Cervical Cancer Cell Proliferation through down-Regulating Phospho-Src-Y416 and Phospho-EGFR-Y1173. *Mol. Cell. Biochem.* **2011**, *348*, 11–19.

(334) Usui, M.; Uno, M.; Nishida, E. Src Family Kinases Suppress Differentiation of Brown Adipocytes and Browning of White Adipocytes. *Genes Cells* **2016**, *21*, 302–310.

(335) Lombardo, L. J.; Lee, F. Y.; Chen, P.; Norris, D.; Barrish, J. C.; Behnia, K.; Castaneda, S.; Cornelius, L. A. M.; Das, J.; Doweyko, A. M.; *et al.* Discovery of *N*-(2-Chloro-6-Methyl- Phenyl)-2-(6-(4-(2-Hydroxyethyl)- Piperazin-1-yl)-2-Methylpyrimidin-4-Ylamino)thiazole-5-Carboxamide (BMS-354825), a Dual Src/Abl Kinase Inhibitor with Potent Antitumor Activity in Preclinical Assays. *J. Med. Chem.* **2004**, *47*, 6658–6661.

(336) Konig, H.; Copland, M.; Chu, S.; Jove, R.; Holyoake, T. L.; Bhatia, R. Effects of Dasatinib on SRC Kinase Activity and Downstream Intracellular Signaling in Primitive Chronic Myelogenous Leukemia Hematopoietic Cells. *Cancer Res.* **2008**, *68*, 9624–9633.

(337) Aplenc, R.; Blaney, S. M.; Strauss, L. C.; Balis, F. M.; Shusterman, S.; Ingle, A. M.; Agrawal, S.; Sun, J.; Wright, J. J.; Adamson, P. C. Pediatric Phase I Trial and Pharmacokinetic Study of Dasatinib: A Report from the Children's Oncology Group Phase I Consortium. *J. Clin. Oncol.* **2011**, *29*, 839–844.

(338) Boschelli, D. H.; Ye, F.; Wang, Y. D.; Dutia, M.; Johnson, S. L.; Wu, B.; Miller, K.; Powell, D. W.; Yaczko, D.; Young, M.; *et al.* Optimization of 4-Phenylamino-3-Quinolinecarbonitriles as Potent Inhibitors of Src Kinase Activity. *J. Med. Chem.* **2001**, *44*, 3965–3977.

(339) Thaimattam, R.; Daga, P. R.; Banerjee, R.; Iqbal, J. 3D-QSAR Studies on c-Src Kinase Inhibitors and Docking Analyses of a Potent Dual Kinase Inhibitor of c-Src and c-Abl Kinases. *Bioorg. Med. Chem.* **2005**, *13*, 4704–4712.

(340) Golas, J. M.; Arndt, K.; Etienne, C.; Lucas, J.; Nardin, D.; Gibbons, J.; Frost, P.; Ye, F.; Boschelli, D. H.; Boschelli, F. SKI-606, a 4-Anilino-3-Quinolinecarbonitrile Dual Inhibitor of Src and Abl Kinases, Is a Potent Antiproliferative Agent against Chronic Myelogenous Leukemia Cells in Culture and Causes Regression of K562 Xenografts in

Nude Mice. *Cancer Res.* **2003**, *63*, 375–381.

(341) Puttini, M.; Coluccia, A. M. L.; Boschelli, F.; Cleris, L.; Marchesi, E.; Donella-Deana, A.; Ahmed, S.; Redaelli, S.; Piazza, R.; Magistroni, V.; *et al*. *In Vitro* and *in Vivo* Activity of SKI-606, a Novel Src-Abl Inhibitor, against Imatinib-Resistant Bcr-Abl+ Neoplastic Cells. *Cancer Res.* **2006**, *66*, 11314–11322.

(342) Tesar, V.; Ciechanowski, K.; Pei, Y.; Barash, I.; Shannon, M.; Li, R.; Williams, J. H.; Levisetti, M.; Arkin, S.; Serra, A. Bosutinib versus Placebo for Autosomal Dominant Polycystic Kidney Disease. *J. Am. Soc. Nephrol.* **2017**, *28*, 3404–3413.

(343) Green, T. P.; Fennell, M.; Whittaker, R.; Curwen, J.; Jacobs, V.; Allen, J.; Logie, A.; Hargreaves, J.; Hickinson, D. M.; Wilkinson, R. W.; *et al*. Preclinical Anticancer Activity of the Potent, Oral Src Inhibitor AZD0530. *Mol. Oncol.* **2009**, *3*, 248–261.

(344) Hennequin, L. F.; Allen, J.; Breed, J.; Curwen, J.; Fennell, M.; Green, T. P.; Lambert-van der Brempt, C.; Morgentin, R.; Norman, R. A.; Olivier, A.; *et al*. *N*-(5-Chloro-1,3-Benzodioxol-4-yl)-7-[2-(4-Methylpiperazin-1-yl)ethoxy]-5- (Tetrahydro-2*H*-Pyran-4-yloxy)quinazolin-4-Amine, a Novel, Highly Selective, Orally Available, Dual-Specific c-Src/Abl Kinase Inhibitor. *J. Med. Chem.* **2006**, *49*, 6465–6488.

(345) Hiscox, S.; Jordan, N. J.; Smith, C.; James, M.; Morgan, L.; Taylor, K. M.; Green, T. P.; Nicholson, R. I. Dual Targeting of Src and ER Prevents Acquired Antihormone Resistance in Breast Cancer Cells. *Breast Cancer Res. Treat.* **2009**, *115*, 57–67.

(346) Chen, Y.; Alvarez, E. A.; Azzam, D.; Wander, S. A.; Guggisberg, N.; Jordà, M.; Ju, Z.; Hennessy, B. T.; Slingerland, J. M. Combined Src and ER Blockade Impairs Human Breast Cancer Proliferation *in Vitro* and *in Vivo*. *Breast Cancer Res. Treat.* **2011**, *128*, 69–78.

(347) Chang, Y.-M.; Bai, L.; Liu, S.; Yang, J. C.; Kung, H.-J.; Evans, C. P. Src Family Kinase Oncogenic Potential and Pathways in Prostate Cancer as Revealed by AZD0530. *Oncogene* **2008**, *27*, 6365–6375.

(348) Azam, M.; Nardi, V.; Shakespeare, W. C.; Metcalf, C. A.; Bohacek, R. S.; Wang, Y.; Sundaramoorthi, R.; Sliz, P.; Veach, D. R.; Bornmann, W. G.; *et al*. Activity of Dual SRC-ABL Inhibitors Highlights the Role of BCR/ABL Kinase Dynamics in Drug Resistance. *Proc. Natl. Acad. Sci. U. S. A.* **2006**, *103*, 9244–9249.

(349) Zhou, T.; Commodore, L.; Huang, W.-S.; Wang, Y.; Sawyer, T. K.; Shakespeare, W. C.; Clackson, T.; Zhu, X.; Dalgarno, D. C. Structural Analysis of DFG-in and DFG-out Dual

Src-Abl Inhibitors Sharing a Common Vinyl Purine Template. *Chem. Biol. Drug Des.* **2010**, *75*, 18–28.

(350) Ohanian, M.; Cortes, J.; Kantarjian, H.; Jabbour, E. Tyrosine Kinase Inhibitors in Acute and Chronic Leukemias. *Expert Opin. Pharmacother.* **2012**, *13*, 927–938.

(351) Parker, W. T.; Yeung, D. T. O.; Yeoman, A. L.; Altamura, H. K.; Jamison, B. A.; Field, C. R.; Hodgson, J. G.; Lustgarten, S.; Rivera, V. M.; Hughes, T. P.; *et al*. The Impact of Multiple Low-Level BCR-ABL1 Mutations on Response to Ponatinib. *Blood* **2016**, *127*, 1870–1880.

(352) Desogus, A.; Schenone, S.; Brullo, C.; Tintori, C.; Musumeci, F. Bcr-Abl Tyrosine Kinase Inhibitors: A Patent Review. *Expert Opin. Ther. Pat.* **2015**, *25*, 397–412.

(353) Weisberg, E.; Choi, H. G.; Ray, A.; Barrett, R.; Zhang, J.; Sim, T.; Zhou, W.; Seeliger, M.; Cameron, M.; Azam, M.; *et al.* Discovery of a Small-Molecule Type II Inhibitor of Wild-Type and Gatekeeper Mutants of BCR-ABL, PDGFRα, Kit, and Src Kinases: Novel Type II Inhibitor of Gatekeeper Mutants. *Blood* **2010**, *115*, 4206–4216.

(354) Kinoshita, T.; Matsubara, M.; Ishiguro, H.; Okita, K.; Tada, T. Structure of Human Fyn Kinase Domain Complexed with Staurosporine. *Biochem. Biophys. Res. Commun.* **2006**, *346*, 840–844.

(355) Dalgarno, D.; Stehle, T.; Narula, S.; Schelling, P.; van Schravendijk, M. R.; Adams, S.; Andrade, L.; Keats, J.; Ram, M.; Jin, L.; *et al*. Structural Basis of Src Tyrosine Kinase Inhibition with a New Class of Potent and Selective Trisubstituted Purine-Based Compounds. *Chem. Biol. Drug Des.* **2006**, *67*, 46–57.

(356) Wang, Y.; Metcalf, C. A.; Shakespeare, W. C.; Sundaramoorthi, R.; Keenan, T. P.; Bohacek, R. S.; van Schravendijk, M. R.; Violette, S. M.; Narula, S. S.; Dalgarno, D. C.; *et al.* Bone-Targeted 2,6,9-Trisubstituted Purines: Novel Inhibitors of Src Tyrosine Kinase for the Treatment of Bone Diseases. *Bioorg. Med. Chem. Lett.* **2003**, *13*, 3067–3070.

(357) Nygaard, H. B.; van Dyck, C. H.; Strittmatter, S. M. Fyn Kinase Inhibition as a Novel Therapy for Alzheimer's Disease. *Alzheimers Res. Ther*. **2014**, *6*, 8.

(358) Nygaard, H. B.; Wagner, A. F.; Bowen, G. S.; Good, S. P.; MacAvoy, M. G.; Strittmatter, K. A.; Kaufman, A. C.; Rosenberg, B. J.; Sekine-Konno, T.; Varma, P.; *et al*. A Phase Ib Multiple Ascending Dose Study of the Safety, Tolerability, and Central Nervous System Availability of AZD0530 (Saracatinib) in Alzheimer's Disease. *Alzheimers. Res.*

Ther. **2015**, *7*, 35.

(359) Papanikos, A.; Freyne, E.J.E.; Ten Holte, P.; Willems, M. . E.; W.C.J.; Mevellec, L.A.; Storck, P. H. Preparation of Quinazoline Derivatives as Antitumor Agents. WO2008006884, **2008**.

(360) Moy, F. J.; Lee, A.; Gavrin, L. K.; Xu, Z. B.; Sievers, A.; Kieras, E.; Stochaj, W.; Mosyak, L.; McKew, J.; Tsao, D. H. H. Novel Synthesis and Structural Characterization of a High-Affinity Paramagnetic Kinase Probe for the Identification of Non-ATP Site Binders by Nuclear Magnetic Resonance. *J. Med. Chem.* **2010**, *53*, 1238–1249.

(361) Bamborough, P.; Drewry, D.; Harper, G.; Smith, G. K.; Schneider, K. Assessment of Chemical Coverage of Kinome Space and Its Implications for Kinase Drug Discovery. *J. Med. Chem.* **2008**, *51*, 7898–7914.

(362) DiMauro, E. F.; Newcomb, J.; Nunes, J. J.; Bemis, J. E.; Boucher, C.; Chai, L.; Chaffee, S. C.; Deak, H. L.; Epstein, L. F.; Faust, T.; *et al*. Structure-Guided Design of Aminopyrimidine Amides as Potent, Selective Inhibitors of Lymphocyte Specific Kinase: Synthesis, Structure-Activity Relationships, and Inhibition of *in Vivo* T Cell Activation. *J. Med. Chem.* **2008**, *51* , 1681–1694.

(363) Wang, Y. D.; Miller, K.; Boschelli, D. H.; Ye, F.; Wu, B.; Floyd, M. B.; Powell, D. W.; Wissner, A.; Weber, J. M.; Boschelli, F. Inhibitors of Src Tyrosine Kinase: The Preparation and Structure-Activity Relationship of 4-Anilino-3-Cyanoquinolines and 4-Anilinoquinazolines. *Bioorg. Med. Chem. Lett.* **2000**, *10*, 2477–2480.

(364) Boschelli, D. H.; Wang, Y. D.; Ye, F.; Wu, B.; Zhang, N.; Dutia, M.; Powell, D. W.; Wissner, A.; Arndt, K.; Weber, J. M.; *et al*. Synthesis and Src Kinase Inhibitory Activity of a Series of 4-Phenylamino-3-Quinolinecarbonitriles. *J. Med. Chem.* **2001**, *44*, 822–833.

(365) Berger, D. M.; Dutia, M.; Birnberg, G.; Powell, D.; Boschelli, D. H.; Wang, Y. D.; Ravi, M.; Yaczko, D.; Golas, J.; Lucas, J.; *et al*. 4-Anilino-7,8-Dialkoxybenzo[*g*]quinoline-3-Carbonitriles as Potent Src Kinase Inhibitors. *J. Med. Chem.* **2005**, *48*, 5909–5920.

(366) Nathan Tumey, L.; Boschelli, D. H.; Lee, J.; Chaudhary, D. 2-Alkenylthieno[2,3-*b*]pyridine-5-Carbonitriles: Potent and Selective Inhibitors of PKCθ. *Bioorg. Med. Chem. Lett.* **2008**, *18*, 4420–4423.

(367) Li, J.; Rix, U.; Fang, B.; Bai, Y.; Edwards, A.; Colinge, J.; Bennett, K. L.; Gao, J.; Song, L.; Eschrich, S.; *et al*. A Chemical and Phosphoproteomic Characterization of Dasatinib

Action in Lung Cancer. *Nat. Chem. Biol.* **2010**, *6*, 291–299.

(368) Wityak, J.; Das, J.; Moquin, R. V.; Shen, Z.; Lin, J.; Chen, P.; Doweyko, A. M.; Pitt, S.; Pang, S.; Shen, D. R.; *et al.* Discovery and Initial SAR of 2-Amino-5-Carboxamidothiazoles as Inhibitors of the Src-Family Kinase p56(Lck). *Bioorg. Med. Chem. Lett.* **2003**, *13*, 4007–4010.

(369) Chen, P.; Norris, D.; Das, J.; Spergel, S. H.; Wityak, J.; Leith, L.; Zhao, R.; Chen, B.-C.; Pitt, S.; Pang, S.; *et al.* Discovery of Novel 2-(Aminoheteroaryl)-Thiazole-5-Carboxamides as Potent and Orally Active Src-Family Kinase p56(Lck) Inhibitors. *Bioorg. Med. Chem. Lett.* **2004**, *14*, 6061–6066.

(370) Blake, R. A.; Broome, M. A.; Liu, X.; Wu, J.; Gishizky, M.; Sun, L.; Courtneidge, S. A. SU6656, a Selective Src Family Kinase Inhibitor, Used to Probe Growth Factor Signaling. *Mol. Cell. Biol.* **2000**, *20*, 9018–9027.

(371) Guan, H.; Laird, A. D.; Blake, R. A.; Tang, C.; Liang, C. Design and Synthesis of Aminopropyl Tetrahydroindole-Based Indolin-2-Ones as Selective and Potent Inhibitors of Src and Yes Tyrosine Kinase. *Bioorg. Med. Chem. Lett.* **2004**, *14*, 187–190.

(372) Kilic-Kurt, Z.; Olgen, A. O.-B. and S. Synthesis, Biological and Computational Evaluation of Novel Oxindole Derivatives as Inhibitors of Src Family Kinases. *Lett. Drug Des. Discov*. **2013**, *10*, 713–718.

(373) Chen, P.; Doweyko, A. M.; Norris, D.; Gu, H. H.; Spergel, S. H.; Das, J.; Moquin, R. V.; Lin, J.; Wityak, J.; Iwanowicz, E. J.; *et al*. Imidazoquinoxaline Src-Family Kinase p56Lck Inhibitors: SAR, QSAR, and the Discovery of (S)-*N*-(2-Chloro-6-Methylphenyl)-2-(3-Methyl-1-Piperazinyl)imidazo-[1,5-*a*]pyrido[3,2-*e*]pyrazin-6-Amine (BMS-279700) as a Potent and Orally Active Inhibitor with Excellent *In Vivo* Antiinflammatory Activity. *J. Med. Chem.* **2004**, *47*, 4517–4529.

(374) Ho, C. Y.; Ludovici, D. W.; Maharoof, U. S. M.; Mei, J.; Sechler, J. L.; Tuman, R. W.; Strobel, E. D.; Andraka, L.; Yen, H.-K.; Leo, G.; *et al*. (6,7-Dimethoxy-2,4-dihydroindeno[1,2-*c*]pyrazol-3-yl)phenylamines: Platelet-Derived Growth Factor Receptor Tyrosine Kinase Inhibitors with Broad Antiproliferative Activity against Tumor Cells. *J. Med. Chem.* **2005**, *48*, 8163–8173.

(375) Artusi, R.; Caselli, G.; Rovati, L. New Fyn Kinase Inhibitors, WO2016146220, **2016**.

(376) Kang, N. J.; Lee, K. W.; Shin, B. J.; Jung, S. K.; Hwang, M. K.; Bode, A. M.; Heo, Y.-S.; Lee, H. J.; Dong, Z. Caffeic Acid, a Phenolic Phytochemical in Coffee, Directly

Inhibits Fyn Kinase Activity and UVB-Induced COX-2 Expression. *Carcinogenesis*. **2009**, *30*, 321–330.

(377) Jelić, D.; Mildner, B.; Kostrun, S.; Nujić, K.; Verbanac, D.; Culić, O.; Antolović, R.; Brandt, W. Homology Modeling of Human Fyn Kinase Structure: Discovery of Rosmarinic Acid as a New Fyn Kinase Inhibitor and in Silico Study of Its Possible Binding Modes. *J. Med. Chem.* **2007**, *50*, 1090–1100.

(378) He, Z.; Tang, F.; Ermakova, S.; Li, M.; Zhao, Q.; Cho, Y.-Y.; Ma, W.-Y.; Choi, H.-S.; Bode, A. M.; Yang, C. S.; *et al*. Fyn Is a Novel Target of (-)-Epigallocatechin Gallate in the Inhibition of JB6 Cl41 Cell Transformation. *Mol. Carcinog.* **2008**, *47*, 172–183.

(379) Jung, S. K.; Lee, K. W.; Byun, S.; Kang, N. J.; Lim, S. H.; Heo, Y.-S.; Bode, A. M.; Bowden, G. T.; Lee, H. J.; Dong, Z. Myricetin Suppresses UVB-Induced Skin Cancer by Targeting Fyn. *Cancer Res.* **2008**, *68*, 6021–6029.

(380) Hwang, M. K.; Kang, N. J.; Heo, Y.-S.; Lee, K. W.; Lee, H. J. Fyn Kinase Is a Direct Molecular Target of Delphinidin for the Inhibition of Cyclooxygenase-2 Expression Induced by Tumor Necrosis Factor-Alpha. *Biochem. Pharmacol.* **2009**, *77*, 1213–1222.

(381) Kim, A. Y.; Lee, C. G.; Lee, D. Y.; Li, H.; Jeon, R.; Ryu, J. H.; Kim, S. G. Enhanced Antioxidant Effect of Prenylated Polyphenols as Fyn Inhibitor. *Free Radic. Biol. Med.* **2012**, *53*, 1198–1208.

(382) Koo, J. H.; Lee, W. H.; Lee, C. G.; Kim, S. G. Fyn Inhibition by Cycloalkane-Fused 1,2-Dithiole-3-Thiones Enhances Antioxidant Capacity and Protects Mitochondria from Oxidative Injury. *Mol. Pharmacol.* **2012**, *82*, 27–36.

(383) Krishnamurty, R.; Brigham, J. L.; Leonard, S. E.; Ranjitkar, P.; Larson, E. T.; Dale, E. J.; Merritt, E. A.; Maly, D. J. Active Site Profiling Reveals Coupling between Domains in SRC-Family Kinases. *Nat. Chem. Biol.* **2013**, *9*, 43–50.

(384) Rauch, J.; Volinsky, N.; Romano, D.; Kolch, W. The Secret Life of Kinases: Functions beyond Catalysis. *Cell Commun. Signal. CCS* **2011**, *9*, 23.

(385) Saito, Y.; Yuki, H.; Kuratani, M.; Hashizume, Y.; Takagi, S.; Honma, T.; Tanaka, A.; Shirouzu, M.; Mikuni, J.; Handa, N.; *et al*. A Pyrrolo-Pyrimidine Derivative Targets Human Primary AML Stem Cells *in Vivo*. *Sci. Transl. Med.* **2013**, *5*, 181ra52.

(386) Parker, L. J.; Taruya, S.; Tsuganezawa, K.; Ogawa, N.; Mikuni, J.; Honda, K.; Tomabechi, Y.; Handa, N.; Shirouzu, M.; Yokoyama, S.; *et al*. Kinase Crystal Identification and ATP-Competitive Inhibitor Screening Using the Fluorescent Ligand

SKF86002. *Acta Crystallogr. D. Biol. Crystallogr.* **2014**, *70*, 392–404.

(387) Calderwood, D. J.; Johnston, D. N.; Munschauer, R.; Rafferty, P. Pyrrolo[2,3-*d*]pyrimidines Containing Diverse N-7 Substituents as Potent Inhibitors of Lck. *Bioorg. Med. Chem. Lett.* **2002**, *12*, 1683–1686.

(388) Radi, M.; Tintori, C.; Musumeci, F.; Brullo, C.; Zamperini, C.; Dreassi, E.; Fallacara, A. L.; Vignaroli, G.; Crespan, E.; Zanoli, S.; *et al.* Design, Synthesis, and Biological Evaluation of Pyrazolo[3,4-*d*]pyrimidines Active *in Vivo* on the Bcr-Abl T315I Mutant. *J. Med. Chem.* **2013**, *56*, 5382–5394.

(389) Schenone, S.; Radi, M.; Musumeci, F.; Brullo, C.; Botta, M. Biologically Driven Synthesis of Pyrazolo[3,4-*d*]pyrimidines As Protein Kinase Inhibitors: An Old Scaffold As a New Tool for Medicinal Chemistry and Chemical Biology Studies. *Chem. Rev.* **2014**, *114*, 7189–7238.

(390) Tintori, C.; Laurenzana, I.; La Rocca, F.; Falchi, F.; Carraro, F.; Ruiz, A.; Este, J. A.; Kissova, M.; Crespan, E.; Maga, G.; *et al.* Identification of Hck Inhibitors as Hits for the Development of Antileukemia and Anti-HIV Agents. *ChemMedChem* **2013**, *8*, 1353–1360.

(391) Ranjitkar, P.; Brock, A. M.; Maly, D. J. Affinity Reagents That Target a Specific Inactive Form of Protein Kinases. *Chem. Biol.* **2010**, *17*, 195–206.

(392) Fang, Z.; Grütter, C.; Rauh, D. Strategies for the Selective Regulation of Kinases with Allosteric Modulators: Exploiting Exclusive Structural Features. *ACS Chem. Biol.* **2013**, *8*, 58–70.

(393) Pene-Dumitrescu, T.; Shu, S. T.; Wales, T. E.; Alvarado, J. J.; Shi, H.; Narute, P.; Moroco, J. A.; Yeh, J. I.; Engen, J. R.; Smithgall, T. E. HIV-1 Nef Interaction Influences the ATP-Binding Site of the Src-Family Kinase, Hck. *BMC Chem. Biol.* **2012**, *12*, 1.

(394) Hassan, R.; Suzu, S.; Hiyoshi, M.; Takahashi-Makise, N.; Ueno, T.; Agatsuma, T.; Akari, H.; Komano, J.; Takebe, Y.; Motoyoshi, K.; *et al.* Dys-Regulated Activation of a Src Tyroine Kinase Hck at the Golgi Disturbs N-Glycosylation of a Cytokine Receptor Fms. *J. Cell. Physiol.* **2009**, *221*, 458–468.

(395) Chutiwitoonchai, N.; Hiyoshi, M.; Mwimanzi, P.; Ueno, T.; Adachi, A.; Ode, H.; Sato, H.; Fackler, O. T.; Okada, S.; Suzu, S. The Identification of a Small Molecule Compound That Reduces HIV-1 Nef-Mediated Viral Infectivity Enhancement. *PLoS One* **2011**, *6*, e27696.

(396) Gwanmesia, P. M.; Romanski, A.; Schwarz, K.; Bacic, B.; Ruthardt, M.; Ottmann, O. G. The Effect of the Dual Src/Abl Kinase Inhibitor AZD0530 on Philadelphia Positive Leukaemia Cell Lines. *BMC Cancer* **2009**, *9*, 53.

(397) Sabat, M.; VanRens, J. C.; Laufersweiler, M. J.; Brugel, T. A.; Maier, J.; Golebiowski, A.; De, B.; Easwaran, V.; Hsieh, L. C.; Walter, R. L.; *et al*. The Development of 2-Benzimidazole Substituted Pyrimidine Based Inhibitors of Lymphocyte Specific Kinase (Lck). *Bioorg. Med. Chem. Lett.* **2006**, *16*, 5973–5977.

(398) Narita Y, Matsuki M, T. K. Treatment of Acute Myeloid Leukemia with an HCK Inhibitor. WO2015181628A1, **2015**.

(399) Kim, J.-E.; Kim, J. H.; Lee, Y.; Yang, H.; Heo, Y.-S.; Bode, A. M.; Lee, K. W.; Dong, Z. Bakuchiol Suppresses Proliferation of Skin Cancer Cells by Directly Targeting Hck, Blk, and p38 MAP Kinase. *Oncotarget* **2016**, *7*, 14616–14627.

(400) Bain, J.; Plater, L.; Elliott, M.; Shpiro, N.; Hastie, C. J.; McLauchlan, H.; Klevernic, I.; Arthur, J. S. C.; Alessi, D. R.; Cohen, P. The Selectivity of Protein Kinase Inhibitors: A Further Update. *Biochem. J.* **2007**, *408*, 297–315.

(401) Berdel, H. O.; Yin, H.; Liu, J. Y.; Grochowska, K.; Middleton, C.; Yanasak, N.; Abdelsayed, R.; Berdel, W. E.; Mozaffari, M.; Yu, J. C.; *et al*. Targeting Serum Glucocorticoid-Regulated Kinase-1 in Squamous Cell Carcinoma of the Head and Neck: A Novel Modality of Local Control. *PLoS One* **2014**, *9*, e113795.

(402) Mansley, M. K.; Wilson, S. M. Effects of Nominally Selective Inhibitors of the Kinases PI3K, SGK1 and PKB on the Insulin-Dependent Control of Epithelial Na^+ Absorption. *Br. J. Pharmacol.* **2010**, *161*, 571–588.

(403) Towhid, S. T.; Liu, G.-L.; Ackermann, T. F.; Beier, N.; Scholz, W.; Fuchss, T.; Toulany, M.; Rodemann, H.-P.; Lang, F. Inhibition of Colonic Tumor Growth by the Selective SGK Inhibitor EMD638683. *Cell. Physiol. Biochem.* **2013**, *32*, 838–848.

(404) Ackermann, T. F.; Boini, K. M.; Beier, N.; Scholz, W.; Fuchss, T.; Lang, F. EMD638683, a Novel SGK Inhibitor with Antihypertensive Potency. *Cell. Physiol. Biochem.* **2011**, *28*, 137–146.

(405) Nazarè, M.; Halland, N.; Schmidt, F.; Weiss, T. .; Dietz, U.; Hofmeister, A. .; Carry, J. C. *N*-[a-(1*H*-pyrazolo[3,4-*b*]pyrazin-6-yl)-Phenyl]-Sulfonamides and Their Use as Pharmaceuticals. WO2013041119, **2013**.

(406) El-Moghazy, S. M.; George, R. F.; Osman, E. E. A.; Elbatrawy, A. A.; Kissova, M.;

Colombo, A.; Crespan, E.; Maga, G. Novel Pyrazolo[3,4-*d*]pyrimidines as Dual Src-Abl Inhibitors Active against Mutant Form of Abl and the Leukemia K-562 Cell Line. *Eur. J. Med. Chem.* **2016**, *123*, 1–13.

(407) Lan, T.; Wang, H.; Zhang, Z.; Zhang, M.; Qu, Y.; Zhao, Z.; Fan, X.; Zhan, Q.; Song, Y.; Yu, C. Downregulation of Beta-Arrestin 1 Suppresses Glioblastoma Cell Malignant Progression Vis Inhibition of Src Signaling. *Exp. Cell Res.* **2017**, *357*, 51–58.

(408) Ceccherini, E.; Indovina, P.; Zamperini, C.; Dreassi, E.; Casini, N.; Cutaia, O.; Forte, I. M.; Pentimalli, F.; Esposito, L.; Polito, M. S.; *et al*. SRC Family Kinase Inhibition Through a New Pyrazolo[3,4-*d*]pyrimidine Derivative as a Feasible Approach for Glioblastoma Treatment. *J. Cell. Biochem.* **2015**, *116*, 856–863.

(409) Anderson, F. E.; Kaminsky, D.; Dubnick, B.; Klutchko, S. R.; Cetenko, W. A.; Gylys, J.; Hart, J. A. Chemistry and Pharmacology of Monoamine Oxidase Inhibitors: Hydrazine Derivatives. *J. Med. Pharm. Chem.* **1962**, *5*, 221–230.

(410) Benoit, G. Hydroxyalcoylhydrazine. *Bull. Soc. Chim. Fr* **1939**, *6*, 708–715.

(411) Musumeci, F.; Sanna, M.; Greco, C.; Giacchello, I.; Fallacara, A. L.; Amato, R.; Schenone, S. Pyrrolo[2,3-*d*]pyrimidines Active as Btk Inhibitors. *Expert Opin. Ther. Pat.* **2017**, *27*, 1305–1318.

(412) Musumeci, F.; Sanna, M.; Grossi, G.; Brullo, C.; Fallacara, A. L.; Schenone, S. Pyrrolo[2,3-*d*]pyrimidines as Kinase Inhibitors. *Curr. Med. Chem.* **2017**, *24*, 2059–2085.

(413) Flanagan, M. E.; Blumenkopf, T. A.; Brissette, W. H.; Brown, M. F.; Casavant, J. M.; Shang-Poa, C.; Doty, J. L.; Elliott, E. A.; Fisher, M. B.; Hines, M.; *et al*. Discovery of CP-690,550: A Potent and Selective Janus Kinase (JAK) Inhibitor for the Treatment of Autoimmune Diseases and Organ Transplant Rejection. *J. Med. Chem.* **2010**, *53*, 8468–8484.

(414) Deisseroth, A.; Kaminskas, E.; Grillo, J.; Chen, W.; Saber, H.; Lu, H. L.; Rothmann, M. D.; Brar, S.; Wang, J.; Garnett, C.; *et al*. U.S. Food and Drug Administration Approval: Ruxolitinib for the Treatment of Patients with Intermediate and High-Risk Myelofibrosis. *Clin. Cancer Res.* **2012**, *18*, 3212–3217.

(415) Gonzales, A. J.; Bowman, J. W.; Fici, G. J.; Zhang, M.; Mann, D. W.; Mitton-Fry, M. Oclacitinib (APOQUEL(®)) Is a Novel Janus Kinase Inhibitor with Activity against Cytokines Involved in Allergy. *J. Vet. Pharmacol. Ther.* **2014**, *37*, 317–324.

(416) Traxler, P.; Allegrini, P. R.; Brandt, R.; Brueggen, J.; Cozens, R.; Fabbro, D.; Grosios,

K.; Lane, H. A.; McSheehy, P.; Mestan, J.; *et al*. AEE788: A Dual Family Epidermal Growth Factor receptor/ErbB2 and Vascular Endothelial Growth Factor Receptor Tyrosine Kinase Inhibitor with Antitumor and Antiangiogenic Activity. *Cancer Res.* **2004**, *64*, 4931–4941.

(417) Valverde, A.; Penarando, J.; Canas, A.; Lopez-Sanchez, L. M.; Conde, F.; Hernandez, V.; Peralbo, E.; Lopez-Pedrera, C.; de la Haba-Rodriguez, J.; Aranda, E.; *et al*. Simultaneous Inhibition of EGFR/VEGFR and Cyclooxygenase-2 Targets Stemness-Related Pathways in Colorectal Cancer Cells. *PLoS One* **2015**, *10*, e0131363.

(418) Yap, T. A.; Walton, M. I.; Hunter, L.-J. K.; Valenti, M.; de Haven Brandon, A.; Eve, P. D.; Ruddle, R.; Heaton, S. P.; Henley, A.; Pickard, L.; *et al*. Preclinical Pharmacology, Antitumor Activity and Development of Pharmacodynamic Markers for the Novel, Potent AKT Inhibitor CCT128930. *Mol. Cancer Ther*. **2011**, *10*, 360–371.

(419) Addie, M.; Ballard, P.; Buttar, D.; Crafter, C.; Currie, G.; Davies, B. R.; Debreczeni, J.; Dry, H.; Dudley, P.; Greenwood, R.; *et al*. Discovery of 4-Amino-*N*-[(1S)-1-(4-Chlorophenyl)-3-Hydroxypropyl]-1-(7*H*-pyrrolo[2,3-*d*]pyrimidin-4-yl)piperidine-4-Carboxamide (AZD5363), an Orally Bioavailable, Potent Inhibitor of Akt Kinases. *J. Med. Chem.* **2013**, *56*, 2059–2073.

(420) Laurent, A.; Rose, Y. Preparation of Pyrrolopyrimidinamines as Protein Kinase Inhibitors and Therapeutic Uses Thereof. WO2015077866, **2015**.

(421) Kaspersen, S. J.; Han, J.; Norsett, K. G.; Rydsa, L.; Kjobli, E.; Bugge, S.; Bjorkoy, G.; Sundby, E.; Hoff, B. H. Identification of New 4-*N*-Substituted 6-Aryl-7*H*-Pyrrolo[2,3-*d*]pyrimidine-4-Amines as Highly Potent EGFR-TK Inhibitors with Src-Family Activity. *Eur. J. Pharm. Sci.* **2014**, *59*, 69–82.

(422) Dincer, S.; Cetin, K. T.; Onay-Besikci, A.; Olgen, S. Synthesis, Biological Evaluation and Docking Studies of New Pyrrolo[2,3-*d*]pyrimidine Derivatives as Src Family-Selective Tyrosine Kinase Inhibitors. *J. Enzyme Inhib. Med. Chem.* **2013**, *28*, 1080–1087.

(423) Baker, B. R.; Joseph, J. P.; Schaub, R. E. Puromycin. Synthetic Studies I. Synthesis of 6-Dimethylaminopurine, An Hydrolytic Fragment. *J. Org. Chem.* **1954**, *19*, 631–637.

(424) Noell, C. W.; Robins, R. K. Aromaticity in Heterocyclic Systems. II. the Application of N.M.R. in a Study of the Synthesis and Structure of Certain lmidazo[1,2-*c*]pyrimidines and Related Pyrrolo[2,3-*d*]pyrimidines. *J. Heterocycl. Chem.* **1964**, *1*, 34–41.

(425) Medina, M.; Avila, J. New Insights into the Role of Glycogen Synthase Kinase-3 in Alzheimer's Disease. *Expert Opin. Ther. Targets* **2014**, *18*, 69–77.

(426) Yang, K.; Belrose, J.; Trepanier, C. H.; Lei, G.; Jackson, M. F.; MacDonald, J. F. Fyn, a Potential Target for Alzheimer's Disease. *J. Alzheimer's Dis. JAD* **2011**, *27*, 243–252.

(427) Zamperini, C.; Dreassi, E.; Vignaroli, G.; Radi, M.; Dragoni, S.; Schenone, S.; Musumeci, F.; Valoti, M.; Antiochia, R.; Botta, M. CYP-Dependent Metabolism of Antitumor Pyrazolo[3,4-*d*]pyrimidine Derivatives Is Characterized by an Oxidative Dechlorination Reaction. *Drug Metab. Pharmacokinet.* **2014**, *29*, 433–440.

(428) Robins, R. K. Potential Purine Antagonists. I. Synthesis of Some 4,6-Substituted Pyrazolo[3,4-*d*]pyrimidines1. *J. Am. Chem. Soc.* **1956**, *78*, 784–790.

(429) Hirst, G. C.; Calderwood, D.; Wishart, N.; Rafferty, P.; Ritter, K.; Arnold, L. D.; Friedman, M. M. Preparation of Pyrazolopyrimidines as Protein Kinase Inhibitors. WO 2001019829, **2001**.

(430) Hanefeld, U.; Rees, C. W.; White, A. J. P.; Williams, D. J. One-Pot Synthesis of Tetrasubstituted Pyrazoles—proof of Regiochemistry. *J. Chem. Soc. Perkin Trans. 1* **1996**, *13*, 1545–1552.

(431) Schindler, T.; Sicheri, F.; Pico, A.; Gazit, A.; Levitzki, A.; Kuriyan, J. Crystal Structure of Hck in Complex with a Src Family-Selective Tyrosine Kinase Inhibitor. *Mol. Cell* **1999**, *3*, 639–648.

(432) E. Ballana, E. Pauls, J. Senserrich, B. Clotet, F. Perron-Sierra, G. C. T.; Este, J. A. Cell Adhesion through alphaV-Containing Integrins Is Required for Efficient HIV-1 Infection in Macrophages. *Blood* **2009**, *113*, 1278–1286.

(433) Ballana, E.; Pauls, E.; Clotet, B.; Perron-Sierra, F.; Tucker, G. C.; Esté, J. A. β5 Integrin Is the Major Contributor to the αV Integrin-Mediated Blockade of HIV-1 Replication. *J. Immunol.* **2011**, *186*, 464–470.

(434) Van Duyne, R.; Guendel, I.; Jaworski, E.; Sampey, G.; Klase, Z.; Chen, H.; Zeng, C.; Kovalskyy, D.; El Kouni, M. H.; Lepene, B.; *et al*. Effect of Mimetic CDK9 Inhibitors on HIV-1-Activated Transcription. *J. Mol. Biol.* **2013**, *425*, 812–829.

(435) Garron, M. L.; Arthos, J.; Guichou, J. F.; McNally, J.; Cicala, C.; Arold, S. T. Structural Basis for the Interaction between Focal Adhesion Kinase and CD4. *J. Mol. Biol.* **2008**, *375*, 1320–1328.

(436) Readinger, J. A.; Schiralli, G. M.; Jiang, J.-K.; Thomas, C. J.; August, A.; Henderson,

A. J.; Schwartzberg, P. L. Selective Targeting of ITK Blocks Multiple Steps of HIV Replication. *Proc. Natl. Acad. Sci. U. S. A.* **2008**, *105*, 6684–6689.

(437) Landires, I.; Nunez-Samudio, V.; Theze, J. Short Communication: Nuclear JAK3 and Its Involvement in CD4 Activation in HIV-Infected Patients. *AIDS Res. Hum. Retroviruses* **2013**, *29*, 784–787.

(438) Lee, E. S.; Kalantari, P.; Tsutsui Section, S.; Klatt, A.; Holden, J.; Correll, P. H.; Power Section, C.; Henderson, A. J. RON Receptor Tyrosine Kinase, a Negative Regulator of Inflammation, Inhibits HIV-1 Transcription in Monocytes/macrophages and Is Decreased in Brain Tissue from Patients with AIDS. *J. Immunol.* **2004**, *173*, 6864–6872.

(439) Pochetti, G.; Montanari, R.; Gege, C.; Chevrier, C.; Taveras, A. G.; Mazza, F. Extra Binding Region Induced by Non-Zinc Chelating Inhibitors into the S1' Subsite of Matrix Metalloproteinase 8 (MMP-8). *J. Med. Chem.* **2009**, *52*, 1040–1049.

(440) Raghu Prasad, M.; Pran Kishore, D. Multistep, Microwave Assisted, Solvent Free Synthesis and Antibacterial Activity of 6-Substituted-2,3,4-trihydropyrimido[1,2-*c*]9,10,11,12-tetrahydrobenzo[*b*]thieno[3,2-*e*]pyrimidines. *Chem. Pharm. Bull.* **2007**, *55*, 776–779.

(441) Fujita, M.; Hirayama, T.; Ikeda, N. Design, Synthesis and Bioactivities of Novel Diarylthiophenes: Inhibitors of Tumor Necrosis Factor-Alpha (TNF-Alpha) Production. *Bioorg. Med. Chem.* **2002**, *10*, 3113–3122.

(442) Lupea X. A., Padure M. Synthesis and Characterization of Some N-Substituted Amides of Salicylic Acid. *Proceedings for Natural Sciences*, **2003**, *104*, 5-10.

(443) Sun, X.; Lv, X. H.; Ye, L. M.; Hu, Y.; Chen, Y. Y.; Zhang, X. J.; Yan, M. Synthesis of Benzimidazoles via Iridium-Catalyzed Acceptorless Dehydrogenative Coupling. *Org. Biomol. Chem.* **2015**, *13*, 7381–7383.

(444) Dreassi, E.; Zizzari, A. T.; Mori, M.; Filippi, I.; Belfiore, A.; Naldini, A.; Carraro, F.; Santucci, A.; Schenone, S.; Botta, M. 2-Hydroxypropyl-β-Cyclodextrin Strongly Improves Water Solubility and Anti-Proliferative Activity of pyrazolo[3,4-*d*]pyrimidines Src-Abl Dual Inhibitors. *Eur. J. Med. Chem.* **2010**, *45*, 5958–5964.

(445) Vignaroli, G.; Calandro, P.; Zamperini, C.; Coniglio, F.; Iovenitti, G.; Tavanti, M.; Colecchia, D.; Dreassi, E.; Valoti, M.; Schenone, S.; *et al*. Improvement of Pyrazolo[3,4-*d*]pyrimidines Pharmacokinetic Properties: Nanosystem Approaches for Drug Delivery. *Sci. Rep.* **2016**, *6*, 21509.

(446) Fallacara, A. L.; Mancini, A.; Zamperini, C.; Dreassi, E.; Marianelli, S.; Chiariello, M.; Pozzi, G.; Santoro, F.; Botta, M.; Schenone, S. Pyrazolo[3,4-*d*]pyrimidines-Loaded Human Serum Albumin (HSA) Nanoparticles: Preparation, Characterization and Cytotoxicity Evaluation against Neuroblastoma Cell Line. *Bioorg. Med. Chem. Lett.* **2017**, *27*, 3196–3200.

(447) Vignaroli, G.; Zamperini, C.; Dreassi, E.; Radi, M.; Angelucci, A.; Sanità, P.; Crespan, E.; Kissova, M.; Maga, G.; Schenone, S.; *et al*. Pyrazolo[3,4-*d*]pyrimidine Prodrugs: Strategic Optimization of the Aqueous Solubility of Dual Src/Abl Inhibitors. *ACS Med. Chem. Lett.* **2013**, *4*, 622–626.

(448) Baghel, S.; Cathcart, H.; O'Reilly, N. J. Polymeric Amorphous Solid Dispersions: A Review of Amorphization, Crystallization, Stabilization, Solid-State Characterization, and Aqueous Solubilization of Biopharmaceutical Classification System Class II Drugs. *J. Pharm. Sci.* **2016**, *105*, 2527–2544.

(449) Vo, C. L.-N.; Park, C.; Lee, B.-J. Current Trends and Future Perspectives of Solid Dispersions Containing Poorly Water-Soluble Drugs. *Eur. J. Pharm. Biopharm.* **2013**, *85*, 799–813.

(450) Huang, Y.; Dai, W.-G. Fundamental Aspects of Solid Dispersion Technology for Poorly Soluble Drugs. *Acta Pharm. Sin. B* **2014**, *4*, 18–25.

(451) Van Eerdenbrugh, B.; Taylor, L. S. Small Scale Screening to Determine the Ability of Different Polymers to Inhibit Drug Crystallization upon Rapid Solvent Evaporation. *Mol. Pharm.* **2010**, *7*, 1328–1337.

(452) Taresco, V.; Louzao, I.; Scurr, D.; Booth, J.; Treacher, K.; McCabe, J.; Turpin, E.; Laughton, C. A.; Alexander, C.; Burley, J. C.; *et al*. Rapid Nanogram Scale Screening Method of Microarrays to Evaluate Drug-Polymer Blends Using High-Throughput Printing Technology. *Mol. Pharm.* **2017**, *14*, 2079–2087.

(453) Sanna, M.; Sicilia, G.; Alazzo, A.; Singh, N.; Musumeci, F.; Schenone, S.; Spriggs, K. A.; Burley, J. C.; Garnett, M. C.; Taresco, V.; *et al*. Water Solubility Enhancement of Pyrazolo[3,4-*d*]pyrimidine Derivatives via Miniaturized Polymer–Drug Microarrays. *ACS Med. Chem. Lett.* **2018**.

(454) Chelli, B.; Maga, G.; Bondavalli, F.; Botta, M.; Crespan, E.; Mosci, F.; Martini, C.; Brullo, C.; Manetti, F.; Bruno, O.; *et al*. Structure-Based Optimization of pyrazolo[3,4-*d*]pyrimidines as Abl Inhibitors and Antiproliferative Agents toward Human Leukemia

Cell Lines. **2008**.

(455) Kruewel, T.; Schenone, S.; Radi, M.; Maga, G.; Rohrbeck, A.; Botta, M.; Borlak, J. Molecular Characterization of c-Abl/c-Src Kinase Inhibitors Targeted against Murine Tumour Progenitor Cells That Express Stem Cell Markers. *PLoS One* **2010**, *5*, e14143.

(456) Manetti, F.; Santucci, A.; Locatelli, G. A.; Maga, G.; Spreafico, A.; Serchi, T.; Orlandini, M.; Bernardini, G.; Caradonna, N. P.; Spallarossa, A.; *et al*. Identification of a Novel Pyrazolo[3,4-*d*]pyrimidine Able To Inhibit Cell Proliferation of a Human Osteogenic Sarcoma *in Vitro* and in a Xenograft Model in Mice. *J. Med. Chem.* **2007**, *50*, 5579–5588.

(457) Sivina, M.; Kreitman, R. J.; Arons, E.; Ravandi, F.; Burger, J. A. The BTK Inhibitor Ibrutinib (PCI-32765) Blocks Hairy Cell Leukaemia Survival, Proliferation and BCR Signalling: A New Therapeutic Approach. *Br. J. Haematol*. **2014**, *166*, 177–188.

ACKNOWLEDGMENTS

Firstly, I would like to express my gratitude to my supervisor, Prof. Silvia Schenone, for her guidance throughout the years of my PhD course, for her helpfulness and for the suggestions during the correction of this thesis.

I am thankful to Francesca, for her support in all my problems and for the time spent answering my questions.

I would like to thank my PhD colleagues, Andrea, Chiara, Elda and expecially Ilaria, for the nice time spent together which I will never forget.

I am grateful to the entire DIFAR department, to Professors, to technicians and to PhD students, for many useful and nice moments.

A special thank to the University of Nottingham, in particular to Prof. Cameron Alexander, my supervisor during my research period in U.K., who gave me the possibility to work in his lab and to learn many new technologies and a big thank to Vincenzo and Giovanna, for their essential assistance in the lab and expecially in publishing our work.

Thanks so much to Sofia, for all the unforgettable moments in our house and for her true friendship.

A special thank to Silvia and Stefania, my big friends, for these many years during I could always have their support and affection.

I would like to thank my amazing extended family, who have sustained me every time with love.

A big thank to my special “Sirocchia”, Valeria, for her unconditional love, and, of course, to my loved nephews Maryam and Iyad, who have changed my life.

I am very grateful to my amazing parents, Paola and Salvatore, for our special relationship, for their love and support during all my life; I can’t describe the emotions which I feel for them.

Finally, I would sincerely thank Ale, my unique love, for all the great time spent together; I will never thank him enough for his support, for the laughs and for his true love. A wonderful future is waiting for us.